Characterization of Peripheral-Membrane Enzymes Required for Lipid A Biosynthesis in Gram-Negative Bacteria

by

Louis Eugene Metzger IV

Department of Biochemistry
Duke University

Date:_____

Approved:

_____
Christian R. H. Raetz, Supervisor

_____
K. V. Rajagopalan

_____
David C. Richardson

_____
Margarethe J. Kuehn

_____
Vytas A. Bankaitis

Dissertation submitted in partial fulfillment of
the requirements for the degree of Doctor of Philosophy in the Department of Biochemistry in the Graduate School
of Duke University

2010

ABSTRACT

Characterization of Peripheral-Membrane Enzymes Required for Lipid A Biosynthesis in Gram-Negative Bacteria

by

Louis Eugene Metzger IV

Department of Biochemistry
Duke University

Date:_____

Approved:

_____
Christian R. H. Raetz

_____
K. V. Rajagopalan

_____
David C. Richardson

_____
Margarethe J. Kuehn

_____
Vytas A. Bankaitis

An abstract of a dissertation submitted in partial fulfillment of the requirements for the degree of Doctor of Philosophy in the Department of Biochemistry in the Graduate School of Duke University

2010

Abstract

Gram-negative bacteria possess an asymmetric outer membrane in which the inner leaflet is composed primarily of phospholipids while the outer leaflet contains both phospholipids and lipopolysaccharide (LPS). LPS forms a structural barrier that protects Gram-negative bacteria from antibiotics and other environmental stressors. The lipid A anchor of LPS is a glucosamine-based saccharolipid that is further modified with core and O-antigen sugars. In addition to serving a structural role as the hydrophobic anchor of LPS, lipid A is recognized by the innate immune system in animal cells and macrophages. The enzymes of Lipid A biosynthesis are conserved in Gram-negative bacteria; in most species, a single copy of each bio-synthetic gene is present. The exception is *lpxH*, which is an essential gene encoding a membrane-associated UDP-2,3-diacylglucosamine hydrolase, which catalyzes the attack of water upon the alpha-phosphate of its substrate and the leaving of UMP, resulting in the formation of lipid X. Many Gram-negatives lack an *lpxH* orthologue, yet these species must possess an activity analogous to that of LpxH. We used bioinformatics approaches to identify a candidate gene, designated *lpxI,* encoding this activity in the model organism *Caulobacter crescentus*. We then demonstrated that *lpxI* can rescue *Escherichia coli* deficient in *lpxH*. Moreover, we have shown that LpxI possesses robust and specific UDP-2,3-diacylglucosamine hydrolase activity *in vitro*. We have developed high-yield purification schema for recombinant *Caulobacter crescentus* LpxI (CcLpxI) expressed in *E. coli*. We crystallized CcLpxI and determined its structure in complex with lipid X at 2.6 Å. CcLpxI, which has no known homologues, consists of two novel domains connected by a linker. Moreover, we have identified a point mutant of CcLpxI which co-purifies with its substrate in a 0.85:1 molar ratio. We have solved the x-ray crystal structure of this mutant to 3.0 Å; preliminary comparison with the product-complexed model revealed striking differences. The findings described herein set the stage for further mechanistic and structural characterization of this novel

enzyme.

In this work, we also isolated and characterized LpxB, an essential lipid A biosynthetic gene which is conserved among all Gram-negative bacteria. We purified *E. coli* and *Hemophilus influeznea* LpxB to near-homogeneity on a 10 mg scale, and we determined that *E. coli* LpxB activity is dependent upon the bulk surface concentration of its substrates in a mixed micellar assay system, suggesting that catalysis occurs at the lipid interface. *E. coli* LpxB partitions with membranes, but this interaction is partially abolished in high-salt conditions, suggesting that a significant component of LpxB's membrane association is ionic in nature. *E. coli* LpxB ($M_r \sim 43$ kDa) is a peripheral membrane protein, and we demonstrated that it co-purifies with phospholipids. We estimated, by autoradiography and mass-spectrometry, molar ratios of phospholipids to purified enzyme of 1.6-3.5:1. Transmission electron microscopy revealed the accumulation of intra-cellular membranes when LpxB was massively over-expressed. Alanine-scanning mutagenesis of selected conserved LpxB residues identified two, D89A and R201A, for which no residual catalytic activity was detected. Our data support the hypothesis that LpxB performs catalysis at the cytoplasmic surface of the inner membrane, and provide a rational starting-point for structural studies. This work contributes to knowledge of the small but growing set of structurally and mechanistically characterized enzymes which perform chemistry upon lipids.

Dedication

To my grandfather, Roger Vincent Foehringer, who was a man of rare courage, a patriot, and a gentleman. He spoke his mind to the lowly and to the powerful alike, never afraid to take a stand for causes in which he believed. He visited me and provided encouragement during the most difficult part of my time at Duke. My doctoral work is dedicated to his memory.

To Professor Christian R. H. Raetz, my thesis advisor, mentor, and friend. In these past six years, we have shared many adventures, dramatic moments of worry and triumph. Chris Raetz guided my growth as a scientist with enormous skill and dedication. Throughout our time together, he was animated by an ardent scientific curiosity, the sparks of which he never failed to transmit. Perhaps more importantly, Chris Raetz taught me much about the value of life, and the virtues of bravery and persistence in the face of overwhelming odds. My work is a tribute to his mentorship.

Table of Contents

List of Figures

List of Tables

1. Introduction

1.1 Gram-negative bacteria

Gram-negative bacteria play underappreciated and complex roles in nature and in human society. Many Gram-negatives, including *Escherichia coli* (*E. coli*) and *Salmonella Typhimurium* (*S. typhimirium*) are dangerous human pathogens (*1-3*). In contrast, the *Rhizobiaceae*, are benign nitrogen-fixing endosymbiotes (*4*). Other species, including *Burkholderia xenovorans*, are employed in the bioremediation of pollution (*5*). Due to their genetic diversity and robustness, Gram-negative species populate environments incompatible with most other forms of life; such extremophiles can provide key evolutionary and chemical insights upon which society-altering biotechnologies are based. Given the significance and ubiquity of Gram-negative species, the detailed elucidation of their biochemical properties is an important scientific goal toward which this work is directed.

Gram-negative bacteria are differentiated from their Gram-positive counterparts by possession of a two-membrane cellular envelope (*see Figure 1*). Gram-positives and Gram-negatives both have an inner membrane composed of a symmetric phospho- and/or sulpho-lipid bilayer (*6*). Exterior to this inner envelope, both possess a surrounding layer of peptidoglycan. In contrast to Gram-positives, Gram-negative species have an additional, asymmetric outer membrane (see Figure 1.1). The inner leaflet of this membrane is composed of phospholipids; the outer leaflet of lipopolysaccharide (LPS), which is anchored by its unique polyacylated disaccharide moiety, lipid A (see Figure 1.1). In most Gram-negatives, core regions of linked hexoses and heptoses are attached to the lipid A at its Kdo (3-deoxy-D-manno-oct-2-ulosonic acid) moiety. Distal to these core sugars are the more variable O-antigen polysaccharide repeats. In most species, the lipid A precursor Kdo_2-lipid IV_A (see Figure 1.1) is the minimal structure required for growth and viability (*7, 8*). LPS, in conjunction with outer-membrane proteins, constitutes a barrier that protects Gram-negatives from environmental toxins, including

amphipathic molecules such as bile salts and cationic antimicobial peptides (CAMPs) (*7*). At the same time, LPS plays a crucial role in host-pathogen recognition and invasion (*9*); the variable O-antigen repeats are recognized by the adaptive immune systems of many organisms, while the lipid A moiety is a potent activator of innate immune response (*10*).

While much attention is focused upon the dangers of community-acquired, multiple-drug resistant Gram-positive bacteria such as methicillin-resistant *Staphylococcus aureus* (*11*), infections by Gram-negative species are equally serious, especially in the developing world (*12, 13*), where they can cause endemic diseases that entail staggering social and economic costs. In addition to the well-studied *E. coli* and *S. typhimirium*, examples include *Rickettsia prowazekii* (*R. prowazekii*), the cause of typhus, *Leptospira interrogans* (*L. interrogans*), the cause of leptospirosis, the opportunistic pathogen *Psuedomonas aeruginosa* (*P. aeruginosa*), and members of the *Brucella* genus. Moreover, Gram-negatives are a major cause of nosocomial infections (*14, 15*).

Since Gram-negatives often face strong selective pressures and possess relatively rapid growth rates, they participate in an evolutionary arms race to evade (or elicit) host immune response (*16-19*). Since the advent of modern microbiology (*20, 21*), the development of effective antimicrobials has been a primary goal. Currently prescribed antibiotics arrest the growth of, or kill, Gram-negatives by a variety of mechanisms (*21*). Some successful compounds, such as quinolones (ciprofloxacin), and the polyaromatic natural product rifampicin, work to inhibit bacterial DNA replication and transcription, respectively. The same effect is achieved by blocking the production of folate, thus inhibiting nucleic acid biosynthesis; this is accomplished by sulfonamines such as sulfamethoxazole. Other antibiotics, including aminoglycosides (kanamycin, streptomycin), tetracylcines, and macrolides (erythromycin, spectinomycin), interfere with bacterial protein translation by interacting with the ribosome. The large β-lactam class, including the penicillins and cephalosporins, inhibit peptidoglycan cross-linking. The assembly of peptidoglycan is also targeted by glycopeptides such as vancomycin. Some cyclic peptides,

including polymyxin B and colistin, disrupt the membrane, leading to bacterial death. Modification of an organism's lipid A can modulate its sensitivity to such amphipathic peptides (*22, 23*). Through selective pressure, the widespread use (or misuse) of antibiotics over many decades has lead to the evolution of multi-drug resistant strains (*24, 25*).

Bacteria employ several mechanisms of resistance, including the increased expression of enzymes that metabolize antibiotics (such as β-lactamases), the over-production of and mutation in efflux pumps, and the re-modeling of membrane structure, including LPS (*26*). Unfortunately, the development of new antibiotics, especially those that target Gram-negative species, has not kept pace with bacterial evolution (*20*). A pressing need therefore exists for the discovery of antibiotics that make use of unique biosynthetic pathways in Gram-negative bacteria. Enzymes responsible for the biosynthesis, assembly, and transport of LPS offer excellent targets against which to develop novel antibiotics to combat the increasingly drug-resistant milieu of pathogenic Gram-negatives.

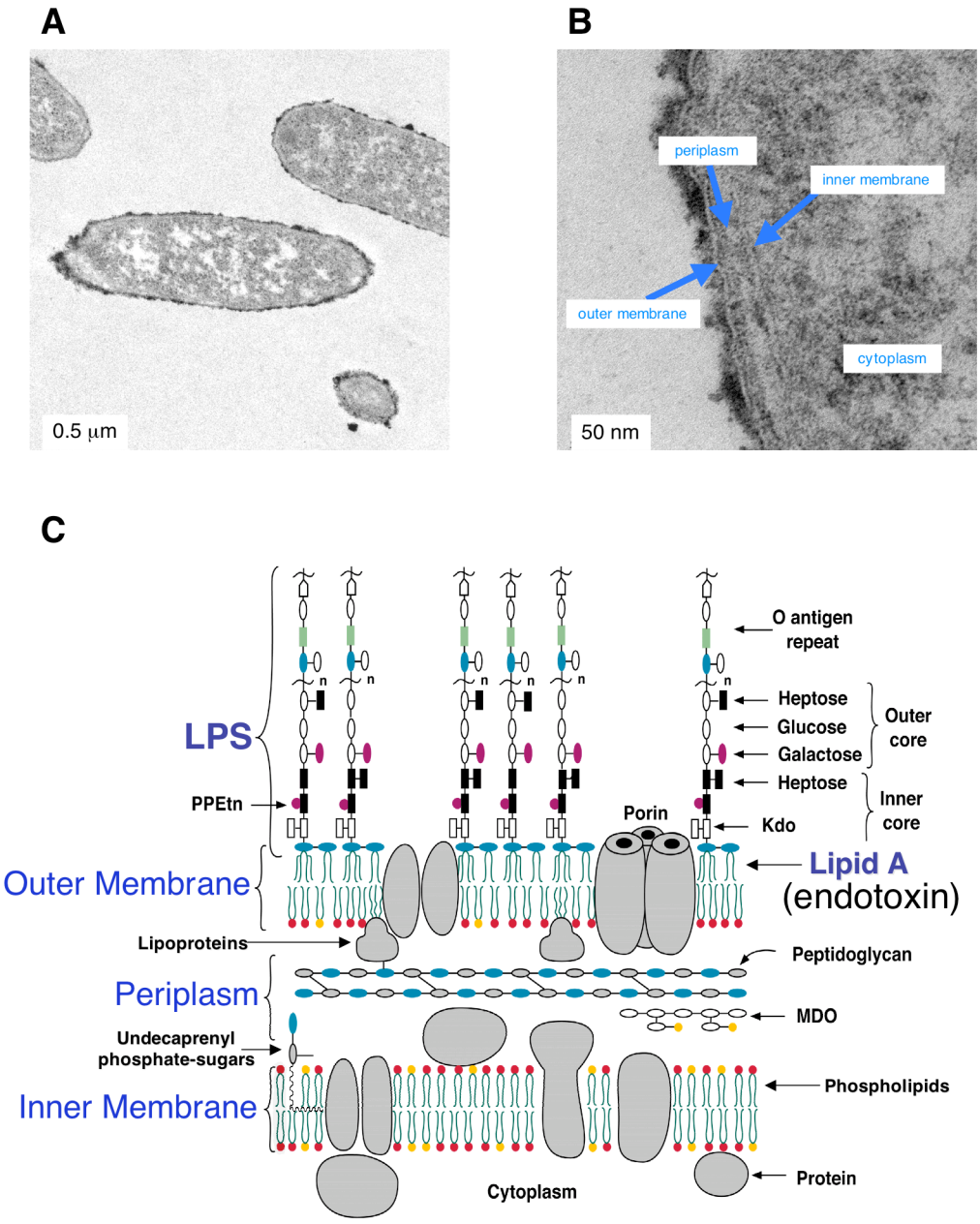

Figure 1.1. Structure of the cell envelope in a model Gram-negative species. Panels A and B show transmission electron micrographs of sectioned *Escherichia coli*, a Gram-negative bacterium. *E coli* strain C41(DE3) cells were grown, prepared, and imaged as described in (*27*). Cross-sections of cells are shown at 6,500-fold (Panel A) and 65,000-fold (Panel B) magnification. The blue arrows and labels on panel B indicate the location of the outer membrane, the periplasm, the inner membrane, and the cytosol. In most Gram-negative species, including *E. coli*, the outer leaflet of the outer membrane is largely composed of lipid A. Panel C (adapted from (*27*)), is a cartoon representation of the Gram-negative bacterial envelope. MDO denotes membrane-derived oligosaccharide.

1.2 The biosynthesis of Lipid A

The biosynthesis of Lipid A the hydrophobic anchor of LPS, has been described during the last twenty-five years by the Raetz laboratory (*28*). Beginning with the identification of the lipid A precursor 2,3-diacylglucosamine 1-phosphate (lipid X), the biosynthetic intermediates and constitutive enzymes of the lipid A pathway have been discovered and characterized (*28*) (see Figure 1.2). The assembly of lipid A is accomplished by a series of nine constitutive enzymes that are conserved among most bacterial species. In *E. coli,* a molecule of uridine diphosphate-*N*-acetyl-D-glucosamine (UDP-GlcNAc) is acylated at its 3-position hydroxyl by a molecule of *R*-3-hydroxymyristate transferred from acyl carrier protein (ACP) by the acyltransferase LpxA (*29*). The resulting UDP-3-*O*-(acyl)-GlcNAc is deacetylated at its 2-position by the metal-dependant enzyme LpxC (*30*). This allows the acyltransferase LpxD (*31*), which has significant homology to LpxA, to catalyze the transfer of a second *R*-3-hydroxymyistate to the deacetylated 2-amine, yielding UDP-2,3-diacylglucosamine. A metal-dependent phosphodiester hydrolase, LpxH (*32-34*), catalyzes the hydrolysis of the UMP moiety of UDP-2,3-diacylglucosamine to give 2,3-diacylglucosamine-1-phosphate (lipid X). LpxB (*35*), an inverting glycosyltransferase (GTase), catalyzes the condensation of lipid X and UDP-2-3-diacylglucosamine to form 2',3'-diacyl-GlcN(β,1'→6)2,3-diacyl-GlcN-1-P (disaccharide monophosphate), releasing UDP. The integral membrane enzyme LpxK phosphorylates the disaccharide monophosphate at its 4' hydroxyl, yielding lipid IV_A (*36*). The GTase KdtA then sequentially catalyzes the transfer of Kdo sugars from CMP-Kdo to the 6' position of lipid IV_A, yielding Kdo_2-IV_A (*37*), the minimum lipid A structure required for growth and viability in most Gram-negative species. The late acyltransferases LpxL and LpxM catalyze the transfer of laurate and myristate, respectively, from ACP to the 3-hydroxyl of Kdo_2-IV_A's 2' (LpxL) and 3' (LpxM) *R*-3-hydroxymyristate substituents (*38, 39*). LpxA, LpxD, and LpxC, for which structures have been reported, are soluble, cytosolic proteins. LpxH and LpxB act upon substrates located in the inner leaflet of the inner membrane, and are membrane-

associated. In most species, LpxK, KdtA, LpxL, and LpxM are cytoplasm-facing integral membrane proteins.

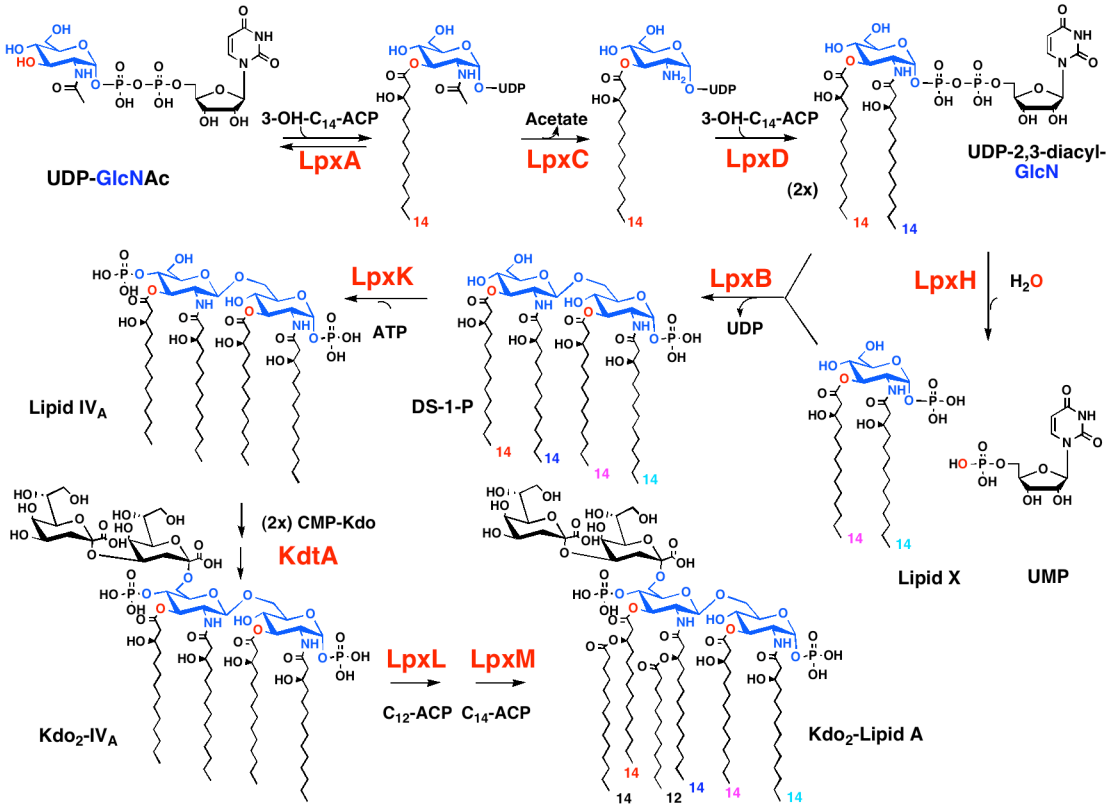

Figure 1.2. Constitutive lipid A biosynthesis in *E. coli*. The GlcN saccharides of the lipid A precursors are drawn in blue; their 3 or 3'-position oxygens are highlighted in red. In the hydrolysis step catalyzed by LpxH, the oxygen of the attacking water is colored red; its placement on the UMP product has been determined by labeling with $H_2{}^{18}O$ (*40*). Enzyme names are denoted in red text, while the names of co-factors and biosynthetic intermediates are in black. The colored numbers below the hydroxy-acyl moeties of lipid A precursors denote acyl chain length. Kdo_2-IV_A is the minimum structure required for growth and viability.

While most Gram-negative species possess each of the constitutive lipid A biosynthetic genes in a single copy, exceptions exist. *Legionella pneumophilia* (*L. pneumophilia*) has two orthologues of *lpxB*; transcription of each is dependent upon growth conditions (*41*). The model plant species *Arabidopsis thaliana* (*A. thaliana*), appears to have multiple *lpxD* genes. The most notable exception occurs in the case of the UDP-2,3-diacylglucosamine hydrolase; some species have two apparent *lpxH* orthologues, while many others, especially alpha-proteobacteria, have none (K. Baninski, thesis). In the case of *P. aeruginosa*, one orthologue, *lpxH1*, has 46% identity and 61% similarity to *E. coli lpxH*, while the other orthologue, initially designated *lpxH2*, has only 28% identity and 39% similarity (*34*). *P. aeruginosa* LpxH1 can complement *E. coli* depleted in LpxH, while *P. aeruginosa* LpxH2 cannot, providing the first clue that LpxH2 orthologues might have a function divergent from UDP-2,3-diacylglucosamine hydrolysis (*34*). Indeed, a *lpxH2* orthologue in *Sinorhizobium meliloti*, renamed *plcP*, has recently been shown to function as a phospholipase C, hydrolyzing the phosphocholine head group from phosphatidylcholine (PC) under low-phosphate growth conditions, thus making diacylglycerol available for recycling into sulfolipids (*42*). Most α-proteobacteria, including members of the geni *Brucella*, *Rhodobacter*, *Sinorhizobium*, *Rickettsia*, and *Caulobacter* lack an *lpxH* orthologue. Several extremophiles, including the *Aqifex aeolicus* (*A. aeolicus*), are also missing this gene. The discovery, purification, and characterization of a bacterial transformational analogue of LpxH will be addressed in this work, as will the purification and characterization of *E. coli* and *H. influenzae* LpxB.

1.3 Lipid A transport and Elongation

In *E. coli* and *S. typhimirium*, the Kdo_2-lipid A is glycosylated at the cytosolic face of the inner membrane by the Waa GTases (*43*), which catalyze the transfer of sugars from nucleotide-charged donors (*43*). In the same compartment, other peripheral-membrane GTases assemble the O-antigen oligosaccharide repeat on membrane-anchored undecaprenyl diphosphate. Multiple lines of evidence suggest that MsbA, an ATP-dependent floppase of the ABC transporter

family, is responsible for flipping core-sugar glycosylated lipid A to face the periplasm (*44, 45*). The nascent O-antigen oligosaccharide repeat, anchored to undecaprenyl diphosphate, is flipped to the periplasmic side of the inner membrane by Wzx (*46*), where a polymerase catalyzes its transfer to a growing chain of O-antigen repeats. The periplasmic enzyme WaaL then ligates the O-antigen polymer to the outer core sugars of Lipid A (*47*). The proteins LptA, LptB, LptC, LptF, and LptG are necessary for the transport of LPS to the outer membrane, employing mechanism still being elaborated (*48-52*). Once delivered to the inner leaflet of the outer membrane, the proteins LptD/LptE are involved in the flipping LPS to the outer leaflet (*53*).

1.4 Lipid A and the innate immune response

LPS plays a crucial role in Gram-negative species' ability to colonize host organisms (*10, 54*). Since LPS is anchored to the outer leaflet of these species' outer membranes, it is readily presented to elements of the innate immune system. In mammals, soluble serum LPS binding protein (LBP) effectively extracts LPS molecules from the outer membrane of the bacterium or from bacterial vesicles (*55, 56*). LPB makes LPS available for binding to monocyte differentiation antigen CD14 (CD14), a protein localized to the outer leaflet of host cells' membranes by a phosphatidylinositol (PI)-glycan anchor (*52*). CD14 then presents LPS to Toll-like receptor 4 (TLR4), the primary TLR implicated in LPS binding and signaling (*54*). While the specificities of the various toll-like receptors are still being determined, TLR2 is known to interact with certain bacterial lipoproteins, TLR3 with RNA, and TLR5 with flagellin (*57*). Members of the type I family of membrane-bound receptors, TLR's possess an exogenous ligand-binding domain (*see Figures 3 and 4*) attached by membrane-spanning linkers to a cytosolic TIR (toll-interleukin receptor) signaling domain (see Figures 1.3 and 1.4). TLR4 has been shown to interact with a soluble protein, myeloid differentiation factor 2 (MD2), to form a heterodimer (see Figures 1.3 and 1.4) (*54*). In its active form, the TLR4/MD2 complex is predicted to form a dimer of heterodimers (*58*) (see Figures 1.3). Structural and biochemical evidence (*10, 54, 59, 60*) suggests that the lipid A

anchor of LPS partially mediates the interaction between TLR4 and MD2 and thereby modulates the conformation and homodimerization of TLR's cytosolic TIR domains. The coupled role of TLR4/MD2 is supported by the observation that mice lacking either *TLR4* or *MD2* do not experience endotoxic shock when dosed with LPS, in contrast to wild-type controls (*61*).

The result of TLR4/MD2-mediated signaling, and thus the nature of the innate immune response, varies depending upon the properties of the molecule presented. A strong agonist of the human immune system, hexa-acylated lipid A (see Figure 1.4), binds to TLR4/MD2, causing conformational changes in both proteins, leading to the homo-dimerization of a TIR domain from each of two dimerized TLR4/MD2 complexes (*58*). This allows for the binding of either MAL or TRAM (*62*), adaptor proteins involved in TLR4-mediated signal transduction, to the activated TIR domain. These recruit MyD88 and TRIF, respectively (*62*). Upon binding to MAL, MyD88 initiates a kinase-dependent signaling cascade which results in the activation of nuclear factor κ-B (NF-κB). NF-κB is subsequently translocated to the nucleus and potenitates the up-regulation of genes that encode cytokines. Following translation, processing, and export from the nucleus, these cytokines cause inflammation that contribute to septic shock. Alternatively, if the TRAM/TRIF adaptor proteins are recruited to the TIR domain of activated TLR4, a signaling cascade is initiated which leads to the increased transcription of both NF-κB-regulated genes, and of genes whose transcription is mediated by interferon regulatory factor-3 (IRF-3). The latter encode immuno-regulatory proteins, such as interferons, which can affect a more benign immune response, resulting in infection clearing and adjuvanticity (*62*).

A true antagonist of TLR4, such as eritoran (see Figure 1.4), binds to the TLR4/MD2 without causing major conformational changes in TLR4/MD2 (*54*). Consequently, the eritoran-bound complex is unavailable to bind to agonists, and is therefore sequestered from potential signaling cascades. In contrast, 1-dephospo- lipid A can both bind to and induce conformational change in human MD2, but it fails to interact with the specific positively-charged residues on TLR4 required for complete activation of the TIR domains (*60*). Similarly, lipid IV_A binds to

MD2/TLR4 and induces a limited conformational change, owing to the reduction in hydrophobic contacts between the missing acyl moieties and MD2, leading only to partial TIR activation (*60*). In instances where partial agonism results in adjuvanticity, partially activated TIR domains are able to transduce signal via the TRAM/TRIF cascade, but not via the MAL/MyD88 pathway. Both 1-dephospo lipid A and lipid IV_A are partial agonists of the innate immune response in mice (*10*), while 1-dephospo lipid A is an antagonist in humans.

Genetic and biochemical evidence suggests an evolutionary relationship between host species' TLR4 and pathogens' LPS structure(s) (*10*). Not surprisingly, amino acid substitutions in the exogenous C-terminal domain of TLR4, and within the binding cleft of MD2, account for species' diverse responses to TLR activators (see Figure 1.2). For instance, *E. coli* lipid IV_A (*see Figure 2*) is antagonist toward human TLR4/MD2, but is an agonist toward the equine orthologue of this complex (*63*); this observation highlights the differential co-evolution of pathogen and host. As the success of a pathogen is partially dependent upon its ability to evade immune response, species such as *Yersinia pestis*, *Francicella tularensis*, and *Psuedomonas aeruginosa* have evolved to produce LPS that displays weak agonism toward human TLR4 (*64-66*), although it is claimed that some of these species' lipid A may activate TRL2 instead (*67*). Conversely, the susceptibility of a host to sustained infection by pathogenic species is partially dependent upon polymorphisms in TLR4 or MD2, which affect LPS binding and concomitant signaling (*67*). Moreover, many pathogens modify their lipid A structures based upon growth conditions (*28*). *Salmonella typhimurium* (*68*), *Yersinia pestis* (*69*) and *Legionella pneumophilia* (*41, 70, 71*) provide excellent examples of environment-dependent modification of lipid A. In addition to mediating host-pathogen relationships, LPS plays a role in benign symbiosis, most notably between species of nitrogen-fixing *Rhizobiacea* and various plants, including legumes (*72*). The biological implications of lipid A modification in these symbiotes is only beginning to be elucidated (Ingram et al., *in press*). Moreover, plants such as *Arabidopsis thaliana* and rice contain orthologues of many of the genes required for lipid A biosynthesis, hinting at a role for lipid A or

its precursors in these organisms. As genetics-guided structure-function analyses are performed upon a variety of TLR4/MD2 orthologues complexed with a diverse array of agonists, partial agonists, and antagonists, the subtle chemical determinants of TLR4 activation will become better understood.

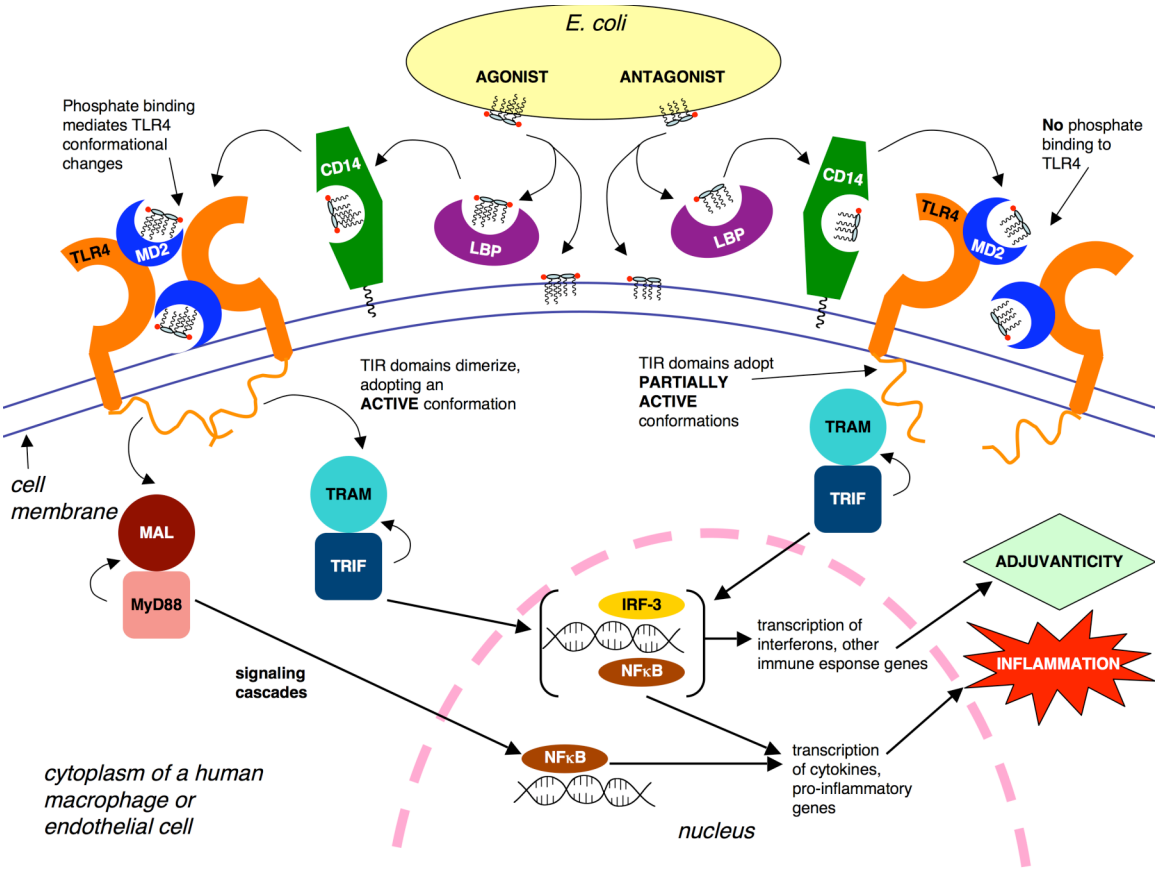

Figure 1.3. Human immune response to bacterial lipid A. This scheme describes two possible outcomes of human infection by a Gram-negative species. A bacterium, circulating in the intracellular matrix, sheds LPS. Lipid A, on the left, an agonist of the innate immune system in humans, is disaggregated and solubilized by LBP (purple), which then presents lipid A to the membrane-anchored receptor CD14 (dark green). CD14, in turn. delivers the agonist LPS to the MD2 (blue) portion of a heterodimer of MD2 and TLR4 (orange). Upon binding, the agonist lipid A mediates the homodimerization of two MD2/TLR4 heterodimers, causing the TLR4s' cytoplasmic TIR domains (orange waves) to interact and to undergo conformational change. This allows for the recruitment of either the TRAM/TRIF (turquoise/navy) or MAL/MyD88 (burgundy/salmon) adaptor-receptor pairs. The binding of MAL/MyD88 to the TIR domain initiates a signaling cascade which results in NFκB-mediated (brown) transcription of cytokines and pro-inflammatory genes. While TIR binding of the TRAM/TRIF adaptor pair also results in NFκB-mediated inflammatory response, it simultaneously leads to IRF3-mediated (gold) transcription of interferons and other immunogenic genes, thereby contributing to adjuvanticity. In contrast, 1-dephospho-lipid A, an antagonist in humans, is able to bind to MD2, but is not able to fully mediate interactions within and between MD2/TLR4 heterodimers due to the loss of interactions between the 1-phosphate and cationic residues on both MD2 and TLR4. Consequently, the TIR domains adopt active configurations TAM/TRIF are recruited, and signaling leads to an immune response consistent with adjuvanticity. This figure is not drawn to scale.

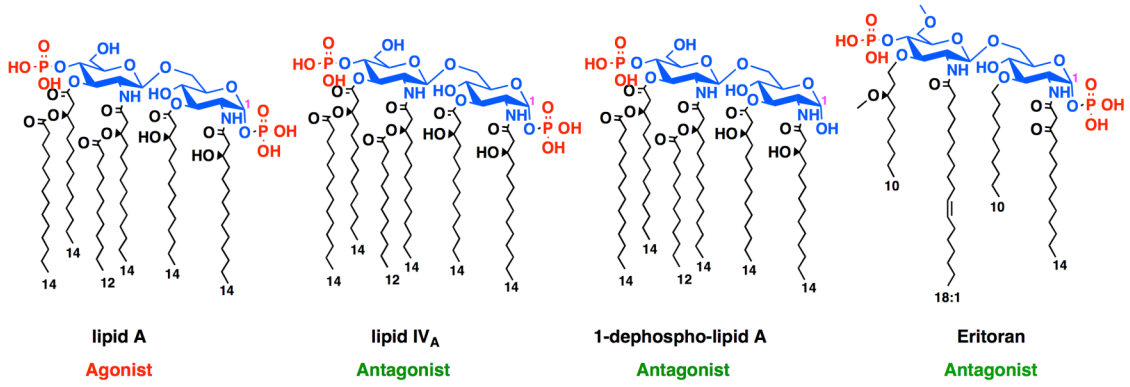

Figure 1.4. Lipid A agonists and antagonists. The glucosamine-based disaccharide scaffold is highlighted in blue, the phosphates in red. The magenta number "1" denotes the 1-position of the disaccharide. In humans, *E. coli* lipid A is an agonist of TLR4, while, lipid IV$_A$, 1-dephospho-lipid A, and eritoran are antagonists.

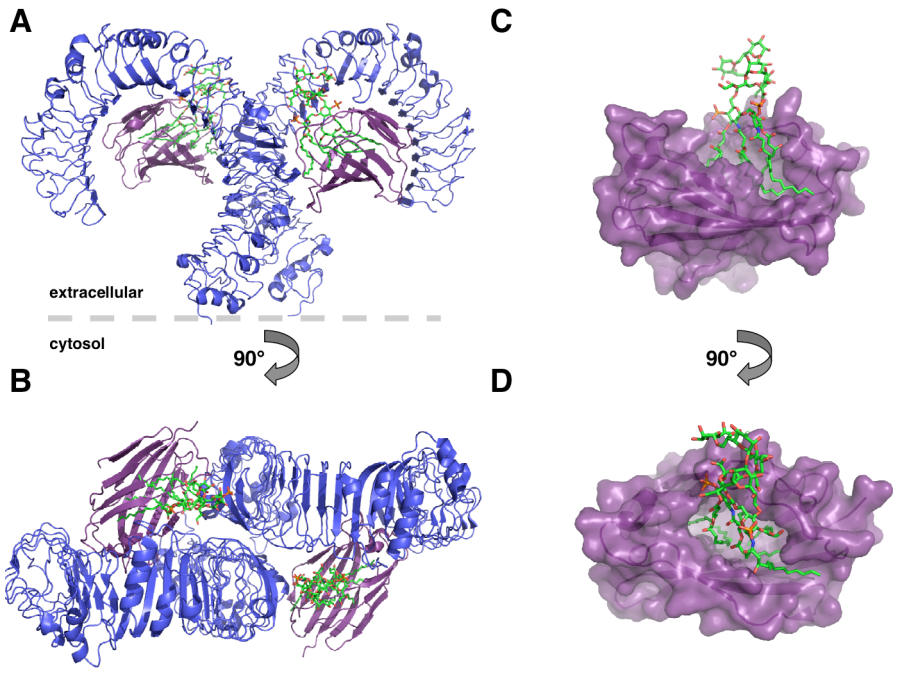

Figure 1.5. Structure of human TLR4/MD2 complex with bound lipid A. The extracellular domain of TLR4 is shown in blue. Human MD2 is displayed in purple. 3-Heptose-Kdo2-lipid A is colored by atom type: green for carbon, red for oxygen, blue for nitrogen, and orange for phosphorous. Panel A shows complex from one side, orientated such that it would be perpendicular to the plasma membrane. Panel B displays the same ensemble, rotated to show the top of the complex. Panels C and D show the MD2/lipid A portion of the complex. A semi-transparent surface demonstrates the depth of the MD2 binding pocket. This figure was generated using PyMOL (*73*), from a set of atomic coordinates contained in PDB ID 3FXI (3.1 Å), and described in (*74*).

1.5 Lipid A modification

As a consequence of host co-evolution and of other divergent selection pressures, Gram-negative bacteria produce a variety of lipid A structures. While all known lipid A's consist of a polyacylated β,1'→ 6 linked disaccharide scaffold, most other attributes of lipid A can be modified, in a species-dependent manner, by several lipid A remodeling enzymes. The oxidase/transaminase enzymes GnnA and GnnB, which are present in many bacteria, catalyze the conversion of the lipid A precursor UDP-GlcNAc to UDP-diamino-*N*-acetylglucosamine (UDP-GlcNAc3N) (*75*). Aided in some cases (*76*) by LpxA orthologues which greatly favor the acylation of UDP-GlcNAc3N over UDP-GlcNAc, species harboring *gnnA* and *gnnB* can produce lipid A with one (*Acidithiobacillus ferrooxidans*, *Campylobacter jejuni*) or both (*Leptospira interrogans*, *Mesorhizobium loti)* β1'→6 linked disaccharides consisting of diamino-*N*-glucosamine (GlcN3N) (*75*) (see Figure 1.6, panels A and B). The lipid A acyltransferases, LpxA, LpxD, LpxL, and LpxM, have differing acyl chain specificities dependent upon organism and/or growth condition (*7, 75*). In *S. typhimerium*, the outer membrane enzymes PagL (*77*) and LpxR (*78*) can catalyze the hydrolysis of the 3-position *R*-hydroxyacyl and the 3′-position R-acyloxyacyl chains, respectively (see Figure 1.6, panel C). In contrast *E. coli* or *S. typhimirium* PagP (*79*) catalyzes the transfer of palmitate to the hydroxyl group of lipid A's 2-position *R*-3-hydroxymyristate under certain growth conditions. In species including *Rhizobiaceae* and *Helicobacter pylori* (*H. pylori*) (*80*), the phosphatase LpxE can dephosphorylate the 1-position of lipid A, while in other species, including *Francicella tularensis* (*F. tularensis*), its distantly related homologue LpxF removes the 4′ phosphate (*81*). In *Rhizobiaceae* lipid A, dephosphorylation by LpxE renders the anomeric carbon of the proximal glucosamine susceptible to oxidation by LpxQ, an outer-membrane oxidase ((*82*), Ingram et al., *in press*, Ingram and Raetz, *in preparation*). An inner-membrane iron-dependent oxidase, LpxO, catalyzes the hydroxylation of the secondary 2′ myristate in *S.*

typhimerium lipid A (*see Figure 6, panel C*). In *E. coli* and *S. typhimirium*, the enzymes EptA and EptB can, respectively, catalyze the transfer of phosphoethanolamine to the 1-position phosphate, and the 7-hydroxyl of lipid A's outer Kdo (*83*). In polymyxin-resistant strains of *E. coli*, ArnT catalyzes the addition of a 4-Amino-4-Deoxy-L-arabinose to the 4′ phosphate of lipid A (*84*).

The lipid A modification enzymes offer a unique array of tools with which to probe the effects of lipid A remodeling upon bacterial viability and pathogenesis (*85, 86*). Their expression in various pathogens shows promise for the development of novel vaccines (*86-88*), and offers insight into the co-evolution of bacterial lipid A modification and the innate immune systems of bacterial hosts (*89*).

1.6 Lipid A as a drug target

As Kdo_2-lipid IV_A is the minimal lipid A structure required for most species' growth and viability, the genes encoding the first seven constitutive biosynthetic enzymes (see Figure 1.2) are essential; their products are potential targets of novel antibiotic inhibitors. The expression, purification, and characterization of these enzymes made possible the identification of inhibitors of LpxA (*90, 91*), LpxC (*92, 93*), and LpxD (Bartling and Raetz, unpublished data). Crystallographic and nuclear magnetic resonance (NMR) characterization of LpxC in complex with nanomolar and micromolar inhibitors (*93-95*) is facilitating the structure-based redesign of these compounds, most notably the nanomolar, biologically active compound Chiron-090. As their enzymology is better characterized and their structures elucidated, LpxH, LpxB, LpK and KdtA will offer additional targets by which to inhibit lipid A biosynthesis.

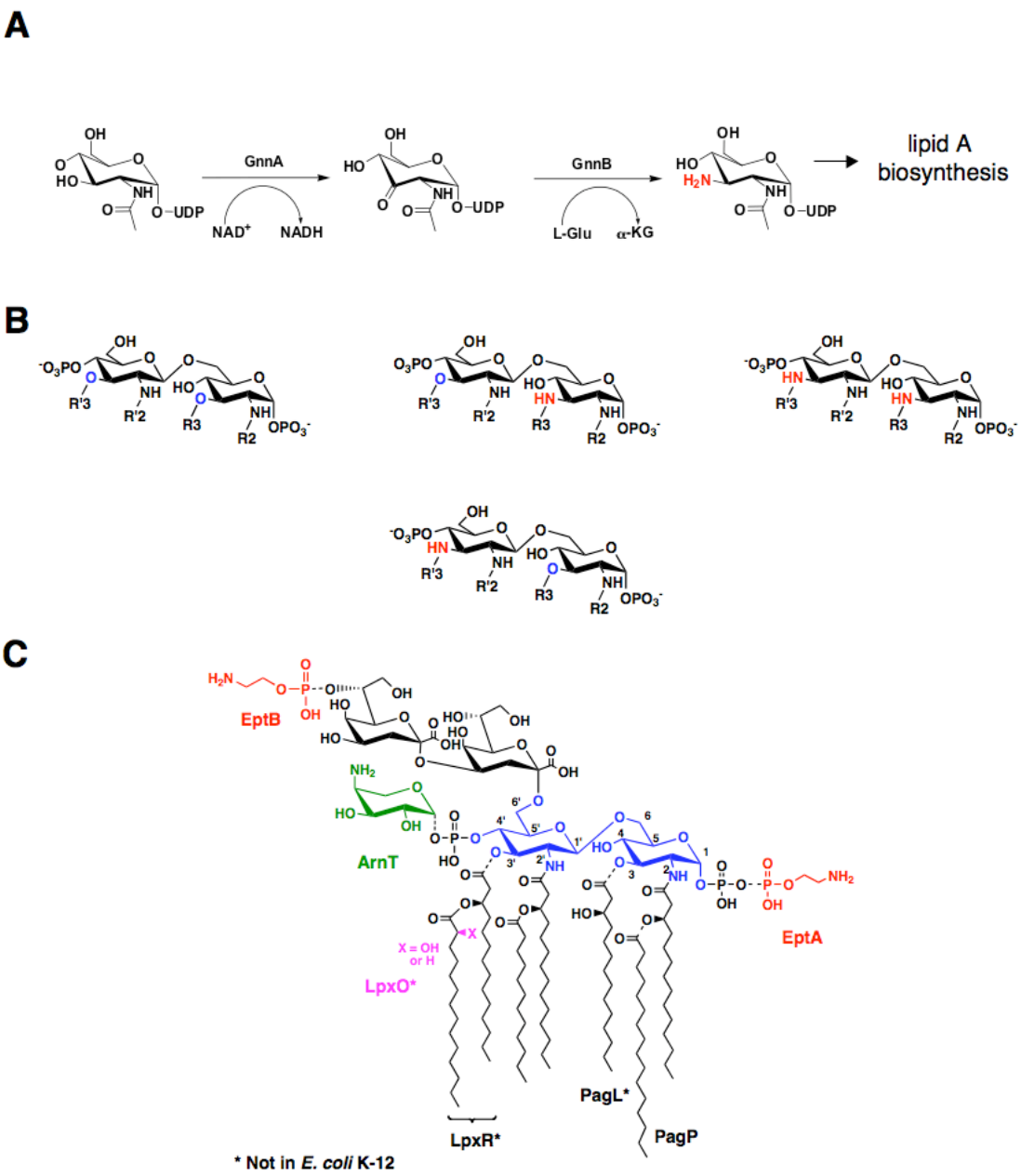

Figure 1.6. Lipid A diversity and modification. Panel A shows the reductase GnnA and the transaminase (GnnB) present in some Gram-negative species, and responsible for the presence of GlcN3N moeties in the disaccharide those species lipid A. Panel B shows the resulting diversity of lipid A disaccharides. Some species, such as *Campylobacter jejuni*, biosynthesize lipid A with mixed scaffolds. Panel C shows some of the possible lipid A modifications in *S. typhimirium* and *E. coli*; the core disaccharide is colored in blue, phosphoethanolamine red, L-4-amino-4-deoxy-arabinose green, and the position of LpxO-catalyzed oxidation in magenta. LpxL and LpxR catalyze the hydrolysis of the acyl moeties under which they appear; the site of cleavage is denoted by a dashed line. The bond formed when PagP catalyzes the transfer of palmitate is also shown as a dashed line.

1.7 The discovery and initial characterization of LpxB, the lipid A disaccharide synthase

LpxB was the first gene to be identified in the lipid A biosynthetic pathway. Its serendipitous discovery resulted from the biochemical analysis of *E. coli* strains possessing a mutant gene in the phospholipid biosynthetic pathway (see Figure 1.7), discovered and characterized by the Kennedy laboratory (*96-106*). The development of a rapid colony autoradiography technique facilitated the isolation of mutants with defective phospholipid biosynthetic enzymes (*107*). The construction of bacterial strains having lesions in Kennedy pathway enzymes allowed for the systematic genetic and biochemical characterization of phospholipid biosynthesis *in vivo* (*107-109*).

In order to investigate the roles of phosphatidylglycerol (PG) and cardiolipin (CL) in membrane function, Raetz and colleagues employed colony autoradiography to screen chemically-mutagenized *E. coli* for deficiency in phosphatidylglycerol-3-phosphate synthase (PgsA) activity (*107*) (see Figure 1.7). Mutants were identified and the chromosomal locations of their respective *pgsA* genes determined. While lysates from these mutants did not display temperature-sensitive (TS) PgsA activity upon shifting from 37 to 42°C, incubation at 70°C resulted in an irreversible loss of activity, in contrast to the wild-type enzyme. Following their transduction into a defined genetic background, only a weak correlation was observed between the level of residual PgsA activity in these mutants and the change in their PG and CL levels relative to the wild-type control (*107*). In order to isolate a "tighter" *pgsA* mutant with multiple lesions (and therefore less PG and CL), a first-step mutant was chemically re-mutagenized and screened for temperature sensitivity. One of these second-step mutants contained less than 1% of the PG and CL normally present in wild-type cells when grown at its non-permissive temperature. Unexpectedly, the thermal stability of PgsA activity in this mutant was similar to that of its parental strain, suggesting that a gene other than *pgsA* had been compromised. Moreover,

chromosomal mapping showed that this second lesion mapped to a site (*pgsB*) distant from *pgsA* on the *E. coli* chromosome. This strain harboring both *pgsA* and *pgsB* mutations was labeled with $^{32}PO_4$ and its phospholipids were extracted by the Bligh-Dyer method (*110*) under both neutral and acidic conditions. Upon resolution in a 2-D TLC system, two previously unknown lipids, X and Y, were significantly enriched in the mutant relative to the parental strain (*107*). Labeling with *N*-acetyl-1-*O*-[1-^{14}C]-glucosamine suggested that these lipids were LPS precursors (*107*). Subsequent experiments confirmed that the TS phenotype observed in the second-step mutant strain was caused by interaction between *pgsA* and *pgsB* lesions (*111*). Transformation of a *pgsB*-encoding plasmid back into the strain harboring both mutant genes (MN7) led to the reversal of lipid X and Y accumulation, further supporting the role of *pgsB* in the biosynthesis of lipids X and Y (*111*). Later studies elucidated the structure of lipid X and identified it as a precursor of lipid A. (*112-114*).

The gene *pgsB* (since renamed *lpxB*) was cloned by Crowell and collaborators (*35*). An inducible plasmid encoding LpxB was transformed into a wild-type *E. coli* background, directing a ~200-fold over-expression of disaccharide synthase activity. The operon upon which *lpxB* is located was subsequently sequenced, and LpxB was predicted to encode a 42.5 kDa protein (*115*). A fusion protein consisting of LpxB with a carboxy-terminal β-galactosidase domain was constructed and subsequently purified using immunoaffinity chromatography. The resulting fusion protein was sequencing, confirming its predicted amino-terminus (*115*). The modeling of LpxB's residue hydrophobicity did not predict transmembrane domains, but suggested the presence of two hydrophobic patches (*115*). When crude lysates of wild-type *E. coli* were subjected to ultracentrifugation at 100,000 × *g* for two hours, ~70% of LpxB activity remained in the supernatant while the remaining activity remained with the membranes (*115*). These data, together with the hydrophobic nature of the LpxB substrates and the insolubility of its product, suggested that LpxB was a peripheral membrane enzyme. Partial purification of *E. coli* LpxB from the strain pSR8/MC1061 was accomplished with dye-affinity chromatography (*116*). By a three-

step purification, a 30% net yield of ~80% pure LpxB was achieved. The development of improved qualitative and quantitative LpxB assays allowed initial kinetic parameters and substrate specificities to be reported (*116*). Additionally, the critical micelle concentrations (CMC's) of lipid X and UDP-2,3,-diacylglucosamine were estimated by fluorescence enhancement and gel filtration chromatography (*116*). More detailed biophysical characterization of lipid X (*117*) further elucidated the unusual solubility characteristics of the LpxB substrates.

1.8 LpxB and glycosyl transferases

LpxB's post-committal place in the lipid A biosynthetic pathway and the near-ubiquity of LpxB orthologues among gram-negative bacteria make it a compelling target for the development of broad-spectrum antibiotics. Moreover, further characterization of LpxB offers the possibility of unique insight into the biochemistry of glycosyl transferases (GTases). Involved in numerous biological processes in every characterized organism, GTases catalyze the glycosytic bond formation between sugars on activated donor substrates and the hydroxyl groups on numerous classes of acceptor molecules (*118*). GTases may either retain or invert the stereochemistry of the sugar substrate. GTases are broadly divided into two superfamilies: GT-A, which includes putative metal-dependent GTases, and GT-B, which encompasses a remarkably diverse subset of metal-independent GTase enzymes including LpxB. Many of the greater than 10,000 predicted GTase-encoding genes likely act upon sugars possessing nucleotide diphosphate leaving groups, of which ~60% are hypothesized to be UDP or TDP (*119*). The GT-A and GT-B superfamilies are themselves organized into theoretical families based upon sequence homology and substrate similarity (*120*). Among the diverse GT-B superfamily, there are currently ~100 CAZy families. Family 19 is exclusively occupied by putative LpxB orthologues, none of which have been strucutrally or mechanistically characterized. Despite the quantity and diversity of GT-B family members, functional and structural characterization is limited to tens of GTases in fewer families. These enzymes' low inter-familial sequence homology and tendency to be membrane-associated

make them difficult to study (*119*). Successful enzymological characterization (*121*), crystallization (*122*), and inhibiton (*123*) of the membrane-associated GTase *E. coli* MurG, an essential enzyme involved in peptidoglycan biosynthesis, demonstrates that rich biological insight can be gained from the study of GT-B type GTases.

In the present work, modern methods of expression cloning and affinity-tagging are employed to express and purify active LpxB to near-homogeneity, allowing for the detailed enzymological characterization of the *E. coli* enzyme, and for the preparation of 10 mg quantities of *E. coli* and *H. influenzae* LpxB for comprehensive crystallographic screening.

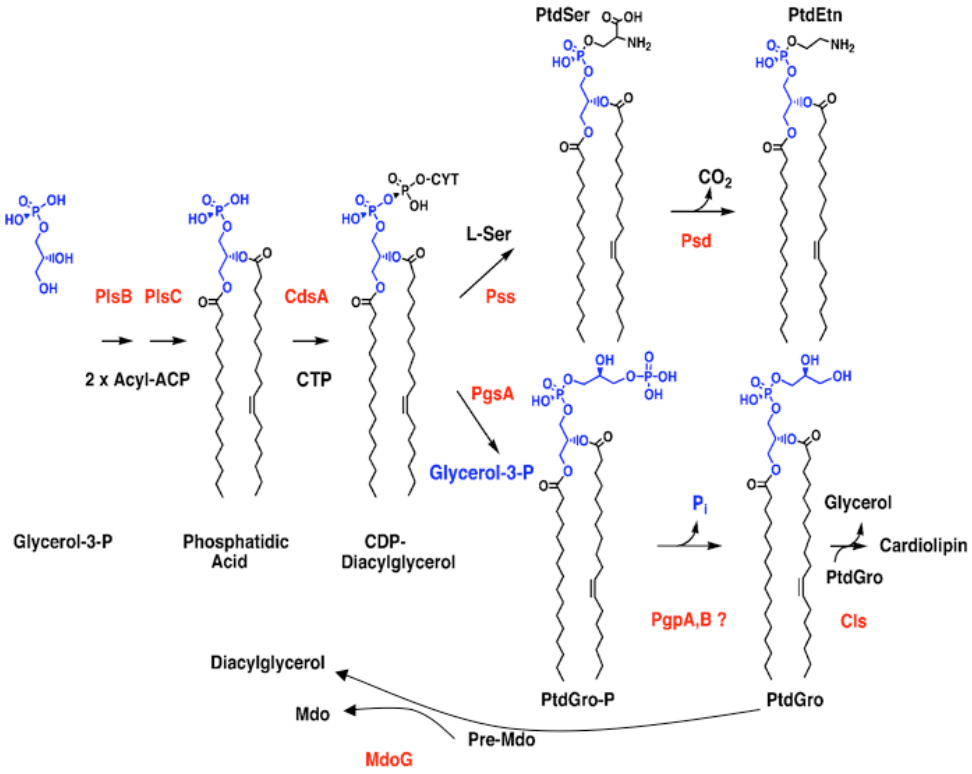

Figure 1.7. Phospholipid biosynthesis in *E. coli*. The glycerol-3-phosphate backbone of the phospholipid biosynthesis intermediates is colored blue, the names of genes encoding enzymes are red, while the names of intermediates, substrates, and products are black. PtdGroP is phosphatidyl glycerol phosphate; PtdGro is phosphatidyl glycerol, PtdSer is phosphatidyl serine, PtdEtn is phosphatidyl ethanolamine, ACP is acyl carrier protein, and Mdo is membrane-derived oligosaccharide. PlsB encodes glycerol-3-phosphate O-acyltransferase; PlsC, 1-acyl-sn-glycerol-3-phosphate acyltransferase; CdsA, CDP-diglyceride synthase; PgsA, phospatidylglycerophosphate synthase; PgpA, phosphatidylglycerophospahtase; Cls cardiolipin synthase; Pss, phosphatidyl serine synthase; Psd, phosphatidylserine decarboxylase.

1.9 The discovery and initial characterization of LpxH, the UDP-2,3-diacylglucosamine hydrolase

Soon after the structure of lipid X was determined by NMR spectroscopy (*124*), NMR analysis of *S. typhimerium* lipid A revealed the presence of a second, linked, 2,3-diacylglucosamine moiety (*125, 126*). It was hypothesized (*127*) that a nucleotide-activated diacylglucosamine species, similar to lipid X, might be the source of this second diacylglucosamine in the lipid A disaccharide. By radio-labeling MN7 and its parental strain R477 with $^{32}PO_4$, and using a modified Bligh-Dyer (*128*) extraction method in which the methanol-water phase was diluted ten-fold with 0.1 N HCl, Raetz and colleagues were able to identify, in addition to lipid X, a second unknown metabolite which accumulated approximately 50-fold in MN7 relative to wild-type *E. coli*. Chemical and enzymological degradation of this unknown compound, coupled with chromatographic analysis in the presence of synthetic NDP-diacylglucosamine standards, suggested that the minor metabolite was UDP-2,3-diacylglucosamine. The abundance of UDP-diacylglucosamine was estimated to be ~400 molecules per cell in wild-type *E. coli*, nearly 10-fold lower than lipid X (*129*). Subsequent pulse-labeling experiments (*130*) identified UDP-2,3,-diacylglucosamine as a precursor of lipid X *in vivo*. Further evidence supporting the role of UDP-2,3,-diacylglucosamine as a lipid A precursor was obtained when crude extracts of *E. coli* were shown to catalyze its conversion to lipid X (*129*), and when partially purified LpxB was used to catalyze the formation of DSMP from purified UDP-2,3,-diacylglucosamine and lipid X (*116*).

The identification of the gene encoding the *E. coli* UDP-2,3-diacylglucosamine hydrolase was made tractable by the observation that upon the *in vitro* assay of crude lysate from a strain in which the gene encoding CDP-diacylglycerol hydolase, *cdh*, is knocked out, residual UDP-diacylglucosamine hydrolase activity remains. (Ray and Raetz, unpublished data). Although Cdh, a promiscuous CDP-diacylglycerol hydrolase enzyme of unknown biological function, acts upon UDP-2,3-diacylglucosamine in cell lysates, it is non-essential for lipid A biosynthesis and cell

viability (*131-134*). Moreover, *cdh* contains a putative signal sequence (*135*) consistent with periplasmic localization. It has been demonstrated that lipid A biosynthesis occurs at the cytoplasmic face of the inner membrane (*136*). To identify the gene responsible for *coli* UDP-2,3-diacylglucosamine hydrolase activity, a *cdh* deletion strain was infected with a library of mapped hybrid bacteriophage λ clones (*137*), and the resulting lysates were assayed for UDP-2,3-diacylglucosamine activity (*33*). From a clone having ~10-fold increased activity over background, and lacking *cdh*, bioinformatics analysis identified *ybbF* (later renamed *lpxH*) as a putative gene encoding the UDP-2,3-diacylglucosamine hydrolase, which was renamed *lpxH* (*33*). Sequence comparison showed LxpH to have a motif ($DXHX_NGDXXDX_NGNH(D/E)$, where X is any residue) characteristic of a metal-dependent phosphoesterase super-family. LpxH activity was confirmed by *in vivo* complementation, radio-labeling of whole cells, and *in vitro* assay (*34, 40*). LpxH was expressed from a high-copy plasmid in *E. coli*, partially purified to ~60% homogeneity, and enzymologically characterized. TLC-based radiographic *in vitro* assays revealed that LpxH has a pH optimum of ~8.0, and a K_M of ~60 μM with respect to UDP-2,3-diacylglucosamine, and an apparent V_{MAX} of ~10 μM/min/mg (*33*). LpxH was shown to have an absolute requirement for both of its substrate's acyl chains, and to lack activity toward CDP-diacylglycerol. ^{31}P NMR analysis of UMP and lipid X, generated from UDP-2,3-diacylglucosamine by partially purified enzyme in the presence of $H_2{}^{18}O$, revealed that LpxH catalyzes the attack of water at the α-phosphorous atom of UDP (*33*). Subsequent characterization showed LpxH's *in vitro* activity to be stimulated greater than 10-fold by divalent cations, with Mn^{2+} producing the largest increase in apparent specific activity (Babinski and Raetz, unpublished data). As many members of the metal-dependant phosphodiesterase family have bi-metallic centers, it is possible that more than one metal is involved in LpxH function. Mutagenesis was used to probe the role of conserved LpxH residues, providing evidence that Asp 122, which is absolutely conserved among LpxH orthologues, may play a role in catalysis. Mutagenesis studies suggested that other absolutely conserved residues, including Asp8, His10, Asp 41, Asn79, Asp81, Asp116, and His195, may be

involved in metal co-factor coordination, either directly or through a shell of ordered water molecules (Babinski and Raetz, unpublished data).

While the purification of *E. coli* LpxH to homogeneity has proven elusive ((*33*), Babinski and Raetz, unpublished data), additional attempts to isolate this protein and its orthologues are warranted. A structural characterization of LpxH, in combination with the large extant body of mutagenesis work (Babinski and Raetz, unpublished), may yield detailed insight into the mechanism of this essential peripheral-membrane hydrolase. Even if structural characterization proves intractable, biophysical analyses performed on near-homogenous LpxH may provide information regarding LpxH's oligomerization state, modality of membrane interaction, and the identity of its physiological metal cofactor(s).

1.10 Metal-dependent Phosphohydrolases

LpxH and its putative transformational analogue(s) catalyze the cleavage of a phosphodiester bond (see Figure 1.2). Phosphohydrolases, which are ubiquitous, play important roles in the post-translational modification of proteins, nucleic acid processing, and numerous other aspects of metabolism, transport, and cellular signaling (*138-147*). In the past decade, biochemical and biophysical techniques have provided significant insight into the mechanisms of different types of metal-dependent phosphohydrolases. Well-characterized members of this functional group include metallo-phosphoesterases that act upon lipids (phospholipases C and D (*148*), sphingomyelin phospodiesterase (*140*)), nucleotides and their precursors (the Nudix enzyme family (*141*), some ribonucleases (*147*), cyclic nucleotide phosphoesterases), and proteins (serine-threonine phosphatases, calcineurin(*149*)). The well-characterized purple acid phosphatases (*150*) have a yet-unknown physiological significance. The mechanisms of these enzymes are diverse, but they generally involve the positioning of a deprotonated water molecule for attack upon the phosphorous of the coordinated phosphate moiety of the substrate. The roles played by metals in these mechanisms vary.

In enzymes such as red kidney bean purple acid phosphatase, an aspartate-coordinated dimetallic center, consisting of Zn^{2+} and Fe^{3+}, positions a hydroxyl for attack upon a phosphorous atom (see Figure 1.8, panels A and B) (*150*). Multiple histidines may provide coordination of the substrate. In the case of bacteriophage λ serine-threonine phosphatase, structural and biochemical evidence suggests that a Mn^{2+} bimetallic center is coordinated by histidine, asparigine, and aspartate residues. A bridge formed by the bimetallic center positions a water for attack upon the phosphate, but the Mn^{2+} cations also coordinate the phosphate: one directly, and the other through an ordered water network (*151*), see Figure 1.8, panels C and D). Members of this enzyme family share a metallo-phosphohydolase motif, $DXHX_NGDXDX_NGNHD/E$, where X denotes any residue, and n is ~25. As with purple acid phosphatases, absolutely conserved histidines are present in the active sites of serine-threonine phosphatases. The Nudix phosphohydrolases, while sharing an active site motif ($GX_5EX_7REUXEEXGU$, where X is any residue and U is a bulky hydrophobic or aliphatic amino acid), catalyze their reactions by diverse mechanisms, using one, two, or three, metals for various catalytic purposes (*152*). These metals are commonly Mg^{2+}, Mn^{2+}, or Co^{2+}, and do not necessarily co-purify with the enzymes (*153*). Different Nudix family members catalyze the attack of water upon α-phosphates (*154*), β-phosphates (*155*), or with GDP-mannose hydrolase, upon the anomeric carbon of the mannose (*156*). The ubiquitous housekeeping dUTPases, present in all living organisms and in some retroviruses (*157*), offer more examples of metallo-phosphohydrolase diversity. In most dUTPase's studied to date, the oxygens of the α-phosphate of dUTP are coordinated by metal atoms, usually Mg^{2+}, within a complex shell of ordered waters (see Figure 1.8, panels E and F), while conserved acidic residues position the catalytic water for attack. Most dUTPases are homotrimers (*157, 158*), with residues contributed by adjacent monomers forming active sites (*159*) (see Figure 1.8, panel F), although some recently-identified orthologues (*160*) are active as monomers.

Having numerous structural motifs and methods of affecting catalysis, the metal-dependent phosphohydrolases provide examples of both convergent and divergent evolution (*141, 161*). Despite sharing a conserved active site sequence, Nudix enzymes have multifarious catalytic strategies, suggesting their divergent evolution from a common ancestor. Another example of such functional drift is the recently-discovered bacterial phospholipase PlcP, which despite sharing a conserved motif with LpxH, catalyzes chemistry upon a different substrate (*42*). Conversely, non-homologous proteins can evolve to perform identical function, becoming transformational analogues (*162*). Like the metal-dependant phosphohydrolases, branches of the enolase superfamily (*163*), provide instances (*164, 165*) of apparently convergent evolution. Since many species of bacteria lack LpxH orthologues, it is likely that a similar functional drift has produced analogous UDP-2,3-diacylglucosamine hydrolase(s). While a lack of homology makes it difficult to identify genes encoding this activity by sequence comparison, the consideration of genomic context can assist in the functional mapping of unknown genes (*166-168*). In this work, we identify and characterize the transformational analogue of LpxH, a metal-dependent phosphodiester hydrolase.

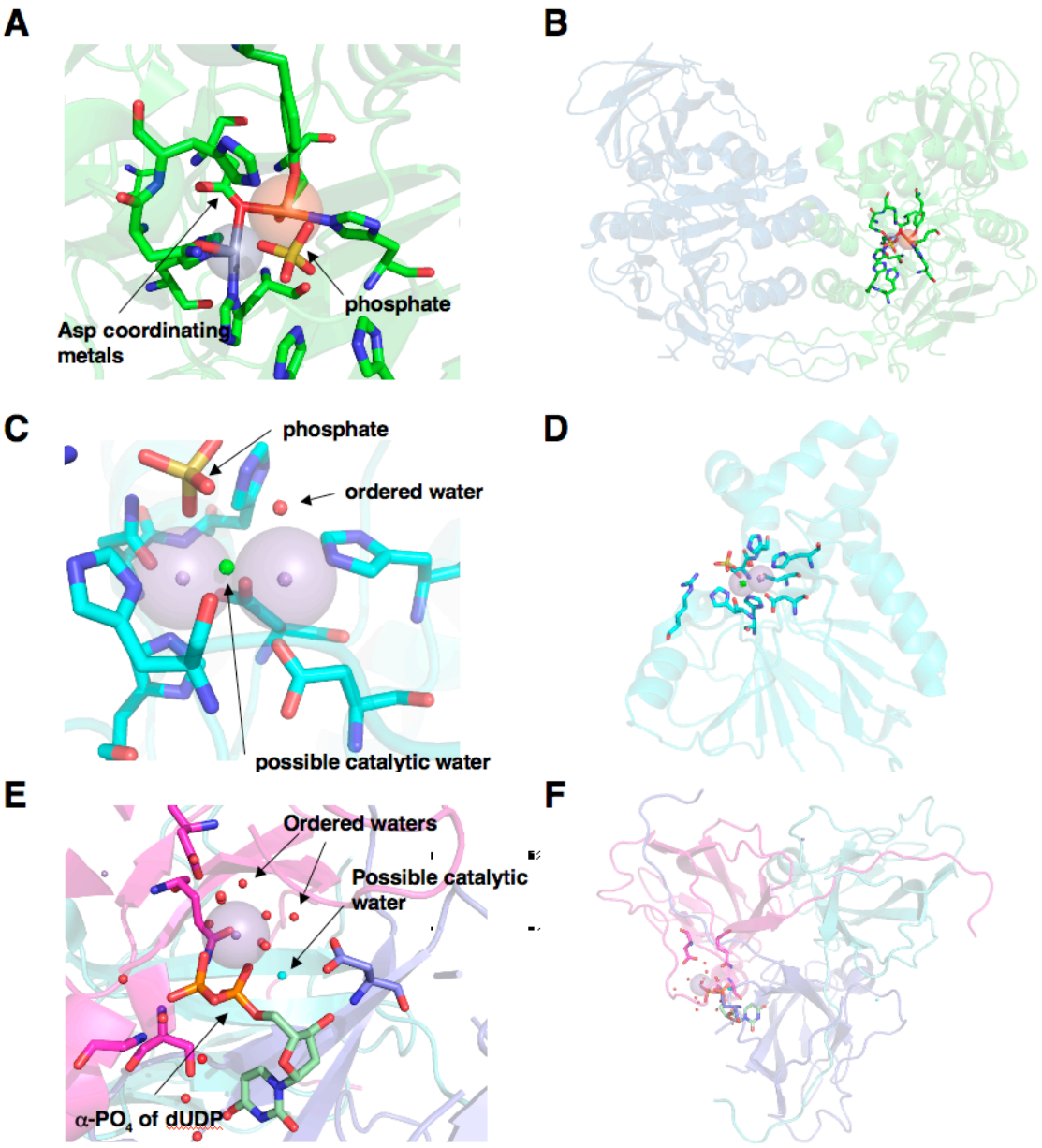

Figure 1.8. Examples of metal-dependent phosphohydrolases. Panel A and B show red kidney bean purple acid phosphatase (PDB 2QFP, 2.4 Å, (*150*)). Panel A is a simplified rendering of the active site, while panel B shows the overall dimer (only one active site is shown). The semi-transparent spheres in panel A are Zn^{2+} (gray) and Fe^{2+} (orange). The coordinations between the metals and active-site residues are rendered as solid bonds in this PDB model (*150*). Panels C and D show bacteriophage λ serine-threonine phospahtase (PDB 1G5B, 2.15 Å, (*151*)). In panel C, the semi-transparent mauve spheres represent Mn^{2+} ions; the green sphere indicates a possible catalytic water. Panel D shows the biological monomer. Panels E and F show *E. coli* dUTPase (PDB 2HR6, 1.84 Å, (*158*)). In panel E, showing a portion of the active site, several ordered waters (red spheres) surround a Mg^{2+} ion (mauve semi-transparent sphere). A teal sphere indicates the position of a possible catalytic water. Panel F shows that the active site is at trimerization interfaces. Hydrogens have been omitted for simplicity.

1.11 Protein-lipid binding

As both LpxB and LpxH catalyze reactions of saccharolipid substrates, it is informative to consider, from a structural perspective, how proteins bind to similar ligands. Excellent examples include Sec14, a potentiator of Golgi vesicle transport and signaling; CD1, a lipid-sampling MHC I-type sensory protein expressed on antigen-presenting cells; and LpxA, an acyltransferase and the first enzyme in the Lipid A biosynthetic pathway. The binding of lipid A by MD2 in complex with TLR4, described in a previous section (*see Figure 5*), constitutes another example of a structurally characterized lipid binding protein.

Sec14 orthologues are peripheral membrane proteins are present on the endoplasmic reticulum and golgi membranes, where they bind to various phospholipids such as phosphatidylcholine (PC) or phosphatidyinositol (PI), and present these to modifying or metabolic enzymes for additional processing (*169, 170*). An emerging model for Sec14 function emphasizes its regulation of lipid metabolism, both through the sequestration of enzymes' lipid substrates, and through their delivery (*169, 170*). One example of Sec14 function is described by a "hetrotypic exchange model," wherein Sec14 samples the membrane surface, binding to PI Sec14 then binds to PC, displacing the PI (Bankaitis et al., *Cell*, in press). The exiting lignad is thereby presented to modifying enzymes, such phosphatidyl inositol 4-OH kinase. High-resolution crystal structures (*169, 170*) (see Figure 1.9, panels A and B) of the yeast Sec14 homologue Sfh1 bound to both PC and PI demonstrate the determinants of Sec14 binding specificity. The acyl chains and head groups of both lipid ligands are buried in Sec41's core; this large internal pocket is made accessible by the displacement of a helical "cap," presumably upon lipid binding. Interestingly, while the acyl chains of PC and PI bind in the same cleft of Sec14, the ligands' head groups reside in different cavities (see Figure 1.9, panels A and B). The PI binding

site is filled with ordered waters (not shown) when PC is bound, and vice-versa; this use of ordered water may explain why Sec14 can accept multiple phospholipid ligands.

CD1 proteins, expressed on the membrane of T-lymphocytes, sequester endogenous and exogenous lipids, presenting them to protein components of the immune systems' signal transduction machinery (*171*). Antigen-presenting cells over-express CD1 orthologues; this expression is stimulated by the presence of cytokines and interferons, and thus by TLR4 and TLR2-mediated signal transduction cascades (*172*). CD1 orthologues allow the immune system to recognize various lipids characteristic of pathogens, including viruses and certain bacteria. The structure of a mouse CD1d orthologue complexed with 3-*O*-galactosyl-1,2,-diacyl-sn-glycerol (BbGL-2f), a glycerolipid produced by the Gram-negative bacterium *Borrelia burgdoferi*, has been determined at high resolution (*172*). The acyl-chains of BbGL-II bind in a long, narrow hydrophobic cleft, while the galactose moiety has relatively few interactions with CD1 residues (*see Figure 9, panels C and D*).

LpxA (*29, 173*), the homotrimeric UDP-GlcNAc acyltransferase responsible for catalyzing the first step in the lipid A biosynthetic pathway, has characterized at high resolution by x-ray crystallography (*90, 91, 174, 175*) (see Figure 1.9, panels E, F and G). *E. coli* LxpA acts upon it natural substrate UDP-GlcNAc, but it can also catalyze the acylation of UDP-GlcNAc3N (*76*). In contrast, *L. interrogans* LxpA exhibits an absolute specificity for UDP-GlcNAc3N (*76*). Crystal structures of both enzymes in complex with their products (*174, 175*) reveal acyl chain binding in a shallow, solvent-exposed hydrophobic cleft (see Figure 1.9, panels E and F), while GlcNAc or GlcNAc3N moieties appear to have several hydrogen-bonding and electrostatic interactions with well-conserved active-site residues. Comparison of these complexes reveals a possible explanation for the specificity of *L. interrogans* LxpA. The backbone carbonyl of a conserved Gln residue in *L. interrogans* is positioned to form a hydrogen bond with the 3-amine of GlcNAc3N

(see Figure 1.9, panel G), but this carbonyl would cause charge-repulsion with the 3-hydroxyl if GlcNAc was substituted for GlcNAc3N. In contrast, the corresponding Gln carbonyl in *E. coli* LpxA is rotated away from the sugar-binding pocket. This may explain why *E. coli* LpxA can act on substrates having either sugar, while *L. interrogans* LxpA is absolutely specific for UDP-GlcNAc3N (*76*). LpxA specificity is also determined by the length of the acyl chain binding pocket (*173, 176*). Mutagenesis and structural analyses have identified residues that act as "hydrophobic rulers" in LpxA; these establish an upper limit upon the length of acyl chains that can be transfered to UDP-GlcNac in a given organism (*173*). As acyl chains are delivered to LpxA by ACP, additional complexity arises from the interfacial interactions between these proteins during catalysis. LpxA likely possesses both acyl-chain and sugar specificities as a consequence of its catalysis of the first step of Lipid A biosynthesis, thereby limiting the heterogeneity of downstream lipid A precursors.

Taken together, the structural characterizations of CD1, Sec14, LpxA, and MD2 orthologues demonstrate the diverse strategies by which proteins interact with their lipid ligands or substrates. In the examples of CD1 in complex with BbGL-II and of MD2/TLR4 in complex with 3-hepto-Kdo_2 lipid A, protein-sugar interactions are sparse, while hydrophobic contact with ligand acyl chains predominates. Sec14 completely buries its substrates' acyl chains in a well-defined cleft, while making use of separate binding pockets to accommodate different ligands' head groups. In contrast, LpxA specificity is exquisitely dependent upon both protein-saccharide and protein-acyl chain interactions. The structural characterization of enzymes that act upon saccharolipids, including LpxB and a transformational analogue of LpxH, will provide additional examples of protein-lipid interactions.

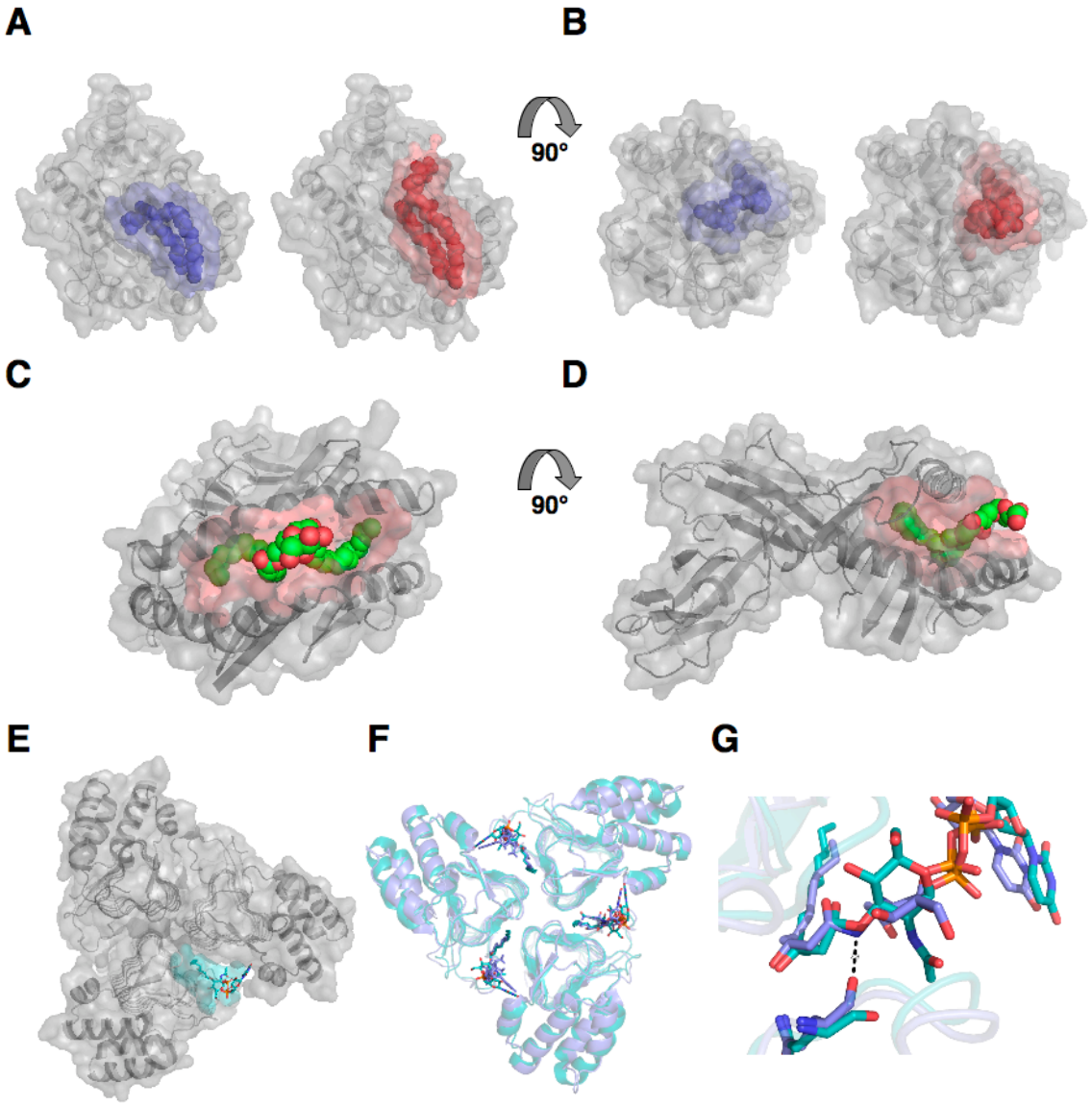

Figure 9. Proteins with lipid ligands. Panels A and B show the yeast Sec14 homologue Sfh1 (PDB 3B7Z, 2.03 Å, (*170*)), complexed to PE (blue) or PI (red) rendered in space-filling spheres. The binding pocket surfaces, modeled using CAVER (*177*), are shown in the colors of their ligands. Panels C and D show mouse CD1d (PDB 3ILQ, 2.05 Å, (*172*)), complexed with 3-*O*-galactosyl-1,2,-diacyl-sn-glycerol (BbGL-2f), a saccharolipid produced by the Gram-negative bacterium *Borrelia burgdoferi*. The ligand, rendered in space-filling spheres is colored by atom type, with carbons green and oxygens red. The binding pocket surface is pink. Panel E show *E. coli* LpxA in complex with its product, uridine-5'-diphosphate-3-O-(R-3-hydroxymyristoyl)- N-acetyl-D-glucosamine (PDB 2QIA, 1.72 Å, (*174*)). One of the trimer's three active sites, its surface modeled in teal is shown. Panel F shows the overlay of the E. coli LpxA complex (in teal) with the *Leptospira interrogans* LpxA product complex (in purple, PDB 3I3X, 2.10 Å, (*175*)). The active sites' Asn carbonyl oxygen in position to clash with the 3-position hydroxyl in the (teal) *E. coli* product, or to hydrogen-bond with the 3-position amine in the *L. interrogans* LpxA product (purple). For clarity, hydrogens and ordered waters have been omitted from these representations.

1.12 Contribution of this work to the field

In Chapter 2, we describe the discovery of a transformational analogue of *lpxH*, designated *lpxI*, and show that its orthologue in *Caulobacter crescentus* (*C. crescentus*) can cover an *lpxH* knockout in *E. coli*. We then demonstrate, by thin-layer chromatography (TLC), that lysates of *E. coli* over-expressing *C. crescentus* LpxI have UDP-2,3-diacylglucosamine hydolase activity *in vitro*. A method is presented for the purification of *C. crescentus* LpxI (CcLpxI) to ~90% homogeneity. With this partially-purified enzyme, we employ an optimized autoradiographic assay for UDP-2,3-diacylglucosamine hydolase activity in order to determine pH, metal, and detergent dependencies. Finally, we use mass-spectrometry to analyze the products of an *in vitro* CcLpxI reaction that is carried out in the presence $H_2{}^{18}O$. Our results reveal that CcLpxI catalyzes the attack of a water on the β-phosphate of UDP-2,3-diacylglucosamine, suggesting that it acts by a different mechanism than LpxH.

In Chapter 3, we describe the cloning and expression of a CcLpxI construct that has been N-terminally tagged with a cleavable poly-histidine tag. We then purify this protein to near-homogeneity on a 100 mg scale. We discover that upon extraction of purified CcLpxI in an acidic two-phase system, a significant quantity of lipid X, the product of the UDP-2,3-diacylglucosamine hydolase reaction, co-purifies with CcLpxI, as judged by TLC and mass-spectrometry. Whole-cell $^{32}PO_4$ labeling allows us to estimate a lipid X to CcLpxI stoichiometry of 0.95:1, and to observe that CcLpxI over-expressing cells accumulate lipid X to ~10% of their total lipids. A selection of six absolutely conserved LpxI residues are mutated to alanines in non-tagged CcLpxI and expressed in *E. coli*; the *in vitro* activity of these cells' crude lysates is determined using the assay described in chapter 2. To follow the *in vivo* activity of the point mutants, whole cells are extracted and subjected to liquid chromatography and ESI mass spectrometric analysis. Lipid X accumulation is observed in cells expressing active LpxI, while cells expressing catalytically compromised mutants accumulate little or no lipid X. Cells over-expressing one mutant, CcLpxI

D225A, massively accumulate the CcLpxI substrate, UDP-2,3-diacylglucosamine. This mutant is modified by the addition of an N-terminal cleavable poly-histidine tag, and is purified to near-homogeneity. CcLpxI D225A is subjected to TLC and LC-MS analysis, confirming that it co-purifies with UDP-2,3-diacylglucosamine. Spectrophotometric measurements suggest that UDP-2,3-diacylglucosamine is present in purified CcLpxI D225A in a 0.85:1 stoichiometry.

In Chapter 4, we identify and optimize conditions under which purified wild-type (WT) CcLpxI and CcLpxI D225A crystallize. We then screen these crystals' X-ray diffraction, and develop protocols for their cryo-protection. As CcLpxI has no sequence homology to known enzymes, a method is needed by which to solve the phasing problem inherent to x-ray crystallography. Consequently, Se-methionine substituted WT CcLpxI and CcLpxI D225A are expressed, purified, crystallized, and cryo-protected. In collaboration with Robert Stroud's Laboratory at the University of California San Francisco, we perform Multi-wavelength Anomalous Scattering (M.A.D.) experiments at the Berkely Advanced Light Source, and use these data to solve the structures of both WT CcLpxI and CcLpxI D225A. Optimal resolution, obtained from native crystals of WT CcLpxI and CcLpxI D225A, is 2.6 A and 3.0 A, respectively. Model-building has revealed that LpxI consists of two domains, each novel, connected by a polypeptide linker. Although refinement is ongoing, the structure of WT CcLpxI has clear electron density consistent with a bound molecule of lipid X. CcLpxI D225A exhibits a drastically different conformation than WT CcLpxI, and contains electron density consistent with the presence of UDP-2,3-diacylglucosamine. These findings offer a rare comparison of the substrate and product complexes of an enzyme that acts upon saccharolipids, and pose interesting questions about the dynamics and energetics of substrate binding, catalysis, and product release.

In Chapter 5, we describe the purification of *E. coli* and *Hemophilus influeznea* LpxB to near-homogeneity on a 10 mg scale using cleavable $(His)^{10}$-tagged constructs. Having developed an optimized autoradiographic assay, we determine that *E. coli* LpxB activity is dependent upon the bulk surface concentration of its substrates in a mixed micellar assay system, suggesting that

catalysis occurs at the lipid interface. *E. coli* LpxB sediments with membranes, but this interaction is partially abolished by high-salt conditions, suggesting that a significant component of LpxB's membrane association is ionic in nature. Therefore, *E. coli* LpxB (M_r ~ 43 kDa) is a peripheral membrane protein, and it co-purified with phospholipids. We estimate, by autoradiography and mass-spectrometry, molar ratios of phospholipids to purified enzyme of 2:1 and 3:1, respectively. Moreover, transmission electron microscopy reveals the accumulation of intra-cellular membranes when LpxB is massively over-expressed. Alanine-scanning mutagenesis of selected conserved LpxB residues identified two, D89A and R201A, for which no residual catalytic activity is detected. Our data support the hypothesis that LpxB performs catalysis at the cytoplasmic surface of the inner membrane, and provide a rational starting-point for structural studies.

2. Discovery and characterization of a novel UDP-2,3-diacylglucosamine hydrolase in Gram-negative bacteria

2.1 Introduction

Most Gram-negative species possess at least one copy of each lipid A biosynthetic gene. An exception exists in the case of UDP-2,3-diacylglucosamine hydolase, the fourth constitutive enzyme in the pathway, and an assential gene in all Gram-negative species (*6*). Several organisms known to produce lipid A, including members of the genera *Brucella* and *Rickettsia*, have no known orthologue of LpxH, a divalent-cation-dependent peripheral-membrane enzyme which catalyzes the attack of water upon the α-phosphorous of UDP-2,3-diacylglucosamine. Here, we describe the discovery of the transformational analogue of *lpxH*, designated *lpxI*, and show that its orthologue in *Caulobacter crescentus* (*C. crescentus*) can cover an *lpxH* knockout in *E. coli*. We then demonstrate, by thin-layer chromatography (TLC), that lysates of *E. coli* over-expressing *C. crescentus* LpxI have UDP-2,3-diacylglucosamine hydolase activity *in vitro*. A method is presented for the purification of *C. crescentus* LpxI (CcLpxI) to ~90% homogeneity. With this partially-purified enzyme, we employ an optimized autoradiographic assay for UDP-2,3-diacylglucosamine hydolase activity in order to determine pH, metal, and detergent dependencies. Finally, we use mass-spectrometry to analyze the products of an *in vitro* CcLpxI reaction that is carried out in the presence $H_2{}^{18}O$. Our results reveal that CcLpxI catalyzes the attack of a water on the β-phosphate of UDP-2,3-diacylglucosamine, suggesting that it acts by a different mechanism than LpxH. Taken together, our findings suggest that we have discovered a transformational analogue (*164*) of LpxH.

2.2 Materials and methods

2.2.1 Cloning and molecular biology

Amplification of DNA segments, from either genomic or plasmid DNA, was accomplished using KOD Hot Start DNA polymerase, 8 mM dNTP stocks (2 mM each of dATP, dTTP, dGTP, and dCTP), and KOD Hot Start reaction buffer, all obtained from EMD Chemicals (Gibbstown, New Jersey, CA). Polymerase chain reactions (PCR) conditions were those recommended by Strategene, except for the inclusion of 1% (v/v) dimethyl sulfoxide and 1 M betaine in the reaction mixtures. The plasmids described in this study (see Table 2.1) were stored in and amplified from *E. coli* strain XL1-Blue (Stratagene, La Jolla, CA). Qiagen Mini-Prep kits and QIAquick Spin kits (Qiagen, Valencia, CA) were used, respectively, to purify plasmids and DNA fragments by protocols described by the manufacturer. Restriction endonucleases, T4 DNA ligase, and calf intestinal alkaline phosphatase were obtained from New England Biolabs (Ipswich, MA). Unless otherwise stated, the following concentrations of antibiotics are used when appropriate: ampicillin (Amp), 100 μg/ml; kanamycin (Kan), 50 μg/ml; chloramphenicol (Cam), 20 μg/ml; tetracycline (Tet), 15 μg/ml.

2.2.2 Construction of plasmids

DNA oligomers (Integrated DNA Technologies, Coralville, IA) were used to amplify *E. coli lpxH*, *C. crescentus* LpxI, and *A. aeolicus LpxI*, from genomic DNA obtained from ATTC (Rockville, MD). Primers (see Table 2.2) were designed to confer a 5′ *Nde*I and 3′ *BamH*I restriction sites upon the ends each of the amplified oligonucleotides. A Mastercycler Gradient thermocycler (Eppendorf, Hamburg, Germany) was used to amplify linear DNA. These PCR products were digested using *Nde*I and *BamH*I, and subsequently ligated into a similarly digested recipient vector, pET21b (Novagen). These ligation reactions were then transformed into the XL1-Blue strain (Stratagene, La Jolla, CA) chemical-competent *E. coli*, according to the

manufacturer's recommended procedure. Plasmids were isolated from transformants, and their sequences confirmed by the Duke Cancer Center DNA Sequencing Facility. The resulting constructs were designated pEcH21b, pCcH21b, and pAaH21b (see Table 2.2). The restriction endonucelases *XbaI* and *SalI* were used digest these plasmids, liberating linear *E. coli lpxH*, *C. crescentus* LpxI, or *A. aeolicus LpxI*, each flanked by 5′ *Xba* and 3′ *Sal*I restriction sites, and containing a pET21b-encoded ribosome binding site 7-base-pairs upstream from the start codon. These segments were then ligated, as above, into appropriately digested pBAD30 (*178*) or pBAD33 plasmids. The resulting plasmids are described in (see Table 2.2).

2.2.3 Construction of *E. coli lpxH* deletion strains

A knockout of *E. coli* LpxH was made by in-frame kanamycin (Kan) substitution. The primers KanFlank_FW and KanFlank_RV (see Table 2.2) were used to amplify a *Kan* cassette from the plasmid pET28b (Novagen). These primers were designed such that they generated 40 base-pair overhangs complementary to the regions of the *E. coli* chromosome immediately flanking *lpxH*. KanFlank_FW also added a ribosome binding site 7 base-pairs 5′ to the *Kan* cassette's start codon. The resulting linear oligonucleotide was electroporated into temperature-shifted *E. coli* strain DY330 (*179*), harboring pBAD30, pBAD30Ec, or pBAD30Cc (strains DY330VC, DY330VC, and DY330VC, respectively, see Table 2.1), as previously described (*180*). The strains were plated on LB-agar supplemented with Kan and Amp, and grown for 18 hours at 30°C. Transformants were re-purified, and colony PCR was performed using primers Kan_FW and Kan_RV (see Table 2.1) to amplify the *lpxH* locus and its 100-base-pair flanking regions. The resulting oligonucleotides were sequenced to confirm their identities. DY330 strains having successful *lpxH::Kan* replacements, covered by pBAD30Ec or pBAD30Cc, were designated DY330ΔHEc and DY330ΔHEc, respectively.

A P1*vir* lysate was prepared (*181*) from DY330ΔHEc, and used to infect *E. coli* W3110A cells harboring plasmids pBAD33, pBAD33Ec, or pBAD33Cc (strains W3110AVC, W3110AEc,

and W3110Acc, respectively, (see Table 2.1). Following infection and outgrowth as previously described (*181*), cells were spread on LB-agar plated supplemented with Cam, Kan, and 5 mM sodium citrate, and allowed to grow for 20 hours at hours at 30°C. Colonies were selected and re-purified twice to remove traces of contaminating phage. Colony PCR was performed to amplify the chromosomal region ± 100 base-pairs from the *lpxH* locus, and the resulting oligonucleotides were confimed by sequencing. The strains thereby created from the transduction of *lpxH::Kan* into W3110AVC, W3110AEc were designated W3110AΔHEc and W3110AΔHCc.

Table 2.1. Strains and plasmids used in this study

Strain	Description	Source or reference
C41(DE3)	F^- *ompT hsd*S_B(r_B^- m_B^-) *gal dcm* (DE3) D(srl-recA)306::Tn*10*	(*182*)
W3110A	F^- *aroA::Tn10 msbA*$^+$, Tet^R	(*183*)
XL1-Blue	*recA1 endA1 gyrA96 thi-1 hsdR17 supE44 relA1 lac [F′proAB lacIqZDM15 Tn10 (*Tet^R*)]*	Strategene
MN7	K-12-derived *pgsA444 lpxB1*; accumulates lipid X	(*111*)
DY330	W3110 Δ*lacU169 gal490* λcI857 Δ(*cro-bioA*)	(*179*)
Ec21XB	XL1-Blue harboring pEcH21b, Amp^R	This work
Cc21XB	XL1-Blue harboring pCcI21b, Amp^R	This work
Aa21XB	XL1-Blue harboring pAaI21b, Amp^R	This work
EcH33XB	XL1-Blue harboring pBAD33Ec, Cam^R	This work
CcI33XB	XL1-Blue harboring pBAD33Cc, Cam^R	This work
AaI33XB	XL1-Blue harboring pBAD33Aa, Cam^R	This work
EcH30XB	XL1-Blue harboring pBAD30Ec, Amp^R	This work
CcI30XB	XL1-Blue harboring pBAD30Cc, Amp^R	This work
DY330VC	DY330 harboring pBAD30, Amp^R	This work
DY330Ec	DY330 harboring pBAD30Ec, Amp^R	This work
DY330Cc	DY330 harboring pBAD30Cc, Amp^R	This work
DY330ΔHEc	DY330 *lpxH::Kan* harboring pBAD30Ec, Kan^R, Amp^R	This work
DY330ΔHCc	DY330 *lpxH::Kan* harboring pBAD30Cc, Kan^R, Amp^R	This work
W3110AVC	W3110A harboring pBAD33, Cam^R	This work
W3110AEc	W3110A harboring pBAD33Ec, Cam^R	This work
W3110ACc	W3110A harboring pBAD33Cc, Cam^R	This work
W3110AAa	W3110A harboring pBAD33Aa, Cam^R	This work
W3110AΔHEc	W3110A *lpxH::Kan* harboring pBAD33Ec, Cam^R, Amp^R	This work
W3110AΔHCc	W3110A *lpxH::Kan* harboring pBAD33Cc, Cam^R, Amp^R	This work
VC_21b	C41(DE3) harboring pET21b, Amp^R	This work
EcH_21b	C41(DE3) harboring pEcH21b, Amp^R	This work
CcI_21b	C41(DE3) harboring pCcI21b, Amp^R	This work
AaI_21b	C41(DE3) harboring pAaI21b, Amp^R	This work
Plasmid	Description	Source or reference
pET21b	high-copy expression vector containing a T7 promoter, Amp^R	Novagen
pET28b	high-copy expression vector containing a T7 promoter, Kan^R	Novagen
pBAD30	arabinose inducible vector, Amp^R	(*178*)
pBAD33	arabinose inducible vector, Cam^R	(*178*)
pEcH21b	pET21b containing *E. coli lpxH*, Amp^R	This work
pCcI21b	pET21b containing *C. crescentus lpxI*, Amp^R	This work
pAaI21b	pET21b containing *A. aeolicus lpxI*, Amp^R	This work
pBAD33Ec	pBAD33 containing *E. coli lpxH*, Cam^R	This work
pBAD33Cc	pBAD33 containing *C. crescentus lpxI*, Cam^R	This work
pBAD33Aa	pBAD33 containing *A. aeolicus lpxI*, Cam^R	This work
pBAD30Ec	pBAD33 containing *E. coli lpxH*, Amp^R	This work
pBAD30Cc	pBAD33 containing *C. crescentus lpxI*, Amp^R	This work

Table 2.2. Primers used in this study

Name	Purpose	Primer sequence (5' to 3' orientation)
EcH_FW	To amplify *E. coli* LpxH, confer a 5′ *ndeI* restriction site	GCTGATTCATTTTCCGTTTTCAGGA
EcH_RV	To amplify *E. coli* LpxH, confer a 3′ *bamH1* restriction site	GAGCTCGAATTCGGATCCTGAAAAC
CcI_FW	To amplify *C. crescentus* LpxI, confer a 5′ *ndeI* restriction site	CTGAATTCATATGCGTAAGCTTGG
CcI_RV	To amplify *C. crescentus* LpxI, confer a 3′ *bamH1* restriction site	GTCAATTGGATCCTCACGGCCGCT
AAI_FW	To amplify *A. aeolicus* LpxI, confer a 5′ *ndeI* restriction site	GCGCGAATTCATATGAAGTCCTTTA
AAI_RV	To amplify *A. aeolicus* LpxI, confer a 3′ *bamH1* restriction site	CGCGCAATTGGATCCCTACTCCTTA
KanFlank_FW	To amplify a Kan^R cassette from pET28b, while adding a ribosome binding site 7 bases 5′ to the start codon. 5′ to the engineered ribosome binding site, this primer is complementary to the 41 base pairs immediately flanking *lpxH* on the *E. coli* chromosome.	GAAGACGTTATCATTGAAAGCGTGACCGTTAGCGAGTAATCAGGAGATATACAA TGAGCCATATTCAACGGGAAAC
KanFlank_RV	To amplify a Kan^R cassette from pET28b, while adding a 3', 49 base pair overhang complementary to the region of the *E. coli* chromosome immediately 3' to the stop codon of *lpxH*.	GCAAGGAAAACGGTTGCGTGGCTGTGAAATCAGCAAAGTTGCGGGTTTTTTAGA AAAACTCATCGAGCATC
Kan_FW	Complementary to a region of the *E. coli* chromosome 100 base pairs 5' to *lpxH*	GTGTTTGCTGAAGTGGTTGACGGCAT
Kan_RV	Complementary to a region of the *E. coli* chromosome 100 base pairs 3' to *lpxH*	CCCAGTCGCTTTTGGACCCCATCACG
pBAD_FW	Complementary to the pBAD promoter	ATGCCATAGCATTTTTATCC
pBAD_RV	Complementary to the pBAD terminator	GATTTAATCTGTATCAGG

2.2.4 UDP-2,3,-diacylglucosamine hydrolase expression and *in vitro* TLC assay

The plasmids pET21b and pCcI21b were transformed into *E. coli* strain C41(DE3) by electoportation and grown for 18 hours at 30°C on LB-agar plates supplemented with Amp. Single colonies of the resulting strains VC21b and CcI21b (see Table 2.1) were used to inoculate 5-ml overnight cultures. These, in turn, were used to inoculate 50 ml cultures of appropriately supplemented LB media, at an initial OD_{600} of ~0.02. Strains VC21b and CcI21b were then grown at 30°C, with aeration at 220 rpm, until the OD_{600} reached ~0.5 (about 5 hours). Expression was induced by adding IPTG to a final concentration of 250 μM. The cells were grown for an additional 5 hours, until the final OD_{600} of the induced cells was ~3. Cells were collected by centrifugation at 3000 x *g*, washed with PBS, and re-suspended in 3 ml of ice-cold PBS. The washed, re-

suspended cells were passed twice through a French Pressure cell at 18,000 psi, and cell debri removed by entrifugation at 10,000 x *g* for 30 minutes. Lysates were analyzed by SDS-PAGE, and were assayed for UDP-2,3,-diacylglucosamine hydrolase activity.

For initial analysis, the addition of 5 μl of diluted lysate from strains VC21b and Ccl21b was used to start the UDP-2,-3-diacylglucosamine hydrolase reactions in a total volume of 25 μl. Non-radiolabeled UDP-2,3,-diacylglucosamine was prepared as previously described (*33*). Briefly, the reactions consisted of 1 mM UDP-2,-3-diacylglucosamine, 20 mM HEPES pH 8.0, and 2 mM $MnCl_2$, and equilibrated at 30°C for 15 minutes in 0.5 ml polypropylene eppendorf tubes. Reactions were started by the addition of crude lysates from VC21b and Ccl21b, diluted as appropriate with PBS. At various time-points, reactions were quenched by spotting 5 μl portions onto 10 x 10 cm High Perfomance silica TLC plates (Merck, Darmstadt, Germay). These were developed and dried as described (*33*). Reaction products were visualized by spraying the dried TLC plate with H_2SO_4 in 10% EtOH, and subsequent charring on a hot plate at 250°C.

2.2.5 Preparation of [β-^{32}P]-UDP-2,3,-diacylglucosamine

[^{32}P]-labeled lipid X was prepared as previously described (*27*). Following purification, the lipid X was re-dissolved in 2 ml of 3:1 $CHCl_3$/MeOH, transferred to a clean screw-capped glass tube, and thoroughly dried under a nitrogen stream. Next, 10 mg of UMP-morpholidate, 50 μl of 0.2 M 1-*H*-tetrazole in acetonitrile, and 1 ml dry pyridine were quickly added. The tube was immediately sealed with a Teflon-coated screw cap, and further secured by several alternating layers of Teflon tape and Parafilm™. The test tube was then subjected to sonication for 5 minutes in a bath sonicator (Avanti Polar Lipids, Alabaster, AL). The reaction mixture was incubated in a table-top water-bath shaker and incubated for at least 20 hours at 37°C, with rotary shaking at 100 rpm. The reaction mixture was dried under nitrogen until no traces of pyridine remained (~2 hours). The residue at the bottom of the tube was redissolved in 100-300 μl of 20 mM HEPES pH 8.0, containing 0.02% (w/v) Triton X-100, and bath-sonicated for 2 minutes. This material was

then aliquoted and stored at -80°C until use. With this method, we could consistently convert greater than 95% of the [^{32}P]-lipid X to [^{32}P]-UDP-2,3,-diacylglucosamine.

2.2.6 Expression and purification of *C. crescentus* LpxI

A colony of *E. coli* strain Ccl21b was used to inoculate a 25 ml overnight in LB medium supplemented with Amp. Following growth for 18 hours at 30°C, this culture was used to inoculate 1L of LB/Amp to an initial OD_{600} of ~0.005. Growth proceeded at 30°C, 220 rpm aeration, until the cells reached an OD_{600} of ~0.5. IPTG was then added to the culture to a final concentration of 0.25 mM, and growth was allowed to proceed for an additional 5 hours. Cells, which typically grew to an OD_{600} of ~3.5, were harvested by centrifugation at 3000 x *g* for 30 minutes, and subsequently washed with buffer containing 20 mM HEPES pH 8.0, 50 mM NaCl, and stored at -80C. In a typical purification, a cell pellet from 500 ml of harvested culture (~4 g wet cell pellet) was re-suspended in ~300 ml lysis buffer (20 mM HEPES pH 8.0, 50 mM NaCl) and lysed by three passages through an ice-cold Cell-Cracker (Microfluidics International Corp., Newton, MA) pressure diruption chamber. Cell debris and membranes were removed by ultracentrifugation at 150,000 x *g* for 1 hour. A Rabbit-Plus peristaltic pump (Rainin Instrument, LLC, Oakland, CA) was used to load membrane-free lysate, at a linear flow rate of ~2 ml/min, onto a 5 ml High-Trap Q Sepharose Fast-Flow anion exchange cartridge (GE Healthcare) which had been previously equilibrated in lysis buffer. The column was then washed with 20 volumes (100 ml) of lysis buffer at 3 ml/min. The column was then attached to an AKTA 600 FPLC system, and eluted with 30-column-volume (150 ml) continuous gradient from 100% v/v Buffer A (20 mM HEPES pH 8.0, 50 mM NaCl) to 100% v/v Buffer B (20 mM HEPES pH 8.0, 200 mM NaCl). The protein, which was collected in 5-ml fractions, began to elute at ~100 mM NaCl. SDS-PAGE was used to determine which fractions to pool; typically 6 fractions (30 ml) were pooled. This partially-purified LpxI was then concentrated to ~10 ml using two 15 ml Amicon Ultra 10,000 molecular weight cutoff centrifuge concentrators which had been washed in Buffer B. An

AKTA 600 FPLC system was used to load the concentrated, pooled Q Sepharose fractions onto a preparatory size exclusion column (Superdex 200 XK26/70; GE Healthcare, Waukesha, WI), equilibrated with Buffer B. The column (included volume ~300 ml) was run at 1.5 ml/min, with the peak of LpxI eluting at ~210 ml. Fractions of 5 ml were collected, and their purity determined by SDS-PAGE. Typically, 4 fractions (20 ml) were pooled and subsequently concentrated to ~25 mg/ml in the manner described above. Protein aliquots were stored at -80°C, and subjected to fast freeze-thaw cycles upon storage and retrieval. CcLpxI was never thawed slowly on ice.

2.2.7 Radiographic *in vitro* assay of CcLpxI

Unless otherwise noted, 25 µL reactions, containing 20 mM HEPES, pH 8.0, 0.5% (w/v) fatty acid free bovine serum albumin (BSA), 0.05% (w/v) Triton X-100, 100 µM UDP-2,3-diacylglucosamine, 2 mM $MgCl_2$, 1000 cpm/µl [β-^{32}P]-UDP-2,3,-diacylglucosamine, and enzyme, were prepared in 0.5 ml polypropylene tube. Prior to the addtion of enzymes, these components were equilibrated at 30 °C for 15 minutes. Reactions were usually initiated by the addition of 5 µl of enzyme. Unless otherwise noted, enzyme samples were diluted in a buffer identical to the assay mixture, but lacking UDP-2,3-diacylglucosamine. At various time points, 3 µl portions were removed and spotted onto 20 × 20 cm silica gel TLC plates (EMD Chemicals, Inc., Darmstadt, Germany). These were developed, dried, scanned, and quantitated as previously described (*33*).

2.2.8 Kinetic parameters, pH optimum, and detergent dependence of CcLpxI

To determine the effect of pH upon its apparent specific activity, partially purified LpxI was as sayed as described above, but with a triple-buffer system consisting of 100 mM sodium acetate, 50 mM bis(2-hydroxyethyl)iminotris(hydroxymethyl)hexane, and 50 mM Tris, replacing HEPES pH 8.0 (*184*). CcLpxI activity was measured from pH 4. 0-9.0. A two-limb pK_a curve was fit to the data using KaleidaGraph. Typically, 5-50 nM enzyme were used.

To determine the K_M and V_{MAX} of CcLpxI with respect to UDP-2,3-diacylglucosamine, the partially purified enzyme was assayed as above, but with the concentration of UDP-2,3-diacylglucosamine varied from 5 to 1000 μM. KaleidaGraph was used to fit velocities to the Michaelis–Menten equation (*185*). The concentration of CcLpxI in the assay was varied between 2 and 200 nM in order to follow linear conversion at different UDP-2,3-diacylglucosamine concentrations.

To probe whether theapparent CcLpxI activity is affected by detergent, the typical assay conditions were employed, except that the concentration of Triton X-100 was varied from 0 to 1.0% w/v. In order to measure LpxI activity in the complete absence of detergent, $^{32}PO_4$ UDP-2,3,-diacylglucosamine was prepared in buffer lacking Triton X-100. An enzyme concentration of 10 nM was used in these assays.

2.2.9 Metal dependence of CcLpxI

To determine whether metals stimulate CcLpxI activity *in vitro*, the standard assay condition was employed, except that the typical 2 mM $MgCl_2$ was replaced by either no additive, or by 2.0, 0.2, and 0.02 mM of chloride salts of each of the following: Mg^{+2}, Ca^{+2}, Co^{+2}, Ni^{+2}, Cu^{+2}, Zn^{+2}, Mn^{+2}, and EDTA. The concentration of CcLpxI in the assay was varied between 2 and 200 nM in order to follow linear conversion in the presence of the different additives. A separate assay, in which $MgCl_2$ was titrated from 0 to 20 mM, was performed in the presence of 20 nM CcLpxI.

2.2.10 Labeling of the CcLpxI reaction with $H_2{}^{18}O$

A reaction similar to that described in section 2.2.3, except with 2 mM $MgCl_2$ substituted for $MnCl_2$, was performed in the presence of either 100% mol/mol $H_2{}^{16}O$ or 45% mol/mol $H_2{}^{18}O$ (Caimbridge Isotopes). A high concentration of partially purified CcLpxI (20 μM) was used to ensure that the reactions proceeded to completion, as judged by TLC and charring with H_2SO_4.

The reactions were allowed to proceed at 30°C for one hour, and were quenched by conversion to 5.2 ml two-phase acidic Bligh-Dyer system (*128*). The organic phases were washed once with pre-equilibrated Bligh-Dyer upper phase, and subsequently dried under a nitrogen stream in glass screw-capped tube. The dried organic phases, containing lipid X, were re-dissolved in 200 μl of 2:1 $CHCl_3$/MeOH, with aliquots of this concentrated material diluted 10 and 100-fold in 2:1 $CHCl_3$/MeOH. The latter dilution was directly injected onto a QSTAR XL time-of-flight mass spectrometer (Applied Biosystems, Foster City, CA), operating in the ESI negative ion mode. A spectrum was collected in the *m/z* range of 60–2000 amu, with intensity counts accumulated over 1 min. Upper phases from the acidic Bligh-Dyer system, containing UMP, were lyophilized. The dried upper phase was then re-dissolved in 500 μl of acidic single phase Bligh-Dyer solvent, and analyzed by mass spectrometry as above.

2.3 Results

2.3.1 Identification of a candidate UDP-2,3-diacylglucosamine hydrolase in species lacking *lpxH*

The Clusters of Orthologous Genes (*186*) database was used to compare the genomes of Gram-negative bacteria lacking *lpxH* orthologues. Hypothesizing that the gene(s) encoding novel UDP-2,3,-diacylglucosamine hydrolase analogue(s) might be located nearby other Lipid A biosynthetic genes, and noting that in many species, *lpxD, fabZ, lpxA*, and *lpxB* cluster on an operon, we searched for species which both lacked a *lpxH* orthologue and which possessed open reading frames of unknown function near or in the *lpxD-fabZ-lpxA-lpxB* operon. By this method, we identified some species, including *C. crescentus* and *M. loti*, in which a ~1000 base-pair open reading frame is inserted between *lpxA* and *lpxB* in those organisms' chromosomes (see Figure 2.1). This gene of unknown function, annotated as DUF1009 (*186*), is present in many of the organisms that produce lipid A but lack genes obviously encoding the known UDP-2,3-

diacyglucosamine hydrolase, *lpxH*. Many species missing *lpxH*, and lacking the *lpxD-fabZ-lpxA-lpxB* operon, such as *A. aeolicus*, also contain DUF1009 orthologues.

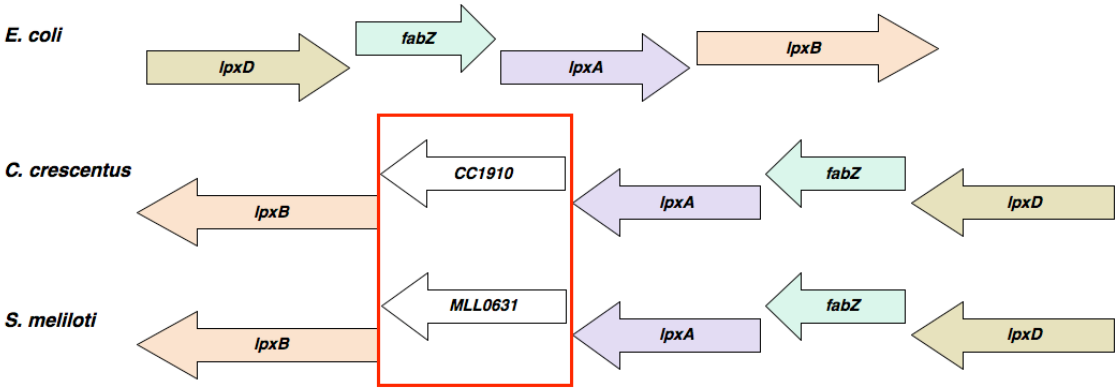

Figure 2.1. Comparison of the *lpxD-fabZ-lpxA-lpxB* operons of *E. coli*, *C. crescentus*, and *M. loti*. Arrows represent open reading frames and their direction of transcription. The DUF1009 orthologues, CC1910 and MLL0631, are highlighted with a red box. Gene lengths are not drawn exactly to scale.

2.3.2 C. *crescentus* gene CC1910 encodes an enzyme having specific UDP-2,3-diacylglucosamine hydrolase activity *in vitro*

The *C. crecentus* DUF1009 orthologue, CC1910, was amplified from genomic DNA, cloned into the high copy pET21b plasmid, and expressed in *E. coli* C41(DE3), yielding strain Ccl21b. This construct was grown in parallel with its empty-vector control (strain VC21b), and induced to over-express the CC1910 gene product. Cells from each strain were harvested and lysed. Over-expression of the expected 29 kDa CC1910 gene product was confirmed by SDS-PAGE (see Figure 2.2, panel A). Equal concentrations of lysate from VC21b and Ccl21b were used to catalyze a TLC *in vitro* UDP-2,3-diacyglucosamine hydrolysis was followed by TLC analysis similar to that described for *E. coli* LpxH (*186*)). Development and charring of the silica plate revealed that Ccl21b lysate contained at least 1000-fold higher UDP-2,3-diacyglucosamine hydrolase activity than its matched vector control (see Figure 2.2, panel B), suggesting that CC1910, hereafter referred to as CcLpxI, is an analogue of LpxH. Upon incubation of the lysates

with CDP-diacylglycerol, under similar assay conditions, no difference in CMP hydrolysis was observed between extracts of VC21b and Ccl21b (data not shown).

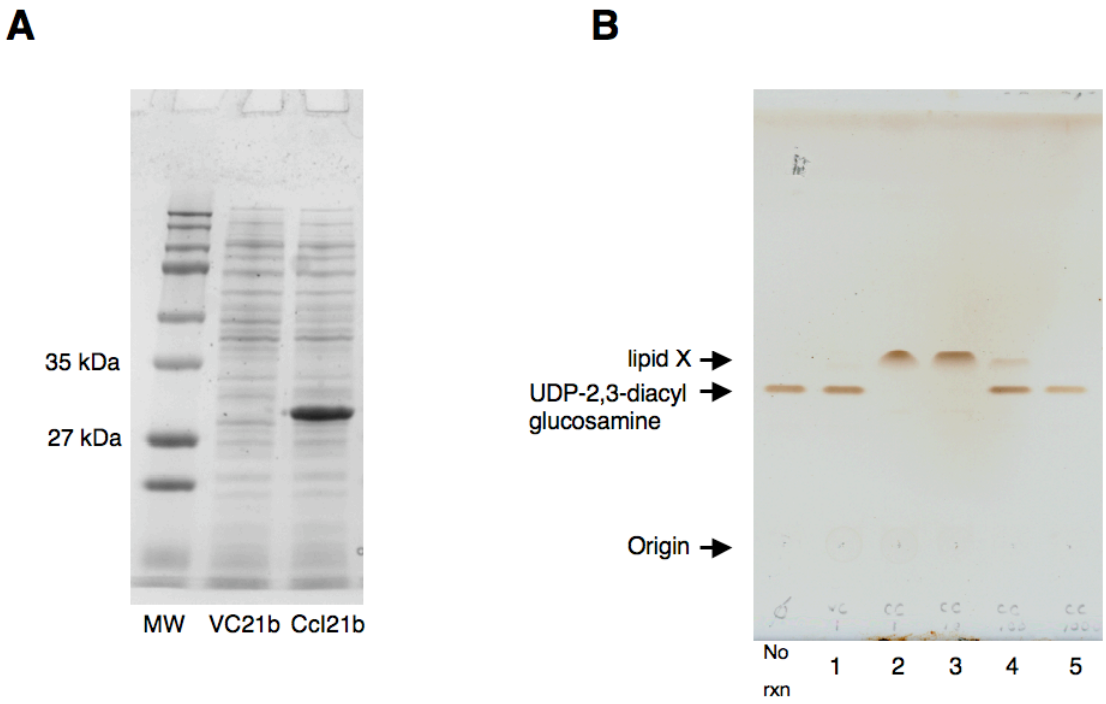

Figure 2.2. Expression and in vitro assay of the CC1910 gene product. Panel A shows a 12% polyacrylamide gel, run in SDS. MW denotes the molecular weight marker, VC21b and Ccl21b denote E. coli C41(DE3) expressing pET21b empty vector and pET21b harboring CC1910, respectively. Each lane contains 20 μg of protein. Panel B shows a silica TLC separation and visualiztion of an in vitro UDP-2,3,-diacylglucosamine hydrolase assay. Lane 1 represents a reaction containing 0.6 mg/ml lysate from strain VC21b. The reactions visualized in lanes 2-5 contain, from left to right, 0.6, 0.06, 0.006, and 0.0006 mg/ml of lysate from Ccl21b. The assay duration was 30 minutes.

2.3.3 *C. crescentus lpxI* can replace *lpxH* in *E. coli*

To determine whether *C. crescentus lpxI* has UDP-2,3-diacyglucosamine hydrolase activity *in vivo*, the essential *lpxH* gene was replaced in *E. coli* DY330 (harboring the λ-red recombinase system, (*179*)) with a *kan* cassette, and plasmids containing either *E. coli lpxH* or *C. crescentus lpxI* were used to complement the resulting *lpxH* deficiency. While an empty vector could not cover for the deletion of chromosomal *lpxH*, plasmids containing *E. coli lpxH* or *C.*

crescentus lpxI allowed this knockout (see Figure 2.3, panel A) to survive. The *lpxH::kan* deletion was subsequently transduced into "wild-type" *E. coli* W3110A harboring *E. coli lpxH* or *C. crescentus lpxI* in a plasmid. The replacement of *lpxH* with *kan* was confirmed by PCR amplification of the *lpxH* locus and its 100 base-pair flanking regions (see Figure 2.3, panel B), and the identities of these PCR products were confirmed by sequencing.

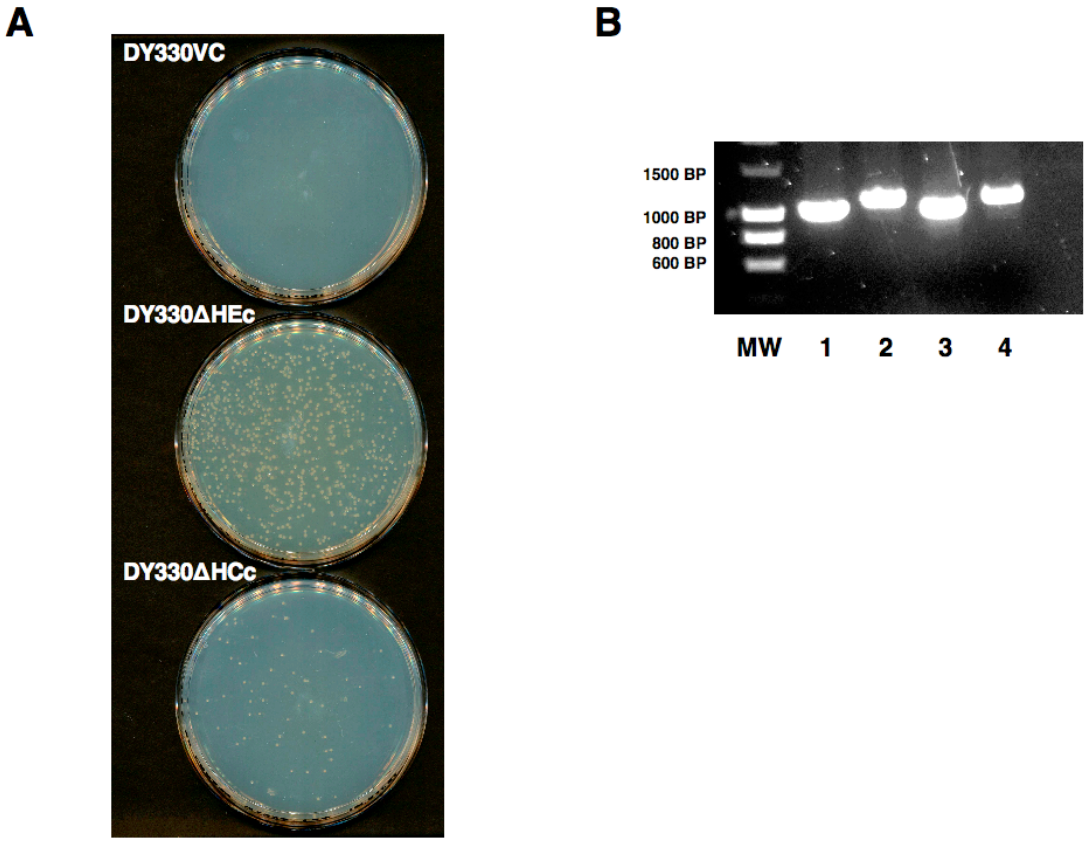

Figure 2.3. *C. crescentus lpxI* encodes a functional UDP-2,3-diacylglucosamine hydrolase *in vivo*. Panel A shows the results of replacing *lpxH* with kan in *E. coli* strain DY330. While the vector control cannot cover for the deletion of *lpxH* (DY330ΔHVC), DY330 harboring vectors containing *E. coli lpxH* (DY330ΔHEc) or *C. crescentus lpxI* (DY330ΔHEc) are viable. In panel B, PCR of the *E. coli lpxH* locus and its flanking 100 base-pairs confirms that *lpxH::kan* was successfully transduced from DY330ΔHEc into *E. coli* W3110A, harboring plasmids containing either *E. coli lpxH* or *C. crescentus lpxI.* Lanes 1 and 2 are PCR products of W3110AEc and W3110AΔHEc*, respectively, while* lanes 3 and 4 show the products amplified from W3110ACc and W3110AΔHCc. The band at ~950 base-pairs is *lpxH* and its flanking regions, while the band at ~1150 base-pairs is *kan* and its flanking regions on the genome.

2.3.4 Expression and purification of CcLpxI

E. coli strain Ccl21b directed the massive expression of a protein band and its putatively associated UDP-2,3-diacylglucosamine hydrolase activity. To characterize CcLpxI, it was purified to greater than 90% homogeneity using ion-exchange and size-exclusion chromatography (see Figure 2.4). The pellet from 500 ml of Ccl21b cells grown to OD_{600} ~3.5 yielded ~30 mg of CcLpxI. The specific activity of the protein increased during the purification, and the total activity yield was ~20% (see Table 2.3). CcLpxI elutes from a sizing column in a symmetric peak (see Figure 2.4, panel A), and its retention time is consistent with either a dimeric or monomeric solution state.

Table 2.3. Purification of CcLpxI from Ccl21b

Step	Protein mass (mg)	Protein volume (ml)	Units (mmol/min)	Specific activity (μmol/min/mg)	Yield (%)	Fold-purification
Membane-free lysate	168	280	4.1	25	100	
Q-sepharose column pooled fractions	34	30	0.9	26	22	1.1
S200 size exclusion column pooled fractions	27	20	0.8	30	20	1.2

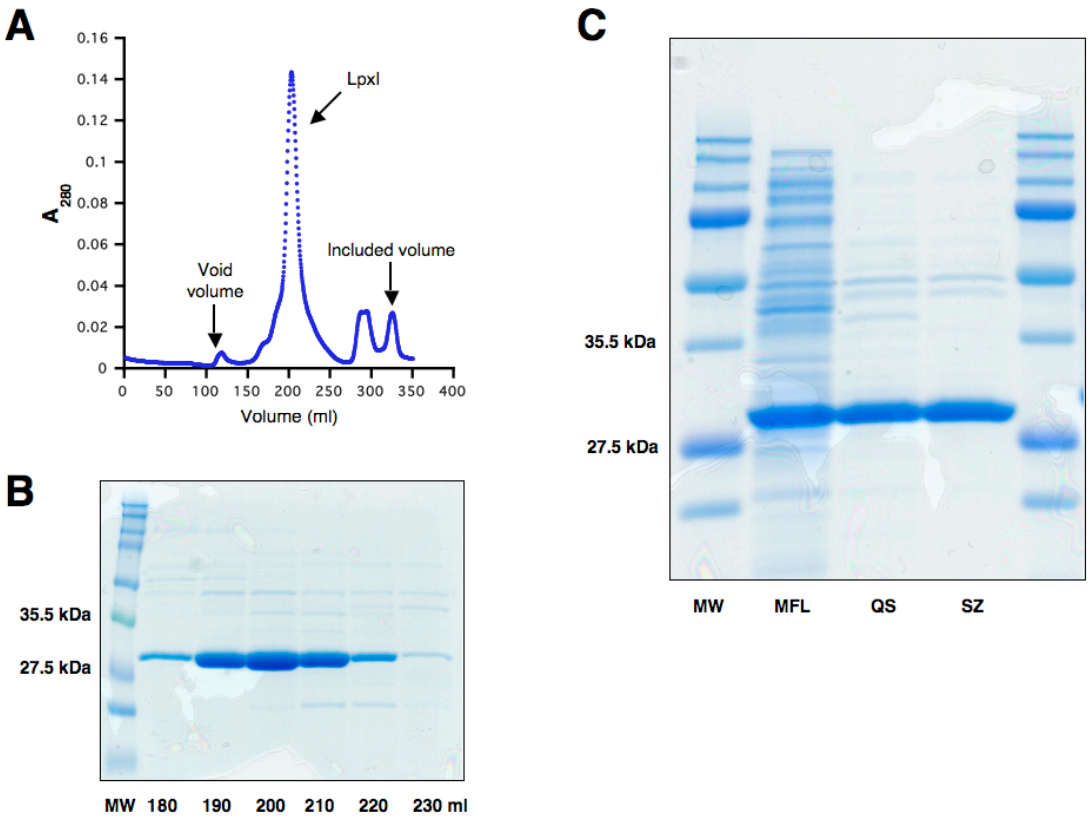

Figure 2.4. Purification of native Cc LpxI. Panel A shows the elution profile of CcLpxI, monitored at A_{280}, from a size exclusion column. Panel B is a 12% polyacrylamide gel run in SDS. Equal volumes of protein sample are loaded in each lane of the gel; lanes correspond to the elution volume of the trace shown in Panel A. Panel C shows an SDS-PAGE analysis protein from each step of the CcLpxI purification. MFL, QS, and SZ denote membrane-free lysate, pooled fractions eluted from a Q-Sepharose anion exchange column, and pooled fraction from a Superdex S200 sizing column, respectively. Approximately 20 μg of protein is loaded in each lane.

2.3.5 Radiographic assay of CcLpxI using [β-^{32}P]-UDP-2,3,-diacylglucosamine

Using [β-^{32}P]-UDP-2,3-diacylglucosamine, we optimized the TLC-based assay for CcLpxI. Using the partially purified protein described above, we demonstrated that CcLpxI activity is linear with time and with enzyme concentration (see Figure 2.5, panels A and B). Moreover, we demonstrate that CcLpxI is capable of quantitatively converting UDP-2,3-diacylglucosamine to lipid X (see Figure 2.5, panel C).

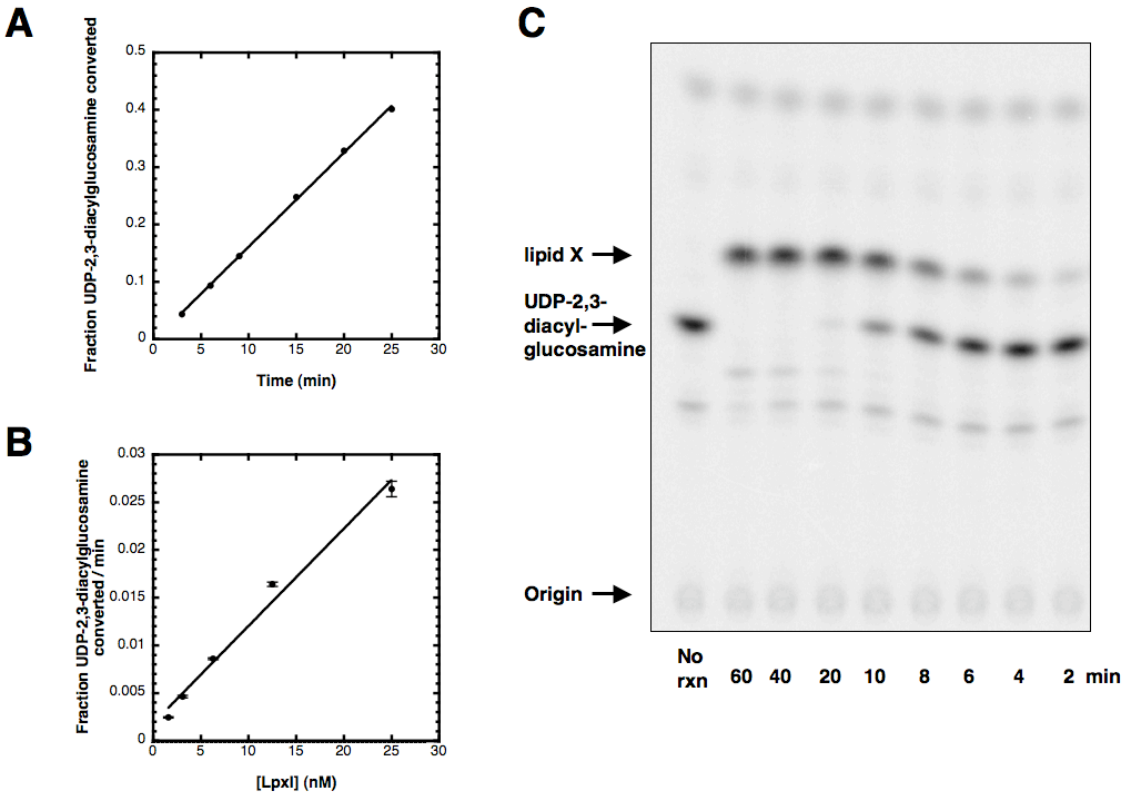

Figure 2.5. CcLpxI activity is linear with time and protein concentration. Panel A shows the fraction of UDP-2,3-diacylglucosamine converted to lipid X under the standard assay conditions described in section 2.2.7, in the presence of 12.5 nM partially purified CcLpxI. Panel B shows the fraction of UDP-2,3-diacylglucosamine converted to lipid X per minute, under the same assay conditions in panel A, as a function of enzyme concentration. Panel C shows an autoradiographic image of a silica TLC plate of a CcLpxI reaction run under identical condtitons, with an enzyme concentration of 40 nM.

2.3.6 Metal dependence of CcLpxI activity *in vitro*

To determine the metal dependence of CcLpxI, partially purified enzyme was assayed in the standard conditions, except that $MgCl^{+2}$ was replaced with 2.0, 0.2, and 0.02 mM of chloride salts of each of the following: Mg^{+2}, Ca^{+2}, Co^{+2}, Ni^{+2}, Cu^{+2}, Zn^{+2}, Mn^{+2}, and EDTA. The apparent specific activity increased 10-fold in the presence of Mg^{+2}, and 6-fold in the presence of Mn^{+2} or Co (see Figure 2.6 panel A), although reactions containing no added divalent cation or EDTA retained substantial activity. The presence of EDTA at either 2.0 or 0.2 mM, completely inhibited CcLpxI. This inhibition was reversible by diluting EDTA-treated enzyme into reactions containing 2 mM Mg^{+2} or Mn^{+2} (data not shown). Zn^{+2} and Cu^{+2} appeared to inhibit CcLpxI at concentrations of 0.2 and 2 mM. LpxI activity was measured under typical assay conditions, and the concentration of Mg^{+2} varied from 0 to 20 mM. CcLpxI activity reached a maximum at 0.2 mM Mg^{+2}, and remained constant up to 20 mM Mg^{+2} (see Figure 2.6, panel B). In order to determine whether divalent cations co-purify with CcLpxI, induction-coupled plasma mass spectrometry was performed in duplicate. In both experiments, no significant levels of metals were detected in the purified protein.

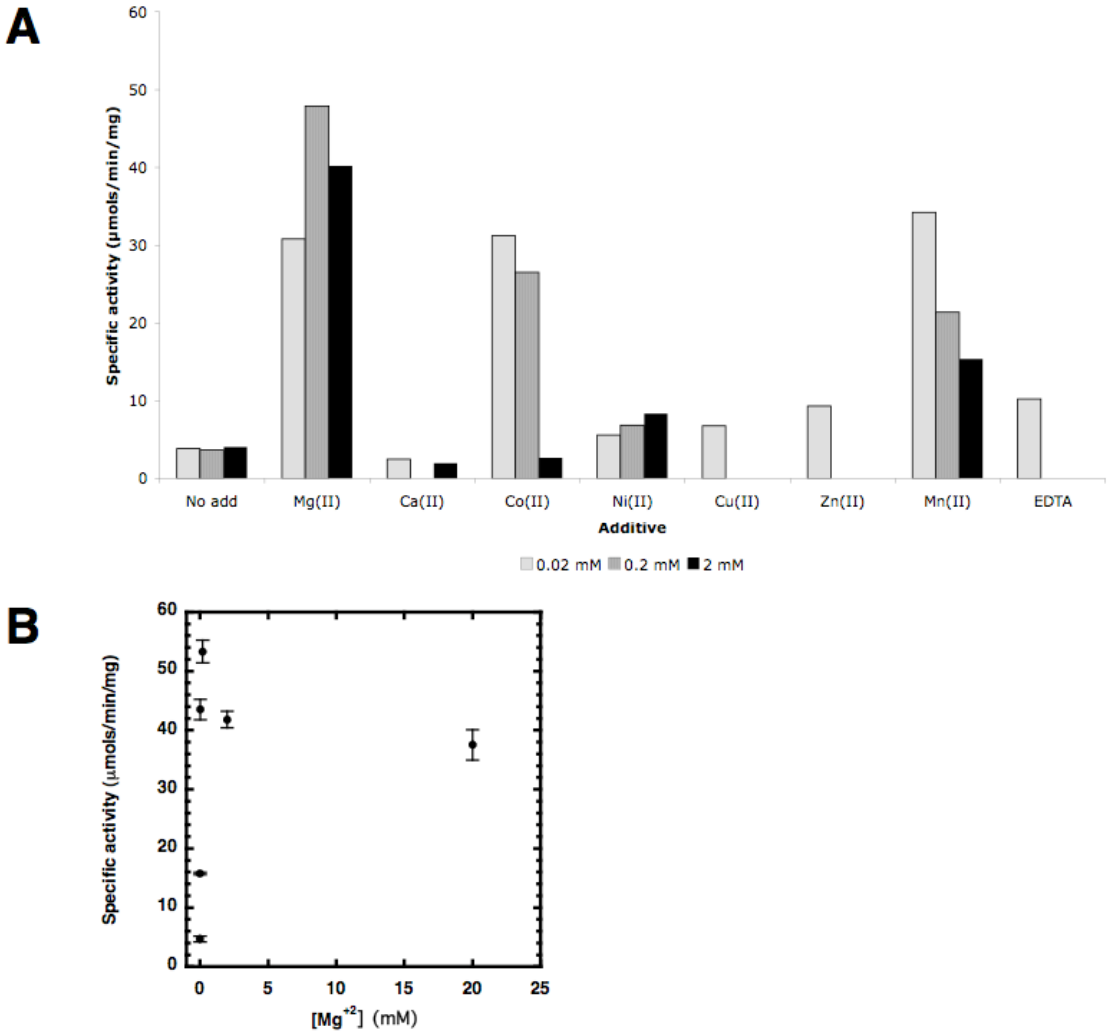

Figure 2.6. Metal dependence of CcLpxI. Panel A shows the specific activity of CcLpxI in the presence of various divalent cations and EDTA. Three sets of assays were performed, which accounts for the three no-additive (denoted No add) controls present at left. Assay conditions were those described in section 2.2.7, with enzyme concentration held at 10 nM in each assay. Figure B shows the standard CcLpxI assay in the presence of 0 to 20 mM $MgCl_2$. The enzyme was assayed at 10 nM.

2.3.8 Apparent kinetic parameters and detergent dependence of CcLpxI

The kinetic parameters of partially purified CcLpxI were determined as described in section 2.2.8. The apparent K_M with respect to UDP-2,3-diacylglucosamine was 105 ± 25 μM, while the apparent V_{max} was 69 ± 5 μmols/min/mg (see Figure 2.7, panel A). A pH rate profile was determined for partially purified CcLpxI, and a two-limb pKa curve was fit to the data using Kaleidograph. The pK_a was estimated to be 6.2 ± 1.2, while the fit pK_b was 9.8 ± 2.2 (see Figure 2.7, panel B). Detergent dependence of CcLpxI was determined by varying the concentration of Triton X-100 in the assay from 0 to 1% w/v. While stimulated ~3-fold in the presence of at least 0.05% w/v Triton X-100, the apparent activity did not decrease in high concentrations of Triton X-100 (see Figure 2.7, panel C).

2.3.9 CcLpxI catalyzes the attack of H_2O on the β-phosphate of UDP-2,3-diacylglucosamine.

In order to determine which phosphorous atom of UDP-2,3-diacylglucosamine is attacked in the hydrolysis reaction catalyzed by CcLpxI, partially purified enzyme was used to fully convert its substrate to product in the presence $H_2{}^{16}O$ or of 45% v/v $H_2{}^{18}O$. The lipid X and UMP products were analyzed in the negative mode by ESI mass spectrometry. For the $H_2{}^{18}O$ labeled reaction, ~45% of the lipid X contained ^{18}O, an observation consistent with water attacking the β-phosphate of UDP-2,3-diacyglucosamine (see Figure 2.8). No ^{18}O incorporation was observed in UMP isolated from the CcLpxI reaction (data not shown).

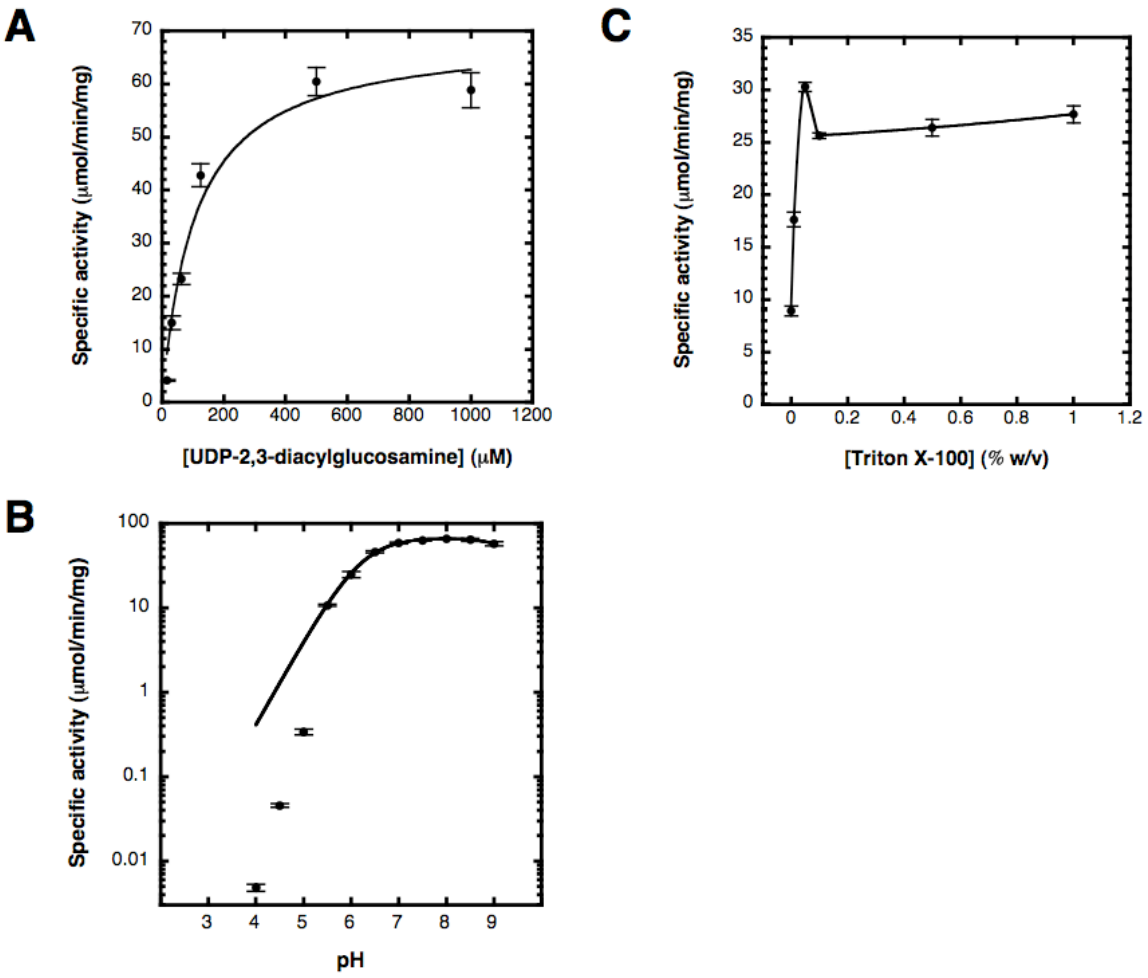

Figure 2.7. Apparent kinetic parameters and detergent dependence of CcLpxI. Panel A shows a Michaelis–Menten curve for CcLpxI with respect to UDP-2,3-diacylglucosamine. The apparent K_M, fit using Kaleidograph, was 105 ± 25 μM, while the apparent V_{max} was 69 ± 5 μmols/min/mg. Panel B shows CcLpxI activity as a function of pH. The pK_a was estimated to be 6.2 ± 1.2; the pK_b, 9.8 ± 2.2. Panel C shows the effect of Triton X-100 concentration upon the apparent specific activity of CcLpxI at [UDP-2,3-diacylglucosamine] = 100 μM.

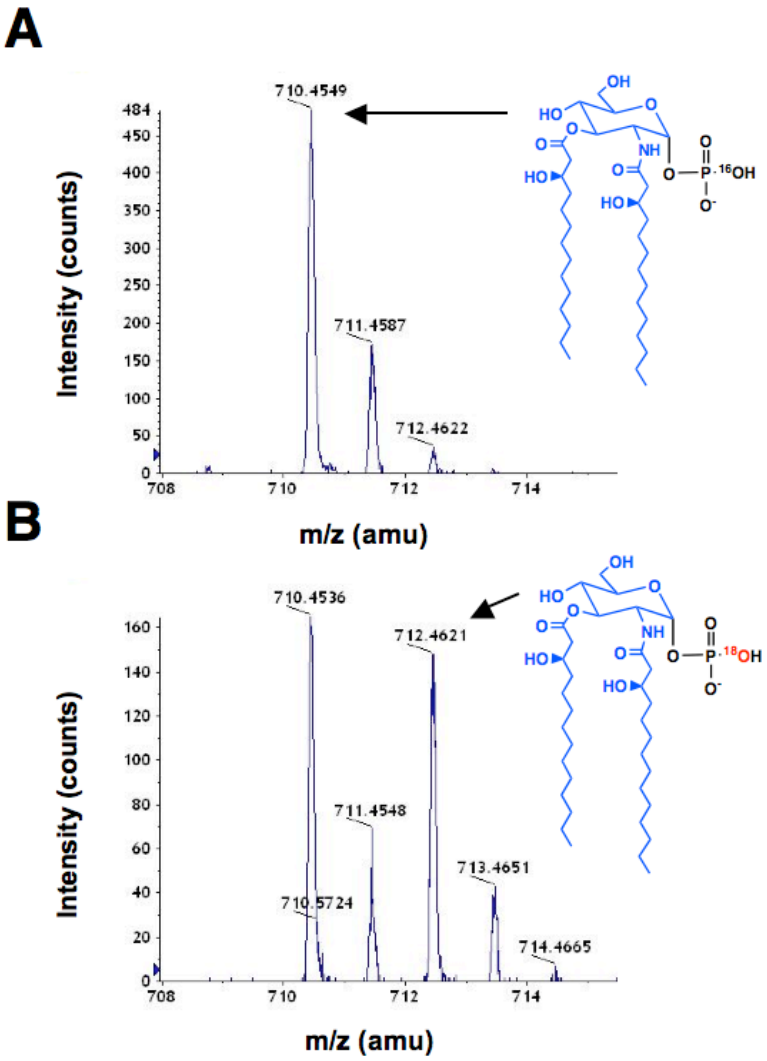

Figure 2.8. Mass spectra of lipid X isolated from CcLpxI-catalyzed UDP-2,3-diacylglucosamine hydrolysis in $H_2{}^{16}O$ or of 45% v/v $H_2{}^{18}O$. Panels A and B show the ESI mass spectra, collected in the negative mode, of lipid X produced by CcLpxI catalyzed hydrolysis of UDP-2,3-diacylglucosamine, in the absence (Panel A) and presence (Panel B) of $H_2{}^{18}O$.

2.4 Discussion

While most Gram-negative bacteria possess other orthologues of the same Lipid A biosynthetic genes in a single copy, this is not true for LpxH, the UDP-2,3-diacylglucosamine hydrolase present in *E. coli*. Here, we describe the identification of a novel UDP-2,3-diacylglucosamine hydrolase present in many species of Gram-negative bacteria, including members of the *Brucella*, *Rickettsia*, and *Leptospira* genera. The candidate for this gene, currently annotated as DUF1009 (*187*), was discovered by its genomic context (see Figure 2.1). Members of the DUF1009 family possess neither sequence identity nor similarity to *E. coli lpxH* and its orthologues. Indeed, DUF1009 orthologues have no conserved histidines, while *lpxH* and members of its metallo-hydrolase superfamily possess absolutely-conserved histidines required for metal-liganding and catalysis (*187*). We amplified the DUF1009 orthologue from *Caulobacter cresentus*, a ubiquitous aquatic Gram-negative species involved in the carbon cycle (*188*). This gene, annotated as CC1910, was cloned into a high-copy vector and expressed in *E. coli*. The expression of this gene resulted in the production of the expected 29 kDa protein (see Figure 2.2, panel A), and E. coli lysates containing this protein displayed greater than 1000-fold increase in UDP-2,3-diacylglucosamine hydrolase activity relative to the vector control (see Figure 2.2, panel B). CC1910, designated *lpxI*, was able to rescue the lethality of a *lpxH* deletion with a kanamycin-resistance cassette in *E. coli*, and for the trasduction of *lpxH::kan* into wild-type E. coli harboring a plasmid containing *C. crescentus lpxI* (see Figure 2.3). Taken together, these data support the notion that lpxI is a specific UDP-2,3-diacylglucosamine hydrolase.

The gene product of *C. crescentus lpxI*, designated CcLpxI, was massively over-expressed in *E. coli* and purified to greater than 90% homogeneity (see Figure 2.4). An improved radiographic UDP-2,3-diacylglucosamine hydrolase assay was described to monitor activity (see Figure 2.5). Partially purified CcLpxI was demonstrated to have optimal activity at pH 8.0, and to have near-optimal activity to at least pH 10.0 (see Figure 2.6). This pH rate profile differs significantly from that described for *E. coli* LpxH (*188*). CcLpxI's apparent kinetic parameters

were measured with respect to UDP-2,3-diacylglucosamine: the K_M was 105 ± 25 μM, while the apparent V_{max} was 69 ± 5 μmols/min/mg (see Figure 2.6). This is similar to the K_M of 60 μM reported for *E. coli* LpxH (*188*). While Co^{+2}, Mn^{+2}, and Mg^{+2} were each shown to stimulate the apparent activity of CcLpxI, Mg^{+2} produced the largest effect (see Figure 2.7). CcLpxI was completely inactive when assayed in the presence of 0.2 mM EDTA, but activity could be restored by the addition of Mg^{+2} in excess of the EDTA. This behavior differs markedly from E. coli LpxH, which is maximally active in the presence of Mn^{+2}, and is not stimulated by Mg^{+2} (*188*). Taken together with the dissimilarity of their conserved morifs, we hypothesize that *E. coli* LpxH and CcLpxI are transformational analogues (*162, 163, 165*), having evolved separately to generate the same product.

The role of metal in CcLpxI remains to be elucidated. Metal-dependent phosphohydolases, including the diverse families of Nudix enzymes (*152*), employ divalent cations in a variety of ways. In some enzymes (*154*), the metal coordinates oxygens of the phosphate, while in others, it positions the water for an attack upon a phosphorous atom. In still other instances, the metal appears to be coordinating a network of ordered waters, which in turn position a "catalytic water" for attack upon the substrate. While CcLpxI does not co-purify with divalet cations, it is clearly dependent upon them for its activity (see Figure 2.7). More detailed experiments, employing cation/EDTA buffers to precisely control metal concentrations, may elucidate the role of divalent cations in CcLpxI activity. For intance, equilibrium dialysis may offer a tractable method by which to estimate the k_d of divalent cations with respect to purified CcLpxI.

To determine which phosphate of UDP-2,3-diacylglucosamine is attacked by water in the CcLpxI catalyzed hydrolysis, reactions were run in the presence and absence of $H_2{}^{18}O$, and their products analyzed by ESI mass spectrometry (see Figure 2.8). In the labeled reaction, ^{18}O-containing lipid X was observed, while the phosphate on UMP was not substituted. These data show that CcLpxI catalyzes the attack of water on the β-phosphate of its substrate, in contrast to E. coli LpxI, which specifically catalyzes the attack on the α-phosphate (*188*), (see Figure 2.9).

This observation, together with the lack of homology between *E. coli* LpxH and CcLpxI, suggests that these enzymes perform catalysis by different mechanisms. Relatively few putative transformational analogues have been explicitly demonstrated to perform catalysis by diffent mechanisms (*188*).

Surveying the distribution of CcLpxI orthologues in Gram-negative bacteria (see Figure 2.10), we observe that among completely sequenced bacterial species, *lpxI* is the predominant putative UDP-2,3-diacyglucosamine hydrolase in δ and α proteobacteria. The presence of *lpxI* -- but not *lpxH* -- orthologues in more ancient species, such as some *Spirochetes* and *Aquificae*, suggest that LpxI may have originally evolved earlier than lpxH orthologues. Moreover, some organisms which make lipid A, including cyanobacteria (*189*), lack orthologues of both lpxH and lpxI, suggesting that a third class of UDP-2,3-diacyglucosamine hydrolase may exist.

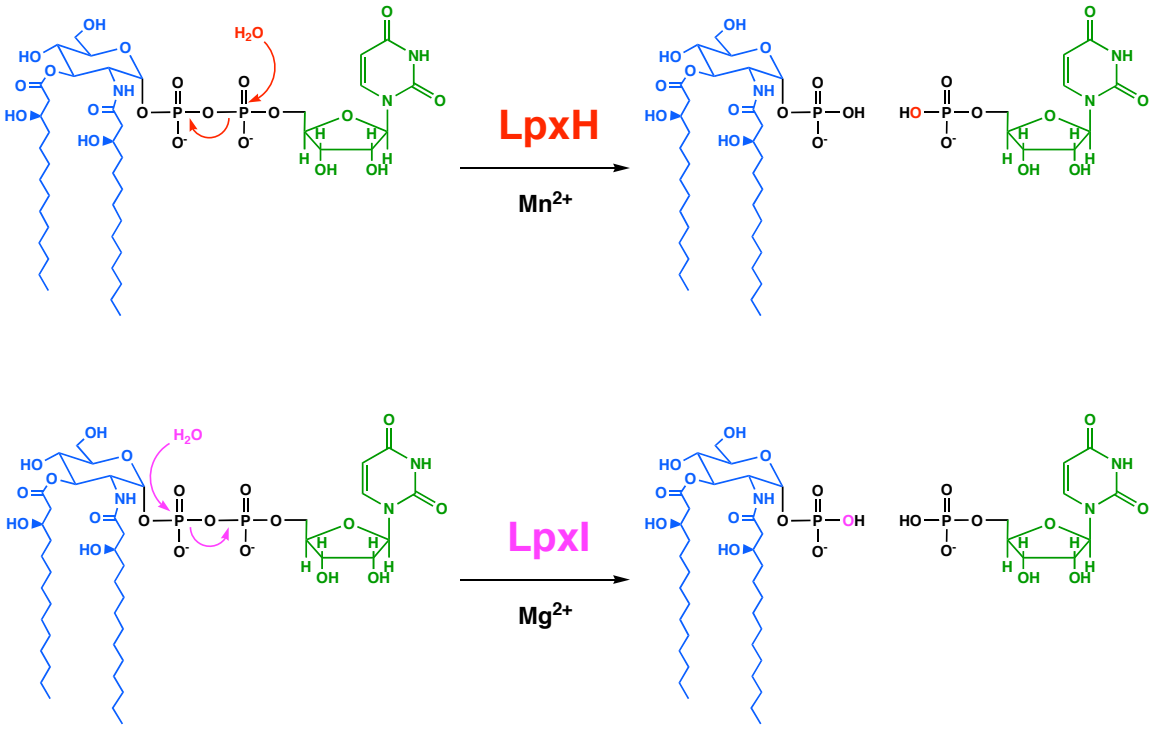

Figure 9. UDP-2,3-diacyglucosamine hydrolysis performed by LpxH vs. LpxI. Oxygen from the water attacking the α-phosphate in the LpxH-catalyzed reaction is shown in red, while oxygen from the β-phosphate in the LpxI-catalyzed reaction is shown in magenta.

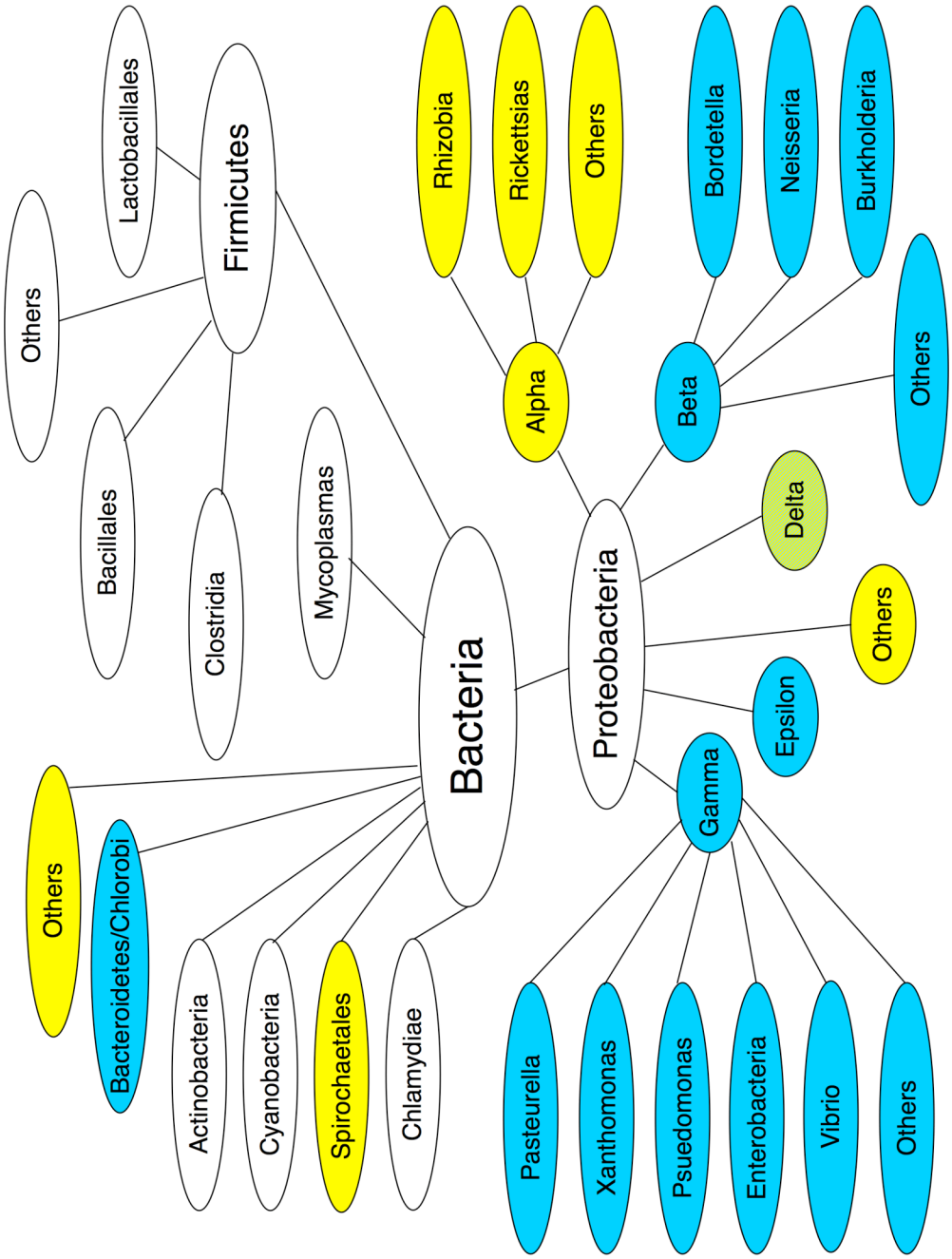

Figure 10. Scheme showing the distribution of LpxH and LpxI orthologues among bacterial species. This figure shows the distribution of LpxH (yellow) and LpxI orthologues (cyan) in bacterial species for which complete geneome sequences are available. Branches represent descent from a common ancestor, but their lengths do not reporesent evolutionary distances. Coloring corresponds to the predominant UDP-2,3-diacyglucosamine hydrolase (LpxH or LpxI) representat in each class of organisms. Yellow and cyan stripes indicate groups in which contain approximately equal proportions of organisms having LpxH and LpxI.

3. Purification and mutagenesis of *Caulobacter Crescentus* LpxI

3.1 Introduction

In the previous chapter, we described the discovery of a novel UDP-2,3-diacylglucosamine hydrolase in the model Gram-negative bacterium *Caulobacter crescentus*. LpxI, a transformational analogue of LpxH, is required for lipid A biosynthesis, and thus for the viability many Gram-negative bacteria, including pathogens such as the *Rickettsiae* and *Brucellae*. In this chapter, we describe the cloning and expression of a CcLpxI construct that has been N-terminally tagged with a cleavable poly-histidine. We then purify this construct to near-homogeneity on a 50 mg scale. We discover that ~99% homogenous CcLpxI co-purifies with its product, lipid X, as judged by TLC and mass-spectrometry. Whole-cell $^{32}PO_4$ labeling allows us to estimate a lipid X to CcLpxI stoichiometry of 0.95, and to observe that CcLpxI over-expressing cells accumulate lipid X to ~10% of their total lipids. A selection of six absolutely conserved LpxI residues are mutated to alanines in wild-type CcLpxI and expressed in *E. coli*; the *in vitro* activity of these cells' crude lysates is determined using the assay described in chapter 2. To follow the *in vivo* activity of the point mutants, whole cells are extracted and subjected to liquid chromatography and ESI mass spectrometric analysis. Lipid X accumulation is observed in cells expressing active LpxI, while cells expressing catalytically compromised mutants accumulate little or no lipid X. Cells over-expressing one mutant, CcLpxI D225A, massively accumulate the CcLpxI substrate, UDP-2,3-diacylglucosamine. This mutant is modified by the addition of an N-terminal cleavable poly-histidine tag, and is purified to near-homogeneity. CcLpxI D225A is subjected to TLC and LC-MS analysis, confirming that it co-purifies with UDP-2,3-diacylglucosamine. Spectrophotometric measurements allow us to estimate that UDP-2,3-diacylglucosamine is present in purified CcLpxI D225A in a 0.85 stoichiometry. Taken together,

these findings poise us to embark upon the detailed structural and functional characterization of CcLpxI.

3.2 Materials and Methods

3.2.1 Molecular biology

Amplification of mutagenized DNA segments from plasmids was accomplished using KOD Hot Start DNA polymerase, 8 mM dNTP stocks (2 mM each of dATP, dTTP, dGTP, and dCTP), and KOD Hot Start reaction buffer, all obtained from EMD Chemicals (Gibbstown, New Jersey, CA). Polymerase chain reactions (PCR) conditions were those recommended by Stratagene, except for the inclusion of 1% (v/v) dimethylsulfoxide and 1 M betaine in the reaction mixtures. The plasmids described in this study (see Table 3.1) were stored in and amplified from *E. coli* strain XL1-Blue (Stratagene, La Jolla, CA). Qiagen Mini-Prep kits and QIAquick Spin kits (Qiagen, Valencia, CA) were used, respectively, to purify plasmids and DNA fragments by protocols described by the manufacturer. Restriction endonucleases, T4 DNA ligase, and calf intestinal alkaline phosphatase were obtained from New England Biolabs (Ipswich, MA). Unless otherwise stated, ampicillin (Amp) was included in bacterial cultures to a final concentration of 100 μg/ml, and induction of plasmid expression was accomplished using 200 μg/ml IPTG.

3.2.1 Construction of a CcLpxI construct having a cleavable N-terminal (His)10 tag

The plasmid pECLpxB-TEV (*27*) (see Table 3.1) was digested using the restriction enzymes *Nde*I and *BamHI*. The linearized plasmid was treated with calf intestinal alkaline phosphatase, separated from its excised insert on a 1% w/v agarose gel, and further purified using a QIAquick Spin kit (Qiagen, Valencia, CA) according to the manufacturer's standard protocol. The plasmid pCc21b was similarly digested, except that it was not treated with calf intestinal alkaline phosphatase. The oligonucleotide liberated from its plasmid by this digestion,

Caulobacter crescentus lpxI having 5′ *Nde*I and 3′ *BamHI* compatible ends, was separated on a 1% w/v agarose gel, excised, and further purified using a QIAquick Spin kit (Qiagen, Valencia, CA). T4 DNA ligase (New England Biolabs) was used, in accordance with its manufacturer's suggested protocol, to ligate the *Caulobacter crescentus lpxI* insert into the empty plasmid liberated by the digestion of pECLpxB-TEV. These ligation reactions were then transformed into XL1-Blue (Stratagene, La Jolla, CA) chemically-competent *E. coli*, according to the manufacturer's recommended procedure. Plasmids were isolated from transformants, and their sequences confirmed by the Duke Cancer Center DNA Sequencing Facility. The resulting construct encoded CcLpxI having an $(His)_{10}$ tag attached by a Tobacco Etch Virus (TEV) protease-cleavable linker to its N-terminus. (see Table 3.1). This plasmid, designated pCcLpxI-TEV, was transformed into *E. coli* C41(DE3) (*182*), yielding the strain CcI-TEV.

3.2.2 *In vitro* UDP-2,3-diacyglucosamine hydrolase assays.

All assay conditions described in this work were identical to those detailed in section 2.2.7. Each 25 μl reaction contained the following components: 100 μM UDP-2,3-diacyglucosamine, 0.5 mg/ml bovine serum albumin (BSA), 0.05% w/v Triton X-100, 20 mM HEPES pH 8.0, and 2 mM $MgCl_2$, and 1000 dpm/μl $^{32}PO_4$ UDP-2,3-diacyglucosamine. All assays were conducted at 30ºC, and quenched by spotting portions of the reaction onto silica TLC plates, which were developed, visualized, and quantified as described in section 2.2.7.

3.2.3 Purification of CcLpxI from strain CcI-TEV

A colony of *E. coli* strain CcI-TEV, which expresses CcLpxI having a N-terminal TEV-cleavable $(His)_{10}$ tag, was used to inoculate a 25 ml overnight culture in LB medium supplemented with Amp. Following growth for 18 hours at 30°C, this culture was used to inoculate 1L of the identical medium to an initial OD_{600} of ~0.05. Growth proceeded at 30°C, 220 rpm aeration, until the cells reached an OD_{600} of ~0.5. IPTG was then added to the culture to a

Table 3.1. Relevant Strains and Plasmids

Strain	Description	Source or reference
C41(DE3)	F$^-$ *ompT hsd*S$_B$(r$_B^-$ m$_B^-$) *gal dcm* (DE3) D(srl-recA)306::Tn*10*	Chapter 2
XL1-Blue	*recA1 endA1 gyrA96 thi-1 hsdR17 supE44 relA1 lac [F′proAB lacIqZDM15 Tn10 (Tet^R)]*	Strategene
VC_21b	C41(DE3) harboring pET21b, Amp^R	Chapter 2
CcI_21b	C41(DE3) harboring pCcI21b, Amp^R	Chapter 2
VC_16b	C41(DE3) harboring pET16b, Amp^R	This work
CcI-TEV	C41(DE3) harboring pCcLpxI-TEV, Amp^R	This work
CcI-Q169A	C41(DE3) harboring pQ169A, Amp^R	This work
CcI-E182A	C41(DE3) harboring pQE182A, Amp^R	This work
CcI-E185A	C41(DE3) harboring pQ185A, Amp^R	This work
CcI-T187A	C41(DE3) harboring pT187A, Amp^R	This work
CcI-Q220A	C41(DE3) harboring pQ220A, Amp^R	This work
CcI-D225A	C41(DE3) harboring pD225A, Amp^R	This work
D225A-TEV	C41(DE3) harboring pD225A-TEV, Amp^R	This work
		This work

Plasmid	Description	Source or reference
pET16b	Expression vector containing a T7 promoter, AmpR, confers a factor Xa-cleavable N-terminal (His)10 tag	Novagen
pCcI21b	pET21b containing C. crescentus lpxI, AmpR	Chapter 2
pECLpxB-TEV	pET16b containing E. coli lpxB wherein the factor Xa cleavage site is replaced by a TEV protease site, AmpR	Chapter 2
pCcLpxI-TEV	Derivative of pECLpxB-TEV wherein the E. coli lpxB insert was excised at the ndeI / BamHI restriction sites, and replaced with C. crescentus lpxI (excised from pCcI21b) at the same restriction sites, AmpR	This work
pQ169A	pCCI21b harboring the mutation Q169A in C. crescentus lpxI, AmpR	This work
pE182A	pCCI21b harboring the mutation E182A in C. crescentus lpxI, AmpR	This work
pE185A	pCCI21b harboring the mutation E185A in C. crescentus lpxI, AmpR	This work
pT187A	pCCI21b harboring the mutation T187A in C. crescentus lpxI, AmpR	This work
pQ220A	pCCI21b harboring the mutation Q220A in C. crescentus lpxI, AmpR	This work
pD225A	pCCI21b harboring the mutation D225A in C. crescentus lpxI, AmpR	This work
pD225A-TEV	pCcLpxI-TEV harboring the mutation D225A in C. crescentus lpxI, AmpR	This work

final concentration of 250 μM, and growth was allowed to proceed for an additional 5 hours. Cells, which typically grew to an OD_{600} of ~3.5, were harvested by centrifugation at 3000 x *g* for 30 minutes, and subsequently washed with 40 ml buffer containing 20 mM HEPES pH 8.0, 50 mM NaCl, and stored at -80°C as a pellet. In a typical purification, a cell pellet from 1L of harvested culture (~8 g wet cell pellet) was re-suspended in ~160 ml lysis buffer (20 mM HEPES pH 8.0, 250 mM NaCl, 25 mM imidazole) and lysed by three passages through an ice-cold Cell-Cracker (Microfluidics International Corp., Newton, MA) pressure disruption chamber. Cell debris and membranes were removed by ultracentrifugation at 150,000 x *g* for 1 hour. The cleared lysate (~160 ml) was then divided equally among four 50-ml polypropylene conical tubes (~40 ml/tube). NiNTA Fast-Flow resin (Qiagen, Valencia, CA), was washed with lysis buffer and mixed in a 50% v/v slurry of the same. Next, 2.5 ml of this NiNTA resin / lysis buffer slurry was added to each conical tube containing cleared lysate, resulting in a total resin bed volume of 5 ml. The batch absorption of the $(His)_{10}$ tagged protein was allowed to proceed for ~30 minutes at room temperature. The conical tubes were gently inverted at intervals of ~5 minutes to ensure complete mixing of the NiNTA resin with the cleared lysate. Between inversions, the tubes were agitated using a table-top nutation apparatus, rotating at ~ 5 rpm. Following batch absorption, the resin/lysate slurry was poured into a glass Bio-Rad column (3.6 cm diameter, 10 cm height). The resin retained on the column bed settled by gravity, while the cleared lysate flowed through the column. The resin was then washed with 20 bed volumes (100 ml) of lysis buffer. At intervals between the addition of wash buffer, the column was capped, and pressure was applied with a syringe, such that the flow-rate was approximately 10 ml/min. Five bed volumes (25 ml) of a more stringent washing step, this time using buffer containing 20 mM HEPES pH 8.0, 250 mM NaCl, and 50 mM imidazole, was applied to the resin as above. A further washing step, this time consisting of five bed volumes (25 ml), was performed with buffer containing 20 mM HEPES pH 8.0 and 50 mM imidazole. Elution of the $(His)_{10}$-tagged CcLpxI was accomplished by applying 20 bed volumes (100 ml) of buffer containing 20 mM HEPES pH 8.0 and 400 mM imidazole to the

resin at the natural flow rate of the resin. Upon its elution from the NiNTA column, monitored by Bradford assay, the 100 ml of $(His)_{10}$-tagged CcLpxI was diluted to 250 ml with 20 mM HEPES pH 8.0, and 0.5 M EDTA pH 7.5 and 1 M DTT were immediately added to final concentrations of 5 mM and 2 mM, respectively. To prevent denaturation at liquid interfaces, it was essential to mix $(His)_{10}$-tagged CcLpxI with its dilution components using a wide-tipped 25 ml plastic pipette, at a transfer rate of less than 25 ml/min. Next, 30 ml of 0.25 mg/ml $(His)_6$-tagged TEV protease (*190, 191*), purified as described in Appendix I, was quickly thawed in room-temperature water and mixed. The 250 ml of diluted $(His)_{10}$-tagged CcLpxI was divided equally into six 50 ml polypropylene conical tubes (~42 ml/tube), and 1.25 mg (5 ml) of $(His)_6$-tagged TEV protease was added to each. The protease was slowly mixed with the $(His)_{10}$-tagged CcLpxI in each tube using a wide-aperture plastic pipette, as described above. Upon complete mixing, the conical tubes were sealed and gently agitated on a table-top nutation apparatus, set to rotate at no more than 1 rpm, for 18 hours at room temperature. The tubes were subsequently opened, and additional (1.25 mg) of freshly-thawed $(His)_6$-tagged TEV protease was gently mixed with the contents of each digestion aliquot, as described above. The tubes were re-sealed, and allowed to nutate at room temperature for an additional 18 hours. The digestion mixture (~300 ml) was then diluted 10-fold by gently mixing it, as above, with 2.7 L of buffer containing 20 mM HEPES 8.0. A 10-ml bed volume of Q-Sepahrose Fast-Flow anion exchange resin (GE Health Sciences), was poured into a 3.6 x 10 cm glass column (Bio-Rad), and washed with 10 bed volumes of 20 mM HEPES pH 8.0. The diluted digestion reaction (3 L) was loaded, by gravity at an average flow rate of ~20 ml/min, onto the Q-Sepahrose Fast-Flow anion exchange column. The column was then washed with 10 column volumes (100 ml) of 20 mM HEPES pH 8.0. Elution of CcLpxI was accomplished by applying 5 column volumes (50 ml) of buffer containing 20 mM HEPES pH 8.0 and 200 mM NaCl, at a flow rate of ~5 ml/min. Fractions were monitored by Bradford assay. Next, a bed volume of 5 ml of NiNTA Fast-Flow resin was poured into a 3.6 x 10 cm glass column and equilibrated in the Q-Sepharose elution buffer. The protein eluted from the Q-Sepharose column

was applied to the NiNTA Fast-Flow column at a flow rate of ~5 ml/min. The flow-through containing CcLpxI (50 ml) was collected. An additional 10 ml of equilibration buffer was used to wash remaining CcLpxI from the column bed, and pooled with the flow-through. Concentrated EDTA pH 7.5 (0.5 M) was added to the resulting 60 ml pooled NiNTA flow-though to a final concentration of 1 mM. Next, the 60 ml protein sample was concentrated to ~10 ml using two 15 ml Amicon Ultra 10,000 molecular weight cutoff centrifuge concentrators. An AKTA 600 FPLC system was then used to load the concentrated sample onto a preparatory size exclusion column (Superdex 200 XK26/70; GE Healthcare, Waukesha, WI), equilibrated in 20 mM HEPES 8.0, containing 200 mM NaCl. The column (included volume ~300 ml) was run at 1.5 ml/min, with the peak of CcLpxI eluting at ~210 ml. Fractions of 5 ml were collected, and their purity determined by SDS-PAGE. Typically, 6 fractions (30 ml) were pooled and subsequently concentrated to ~25 mg/ml in the manner described above. Protein aliquots were stored at -80°C, and processed by freeze-thawing upon storage and retrieval.

3.2.4. Extraction of lipids from purified CcLpxI and analysis by mass spectrometry

To determine whether CcLpxI, a peripheral membrane enzyme, co-purified with phospholipids, we extracted 0.2 mg of protein, purified by the method above, with a 5.8 ml acidic two-phase Bligh-Dyer system (*128*). The extraction was performed as previously described (*27*). A portion of the organic phase was directly diluted 10-fold into 2:1 $CHCl_3$/MeOH and directly injected a onto a QSTAR XL time-of-flight mass spectrometer (Applied Biosystems, Foster City, CA), operating in the ESI negative ion mode. A spectrum was collected in the *m/z* range of 60–2000 amu, with intensity counts accumulated over 1 min.

3.2.5. ^{32}P labeling of *E. coli* expressing CcLpxI

To determine whether *E. coli* expressing CcLpxI accumulate lipid X *in vivo*, we performed total ^{32}P labeling of strains CcI-TEV (expressing $(His)_{10}$-tagged CcLpxI) and VC-16b (the vector control). In each case 25 ml cultures were inoculated to an initial OD_{600} of ~ 0.05 from 5 ml overnight growths in LB medium supplemented with ampicillin. Upon inoculation, each 25 ml culture was labeled with 250 μCi $^{32}P_i$, or 10 μCi/ml of culture. Subsequent OD_{600} measurements were performed on matched non-radiolabeled cultures grown in parallel with the labeled cells. The strains were grown at 30°C in a water-bath rotary shaker at 220 rpm. Upon reaching an OD_{600} of ~0.5, the cultures were induced with IPTG to a final concentration of 250 μM. The cells were grown at 30°C for 3 hours following induction, whereupon they were harvested by centrifugation for 10 minutes at 5000 x *g*, washed with 20 ml PBS , and stored at -20°C as pellets.

To extract the radiolabeled phospholipids, CcI-TEV and VC-16b pellets were first extracted using a two-phase neutral Bligh-Dyer (*128*) system. The upper phase was removed and set aside, while the neutral lower phase (L1) was washed twice with pre-equilibrated neutral upper phase. The neutral upper phase was washed twice with pre-equilibrated neutral lower phase, and subsequently converted to an acidic two-phase Bligh-Dyer system. The acidic upper phase was removed, and the acidic lower phase (L2) was washed twice with pre-equilibrated upper phase. Most *E. coli* phospholipids, including PE, PG, and CL, partition to L1. Some acidic phospholipids, such as PS, PA, and lipid X, partition to L2. Scintillation counting was used to quantify the number of ^{32}P counts partitioning into the L1 and L2 phases of extracted CcI-TEV and VC-16b cells. The L1 and L2 phases were dried under nitrogen, and then redissolved in appropriate volumes of $CHCl_3$/MeOH (2:1, v/v) to obtain 5000 CPM/μl. Having very few counts, the L2 extracted from VC-16b was redissolved in the same volume of solvent as the L2 extracted from CcI-TEV. To quantitate the relative percentages of phospholipids, 5000-DPM portions of L1 and L2 fractions were spotted on 10 x 10 cm High Performance TLC plates (Merck, Darmstadt, Germany), and developed in a solvent system consisting of $CHCl_3$/MeOH/Acetic acid (65/25/10,

v/v/v), dried, and exposed to PhosphoImager screens (GE Health Sciences). After overnight exposure, images from these screens were scanned and peaks quantified as described in Chapter 2. Phospholipids in L1 were identified by their relative R_F values.

3.2.6. Estimation of the stoichiometry of CcLpxI to lipid X by ^{32}P labeling

To estimate the stochiometric ratio of CcLpxI to lipid X, we purified $(His)_{10}$-CcLpxI from radio-labeled whole cells. Again, 25 ml cultures of Vc-16b and CcI-TEV were inoculated and grown as described above. Three matched pairs (a pair consisting of VC-16b and CcI-TEV) of these 25 ml cultures were grown in parallel; two identical pairs of 25 ml cultures were radiolabeled with 10 μCi $^{32}P_i$/ml of culture upon inoculation, whereas the other pair was not labeled. The 25 ml cultures were induced, outgrown, and harvested as described above.

To establish the total number of ^{32}P-labeled lipids in L1 and L2, one matched pair of 25 ml radiolabeled cultures was extracted as described above, and the number of ^{32}P counts in each strain's L1 and L2 determined by scintillation counting. The remaining two matched pairs of VC-16b and CcI-TEV cultures, one of which was radio-labeled, were re-suspended in 20 ml of lysis buffer containing 20 mM HEPES pH 8.0, 250 mM NaCl, and 25 mM imidazole, and broken by sonic disruption as previously described (*128*). The lysates were cleared by ultracentrifugation at 150,000 x *g* for 1 hour. Four 1.6 x 5 cm polypropylene columns, each containing 500 μl of NiNTA Fast-Flow resin, were equilibrated with lysis buffer. The four membrane-free lysate samples, two from radiolabeled cells, were loaded onto their respective NiNTA columns by gravity. Each column was washed with 10 bed volumes (5 ml) of lysis buffer, followed by 10 volumes (5 ml) of buffer containing 20 mM HEPES pH 8.0 and 50 mM imidazole. Elution was accomplished with 10 volumes (5 ml) of buffer containing 20 mM HEPES and 400 mM imidazole. For the non-radiolabled cultures, protein concentration was measured by the Bradford Coomassie method (REF); CcLpxI expression and purification was verified by SDS-PAGE. The amount of ^{32}P eluted from the radio-labeled cells were measured by scintillation counting. The molar ratio of the ^{32}P-

phospholipids to the purified $(His)_{10}$-CcLpxI sample from which they were extracted was estimated as follows: the assumption that 10 μg of phospholipids can be extracted per OD_{600} unit/ml of *E. coli* culture (*108*); the measured amount of $(His)_{10}$-CcLpxI protein purified from the 25 mL of culture; and the assumption that the average molecular weight of *E. coli* phospholipids is 720 g/mol.

3.2.7. Cloning and Expression of CcLpxI Point Mutaants

To probe the role(s) played by absolutely conserved residues, site directed alanine-scanning mutagenesis was performed. The plasmid pCcI21b, encoding non-tagged CcLpxI, was mutagenized by a method analogous to that previously described (*108*). Oligonucleotide primers, listed in Table 3.2, were used to create pQ169A, pE182A, pE185A, pT187A, pQ220A, and pD225A. Upon confirmation of their sequences, these plasmids were transformed into C41(DE3) (Table 3.1). The resulting six strains, together with the VC-21b vector control and the CcI-21b wild-type strain, were grown, induced, and harvested on a 50 ml scale, exactly as described in Chapter 2. Each cell pellet was re-suspended in 3 ml of PBS, and lysed by two passes through a French Pressure cell at 18,000 psi. Membranes were removed by ultracentrifugation at 150,000 x *g* for 1 hour. The resulting membrane-free lysates were diluted with PBS such that each had a concentration of ~2.0 mg/ml, as determined by the Bradford Coumassie assay. The point mutants were assayed exactly as described in section 3.3.2. Each membrane-free lysate was assayed at final concentrations ranging from 200 ng/ml to 0.4 mg/ml. In instances where activity was measured above background, a specific activity was calculated. The relative expression levels of mutant CcLpxI constructs were monitored by SDS-PAGE.

3.2.8. Whole-cell lipid extraction and LC-MS analysis of CcLpxI point mutants

To determine whether *E. coli* expressing catalytically-compromised CcLpxI accumulate lipid X or UDP-2,3-diacylglucosamine *in vivo*, we directly extracted freshly-harvested cells. The strains VC-21b, CcI21b, CcLpxI-Q169A, CcLpxI-E182A, CcLpxI-E185A, CcLpxI-T187A, CcLpxI-

Q220A, and CcLpxI-D225A were grown in 50 ml cultures as described above. The cells were harvested by centrifugation at 3000 x *g* for 30 minutes, and washed with PBS. Each pellet was quickly re-suspended in 1.6 ml of 0.1 N HCl, and the re-suspended pellets were transferred to 15 ml screw-capped glass tubes. Next, 2 ml of $CHCl_3$ and 4 ml of MeOH were added to each tube to create a single-phase acidic Bligh-Dyer solvent system. Each extraction was allowed to proceed at room temperature for ~15 minutes; tubes were vigorously shaken using a vortex mixer at intervals of ~5 min. Debris were then removed by centrifugation at 5000 x *g* for 20 minutes. The supernatants were transferred to fresh screw-capped tubes, and 100 μl portions of each extraction mixture were prepared in 1 ml LCMS vials).

LC-MS analysis of the samples, using a C8 reverse phase column run in a MeOH/acetonitrile/ ammonium acetate system, with subsequent monitoring by ESI-MS, in the negative mode, was performed as previously described (*108*). A 20 μl sample of each 7.6 ml single-phase acidic Bligh-Dyer extraction (0.25% of the total single-phase volume) was loaded onto a ~600 μl C8 reverse phase column (2.5% of bed volume). ESI-MS was performed by a QSTAR XL time-of-flight mass spectrometer coupled to an LC system (*192*). Data were analyzed with the aide of the Analyst QS software package.

3.2.9. Construction, expression, and purification of $(His)_{10}$-tagged CcLpxI D225A

To determine whether the D225A mutant of CcLpxI co-purified with its substrate, we used primers D225A_FW and D225A_RV to mutagenize plasmid pCcLpxI-TEV, by previously described methods (*108*). The resulting plasmid, pD225A-TEV, was transformed into *E. coli* C41(DE3), yielding the strain D225A-TEV (see Table 3.1). Strain D225A-TEV was grown, and the expression of CcLpxI-D225A was induced in the manner described for the wild-type protein. Since CcLpxI D225A appeared to be inactive, the purification yield was measured by protein mass. Purity was judged by SDS-PAGE. The UDP-2,3-diacyglucosamine co-purifying with the

point mutant could also be followed by spotting it on a silica TLC plate, and developing and imaging the lipid as described in Chapter 2.

3.2.10. Estimating the stoichiometry of CcLpxI D225A to its co-purifying UDP-2,3-diacylglucosamine

The stoichiometry of UDP-2,3-diacyglucosamine was estimated by measuring the absorbance of the co-purifying uridine substrate moiety at A_{262}. Given the extinction coefficient of uridine, the known concentration of purified CcLpxI D225A, and the observation that the A_{262} of the wild-type protein is at least 5-fold lower than the substrate-bound point mutant, we were able to calculate the stoichiometry.

Table 3.2. Oligonucleotide primers used in this work

Name	Purpose	Primer sequence (5' to 3' orientation)
Q69A_FW	To mutate D169 to A in *C. crescentus lpxI*	GCATCGGGGCGGGCGCGGTCGTG
Q69A_RV		CACGACCGCGCCCGCCCCGATGTC
E182A_FW	To mutate E182 to A in *C. crescentus lpxI*	GTCGCCGTCGCGGCGCAGGAGG
E182A_RV		CCTCCTGCGCCGCGACGGCGAGC
E185A_FW	To mutate E185 to A in *C. crescentus lpxI*	CGAGGCGCAGGCGGGCACCGACG
E185A_RV		CGTCGGTGCCCGCCTGCGCCTCG
T187A_FW	To mutate T187 to A in *C. crescentus lpxI*	GAGGAGGGCGCCGACGCCATG
T187A_RV		CATGGCGTCGGCGCCCTCCTGC
Q220A_FW	To mutate Q220 to A in *C. crescentus lpxI*	AACCGATCGCGGAGACGCGCGTCG
Q220A_RV		CGACGCGCGTCTCCGCGATCGGTTT
D225A_FW	To mutate D225 to A in *C. crescentus lpxI*	GCGCGTCGCTCTGCCGACGA
D225A_RV		TCGTCGGCAGAGCGACGCGC

3.3 Results

3.3.1 Expression and purification of CcLpxI from a $(His)_{10}$ tagged CcLpxI construct

CcLpxI was purified from *E. coli* strain CcI-TEV, making use of a TEV-protease cleavable N-terminal $(His)_{10}$ tag and Immobilized Metal Affinity Chromatography (IMAC) with Ni^{+2}-conjugated resin. While the $(His)_{10}$-CcLpxI bound tightly to the NiNTA resin and could be purified to near-

homogeneity in a single step (see Figure 3.1, panel A), this construct tended to aggregate and precipitate upon elution from the sizing column. Aggregation was worsened by storage at 4°C, and $(His)_{10}$-CcLpxI, when frozen at -80°C at 0.25-2.0 mg/ml, precipitated during subsequent thawing. As non-tagged CcLpxI appeared to be very stable and more soluble, we chose to cleave the tag from $(His)_{10}$-CcLpxI immediately after eluted from the NiNTA column. As the buffer required for optimal TEV-protease activity contained EDTA and DTT, which are incompatible with NiNTA resin, we performed a buffer-exchange of the digested CcLpxI by binding it to a Q-Sepharose anion exchange column. We then eluted the cleaved CcLpxI from the Q-sepharose anion exchange column, and passed it over a second NiNTA column to remove non-cleaved $(His)_{10}$-CcLpxI, cleaved $(His)_{10}$-tag, $(His)_6$-tagged TEV protease, and other contaminants. Subsequent size exclusion chromatography yielded highly purified CcLpxI (see Figure 3.1, panel B).UDP-2,3-diacylglucosamine hydrolase assays indicated a 68% overall yield in activity, and a 3.7-fold increase in specific activity (see Table 3.3) in this purification scheme. From ~8 g of wet cell pellet, ~60 mg of highly purified CcLpxI were obtained. The specific activity of the purified enzyme, ~26 μmol/mg/ml, was similar to that measured for LpxI purified without a tag (see Chapter 2).

3.3.2 Extraction of lipids from purified CcLpxI and analysis by mass spectrometry

As CcLpxI works acts upon a membrane-bound substrate, we hypothesized that it may co-purify with inner-membrane phospholipids. We therefore extracted CcLpxI, purified extensively as described in section 3.2.3, in an acidic Bligh-Dyer (*128*) solvent system. When this material was analyzed by ESI-MS, operating in the negative-mode, we observed a strong singly-charged species with a *m/z* of 710.397, consistent with lipid X (exact mass of $[M-H]^{-1}$ calculated to be 710.42), the product of CcLpxI (see Figure 3.2). The identity of this species was confirmed by MS/MS analysis (data not shown). A minor species of lipid X, in which a hydroxylaurate is

substituted for a hydroxymyristate chain, was observed at *m/z* of 682.383 (calculated $[M-H]^{-1}$ 682.39). Peaks corresponding to other *E. coli* phospholipids were not observed.

Table 3.3. Purification of CcLpxI from CcI-TEV

Step	Protein mass (mg)	Protein volume (ml)	Units (mmol/min)	Specific activity (μmol/min/mg)	Yield (%)	Fold-purification
Membrane-free lysate from strain CcI-TEV	334	160	2.2	7	100	
TEV-digested CcLpxI, after elution from Q-Sepharose resin and passage through NiNTA resin	104	60	2.1	20	95	2.9
S200 size exclusion column pooled fractions	60	30	1.5	26	68	3.7

3.3.3 ^{32}P labeling of *E. coli* expressing CcLpxI

To determine whether whole cells expressing CcLpxI accumulate lipid X, we labeled the vector control strain VC-16b and the $(His)_{10}$-CcLpxI-expressing strain CcI-TEV with $^{32}P_i$ upon inoculation, and later, upon reaching an OD_{600} of ~ 0.5, induced with IPTG, and grown for another three hours. The cells were harvested and their radiolabeled phospholipids quantified by scintillation and autoradiography of TLC-separated components. The CcI-TEV strain accumulated nearly 52-fold more radiolabeled species in its L2 phase than its vector control, an observation consistent with the accumulation of lipid X in the cells (see Table 3.4). We were surprised to observe that in comparison to VC-16b, the relative abundance of PG in CcI-TEV was nearly three times lower. While the number of ^{32}P counts in the L2 extracted from VC-16b is approximately 0.2% of the total radiolabeled phospholipids, the L2 from CcI-TEV comprises

greater than 10% of that strain's ^{32}P-labeled lipids (see Table 3.4). These observations can be appreciated in Figure 3.3, where Cc-TEV accumulates a phospholipid having an R_F consistent with lipid X. A smaller band, running below the putative lipid X in this solvent system, also accumulates in CcI-TEV relative to VC-16b.

3.3.4 Estimation of the stoichiometry of CcLpxI to lipid X by ^{32}P labeling

To estimate the stoichiometry of CcLpxI to lipid X, we purified $(His)_{10}$-CcLpxI from radio-labeled whole cells. Using the data described in Table 3.5, and assumptions detailed in the methods section, we estimate that the molar ratio of lipid X to $(His)_{10}$-CcLpxI to in CcI-TEV is ~0.95. If we divide the number of ^{32}P counts co-purifying with $(His)_{10}$-CcLpxI by the total number of counts in the L2 of strain CcI-TEV, we obtain a ratio of 0.25. Thus, while $(His)_{10}$-CcLpxI co-purifies in a nearly 1:1 stoichiometry with its product, at least 75% of the accumulated lipid X is present elsewhere in the cell. LpxI does not bind any of the other major *E. coli* lipids, such as PE, PG, or CL. Furthermore, LpxI does not bind related minor lipids, such as PA or undecaprenyl phosphate.

3.3.5 Expression and activity assay of mutants of residues completely conserved among CcLpxI orthologues

Six point mutants of CcLpxI, representing residues that are absolutely conserved among CcLpxI orthologues, were constructed and their expression was tested. Membrane-free lysates were prepared from *E. coli* strains over-expressing the various point mutants. These lysates' UDP-2,3-diacylglucosamine hydrolase activities were assayed. While the wild-type CcI21b control strain displayed robust expression of CcLpxI, a band corresponding to CcLpxI-Q169A was not visible by SDS-PAGE (see Figure 3.4). The CcLpxI-E185A expression pattern consisted of multiple bands of lower apparent molecular mass than full-length CcLpxI. These may be due to proteolysis of CcLpxI-E185A. As judged by SDS-PAGE, the other mutants' expression levels are within two-fold of the wild-type protein.

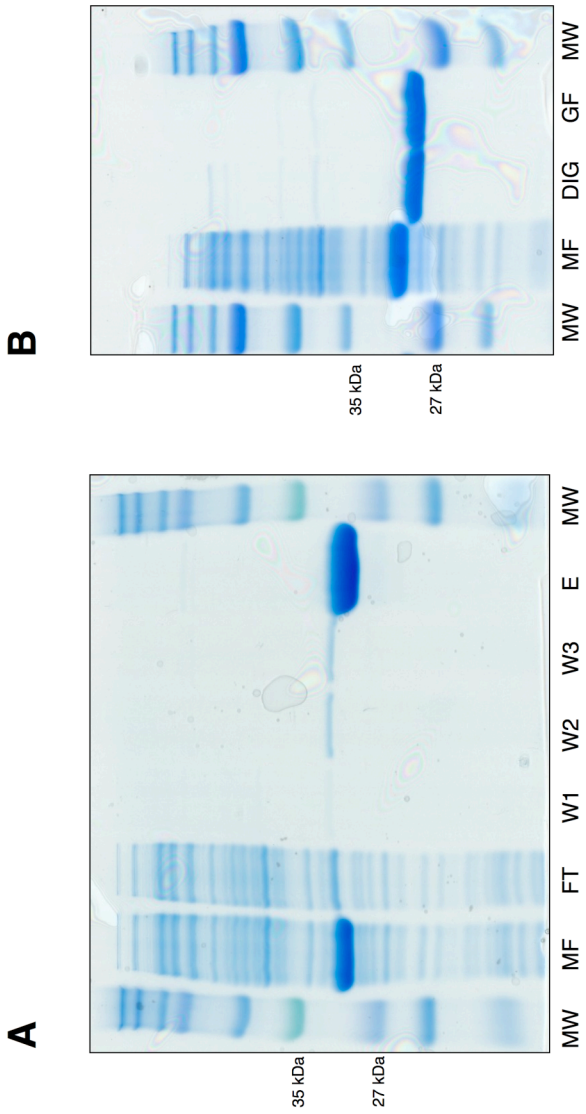

Figure 3.1. Purification of CcLpxI from strain Ccl-TEV. Ccl-TEV expresses CcLpxI having an N-terminal $(His)_{10}$ tag, attached by a Tobacco Etch Virus protease (TEV)-cleavable linker. Panel A is a 12% polyacrylamide gel showing the steps purification of $(His)_{10}$ tagged CcLpxI on a 5 ml NiNTA Fast-flow column. MF denotes membrane free lysate (35 column volumes); FT, flow-through material (32 column volumes); W1 is a 10 column-volume wash step with buffer containing 20 mM HEPES pH 8.0, 250 mM NaCl, and 25 mM imidazole; W2 is an identical washing step, except that the buffer contains 50 mM imidazole; W3 is a 10 column-volume wash consisting of 20 mM HEPES pH 8.0 and 50 mM imidazole; E is a 20 column-volume elution in buffer containing 20 mM HEPES pH 8.0 and 400 mM imidazole. Protein from each purification step is loaded in equal volumes (10 μl) on the gel. Panel B summarizes the steps in a representative purification from ~8 g Ccl-TEV wet cell pellet. MF is membrane-free lysate (160 ml). DIG is $(His)_{10}$ tagged CcLpxI after tag cleavage by TEV protease, buffer exchange on a Q-sepahrose column, and passage through a NiNTA column to remove the cleaved tag (60 ml). GF is pooled CcLpxI after passage through an S200 Superdex size-exclusion column (30 ml). In this 12% polyacrylamide gel, 15 μg of protein are loaded in each lane.

Table 3.4. Distribution of phospholipids in ^{32}P-labeled *E. coli*

Total counts of ^{32}P in Bligh-Dyer phases L1 and L2 (x 10-3)

	L1	L2	Total	L2/Total
				(%)
VC-16b	4900	10	4910	0.2
CcI-TEV	3790	440	4230	10.4

Distribution of phospholipid species in L1

	PE	PG	CL	Unk1	Total
	(%)	(%)	(%)	(%)	
VC-16b	68	25	3.5	2.5	100
CcI-TEV	76	9	10	5	100

Table 3.5. Quantities of ^{32}P present in components of *matched cultures* of VC-16b and CcI-TEV cells

Total counts of ^{32}P in Bligh-Dyer phases L1 and L2 (x 10^{-3})

	L1	L2	Total	L2/Total
				(%)
VC-16b	6400	< 1	6400	< 0.2
CcI-TEV	2700	210	2910	7.8

Total counts of ^{32}P in protein purified from whole cells using NiNTA resin

	Counts	Mass of protein recovered
	(10^3 CPM)	(μg)
VC-16b	None detected	None detected
CcI-TEV	52	127

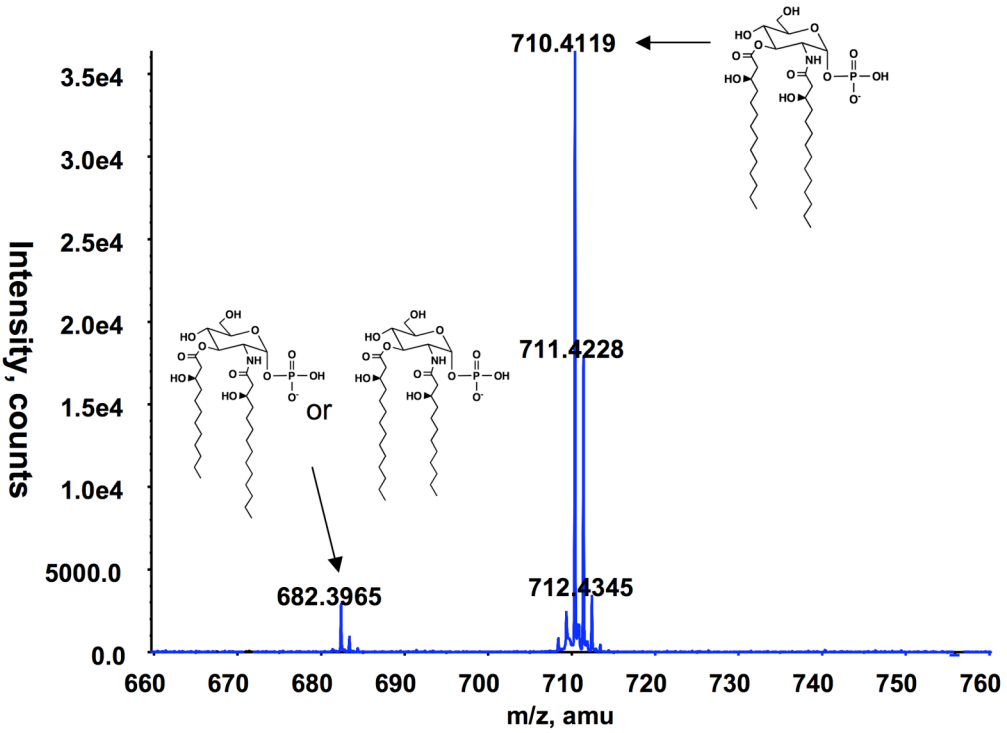

Figure 3.2. Lipid X is extracted from purified CcLpxI. CcLpxI was extracted in an acidic two-phase Bligh-Dyer system (REF Bligh-Dyer), and the organic phase directly analyzed by ESI mass spectrometry (negative mode). This phase, into which most *E. coli* phospholipids partition, contained primarily lipid X. The mass spectrograph above, obtained by direct injection of the lower phase, shows the two lipid X species that were observed. A small fraction of the lipid X contains one hydroxy-lauryate instead of the more abundant hydroxy-myristate. No other phospholipid species were observed in the full spectrum (not shown).

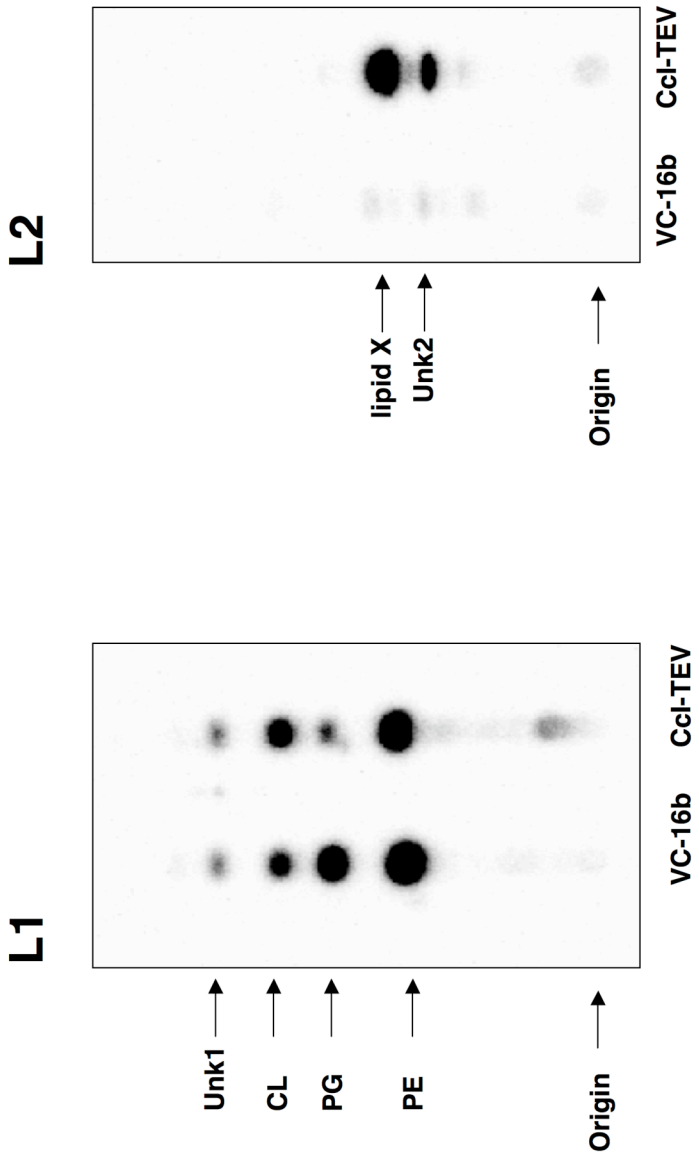

Figure 3.3. Phospholipid distribution in ^{32}P-labeled *E. coli* expressing CcLpxI. Here, we show the PhosphorImager analysis of a silica TLC plate upon which the total extracted phospholipids from ^{32}P-labeled *E. coli* have been separated. In the L1 plate, ~5000 CPM are spotted in each lane. For the L2 plate, equal volumes of redissolved lipids are spotted (representing L1 indicates the neutral lower phase of the Bligh-Dyer (REF) extraction system, while L2 denotes the acidic lower phase derived from the first upper phase. Most phospholipids, including PE, PG, PA, and CL, extract in L1. Other phospholipids, such lipid X, extract in L2. In L1, Unk1 labels a lipid of unknown identity, while Unk2 indicates an unknown lipid, since determined by ESI-MS/MS to be lipid X with ethanolamine added to its phosphate, possibly as the result of the EptA activity. Lanes corresponding to the vector control VC-16b and the CcLpxI-expressing strain CcI-TEV are indicated.

The measurement of these point mutants' specific activities in *E. coli* membrane-free lysates (see Table 3.6) reveals them all to be catalytically compromised *in vitro*. The activities of CcI-Q169A, CcI-E182A, CcI-Q220A, and CcI-D225A are within two-fold of the background UDP-2,3-diacyglucosamine activity present in the *E. coli*. CcI-E185, CcI-T187, possess apparent specific activities of 5.3-fold and 12.4-fold, respectively, of the background activity. In contrast, strain CcI21b, in which wild-type CcLpxI is expressed, has a specific activity ~2800-fold higher than the *E. coli* vector control strain (see Table 3.6).

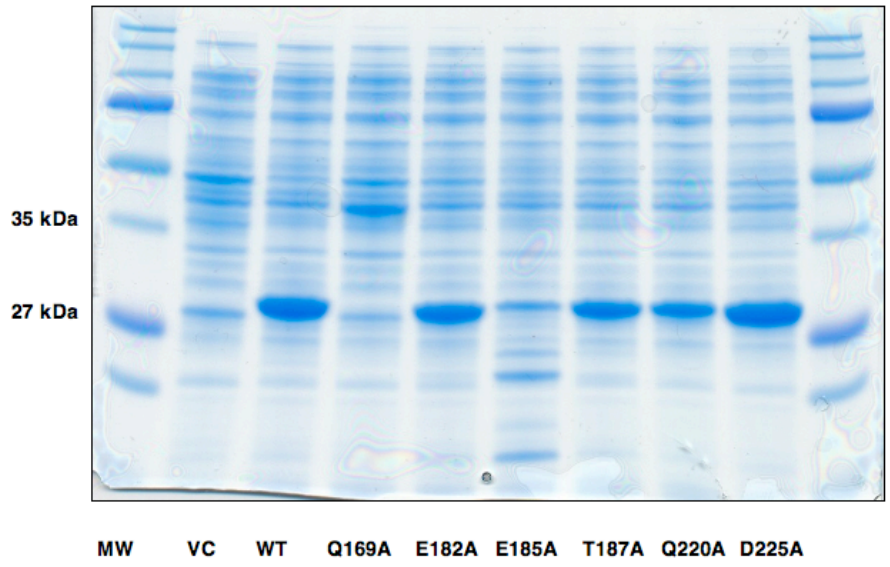

Figure 3.4. Expression of CcLpxI alanine point mutants. Each lane of this 12% polyacrylamide gel is loaded with 15 μg of membrane-free lysate. VC denotes strain VC-21b and WT denotes CcI-21b. Q169A, E182A, E185A, T187A, Q220A, and D225A label membrane-free lysate from strains CcI-Q169A, CcI-E182A, CcI-E185A, CcI-T187A, CcI-Q220A, and CcI-D225A.

3.3.6. Whole-cell lipid extraction and LC-MS analysis of CcLpxI point mutants

Having determined that wild-type CcLpxI co-purified with its product lipid X in a nearly 1:1 stoichiometry, we hypothesized that catalytically compromised point mutants might cause the

accumulation of UDP-2,3-diacyglucosamine by sequestration of this minor but critical lipid A precursor. Moreover, we hypothesized that mutant activity, as measured *in vitro*, should correlate to the accumulation of the CcLpxI product, lipid X, in whole cells.

Table 3.6. Specific activities of membrane-free lysates from strains expressing CcLpxI point mutants

Construct	Description	Specific activity (nmols/min/mg)	Fold-background activity
VC-21b	Vector control	6.02	1
CcI-21b	Wild-type	13,100	2,180
CcLpxI-Q169A	absolutely conserved	5.11	Near background
CcLpxI-E182A	absolutely conserved	6.79	Near background
CcLpxI-E185A	absolutely conserved	31.8	5.3
CcLpxI-T187A	absolutely conserved	74.7	12.4
CcLpxI-Q220A	absolutely conserved	12.6	2.1
CcLpxI-D225A	absolutely conserved	15.1	2.5

In the VC-21b cells, we see no evidence of lipid X accumulation (which represents about 0.01% of the total lipid of wild-type cells), whereas lipid X is the predominant species (by ion yield) in the total spectrum of CcI21b (see Figure 3.5). The mutant strains CcI-E185A and CcI-T187A accumulate lipid X in their total lipid extracts. For CcI-E185A, lipid X is the predominant phospholipid species by ion yield (similar to the CcI21b wild-type). Strain CcI-D225A also appears to contain lipid X at a level slightly higher than the baseline signal (see Figure 3.5). Interestingly, PG species appear to be significantly depleted, relative to wild-type levels, in the

strains that express CcI21b and E185A (data not shown). This is consistent with our earlier observation of PG depletion in whole radio-labeled cells wherein CcLpxI is expressed.

We also looked for the accumulation of the LpxI substrate, UDP-2,3-diacylglucosamine, in total lipid extracts of the strains over-expressing CcLpxI mutants. Previous studies have shown the steady-state level of UDP-2,3-diacylglucosamine in *E. coli* to be ~10-fold lower than lipid X (~0.02% of the total *E. coli* phospholipids). The expected exact mass of the doubly-charged species of UDP-2,3-diacyglucosamine is 507.72 amu. In CcI-D225A, we observed a doubly-charged species with an *m/z* of 507.75 amu (see Figure 3.6). This molecule's MS/MS fragmentation pattern, measured for the singly charged species (see Figure 3.7) was consistent with that expected for UDP-2,3-diacylglucosamine. No species of UDP-diacylglucosamine were observed in *E coli* expressing empty vector, wild-type CcLpxI, or the other CcLpxI point mutants (see Figure 3.6). The observable accumulation of UDP-2,3-diacylglucosamine in CcI-D225A represents a remarkable sequestration of this low steady-state (but high-flux) lipid A precursor.

3.3.7. Expression and purification of CcLpxI D225A

A TEV-protease cleavable $(His)_{10}$-tagged CcLpxI D225A mutant was constructed. The expression of the tagged construct was judged by SDS-PAGE to be at a similar level as wild-type CcLpxI. This construct was purified to near-homogeneity on a scale of ~ 5 mg per gram of wet cell pellet. Conveniently, the purification of this mutant could be followed by the monitoring of its absorbance at A_{262} (see Figure 3.8). Moreover, we employed TLC analysis of the purified protein to demonstrate that UDP-2,3-diacyglucosamine purified with CcLpxI.

Purified CcLpxI was analyzed spectrophotometrically at λ = 260 nM to determine the ratio of UDP-2,3-diacylglucoasmine to CcLpxI-D225A. Background A_{260} was measured for purified wild-type CcLpxI; this was subtracted from purified CcLpxI-D225A of the same concentration to estimate absorbance of co-purifying UDP-2,3-diacylglucosamine. From three separate

experiments, we determined a UDP-2,3-diacylglucosamine to purified CcLpxI-D225A stoichiometry of 0.85 ± 0.05.

To determine whether purified CcLpxI retained any UDP-2,3-diacylglucosamine hydrolase activity, we assayed the enzyme, as described in Chapter 2, for 1 hour at a final concentration of 2.0 mg/ml. No activity was observed.

3.3.8. LC-MS analysis of purified CcLpxI and CcLpxI-D225A

Purified CcLpxI and CcLpxI-D225A, were extracted, in 2 mg portions, in 1.9 ml acidic single-phase Bligh-Dyer systems. Denatured protein was removed by centrifugation, and 40 μl portions of the supernatants were subjected to Normal-phase LCMS analysis, by a method previously described (*192*). Extracted ion currents corresponding to lipid X extracted from purified CcLpxI, and doubly-charged UDP-2,3-diacyglucosamine extracted from CcLpxI-D225A are shown in Figure 3.9. In this chromatography system, lipid X elutes earlier (21.11 minutes) than UDP-2,3-diacylglucosamine (22.11 minutes). To determine whether purified CcLpxI-D225A converts UDP-2,3-diacyglucosamine over time, we incubated it, at 2 mg/ml at room temperature for one week. We then extracted 2 mg of this protein, and subjected it to LCMS analysis, exactly as described above. No changes in the amount of co-purifying UDP-2,3-diacyglucosamine or lipid X were observed.

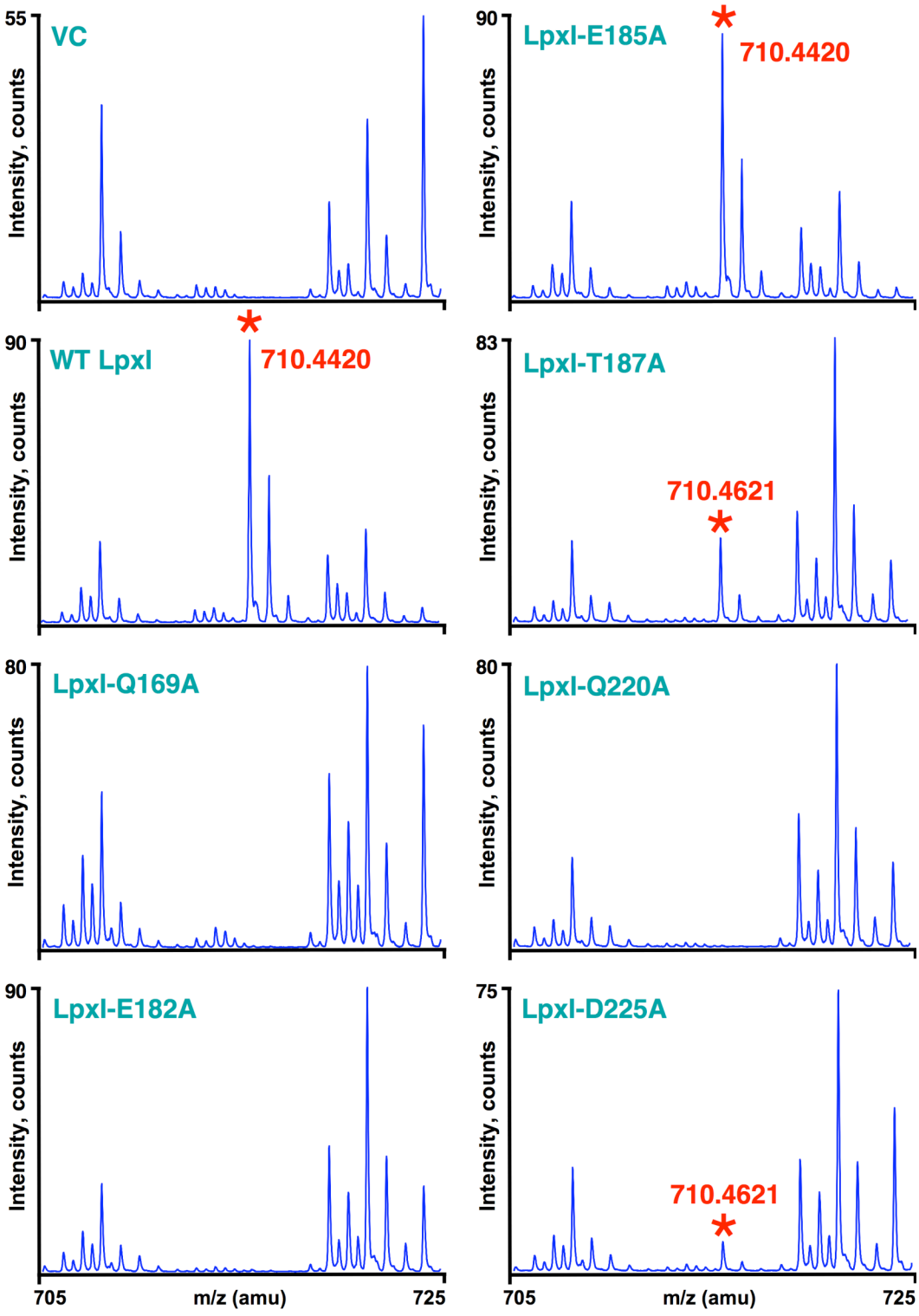

Figure 3.5. ESI-MS of total lipid extracts from *E. coli* strains harboring CcLpxI point mutants: lipid X region. Strain names are teal, the spectral trace is blue, and species corresponding to lipid X are marked with a red asterix and mass label.

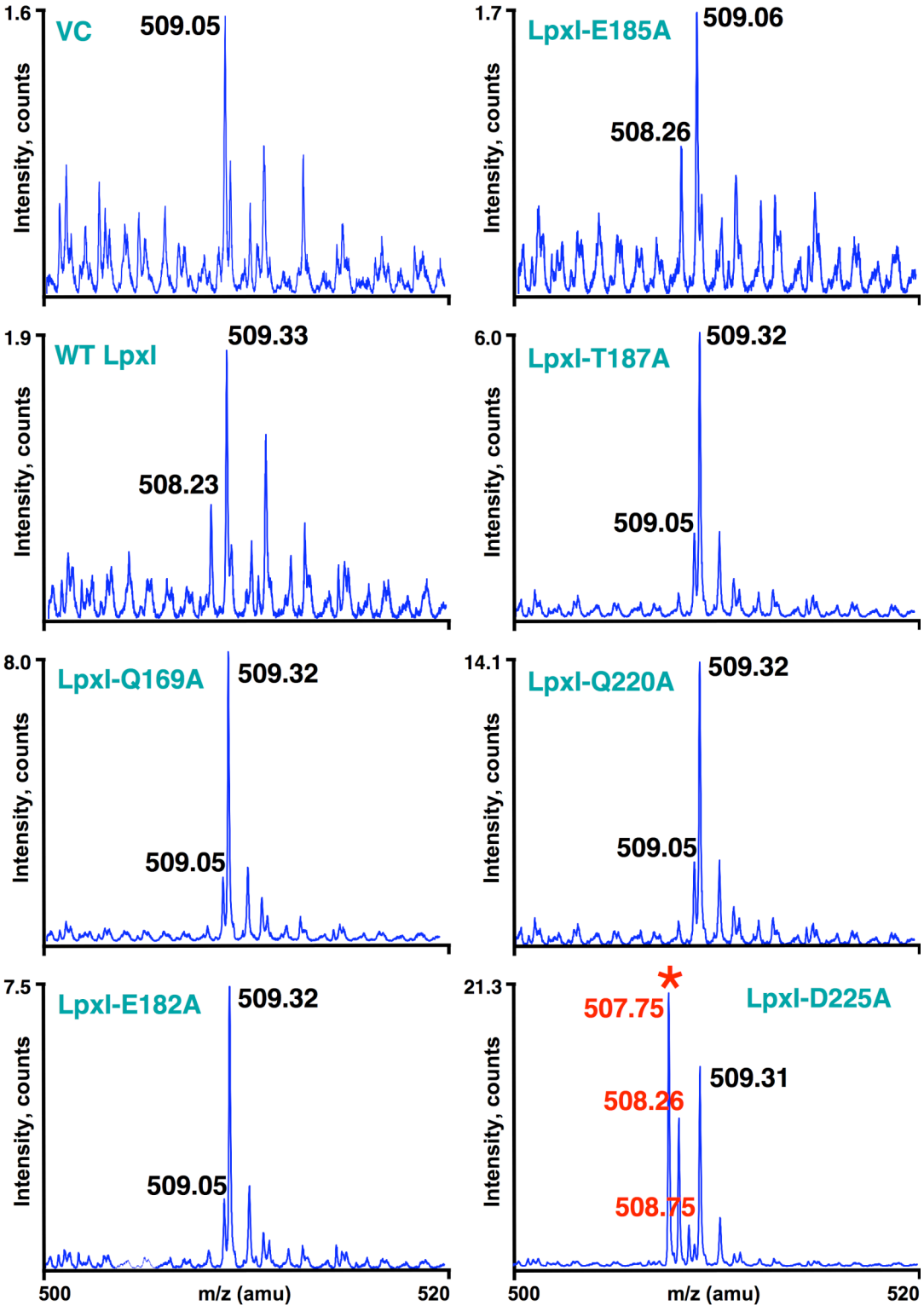

Figure 3.6. ESI-MS of total lipid extracts from *E. coli* strains harboring CcLpxI point mutants: UDP-2,3-diacylglucosamine. Strain names are teal, the spectral trace is blue, and species corresponding to UDP-2,3-diacylglucosamine are marked with a red asterix and mass.

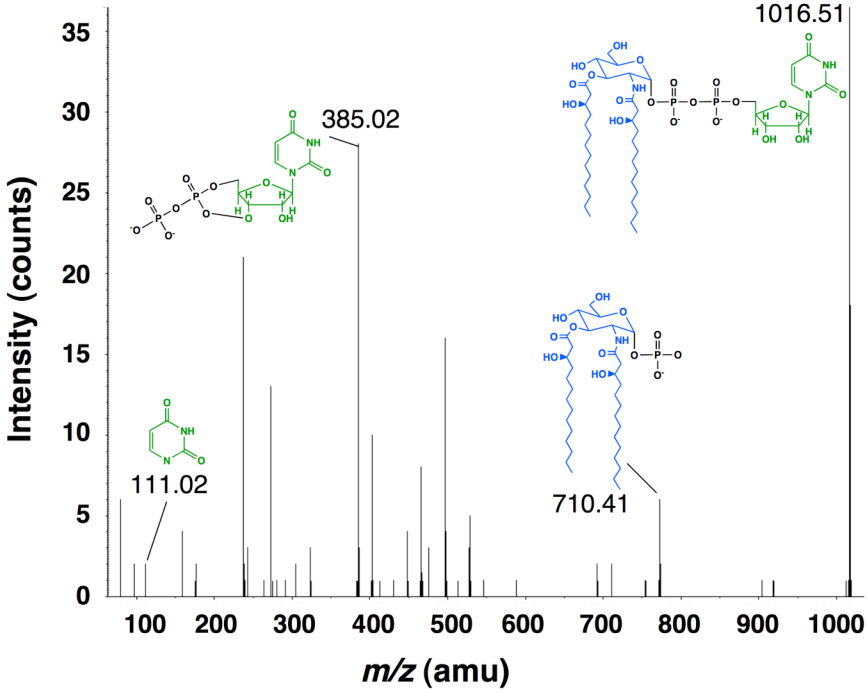

Figure 3.7. ESI-MS/MS of UDP-2,3-diacylglucosamine in total lipid extracts from *E. coli* strain Ccl-D225A. A selection of characteristic UDP-diacylglucosamine fragments are labeled with their experimental mass (amu). The chemical structures of these compounds are included for reference.

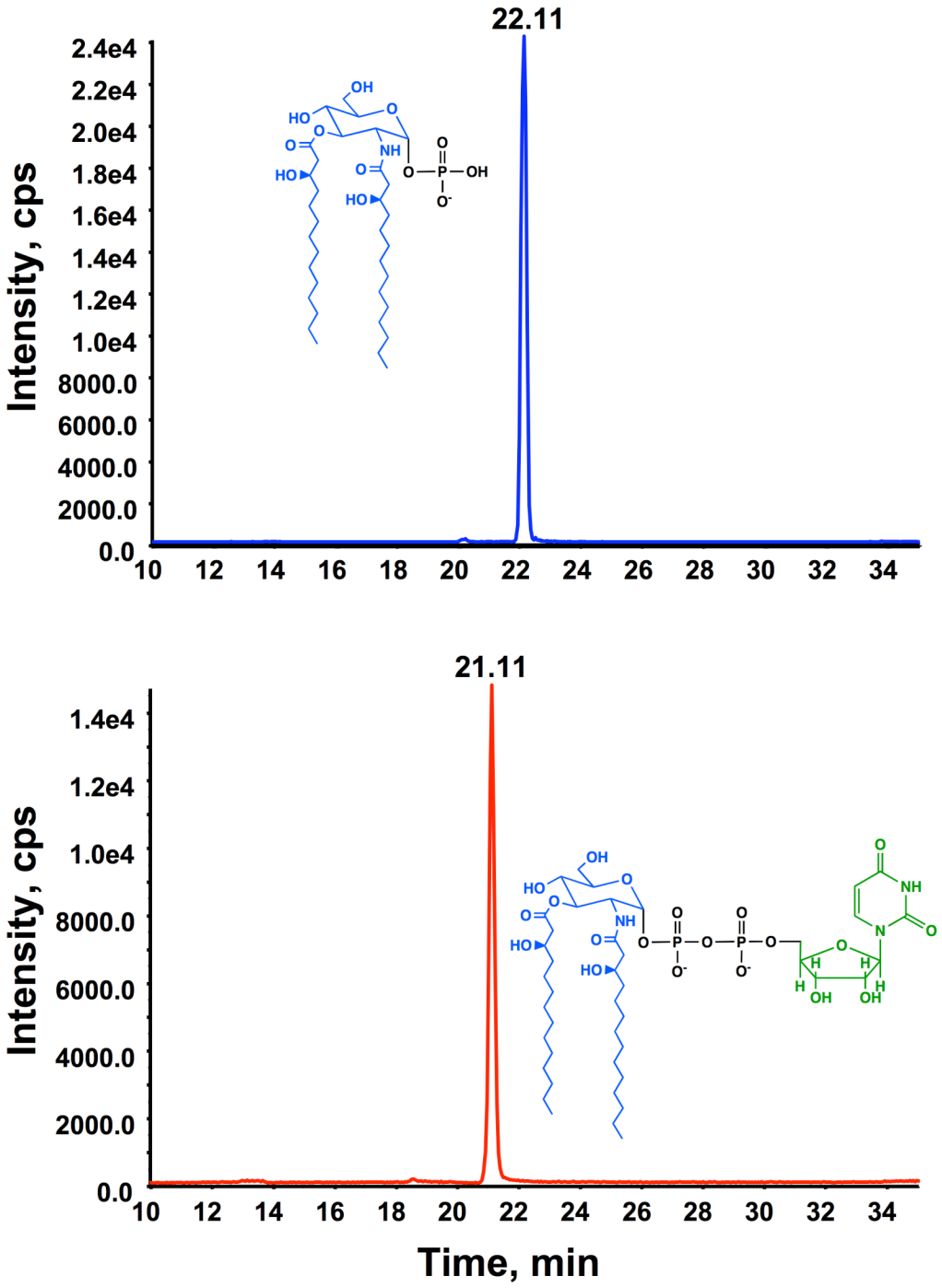

Figure 3.8. Normal phase LC/MS analysis of lipid extracted from purified CcLpxI and CcLpxI-D225A. The top spectrum (blue) shows the extracted ion current corresponding to lipid X extracted from 40 μg of purified CcLpxI. The bottom spectrum (red) is the extracted ion current corresponding to UDP-2,3-diacylglucosamine extracted from the same mass of CcLpxI-D225A.

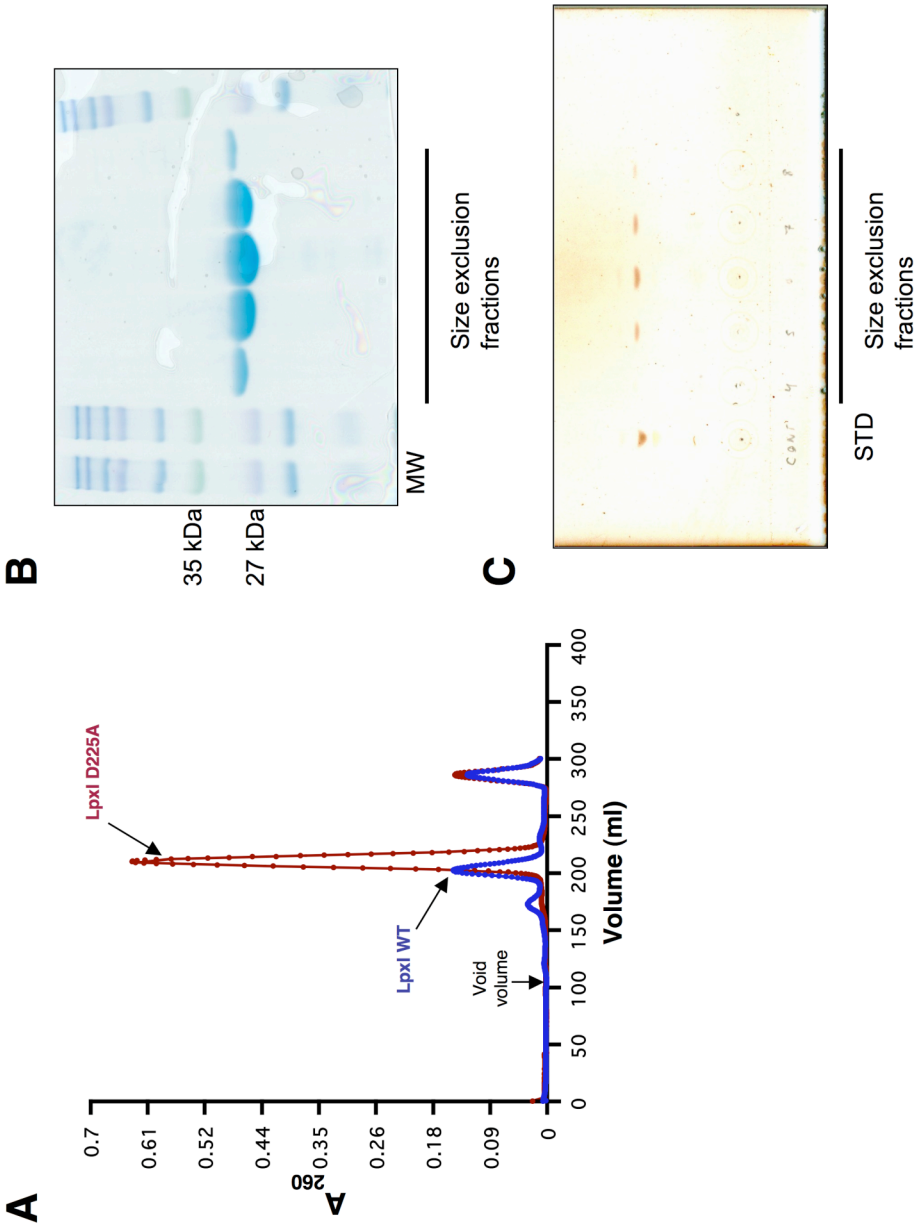

Figure 3.9. Purification of CcLpxI D225A . Panel A shows the overlay of two absorbance traces, both monitored at A_{260}, from two separate size-exclusion chromatographies performed on both wild-type and D225A CcLpxI. The red trace corresponds to ~ 40 mg of CcLpxI D225A, while the blue trace follows ~ 60 mg of wild-type CcLpxI. The chromatography for both proteins was carried out in matched buffer, and on the same Superose S200 sizing column. Note that the CcLpxI D225A peak, normalized for injection volume, is positioned at a lightly higher elution volume than the peak of wild-type CcLpxI. Panel B shows an SDS-PAGE analysis of the sizing column fractions from a purification of the CcLpxI D225A mutant. Each lane contains 10 μl of a 5 ml sizing-column fraction. In panel C, 5 μl portions of the same fractions are spotted, separated, and detected on a silica TLC plate following charring with H_2SO_4. A UDP-2,3-diacygucosamine standard is present at the far left side of the plate.

3.4 Discussion

LpxI is a UDP-2,3-diacylglucosamine hydrolase present in many Gram-negative bacteria. It plays an essential role in the biosynthesis of lipid A, the hydrophobic anchor of LPS. We previously described the discovery and characterization of the *Caulobacter crescentus* orthologue of this gene product (CcLpxI). While we previously reported a partial purification of non-tagged CcLpxI, we present here a robust purification scheme making use of TEV-protease cleavable N-terminally $(His)_{10}$-tagged CcLpxI. Our purification protocol allows us to purify CcLpxI from *E. coli* on a 50-100 mg scale to near-homogeneity, with a 68% activity yield (Table 3.3 and Figure 3.1). Moreover, we show that CcLpxI purified by this method has an apparent specific activity similar to that of the wild-type protein purified in Chapter 2.

To determine whether phospholipids co-purify with CcLpxI, we extract the pure protein and subjected it to ESI-MS analysis. To our surprise, we find that lipid X, the product of CcLpxI, co-purifies with the enzyme (see Figure 3.2). We isolate $(His)_{10}$-tagged CcLpxI from *E. coli* that were grown in the presence of ^{32}P, and thereby calculate a lipid X to CcLpxI ratio of 0.95. We analyze the phospholipid composition of ^{32}P-labelled *E. coli* in which CcLpxI was over-expressed, and find that lipid X is enriched > than 50-fold relative to the vector control (see Table 3.4 and Figure 3.3). We also observe that CcLpxI over-expression causes a nearly 3-fold decrease in the percentage of phosphatidylglycerol (PG), suggesting that the presence of excess lipid X in the membranes substitutes for that anionic phospholipid.

We conduct alanine-scanning mutagenesis of a subset of CcLpxI's absolutely conserved residues: Q169, E182, E185, T187, Q220, and D225, and express these mutants in *E. coli*. We then prepare membrane-free lysates from *E. coli* that over-express these mutants, and measure these lysates' UDP-2,3-diacylglucosamine hydrolase activities *in vitro* (see Table 3.6). CcLpxI-Q169 does not express robustly, not does it have activity above background levels (see Figure 3.4 and Table 3.6). While CcLpxI-Q169 appears to be proteolyzed *in vivo* (see Figure 3.4), it has activity 5-fold greater than the background levels. CcLpxI-E182A, CcLpxI-T187A, CcLpxI-Q220A,

and CcLpxI-D225A express at levels similar to wild-type CcLpxI (Figure 3.4). Of these, only *E. coli* lysate containing CcLpxI-E185A has activity greater than ~2-fold background (see Table 3.6).

Since CcLpI co-purifies in a nearly 1:1 ratio with its product, we hypothesized that catalytically-deficient mutant(s) might sequester UDP-2,3-diacylglucosamine, and that this enzyme-bound substrate accumulation might be observable in whole cells. To test this, we perform LC-MS/MS analysis upon total lipid extracts of *E. coli* over-expressing wild-type or mutant CcLpxI. As a control, we first look for lipid X in these total cell extracts, and we observe significant accumulation in strains harboring wild-type CcLpxI, CcLpxI-E185A, CcLpxI-T187A, and a small accumulation in LpxI-D225A (see Figure 3.5). When we monitor UDP-2,3-diacylglucosamine, we only observe it in CcLpxI-D225A (see Figure 3.6), a finding confirmed by MS/MS (see Figure 3.7).

We purify CcLpxI-D225A to near-homogeneity (see Figure 3.9), attaining a total protein yield comparable to that of the wild-type enzyme. We follow CcLpxI-D225A protein during its purification by TLC and A_{260}, monitoring the co-purifying UDP-2,3-diacylglucosamine (Figure 3.9). Moreover, we show by LCMS that total lipid extracts of this purified construct contain UDP-2,3-diacylglucosamine (see Figure 3.8). By comparing the A_{260} of CcLpxI to that of equally-concentrated CcLpxI-D225A, we estimate a UDP-2,3-diacylglucosamine to CcLpxI-D225A stoichiometry of 0.85 ± 0.05.

The implications of this work are manifold. By developing a robust purification method for CcLpxI, we facilitate future mechanistic studies of this unique hydrolase. Moreover, our finding that CcLpxI co-purifies in a nearly 1:1 stoichiometry with lipid X puts it in the company of relatively few characterized enzymes (*192*). Since most enzymes are designed to release their product, it is possible that UDP-2,3-diacylglucosamine hydrolysis is required for the release of lipid X by CcLpxI. This hypothesis may be addressed in the future by washing immobilized CcLpxI with compounds including UDP, UDP-glucosamine, lipid X, UDP-2,3-diacylglucosamine, phospholipids, and detergents, to determine which of these can displace lipid X. To determine

whether the UDP-2,3-diacylglucosamine sequestered by CcLpxI is transiently released (*193*), purified CcLpxI and CcLpxI-D225A will be mixed, and time-dependent change in this mixture's ratio of lipid X to UDP-2,3-diacylglucosamine will be monitored.

The striking accumulation of UDP-2,3-diacylglucosamine, a minor but essential *E. coli* phospholipid, exemplifies the enourmous perturbations possible in high-flux metabolic pathways. In wild-type *E. coli*, the steady-state level of UDP-2,3-diacylglucosamine has been estimated to be ~400 molecules per cell (*136*). In *E. coli* which over-produce CcLpxI-D225A, we observe UDP-2,3-diacylglucosamine accumulation which may exceed 10% of the cells' total lipid composition. This represents a 500-fold increase over steady-state levels of this metabolite. A practical application of this finding may be the facile isolation of UDP-2,3-diacylglucosamine from whole cells, for use with in the study of LpxB, another lipid A biosynthetic enzyme (*136*).

As many enzymes are stabilized in the presence of their substrates or products, complexes are especially amenable to crystallographic characterization (*194*). By obtaining 50-mg quantities of CcLpxI (with bound lipid X) and CcLpxI-D225A (with bound UDP-2,3-diacylglucosamine), we are poised to embark upon crystallographic trials. To our knowledge, CcLpxI and its orthologues are not homologous to any other known proteins. The present study provides a basis for future biochemical and structural characterization of this unique family of metal-dependent UDP-diacylglucosamine hydrolases.

4. Crystallization and initial structural characterization of *Caulobacter crescentus* LpxI and its D225A mutant

4.1 Introduction

In Chapter 3, we demonstrate that the bacterial UDP-2,3-diacylglucosamine hydrolase CcLpxI co-purifies with its product, lipid X. Moreover, we identify a point mutant, CcLpxI-D225A, which co-purifies with its substrate. In this chapter, we present the crystal structures of wild-type CcLpxI in complex with its product, lipid X, solved to 2.6 Å, and of CcLpxI-D225A, solved to 3.0 Å. We show that CcLpxI represents a novel, two-domain protein fold. The N-terminal domain, which binds to lipid X, represents one of only a dozen lipid binding domains described to date (*195, 196*). Comparison of the CcLpxI and CcLpxI-D225A structures reveals large conformational differences, consistent with a model wherein the two domains come together to form a UDP-2,3-diacylglucosamine binding and/or catalytic site. Sedimentation equilibrium experiments show both CcLpxI and CcLpxI-D225A to exist as dimers in solution. Moreover, these two constructs are shown to have different sedimentation coefficients, a finding that is consistent with the domain re-arrangements observed in their crystal structures. The work described herein sets the stage for further structural and mechanistic study of this unique hydrolase.

4.2 Materials and Methods

4.2.1 Molecular Biology

Plasmids pD225A-TEV and pCcLpxI-TEV (see Chapter 3, Table 3.1) were transformed into chemically-induced competent *E. coli* B834(DE3) cells (Novagen) according to the manufacturer's protocols. The resulting strains were named B834(DE3)/pD225A-TEV and B834(DE3)/pCcLpxI-TEV. Strain B834(DE3) is a methionine auxotroph (REF), and is therefore suitable for the expression of selenomethionine (Se-Met) labeled protein. Unless otherwise noted, the preceding strains were grown in the presence of 100 μg/ml ampicillin, and expression was induced with 0.25 mM IPTG.

4.2.2 Expression and Purification of CcLpxI and CcLpxI-D225A

Strain B834(DE3)/pD225A-TEV or B834(DE3)/pCcLpxI-TEV was freshly transformed and re-purified on LB-agar plates supplemented with 100 μg/ml ampicillin. A modified version of the defined medium PASM-5052 (*197*), hereafter designated PASM-5052Met, was prepared. Modifications to PASM-5052 included the elimination of glycerol and lactose from the media, and the inclusion of 0.5% w/v glucose and of methionine (Met) to 25 μg/ml. Briefly, PASM-5052Met consisted of 50 mM Na_2HPO_4, 50 mM KH_2PO_4, 25 mM $(NH_4)2SO_4$, 2 mM $MgSO_4$, trace metals (consisting of $CaCl_2$, $MnCl_2$, $ZnSO_4$, each 1 mM; $CoCl_2$, $NiCl_2$, each 200 μM; $FeCl_3$, $CuCl_2$, Na_2MoO_4, $Na_2Se_2O_3$, H_3BO_3, each 100 μM), 0.5% w/v glucose, 200 μg/ml of each amino acid except Cys, Tyr, and Met, 25 μg/ml native Met, and 125 μg/ml SeMet, and 100 μg/ml ampicillin. The Met was added to the media immediately before use, while the SeMet was added ~15 minutes prior to induction. The media was sterilized by passage through a 0.2 μm filter before use. Single colonies of B834(DE3)/pD225A-TEV or B834(DE3)/pCcLpxI-TEV were used to inoculate a 25 ml overnight culture, consisting of PASM-5052Met wherein the SeMet was replaced by Met. After growth at 30°C for ~18 hours at 220 RPM, 20 ml of the overnight culture was used to inoculate 4 L of PASM-5052 (5 ml inoculum/liter). The strain was grown at 30°C and aerated at 220 RPM until it reached an OD_{600} of ~0.7, whereupon the medium was supplemented to 125 μg/ml SeMet by adding 25 ml of a 20 mg/ml stock. The cells were grown for an additional 15 minutes, to an OD_{600} of ~0.9, prior to induction with 0.25 μM IPTG. The strains were induced for ~5 hours at 30°C/220 RPM. The cells were washed and harvested as described in section 3.2.3.

The purification of CcLpxI from B834(DE3)/pCcLpxI-TEV or of CcLpxI-D225A from B834(DE3)/pCcLpxI-TEV was performed as previously described (see section 3.2.3). Following purification, the constructs were concentrated to 20-30 mg/ml and stored in aliquots at -80°C. The

extent of SeMet incorporation was assessed by ESI mass-spectrometry, monitoring in the positive mode (*198*), and purity was assessed by SDS-PAGE.

4.2.4 Crystallization of CcLpxI

A Phoenix crystallization robotic system (Art Robbins Instruments, LLC.) was used to screen native, purified CcLpxI (see section 3.2.3) against several commercial screens. These were performed by sitting-drop vapor diffusion in 96-well Intelliplate-3 (Art Robbins Instruments, LLC.) plates. Typically, ~50 μL of screening solution was aliquoted into each well, while 1 μL sitting drops, consisting of CcLpxI and screening solution, were mixed at either 2:3, 1:1, or 3:2 v/v ratios. The protein buffer consisted of 20 mM HEPES pH 8.0 and 200 mM NaCl; CcLpxI having a concentration between 20 and 30 mg/ml was used. Screens were conducted at 4°C and 20°C, in the presence or absence of 5 mM UMP, 1-5 mM $MgCl_2$, or 1-10 mM $MnCl_2$. Initial crystallization conditions were identified from the Qiagen PACT II and III screens (Qiagen), incubated at 4°C, with protein to screening buffer ratios of 1:1 to 3:2 v/v. These initial crystals, which arose in 3-10 days, formed in the presence of polyethylene glycols (PEGs) having 400-10,000 dA average molecular weights, and slightly acidic buffer (pH 5.5-6.8). None of the 4°C hits were transferable to 20°C. Optimization of initial CcLpxI crystals was accomplished by varying PEG type and concentration, buffer type and pH, and by the addition of cryo-protectants (ethylene glycol, glycerol, and PEG400) to the screening solution. We identified the following optimal crystallization conditions for native CcLpxI: 10 μL mixed drops of CcLpxI (20-30 mg/ml) and well solution, were set up in a ratio of 7:3 v/v over reservoirs of 0.5 ml well solution in 24-well Chryschem plates (Hampton Research, Inc). The well solution consisted of 100 mM MES pH 5.7, 3-7% w/v PEG 6000, and 2.5% v/v glycerol. Trays were set up at room temperature (using room-temperature well solution and CcLpxI), sealed with Crystal Clear Sealing Tape (Hampton Research, Inc.), and allowed to equilibrate at 4°C. Crystals, with typical dimensions of ~200 x 200 x 400 μm, formed

between 1 and 3 days, and continued to grow for 5-7 days. CcLpxI incorporating SeMet, purified as described above, was crystallized in conditions identical to those of the native enzyme.

4.2.5 Cryo-protection of CcLpxI crystals

A cryo-protection scheme was developed; its efficacy was assessed by screening cryo-protected crystals for their ability to diffract x-rays when frozen in a -170°C liquid nitrogen stream, and subjected to a 1.54 Å x-ray beam using a rotating-anode R-Axis IV++ source (Rigaku, Inc.). Because they were initially too fragile to harvest with nylon cryo-loops (Hampton Research, Inc.), CcLpxI crystals were cryo-protected and vitrified by incubation in pre-chilled, 4°C cryo-protection buffer, consisting of 47 mM HEPES pH 8.0, 100 mM MES, pH 5.7, 500 mM NaCl, 7% w/v PEG 6000, and 5-40% v/v glycerol (increasing in 5% w/v steps). All steps of cryo-protection were carried out at 4°C. Crystals were allowed to remain in their 10 μL sitting drops, while a pipette was used to carefully remove 5 μL from each. This was then replaced with an equal volume (5 μL) of cryo-protection buffer containing 5% v/v glycerol. Following an incubation of at least 10 minutes, this step was repeated with another 5 μL of cryo-protection buffer containing 5% v/v glycerol. The procedure was then iterated, with half of the well volume being replaced twice for each 5% v/v increase in glycerol, up to 40%. The crystals were harvested with appropriately-sized nylon loops, frozen by immersion in liquid nitrogen, and stored in polypropylene cryo-vials (Hampton Research, Inc). CcLpxI incorporating SeMet, crystallized as described above, was cryo-protected in conditions identical to those of the native enzyme.

4.2.6 Crystallization of CcLpxI-D225A

CcLpxI-D225A was screened for initial crystallization conditions, both manually and with the aid of a Phoenix robotic system (Art Robbins Instruments, LLC.). Vapor diffusion screens were set up at both 4°C and 20°C, with varying ratios of protein to well-solution. Initial crystallization conditions were identified in which $(NH_4)_2SO_4$, typically at concentrations of 1.2-1.8 M, was the precipitant, while other well-solution components, including buffer, pH, and ionic strength, were varied.

Optimal crystals were grown in 24-well plates, at 20°C, by hanging-drop vapor diffusion. The well solution consisted of 100 mM Tris pH 7.5, 180 mM NaCl, 1.3 M $(NH_4)_2SO_4$, and 6% v/v glycerol. Drops, typically consisting of 2:1 or 3:1 v/v ratios of CcLpxI-D225A to well solution, were prepared on glass cover-slips and suspended over 0.75 ml well solution. Large crystals, often exceeding 500 μm in one direction, appeared in 1-2 days at 20°C, and continued to grow for another 3-5 days. CcLpxI-D225A incorporating SeMet, purified as described above, was crystallized in conditions identical to those of the Met-containing enzyme.

4.2.7 Cryo-protection of CcLpxI-D225A crystals

The cryo-protection buffer was identical to the CcLpxI-D225A well solution (100 mM Tris pH 7.5, 180 mM NaCl, 1.3 M $(NH_4)_2SO_4$, and 6% v/v glycerol), except that it contained 20% v/v glycerol. An equal volume of this buffer was added to an equilibrated drop containing crystals, and allowed to incubate at room temperature for 2-5 minutes. A nylon loop of the appropriate diameter was then used to transfer a crystal into a 1 μL drop of cryo-protection solution. Upon transfer, crystals were incubated for ~ 1 minute, and then flash-frozen in liquid nitrogen as described above. CcLpxI-D225A incorporating SeMet, crystallized as described above, was cryo-protected in conditions identical to those of the Met-containing enzyme.

4.2.9 Data Collection and Refinement

For both CcLpxI and CcLpxI-D225A, native data sets were collected at the Advanced Light Source, Beamline 8.3.1, under a -170°C nitrogen cryo-stream. Native crystals of CcLpxI and CcLpxI-D225A diffracted to 2.6 and 3.0 Å, respectively. For phasing, single-wavelength anomalous diffraction (SAD) and multiple-wavelength anomalous diffraction (MAD) datasets were collected for Se-Met derivatives of CcLpxI and CcLpxI-D225A, MAD datasets were collected at the Se absorption peak, while three-wavelength MAD datasets were obtained at the near, peak, and far Se adsorption edges. These datasets diffracted to 2.8 and 3.3 Å, respectively. Data

collection strategies were calculated using Elves (*199*). Data indexing and scaling was accomplished using HKL2000.

Phenix Solver (*200*) was used to determine the initial phases for the CcLpxI and CcLpxI-D225A datasets. Following solvent flattening, 6 discrete Se sites were identified for CcLpxI, while 5 were identified for CcLpxI-D225A. Using Phenix (*200*), phases determined from the Se-Met derivatives were used to solve native data sets. Model building was performed using Coot (*201*), while Phenix (*200*) and Refmac5 (*202*) were used for refinement. For all datasets, 5% of the reflections were excluded from refinement, to allow for the calculation of R_{free} values. MolProbity (*203*) was used for structural validation between iterations of refinement. Structures were visualized with PyMOL (*73*), and Chimera (*204*). These programs were also used for surface area, distance, and coulombic surface calculations. Model-building and refinement are ongoing.

4.2.10 Analytical ultracentrifugation

Sedimentation equilibrium experiments were used to estimate the molecular weights of purified CcLpxI and CcLpxI-D225A. Samples were prepared by diluting concentrated protein stocks into their storage buffer (20 mM HEPES pH 8.0, 200 mM NaCl). For each construct, concentrations of 1, 2, and 3 mg/ml were each centrifuged at 8,060, 18,150, and 201,600 x *g*, in a Beckman An-60Ti rotor, using a Beckman Optima XL-A analytical ultracentrifuge. Centrifugation was performed at 20°C. Samples were paired with reference cells containing buffer identical to that which with they were diluted. Absorbance was monitored at 240 nm. The program SEDNTERP was used to calculate the buffer density (ρ = 1.0088), and the amino acid sequence of CcLpxI was used to calculate its partial specific volume (υ_{bar} = 0.7371). Best-fit buoyant molecular weight (MW^b) was estimated using the XL-A XLI-1 software suite, from which molecular weight was calculated from the equation: $MW = MW^b/(1-\upsilon_{bar}\rho)$ (*205-207*).

Sedimentation velocity experiments were used to determine the sedimentation coefficients of CcLpxI and CcLpxI-D225A. The proteins were diluted, as above, to 0.7, 1.4, 2.1,

2.6, and 3.1 mg/ml. These samples, paired with reference cells containing the protein buffer, were centrifuged at 2900 x *g* in a Beckman An-60Ti rotor using a Beckman Optima XL-A analytical ultracentrifuge. For CcLpxI, absorbance was monitored at 245 nm, while CcLpxI-D225A was monitored at both 245 and 260 nm. Data were processed using ProteoLab XL-A software, and weight-average sedimentation coefficients (*s*) were determined by second-moment integration of the sedimentation absorbance profiles between the meniscus and solution plateaus (*208*).

4.3 Results

4.3.1. Expression and purification of Se-Met derivatized CcLpxI and CcLpxI-D225A

The over-expression of Se-Met derivatized CcLpxI and CcLpxI-D225A, as judged by SDS-PAGE, was similar to that of the native proteins (compare Figure 4.1 to Figure 3.1). Purification of both constructs proceeded identically to the wild-type, and gave similar yields. The amount of LpxI purified from 1L of *E. coli*, grown as described above, was typically 20-30 mg.

4.3.2. Crystallization and cryo-protection of CcLpxI

Native and Se-derivatized CcLpxI were crystallized and cryo-protected in identical conditions. Mixed drops of CcLpxI (20-30 mg/ml) and well solution, were set up in a ratio of 7:3 v/v in sitting-drop vapor-diffusion chambers. The well solution consisted of 100 mM MES pH 5.7, 3-7% w/v PEG 6000, and 2.5% v/v glycerol. Crystals, with typical dimensions of ~200 x 200 x 400 μm, formed at 4°C in between 1 and 3 days, and continued to grow for 5-7 days. Typically, the crystals were rectangular pyramids and bi-pyramids (see Figure 1, panels A and B). This crystallization condition was robust, and was reproducible with reagents from different suppliers.

Crystals of CcLpxI were fragile, and disintegrated when touched with nylon loops or other crystal-harvesting implements. Therefore, CcLpxI was cryo-protected *in situ*, as described above, by gradually exchanging the sitting-drop buffer with glycerol-containing cryo-protection solutions,

until a final concentration of 40% v/v glycerol was achieved. During cryo-protection, the dimensions of the crystals decreased slightly, as expected for a vitrification process. In concentrations of glycerol greater than 30% v/v, the CcLpxI crystals could be manipulated without damaging them. While other cryo-protectants were tested, including PEG400, xylitol, MPD, and ethylene glycol, screening revealed that optimal X-ray diffraction could be obtained by cryo-protection with buffers containing 40% v/v glycerol.

While most crystal screening and optimization was performed with CcLpxI that had been purified to near-homogeneity (see Chapter 3), protein of ~90% purity, isolated as described in Chapter 2, crystallized readily under these conditions. To determine whether the protein crystals were CcLpxI, a number of crystals, grown with ~90% pure enzyme stock, were washed extensively by buffer exchange during the *in situ* cryo-protection process. The washed crystals were then dissolved in 2% SDS for 40 minutes at 42°C, and analyzed by SDS-PAGE. This experiment (see Figure 4.1, panel E) revealed a band consistent with the molecular mass of CcLpxI to be present in all crystals that were analyzed. Moreover, crystallization served as an effective purification method (see Figure 4.1 panel E).

4.3.3. Crystallization and cryo-protection of CcLpxI-D225A

Native and Se-derivatized CcLpxI-D225A were crystallized and cryo-protected in identical conditions. Optimal crystals were grown at 20°C, by hanging-drop vapor diffusion. The well solution consisted of 100 mM Tris pH 7.5, 180 mM NaCl, 1.3 M $(NH_4)_2SO_4$, and 6% v/v glycerol. Large crystals, in the form of hexagonal prisms and spears, often exceeded 500 μm in length (see Figure 4.1, panels C and D). Crystals appeared in 1-2 days, and continued to grow for another 3-5 days. This crystallization condition was robust, and was reproducible with reagents from different suppliers.

In contrast to CcLpxI, CcLpxI-D225A crystals were not very fragile, and could be easily harvested using nylon loops. As CcLpxI-D225A crystals were grown in 6% v/v glycerol, cryo-protection, as described above, was facile.

4.3.4. Data collection and refinement

Diffraction data were collected at the Advanced Light Source, Beamline 8.3.1, under a -170°C nitrogen cryo-stream. For CcLpxI, the highest-resolution dataset was 2.6 Å. (see Table 4.1). As no homologues existed with which to phase CcLpxI, SAD datasets were collected on Se-Met derivatized crystals at the Se adsorption peak. The highest resolution Se-Met crystals diffracted to 2.6 Å. Phases were determined by MAD, as described above. The experimentally determined model of Se-Met CcLpxI was then used to phase the 2.6 Å dataset of native CcLpxI by molecular replacement (MR). The current R_{crys} for the 2.6 Å dataset is 23.2%, while the R_{free} is 28.6%. The refinement statistics from both datasets are summarized in see Table 4.1. Refinement of the 2.6 Å structure is still ongoing, and the listed data are provisional.

For CcLpxI-D225A, the highest-resolution dataset was 3.0 Å. (see Table 4.1). While we had the option of using CcLpxI to phase CcLpxI-D225A by molecular replacement, we felt that this would introduce unacceptable model bias, especially if the two domains of the two constructs were in radically different orientations. We therefore determined CcLpxI-D225A phases experimentally. SAD and MAD datasets were collected on Se-Met derivatized crystals at the Se adsorption peak, near, and far edges. The highest resolution Se-Met dataset diffracted to 3.0 Å. Phases were determined by MAD, as described above. The current R_{crys} for the 2.6 Å dataset is 30.0%, while the R_{free} is 42.5%. The refinement statistics from both datasets are summarized in Table 4.1. Refinement of the 3.0 Å structure is still ongoing, and the listed data are very preliminary.

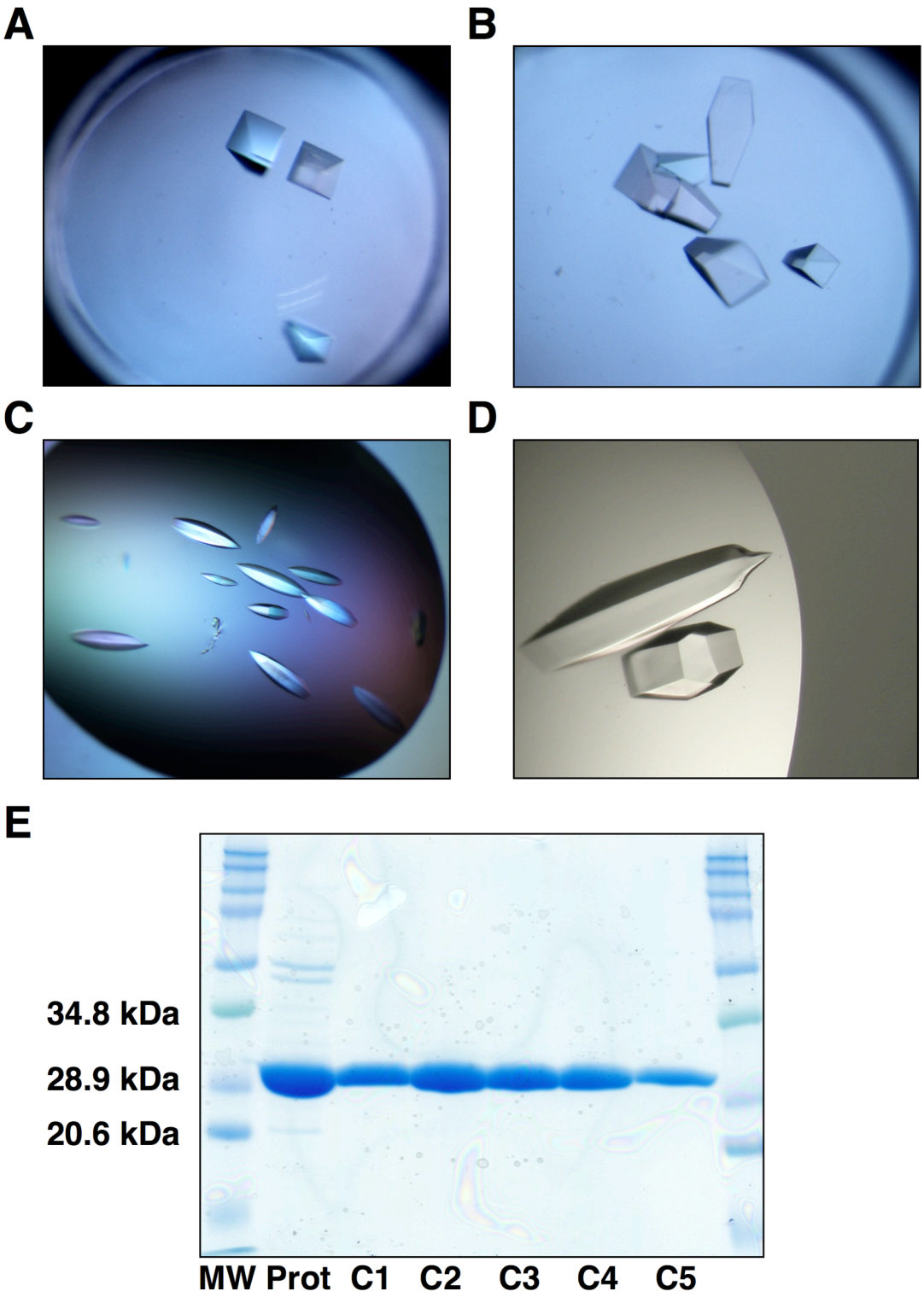

Figure 4.1. Crystallization of CcLpxI and CcLpxI-D225A.

Figure 4.1. Crystallization of CcLpxI and CcLpxI-D225A. Panels A and B depict crystals of CcLpxI, grown by sitting-drop vapor-diffusion at 4°C, in a 7:3 v/v ratio of purified CcLpxI (20 mg/ml) and well solution consisting of 100 mM MES pH 5.7, 3-7% w/v PEG 6000, and 2.5% v/v glycerol. Crystals, with typical dimensions of ~200 x 200 x 400 μm, formed between 1 and 3 days, and continued to grow for 5-7 days. Panels C and D depict crystals of CcLpxI-D225A, grown by hanging-drop vapor diffusion at 20°C, in a 2:1 v/v ratio of purified CcLpxI (30 mg/ml) and well solution consisting of 100 mM Tris pH 7.5, 180 mM NaCl, 1.3 M $(NH_4)_2SO_4$, and 6% v/v glycerol. Crystals appeared in 1-2 days, and continued to grow for another 3-5 days. Panel E shows a Coumassie-stained 12% polyacrylamide gel from an SDS-PAGE experiment in which washed crystals of CcLpxI were heat-denatured and separated by mass. "MW" denotes the molecular weight standard, "Prot" indicates ~90% pure CcLpxI, and lanes "C1-C5" are five separate crystals grown from that protein stock.

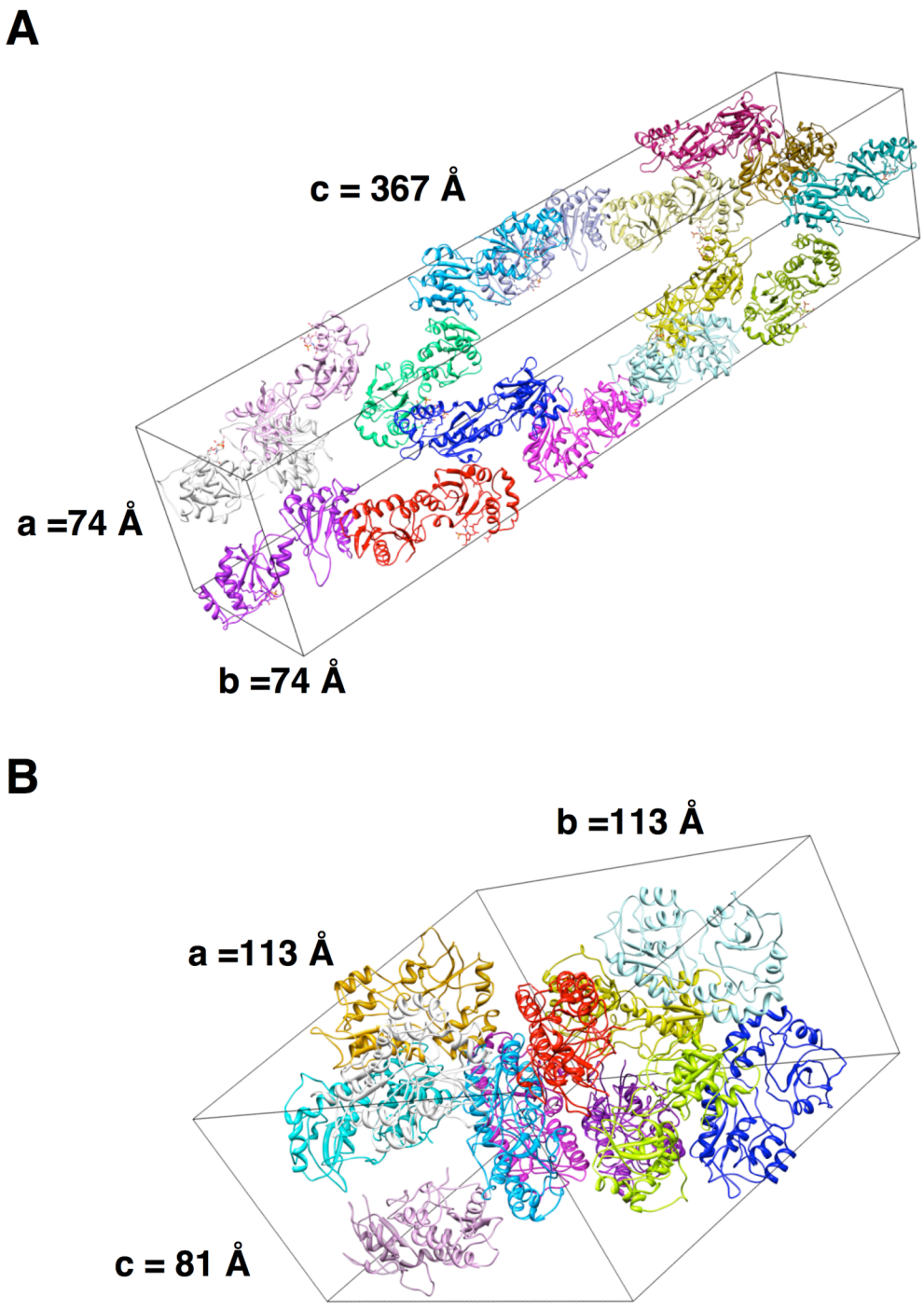

Figure 4.2. Unit cells of CcLpxI and CcLpxI-D225A.

Figure 4.2. Unit cells of CcLpxI and CcLpxI-D225A. Panel A shows the unit cell of CcLpxI crystals. The unit cell dimensions are a = 74, b = 74, c = 367 Å, where $\alpha = \beta = \chi = 90°$. Each asymmetric unit consists of one CcLpxI molecule, while unit cell contains 16 CcLpxI monomers (shown here in ribbons, each rendered in a different color). Panel B shows the unit cell of CcLpxI crystals. The unit cell dimensions are a = 113, b = 113, c = 81 Å, where $\alpha = \beta = 90°$, and $\chi = 120°$. Each asymmetric unit contains 1 CcLpxI-D225A molecule, while each unit cell contains 12 CcLpxI-D225A monomers.

Figure 4.3. CcLpxI topology diagram

Figure 4.3. CcLpxI topology diagram. In the top portion of the figure, CcLpxI is represented by a topology diagram. Flat arrows are β-sheets and cylinders are α-helices. Arrows show the N-terminal to C-terminal connectivity. Structural elements colored in blue belong to the "Lipid X Binding Domain" (LXD), while the "LpxI Catalytic Domain" (ICD) is colored orange. The domains are joined by an α-helical linking region, which is colored dark green. In the lower portion of the figure, the sequences of five LpxI orthologues are aligned. Residue numbering corresponds to the *Caulobacter cresentus* LpxI peptide sequence. Colored boxes, representing elements of CcLpxI secondary structure, are aligned with the CcLpxI sequence. Absolutely conserved residues are colored red, and highlighted in yellow. CcLpxI residues containing atoms within 4 A of lipid X (in the wild-type CcLpxI structure) are highlighted in light green; corresponding residues in other orthologues are underlined.

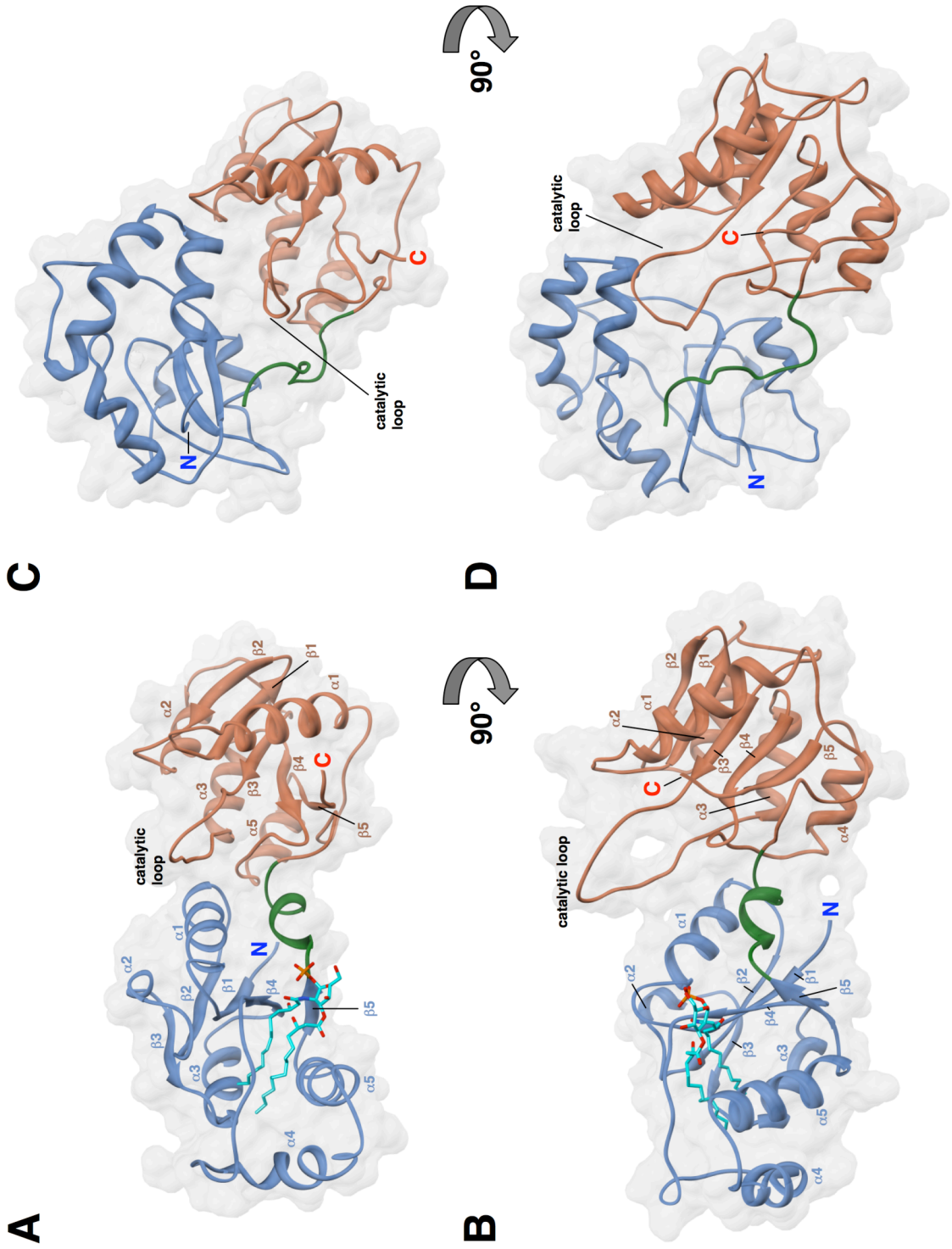

Figure 4.4 Ribbon diagrams of CcLpxI and CcLpxI-D225A

Figure 4.4. Ribbon diagrams of CcLpxI and CcLpxI-D225A. The overall structures of CcLpxI and CcLpxI-D225A are shown in the same color scheme as Figure 3: the LXD is shown in blue, the ICD in orange, and the linking peptide as dark green. Panels A and B show two orientations of CcLpxI with its product, lipid X (in teal), bound to the LXD. Panels C and D show CcLpxI-D225A in similar orientations. In all panels, the ICD domains of CcLpxI and CcLpxI-D225A are orientated such that they overlay. We can therefore see the relative difference in LXD position between CcLpxI (panels A and B) and CcLpxI-D225A (panels C and D). In panels A and B, elements of secondary structure are lableled in colors corresponding to their domain. In all panels, the N and C termini are indicated with blue and red "N" and "C," respectively. The relative position of the "catalytic loop," which lies between α3 and β3 of the ICD, is indicated.

Table 4.1 Data collection and refinement statistics

	LpxI SeMet	LpxI Native	LpxI-D225A SeMet	LpxI-D225A Native
Crystal data				
Space Group	$I4_122$	$I4_122$	$P6_122$	$P6_122$
Unit Cell (Å)	a = 74.66,	a = 74.38	a = 112.73	a = 112.97
	b = 74.66	b = 74.38	b = 112.73	b = 112.97
	c = 366.09	c = 367.701	c = 81.288	c = 81.35
z[a]	1	1	1	1
X-Ray data collection statistics				
Wavelength (Å)	0.9796	1.11	0.9796	1.11
Resolution (Å)	50 – 2.8	50.0 – 2.60	37.5-3.0	48.9-3.0
Total reflections	1,050,618	424,267		
Unique reflections	23,929	15,522	6464	6485
Completeness (last shell) (%)[b]	94.2 (56.55)	99.68 (51.70)	99.69 (37.52)	98.00 (48.9)
R_{merge} (last shell)	9.0 (63.4)	5.4 (61.7)		
I/σ (last shell)	17.8 (3.18)	41.46 (3.86)		
Phasing statistics				
Method	SAD	MR	MAD	MR
Figure of Merit	0.40			
FOM after solvent flattening	0.68			
Refinement statistics				
R_{cryst}, %[c]		23.2		30.0
R_{free}, %[c]		28.6		42.5
Mean B-factors, Å^2		99.9		99.9
rmsd bonds, Å		0.011		0.011
rmsd angles, °		1.44		1.73
Ramachandran plot outliers, %				

[a] z is the number of equivalent structures per asymmetric unit

[b] $R_{merge} = \Sigma | I_{hkl} - < I_{hkl} > | / \Sigma I_{hkl}$, where I_{hkl} is the measured intensity of hkl reflection and $<I_{hkl}>$ is the mean of all measured intensity of hkl reflection

[c] $R_{cryst} = \Sigma_{hkl} | |F_{obs}| - |F_{calc}| | / \Sigma_{hkl} |F_{obs}|$, where F_{obs} is the observed structure factor amplitude and F_{calc} is the structure factor calculated from model. R_{free} is computed in the same manner as is R_{cryst}, with the test set of reflections (5%).

4.3.5. Overall structures of CcLpxI and CcLpxI D225A

CcLpxI (both native and Se-Met derivatized) crystallized in the tetragonal space-group $I4_122$. The unit cell had the following dimensions: a = 74, b = 74, c = 367 Å, where $\alpha = \beta = \chi = 90°$. Each asymmetric unit contained one CcLpxI molecule. Each unit cell contained 16 CcLpxI monomers (see Figure 4.2, panel A). A Matthew's coefficient (V_m) (*208*) was calculated to be 2.45 $Å^3$/Da (72.17 % solvent). The unusually high solvent content of the CcLpxI crystals may account for their fragility prior to vitrification. CcLpxI-D225A (both native and Se-Met derivatized) crystallized in the hexagonal space-group $P6_122$. The unit cell had the following dimensions: a = 113, b = 113, c = 81 Å, where $\alpha = \beta = 90°$, and $\chi = 120°$. Each asymmetric unit contained 1 CcLpxI-D225A molecule, while each unit cell contained 12 CcLpxI-D225A monomers (see Figure 2, panel B). The V_m was 2.58 $Å^3$/Da (52.39 % solvent).

CcLpxI has two domains, connected to each other by a linker region (see Figures 4.3 and 4.4). The N-terminal domain (residues 1 through 120) is comprised of 5 α-helices and 5 β-sheets. With the exception of helices α4 and α5, the α-helices and β-sheets alternate. Hereafter, this N-terminal domain is referred to as the "lipid X binding domain" (LXD). The lipid X binding pocket is comprised of β-sheets 1-5 on one side, and by α-helices 3-5 on the other side (see Figures 4.3 and 4.4). A linking region (residues 124-144), containing an α-helix, connects the LXD to the C-terminal domain of CcLpxI. This second domain (residues 144-280) is comprised of 4 α-helices and 5 β-sheets. Except for sheets β1 and β2, the α-helices and β-sheets alternate (see Figures 4.3 and 4.4). Hereafter, this C-terminal domain is referred to as the "LpxI catalytic domain" (ICD). The ICD contains absolutely-conserved residues, shown in Chapter 3 to be necessary for catalysis. Three of these residues, Q220, D225, and R223, are present on a loop between ICD β3 and α3 (see Figures 4.3 and 4.4). This loop, stretching from P216 to P227, and hereafter designated the "catalytic loop," is labeled in Figure 4. Based upon three-dimensional structural homology searches (*209*), both domains of CcLpxI appear to be a novel protein folds.

4.3.6. Backbone comparison CcLpxI and CcLpxI-D225A

The LXD's of CcLpxI and CcLpxI-D225A can be superimposed with respect to their Cα backbones with an RMSD of 1.064 Å. A similar alignment of these constructs' ICD's yields an RMSD of 0.728 Å (see Figure 4.5). When full-length CcLpxI and CcLpxI-D225A are aligned with respect to either their LXD or CID, a striking conformational difference is revealed. Taking an alignment about the ICD, we observe a large reorientation of the LXD. As shown in Figure 4.5 (panels A and B), the entire LXD is rotated 72° in the x/y plane, and 78° in the y/x plane. While the LXD and ICD of each structure retain their basic folds, linking helix in CcLpxI is stretched into a loop in the CcLpxI-D225A mutant.

4.3.7 Ligand binding in CcLpxI

Analysis of the CcLpxI electron density maps revealed density into which enzyme backbone and side-chains could not be readily fit (see Figure 4.6, panel A). Further refinement allowed for the modeling of lipid X into this density. Chimera (*209*) was used to determine which CcLpxI residues contained atoms within 4 Å of the modeled ligand. These residues (Figure 4.6, panel B), include L33, V49, I51, F54, I57, F71, A72, V75, S76, P78, L96, D104, D105, L107, V111, and F115. Not surprisingly, most of the lipid X binding pocket surface (Figure 4.6, panels D and E) is comprised of hydrophobic side-chains. The surface are of this binding pocket was calculated to be ~ 490 $Å^2$.

4.3.8 Putative ligand electron density in CcLpxI-D225A

Although analysis and refinement of the CcLpxI-D225A model is ongoing, we observe density in addition to that expected for the protein (see Figure 4.7, panels A, B and C). Some of this density is present in the LXD, and is surrounded by lipid X binding-pocket residues F54, F71, and F115. A large region of unassigned positive density (green mesh) is observed near the ICD,

immediately beneath the labeled D225A residue. This density is nearby absolutely-conserved residues, as shown in Figure 7, panel B.

4.3.9 Comparison of LXD and ICD residues in CcLpxI vs. CcLpxI-D225A

The LXD's of CcLpxI vs. CcLpxI-D225A are reasonably superimposable (RMSD with respect to Cα atoms of 1.064 Å). When overlaid, the lipid X binding residues retain similar conformations in both CcLpxI and CcLpxI-D225A (see Figure 4.8). In contrast, larger intra-domain differences exist in these constructs' ICD's (see Figure 4.9). While the absolutely-conserved residues nearest to the putative ligand density (Q169, T187, E182, E185, R193, K214, and T233) are positioned similarly in both models (see Figure 4.9), other residues, including D166 and the catalytic loop residues Q220, R223, and D225) have moved. The largest translational differences, as judged by Cα distances, were found in CcLpxI vs. CcLpxI-D225A residues D166 and Q220. The former was displaced 5 Å, the latter by 4.2 Å. The movement of Q220 is indicative of an overall hinging of the catalytic loop in CcLpxI-D225A relative to CcLpxI (see Figure 4.9, panel D).

4.3.10. Modeling surface charges of CcLpxI and CcLpxI-D225A molecules

A Coulombic surface was modeled onto both CcLpxI and CcLpxI-D225A (see Figure 4.10). The models predicted predominantly anionic surfaces for both molecules. In general, few patterns were apparent. An exception was for CcLpxI (see Figure 4.10, panel A, "top" and "bottom" views), where one side of the molecule ("bottom") was predicted to be significantly more positively charged than the other ("top") side.

4.3.11. Analytical ultracentrifugation

The apparent molecular masses of purified CcLpxI and CcLpxI-D225A were measured by sedimentation equilibrium as described in section 4.2. For CcLpxI, two separate experiments yielded apparent molecular masses of 58.9 and 56.9 kDa. For CcLpxI-D225A, two experiments yielded masses of 63.7 and 57.0 kDa.

The sedimentation coefficient of CcLpxI, *s* was measured to be 3.56 ± 0.11 svedbergs (n = 5). For CcLpxI-D225A, *s* = 3.85 ± 0.09 (n = 5), a statistically significant increase relative to the coefficient measured for CcLpxI.

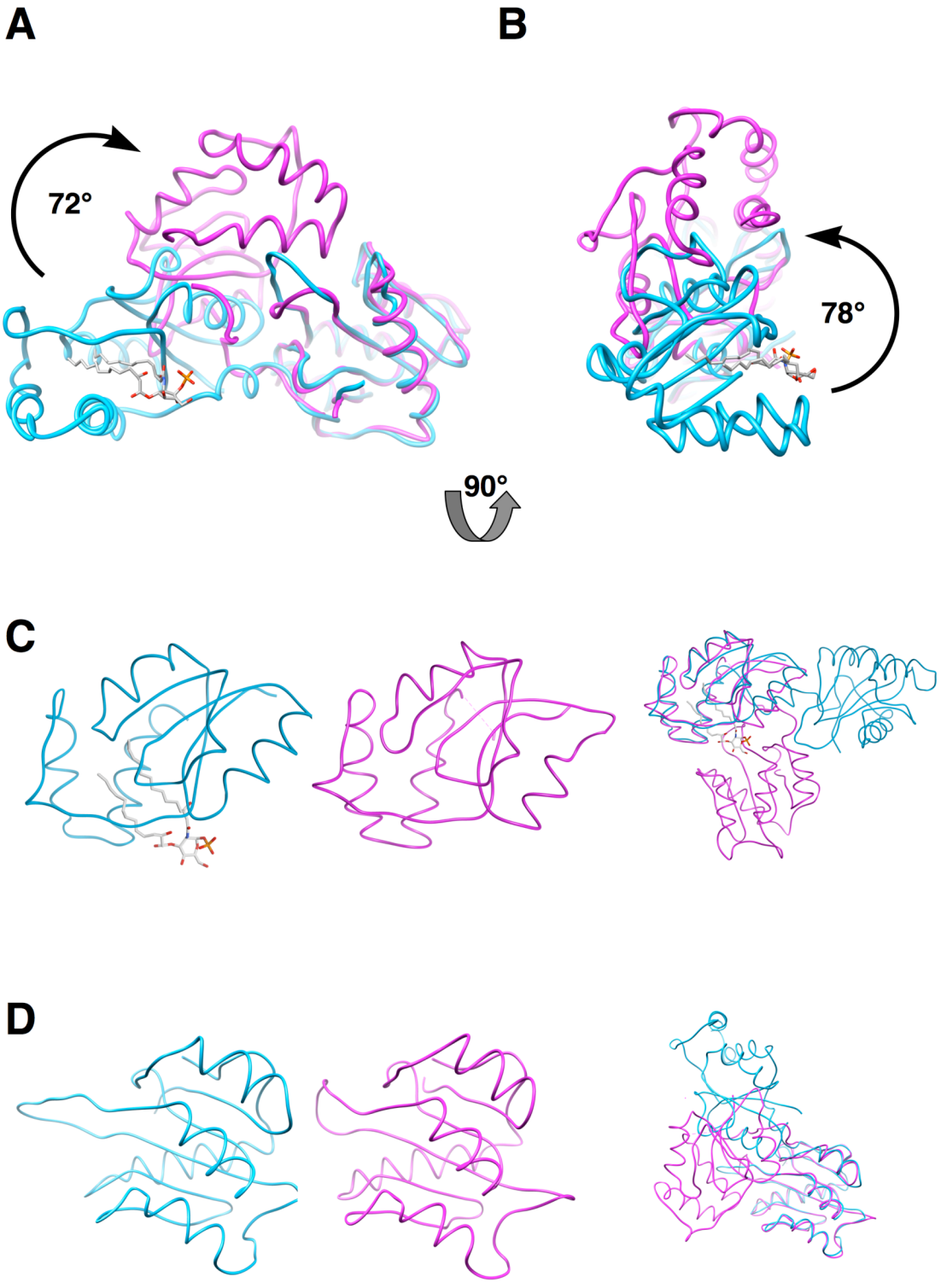

Figure 4.5. Macromolecular comparison of CcLpxI to CcLpxI-D225A

Figure 4.5. Macromolecular comparison of CcLpxI to CcLpxI-D225A. In each panel, teal ribbons represent the Cα backbone trace of CcLpxI, while magenta ribbons represent that of CcLpxI-D225A. Lipid X is shown with grey carbon atoms; non-carbon atoms are colored according to the following scheme: red for oxygen, blue for nitrogen, and orange for phosphorous. Panel A shows CcLpxI and CcLpxI-D225A aligned with respect to the Cα backbone of their ICD domains (RMSD = 0.728 Å with respect to the aligned domain). From this orientation, we measure a 72° difference in the orientation of the superimposed molecules' LXD domains. Panel B shows the same alignment, but turned 90° right with respect to the orientation in panel A. Here, we observe a 72° difference in the orientation of the LDX domains in CcLpxI vs. CcLpxI-D225A. Panel C shows the CcLpxI LXD (left), the CcLpxI-D225A LXD (center), and the alignment of full-length CcLpxI and CcLpxI-D225A with respect to the Cα backbone of their LXD domains (right). The RMSD of the aligned LXD's is 1.064 Å. Panel D shows the CcLpxI ICD (left), the CcLpxI-D225A ICD (center), and the alignment of full-length CcLpxI and CcLpxI-D225A with respect to the Cα backbone of their ICD domains (right). The RMSD of the aligned ICD's is 0.728 Å.

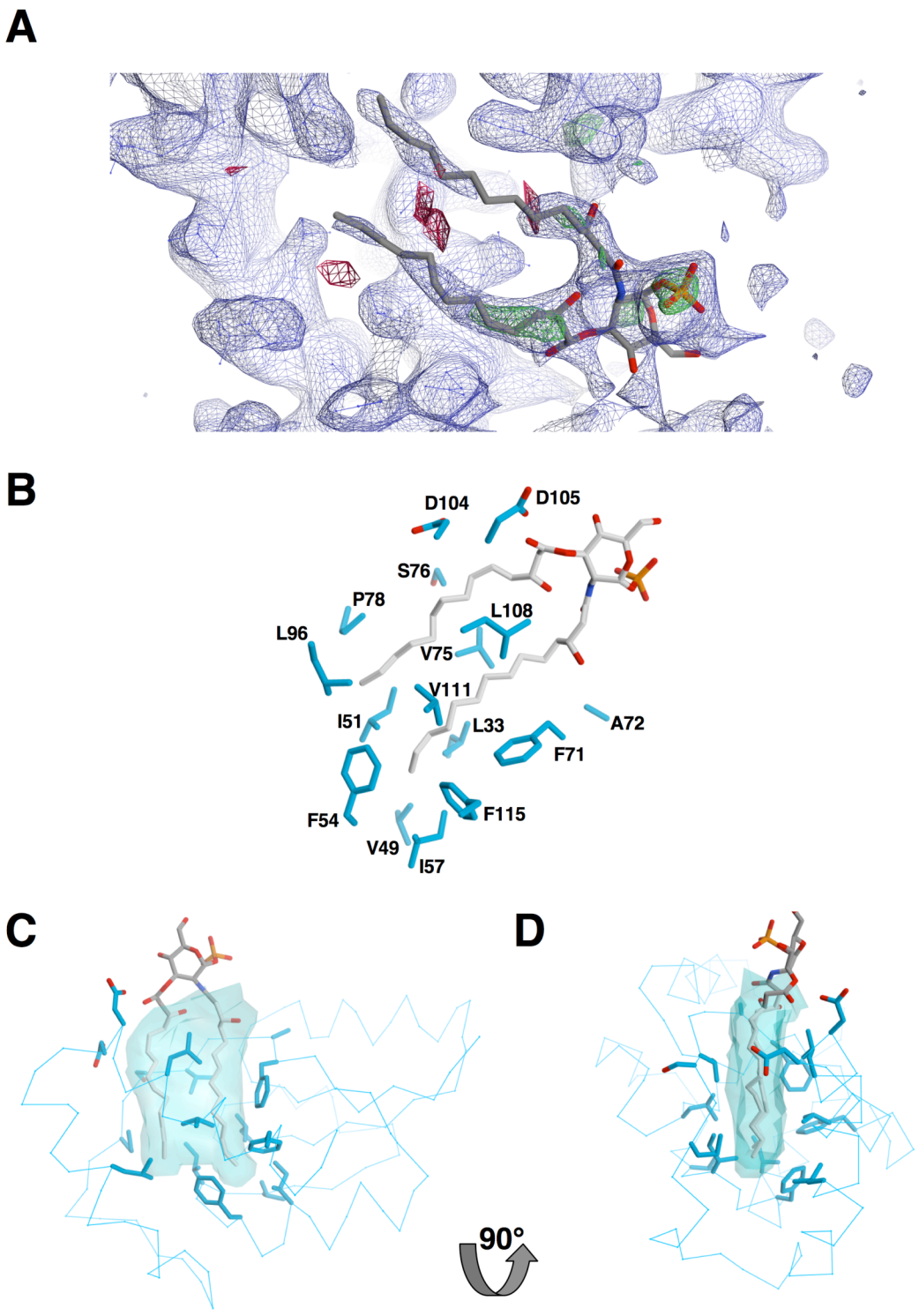

Figure 4.6. Binding modality of lipid X to CcLpxI

Figure 4.6. Binding modality of lipid X to CcLpxI. Panel A shows OMIT electron density maps surrounding the lipid X ligand bound to CcLpxI. Blue mesh corresponds to a $2F_o$-F_c map contoured at 1.1 σ, green and red meshes represent positive and negative density, respectively, from F_o-F_c maps contoured at ± 3.0 σ. Lipid X is shown in stick representation with the following coloring scheme: grey for carbons, red for oxygen, blue for nitrogen, and orange for phosphorous. Panel B shows the CcLpxI side-chains of residues within 4 Å of the modeled lipid X. Residues are shown in teal and are labeled in black. Lipid X is colored as in panel A. Panels C and D show the binding pocket of CcLpxI, as modeled by Chimera (REF). The side-chains of residues within 4 Å of lipid X are shown as teal sticks, while the Cα trace of CcLpxI's LXD is rendered in teal lines. Panel D is identical to panel C, but turned 90° right with respect to the former. The calculated surface area of the shaded lipid X binding pocket is 490 $Å^2$.

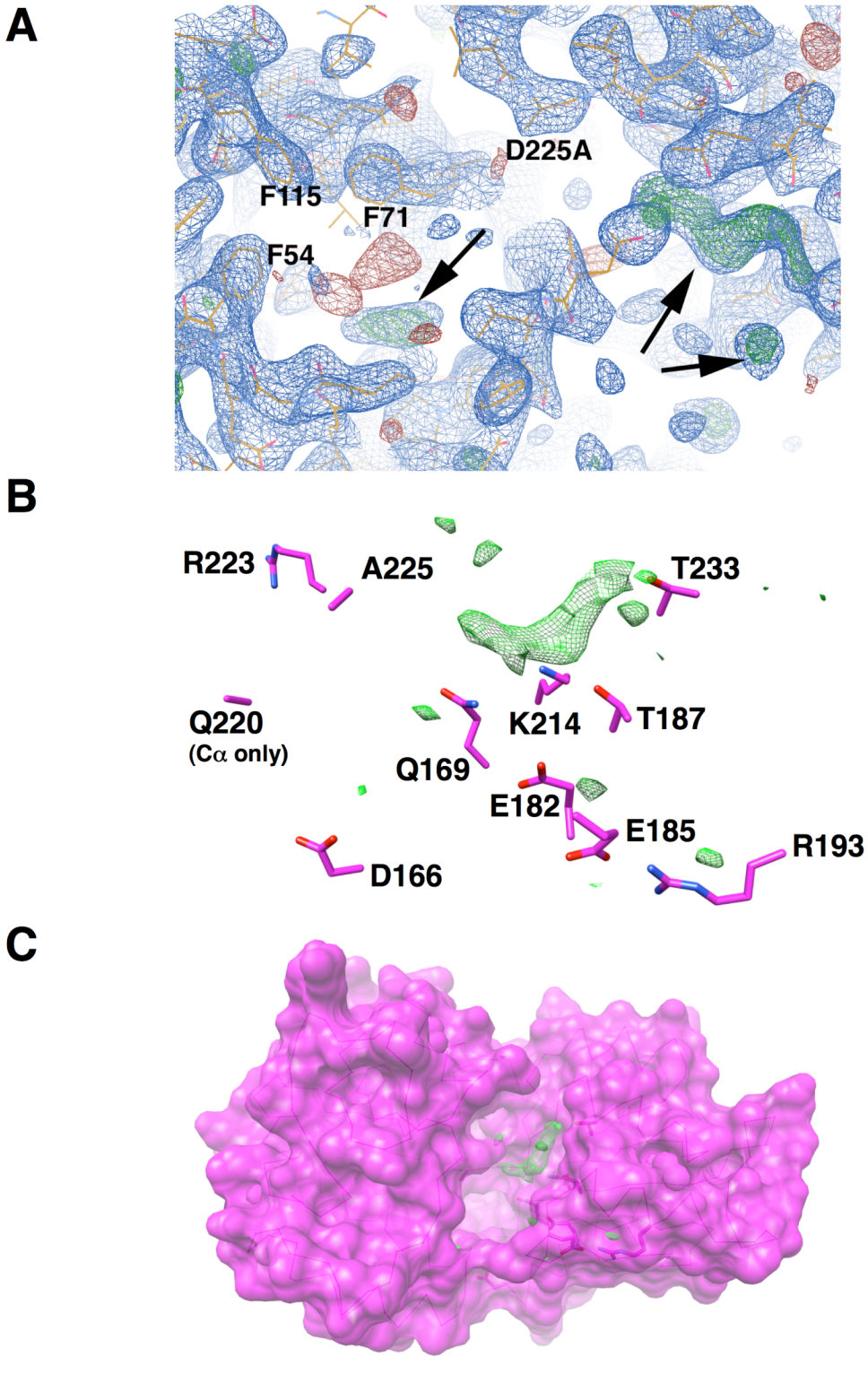

Figure 4.7. Putative UDP-2,3,-diacyglucosamine electron density in CcLpxI-D225A

Figure 4.7. Putative ligand electron density in CcLpxI-D225A. While refinement and model-building for the CcLpxI-D225A diffraction data are ongoing, this figure shows electron density consistent with the presence of the UDP-2,3-diacyglucosamine ligand. Panel A shows OMIT electron density maps centered about a large internal cleft in the CcLpxI-D225A strucutre. Blue mesh corresponds to a $2F_o$-F_c map contoured at 1.2 σ, green and red meshes represent positive and negative density, respectively, from F_o-F_c maps contoured at 3.0 σ. Residues F54, F71, and F115, present in the LXD, are labeled. A single arrow near these residues points to positive density consistent with ligand density (possibly acyl chains) in the LXD. In the left portion of the image, two arrows point to large regions of positive density near the ICD of CcLpxI-D225A. Residue A225 is also labeled. Panel B shows the positions of absolutely conserved residues present in the CcLpxI-D225A model. These residues' side-chains are shown in teal and are labeled in black. Note that only the Cβ of Q220 has been fit to the electron density, as model-building and refinement are ongoing. Green mesh corresponds to a F_o-F_c map contoured at +3.0 σ. Panel C shows a solvent-accessible surface, modeled using Chimera, for full-length CcLpxI-D225A. Green mesh corresponds to a F_o-F_c density (3.0 σ).

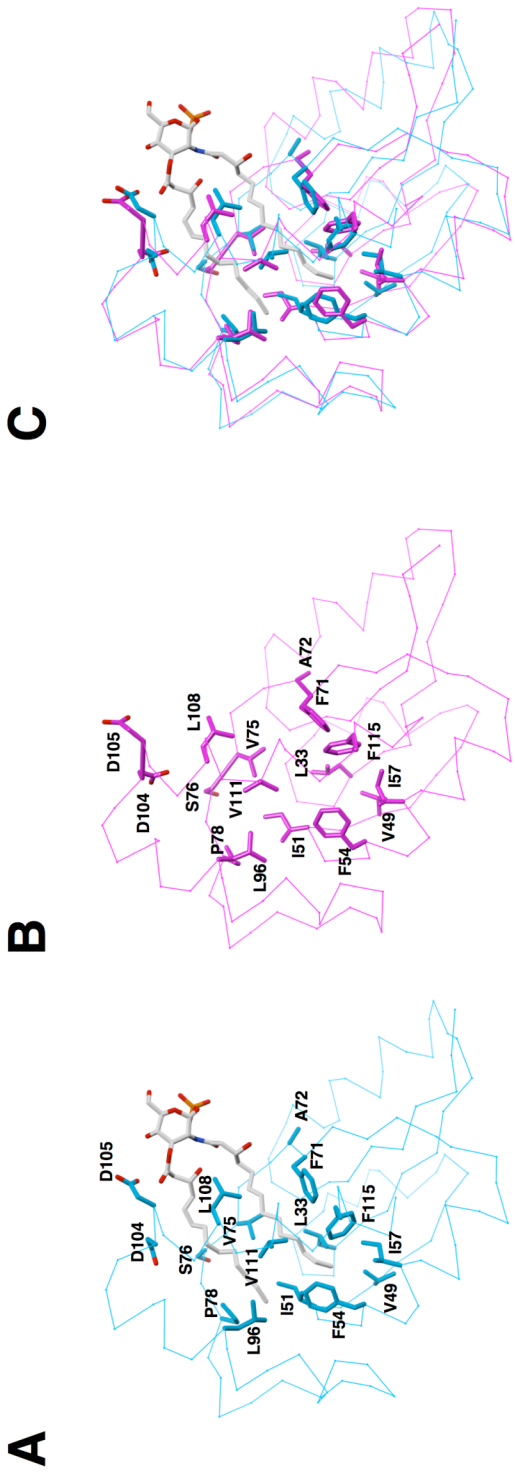

Figure 4.8. A comparison of CcLpxI and CcLpxI-D225A LXD's.

Figure 4.8. A comparison of CcLpxI and CcLpxI-D225A LXD's. This figure compares the LXD in CcLpxI (teal) with the LXD of CcLpxI-D225A (magenta). Panel A shows CcLpxI residues (teal sticks) having atoms within 4 Å of the modeled lipid X. The Cα trace is shown in narrow teal lines. Lipid X is shown in sticks, and colored according to the following scheme: grey for carbons, red for oxygen, blue for nitrogen, and orange for phosphorous. Residues are labeled in black. Panel B shows the LXD of CcLpxI-D225A, oriented and rendered identically to panel A, except that residue side-chains and the backbone trace are colored in magenta. Panel C shows the alignment of the LXD's in panels A and B according to Cα position (RMSD = 1.064 Å). Lipid X is positioned with respect to the LXD of CcLpxI, exactly as in figure A. Residue labels are omitted for clarity.

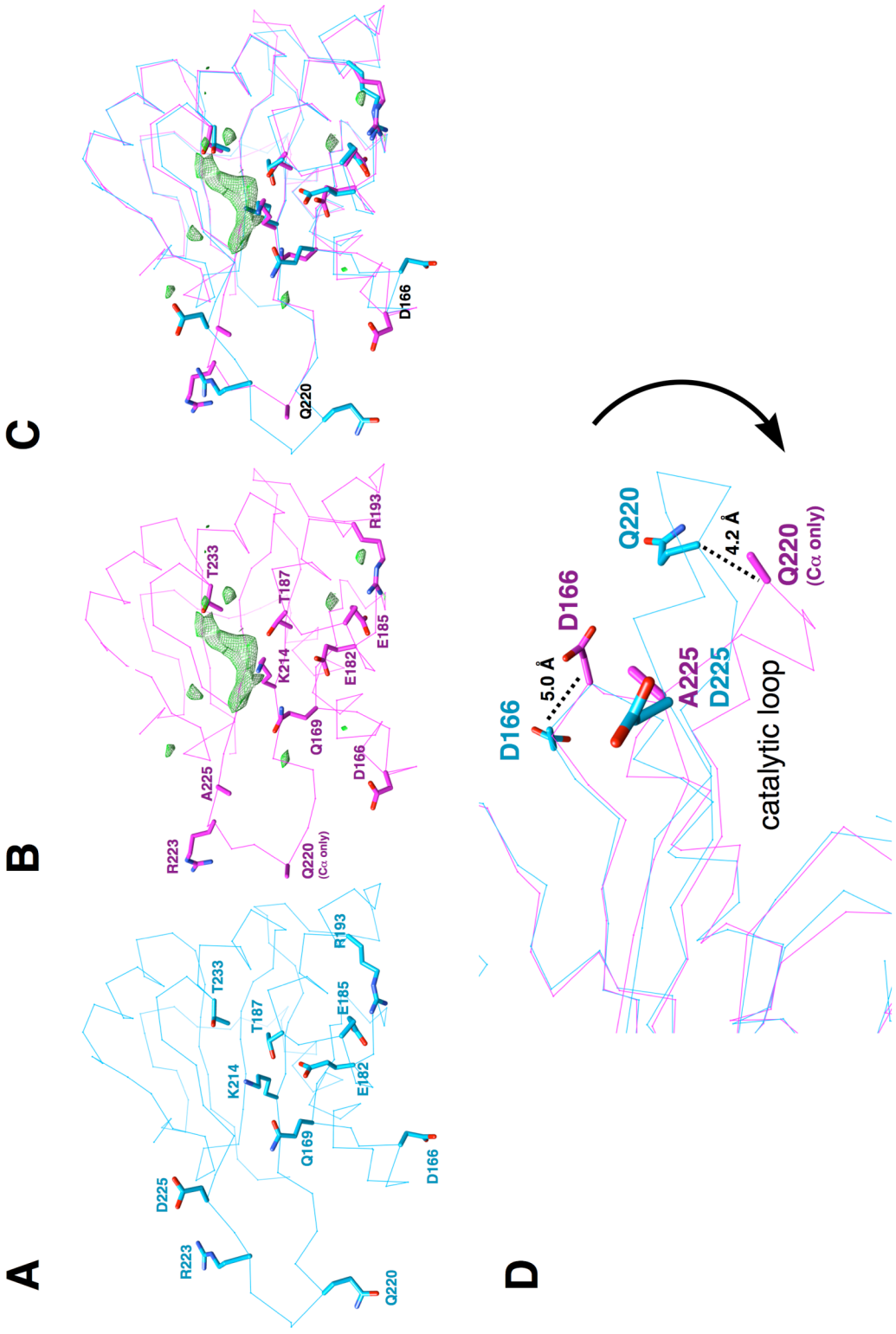

Figure 4.9. ICD orientation in CcLpxI vs. CcLpxI-D225A

Figure 4.9. A comparison of CcLpxI and CcLpxI-D225A ICD's. This figure compares the ICD in CcLpxI (teal) with that of CcLpxI-D225A (magenta). Panel A shows absolutely conserved residues (teal sticks) in the CcLpxI ICD. The Cα backbone is traced in teal. Panel B shows the ICD of CcLpxI-D225A, oriented and rendered identically to panel A, except that residue side-chains and the backbone trace are colored in magenta. Green mesh corresponds to to F_o-F_c density (3.0 σ) in the CcLpxI-D225A model. Panel C shows the alignment of the ICD's in panels A and B according to Cα position (RMSD = 0.728 Å). Residues whose Cα positions vary drastically in the overlaid models are labeled in black (Q220 and D166). Panel D shows a close view of the superimposed structures. Q220 is shown on the catalytic loop, and the distance between the position of its Cα atom in CcLpxI vs CcLpxI-D225A is indicated by a dotted line. The difference in the position of Cα in D166 is similarly indicated. D225/A225, present on the catalytic loop, is shown for reference.

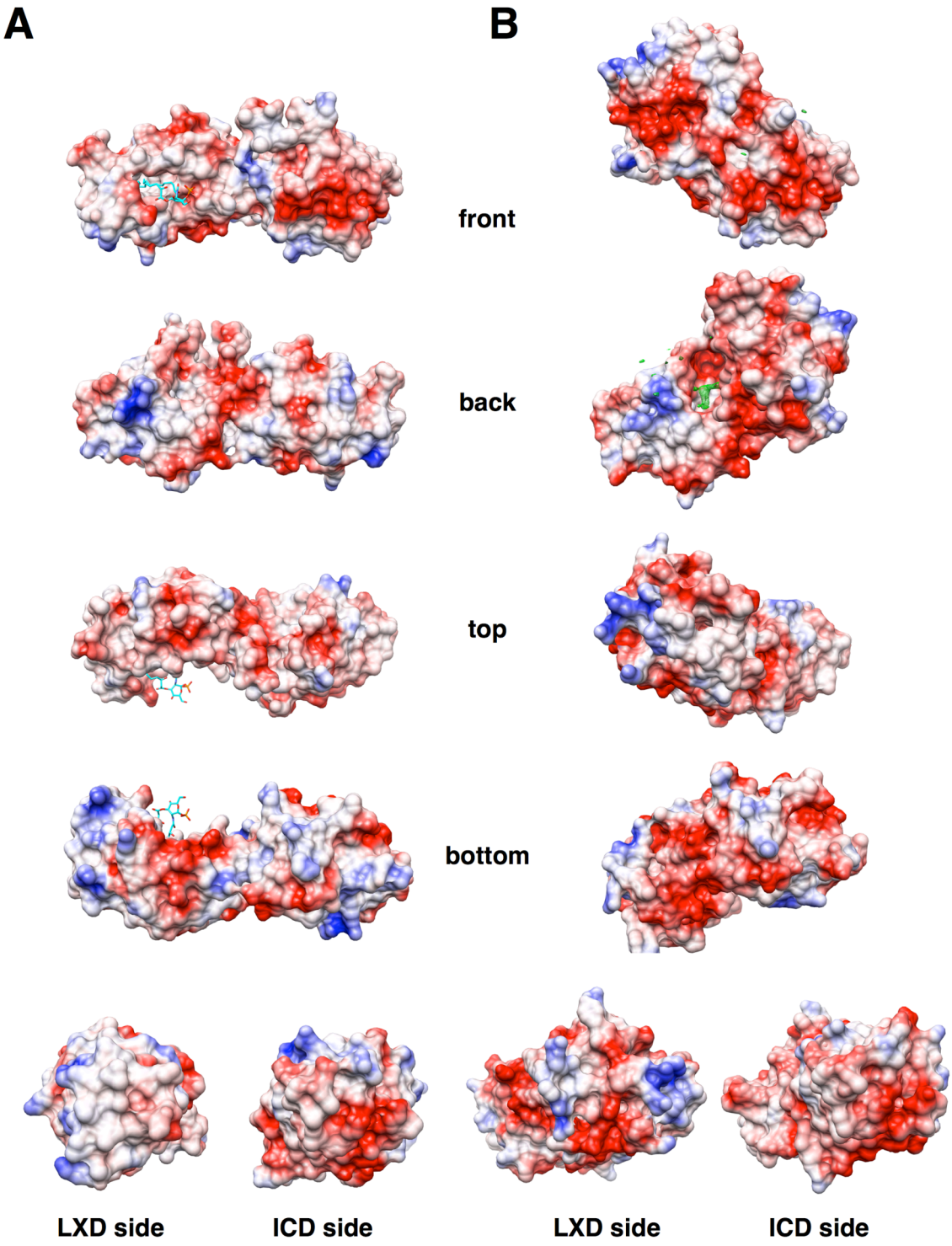

Figure 4.10. Hypothetical surface charge on CcLpxI vs. CcLpxI-D225A molecules

Figure 4.10. Hypothetical surface charge on CcLpxI vs. CcLpxI-D225A molecules. This figure shows predicted Coulombic charges on the surface of CcLpxI and CcLpxI-D225A molecules. Charges were calculated using Chimera, according to the following parameters: distance-dependent dielectric constant = 4, cutoff distance from protein surface = 1.4 Å. Relative charges are shown as followed, blue is positive, white is neutral, and red is negative. Panel A shows Coulombic surfaces on CcLpxI, from each possible perspective. Lipid X is rendered colored in teal. Similarly, Panel B shows Coulombic surfaces on CcLpxI-D225A. Green mesh corresponds to F_o-F_c density (3.0 σ), consistent with the presence of a ligand, near the ICD.

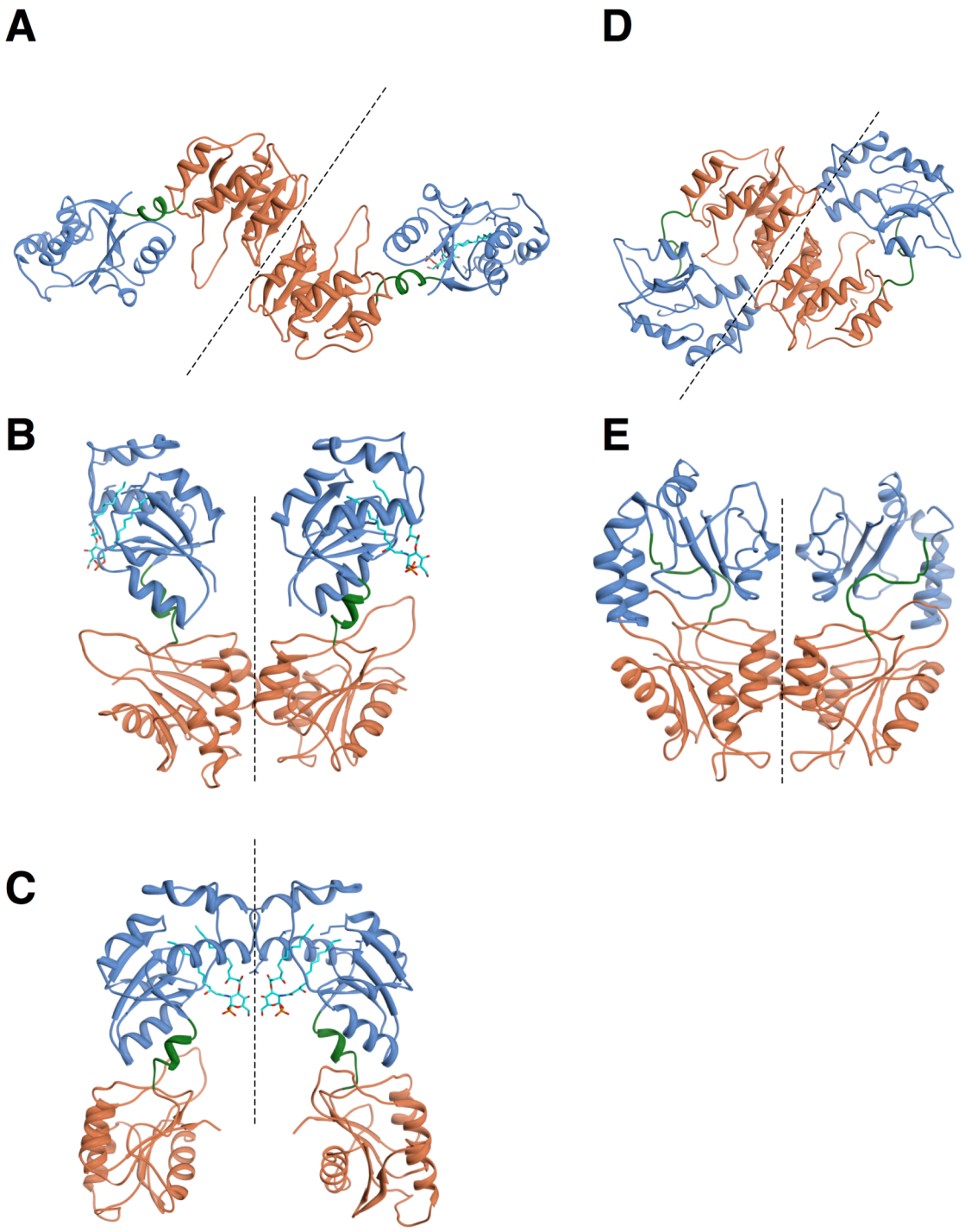

Figure 4.11. Crystal contacts in CcLpxI and CcLpxI-D225A

Figure 4.11. Crystal contacts in CcLpxI and CcLpxI-D225A. This figure shows a series of crystallographic contacts between monomers of either CcLpxI (Panels A, B, and C) or CcLpxI-D225A (Panels D and E). Putative crystal contacts were visualized using Chimera at a cutoff distance of 3.0 Å . The pairs of molecules are colored as in Figure 4: the LXD is blue, the linker is dark green, and the ICD is orange. For CcLpxI, lipid X is shown in teal. Dashed lines represent the plane at which these contacts occur. Note that in pairs of panels A and D the ICD domains (orange) are shown in the same relative orientation. The ICD's in panels B and E are similarly matched.

4.4 Discussion

Here, we report the crystallization and initial structural characterization of *C. crescentus* LpxI (CcLpxI), a UDP-2,3-diacyglucosamine hydrolase. LpxI, which we previously demonstrated to be a transformational analogue of LpxH (Chapter 2), is responsible for Lipid A biosynthesis in several pathogen genera, including *Rickettsia*, *Brucella*, and *Leptospira*. A metal-dependent hydrolase, LpxH catalyzes the attack of water upon the α-phosphate of UDP-2,3,-diacylglucosamine (see Chapter 2). CcLpxI, working by a different mechanism, catalyzes the attack of water on the β-phosphate.

Crystals of wild-type CcLpxI were obtained in the presence of lipid X, which co-purifies with CcLpxI in a molar ratio of 0.95:1 lipid X/CcLpxI. These crystals diffracted to 2.6 Å. As CcLpxI has no structurally-characterized orthologues, phasing was accomplished using anomalous x-ray diffraction of Se-Met derivatized protein crystals at the Se adsorption edge. Phasing of diffraction data from native protein and subsequent model-building and refinement, reveal an overall structure of CcLpxI having two distinct domains: an N-terminal lipid X binding domain (LXD), and a C-terminal LpxI catalytic domain (ICD) (see Figures 3 and 4). To our knowledge, both domains of this structure represent a novel protein folds. While refinement and model-building are ongoing (R_{crys} = 23.2%, R_{free} = 28.6%), we have been able to fit all absolutely-conserved CcLpxI residues to electron density. Moreover, sufficient data are available that allow us to include lipid X in the CcLpxI model (see Figure 6). Analysis of the lipid X binding pocket of the LXD reveals a deep binding cleft which surrounds the ligand acyl chains (see Figure 4.6). This binding pocket, which has a hydrophobic surface of ~490 Å^2, is strikingly similar to that observed in Sec14 (*170*) and in various PH-domain (LBD)-fused proteins (*195, 196*). Relatively few residues are positioned such that they might interact with the head group of lipid X. For this reason, the modality of lipid X binding to CcLpxI is reminiscent of how lipid A binds to human Toll-like receptor 4 (*54, 60*), or of

the recognition of exogenous lipids by many members of the CD1 family of receptors (*171, 172*). In this regard, LpxI differs from the lipid A biosynthetic enzyme LpxA, for which structural characterization of the product-bound orthologues revealed an exquisite specificity for its ligand head-group (*174, 175*).

In addition to product-bound wild-type CcLpxI, we crystallized a mutant construct (CcLpxI-D225A) that we had previously shown to co-purify, in a stochiometric amount (ratio of 0.85) with its substrate UDP-2,3-diacyglucosamine (see Chapter 3). In order to avoid introducing bias from the product-liganded CcLpxI structure into a model of CcLpxI-D225A, phase determination was accomplished by MAD using Se-Met derivatized protein. The highest-resolution data obtained for CcLpxI-D225A were 3.0 Å. While refinement and model-building are incomplete (R_{crys} = 30.0%, R_{free} is 42.5%), we have been able to fit nearly all of the protein backbone and absolutely-conserved CcLpxI residues into electron density. Unassigned F_o-F_c density in both the LXD and CID of CcLpxI-D225A may be UDP-2,3-diacyglucosamine (see Figure 4.7). Significantly, some of the absolutely-conserved residues closest to this unassigned density, including E182 and Q169, appear to be required for CcLpxI activity (Chapter 3).

A comparison of the LXD's of CcLpxI and CcLpxI-D225A reveals that these domains' Cα backbones overlay with an RMSD of 1.064 Å. Moreover, the positions of lipid X binding pocket residues do not differ significantly between the two constructs (see Figure 4.8). Taken together, these observations suggest that the LXD may be a relatively rigid domain. This may arise from side-chain ordering upon ligand binding (*210*). Overlay of the ICD's of CcLpxI and CcLpxI-D225A gives a RMSD of 0.728 Å. While the positions of absolutely conserved residues' side-chains are relatively static in the regions surrounding putative ligand density (see Figure 4.9) others, such as D166 and Q220 differ significantly between the constructs. Notably, the catalytic-loop residue Q220, which *in vivo* studies (Chapter 3) shows to be essential for LpxI-driven lipid X accumulation in *E. coli*, has a ΔCα of 4.2 Å. This translation results from a significant reorientation of the catalytic loop between the two structures (see Figure 4.9). Despite this, the two contructs' CID

Cα peptide backbones overlay remarkably well (see Figure 4.5, Figure 4.9). This is consistent with a catalytic model in which the LXD and CID each form halves of an inter-domain active site.

While the LXD and CID domains are largely superimposible, these domains' relative orientations differ greatly between the two constructs (see Figure 4.5). While CcLpxI adopts an extended conformation, with the LXD and CID spread far apart, these domains are positioned more closely together in CcLpxi-D225A. A striking relative domain translation of 72° with a 78° rotation is observed when comparing the models (see Figure 4.5). Such large inter-domain conformational changes, rarely observed between two liganded complexes (*211-214*), are consistent with a two-domain model of LpxI catalysis.

While the observed conformational differences between CcLpxI and CcLpxI-D225A may represent states on a true dynamic continuum during catalysis, we cannot exclude that these conformations are artifacts of crystal packing. To probe the solution behavior of CcLpxI and CcLpxI-D225A, we determined their sedimentation velocities. We measured the sedimentation coefficient of CcLpxI to be 3.56 ± 0.11 svedbergs (n = 5), while CcLpxI-D225A had a sedimentation coefficient of 3.85 ± 0.09 svedbergs (n = 5). These data demonstrate a small but statistically significant increase in sedimentation velocity for CcLpxI-D225A in comparison to CcLpxI. The latter, its crystallographic model having a maximum length of ~75 Å, would be expected to have a higher frictional coefficient as a result of its extended conformation relative to CcLpxI-D225A (maximum length of ~64 Å). Consequently, we would expect the sedimentation velocity of CcLpxI to be lower than that of CcLpxI-D225A. This is precisely what we observe. These data are consistent with a model wherein significant domain rearrangement occurs in conjunction with substrate binding (or product release).

CcLpxI works on a membrane-bound substrate (UDP-2,3-diacylglucosamine), and produces a membrane-bound product (lipid X). However, when over-expressed in *E. coli*, CcLpxI partitions to the cytosol. This suggests that membrane association is likely to be transient. Calculated Coulombic surfaces of the CcLpxI and CcLpxI-D225A models (see Figure 4.10)

suggest an overall anionic surface charge. This is consistent with CcLpxI's relatively low isoelectric point (pH = 5.5). While no large basic patches, which might be responsible for transient binding to anionic phospholipids head-groups, are revealed (see Figure 10, panel B, "bottom" orientation), one side of wild-type CcLpxI is enriched in electropositive surface relative to the others. It is possible that this surface may be involved in transient interaction with the cytosolic face of the inner membrane.

The solution molecular masses of CcLpxI and CcLpxI-D225A were estimated by sedimentation equilibrium. For both constructs, sedimentation equlibrium was consistent with molecular masses of ~60 kDa, and therefore dimers of CcLpxI. Analysis of crystal contacts (see Figure 4.11) revealed two possible dimerization interfaces. Additional mutagenesis will be necessary in order to identify the biological interface, but we prefer the dimerization interface shown in figure 4.11, panels A and D. We hypothesize that this plane represents the biological interface, due to the proximity of absolutely-conserved residues of the ICD. Some of these residues, including E185 and R193, may play a role in dimerization. Of particular note is the conserved planar stacking between R193 residues on adjacent CcLpxI monomers.

We have crystallized and solved the structure of CcLpxI, an essential enzyme in many Gram-negative bacteria, and one that performs catalysis upon an unusual saccharolipid substrate. We have thereby discovered a new protein fold. Co-crystallization of CcLpxI's product, lipid X, allowed us to define a distinct lipid X binding region in this two-domain enzyme. To date, only eleven families of lipid binding domains have been described (*215-217*). We have crystallized and solved the structure of a catalytically incompetent mutant, CcLpxI-D225A, which co-purifies stoichiometrically with its substrate, UDP-2,3-diacylglucosamine. While modeling and refinement are still in their initial stages, and the ligand has not yet been built into its putative electron density, the comparison of CcLpxI-D225A to CcLpxI reveals a large conformational change. Sedimentation velocity determination suggests that CcLpxI and CcLpxI-D225A may exist in different conformational states in solution. This is consistent with a model in which each

domain of CclpxI forms one-half of a catalytic site, and active site assembly is made possible by large inter-domain rearrangements. Less clear is the mechanism for product release, and for the role of Mg^{2+} in catalysis. The present work has set the stage for the detailed mechanistic characterization of this unique hydrolase.

While detailed mechanistic hypotheses cannot be developed based upon the present data, it is clear that CcLpxI operates differently than most other nucleotide pyrophosphatases. While such phosphatases perform catalysis by a variety of mechanisms and with sundry ensembles of active-site residues, most appear to do so without major macro-molecular rearrangement (as with CcLpxI). To our knowledge, CcLpxI is the only example of a nucleotide pyrophosophatase that remains bound to its non-nucleotide product following catalysis. This ususual behavior may have thermodynamic underpinnings: the entropic cost of de-solvating lipid X may offer too great a barrier to product release. We therefore speculate that with CcLpxI, phosphodiester bond hydrolysis, substrate binding, or both, drive the release of lipid X. In this regard, CcLpxI may more closely resemble two-domain glycosyl-transferases, wherein acceptor nucleotide-sugar hydrolysis appears to drive domaim movements and/or product release (*118*).

4.5. Contributions to this work

The author determined the optimal crystallization and cryoprotection conditions for CcLpxI, and performed MAD experiments on CcLpxI jointly with his collaborator, John K. Lee, Ph.D., a member of the Stroud Laboratory at the University of California San Francisco. While the crystallization of CcLpxI-D225A was piloted by both parties, optimally-diffracting crystals were obtained by Dr. Lee, and their x-ray diffraction data collected by him. Dr. Lee has also taken a lead role in structural refinement and validation efforts for both constructs. The author and Dr. Lee have contributed equally to the generation of the data presented in this chapter.

5. Purification and Characterization of the Lipid A Disaccharide Synthase (LpxB) from *Escherichia coli*: a Peripheral Membrane Protein

5.1 Introduction

Gram-negative bacteria possess an asymmetric outer membrane in which the inner leaflet is composed primarily of glycerophospholipids while the outer leaflet contains mostly lipopolysaccharide (LPS) (*28, 218, 219*). LPS forms a structural barrier that protects Gram-negative bacteria from antibiotics and other environmental stressors (*218*). The lipid A anchor of LPS is a glucosamine-based saccharolipid that is further glycosylated with core and O-antigen sugars (*28, 218-220*). Lipid A biosynthesis is required for viability in most species of Gram-negative bacteria (*219*). The minimum structure required for growth is usually lipid A derivatized with two Kdo (3-deoxy-D-*manno*-oct-2-ulosonic acid) residues (*219, 221*). In addition to serving a structural role as the hydrophobic anchor of LPS, lipid A is recognized as foreign by receptors of the innate immune system (*222-224*). In macrophages, lipid A stimulates the TLR4 (toll like receptor 4)/MD2 complex, which in turn activates a signal transduction cascade for the production of cytokines and other mediators of inflammation (*224-227*). In endothelial cells, lipid A also stimulates tissue factor production (*228, 229*). The over-production of these pro-inflammatory molecules can damage the microvasculature, contributing to Gram-negative septic shock and organ failure (*230*). Synthetic *Escherichia coli* lipid A by itself potently activates TLR4/MD2 and mimics many features of Gram-negative sepsis when injected into animals (*231*). Given lipid A's importance for bacterial viability and pathogenesis, the enzymes of its biosynthetic pathway are promising targets for the design of new antibiotics (*219, 232, 233*).

The biosynthesis of *E. coli* lipid A is catalyzed by nine constitutive enzymes, which are conserved in most Gram-negative bacteria (*28, 219*). The genes encoding these enzymes are usually present in single copy. The first three enzymes, LpxA, LpxC and LpxD (Scheme 1),

convert UDP-GlcNAc to UDP-2,3-diacylglucosamine (UDP-2,3,-diacyl-GlcN), whereupon LpxH (*34, 40*) cleaves off the UMP moiety to generate 2,3-diacylglucosamine-1-phosphate (2,3-diacyl-GlcN-1-P), also termed lipid X (*125*). Next, LpxB, an inverting glycosyl transferase (*116, 129*), condenses another molecule of UDP-2-3-diacyl-GlcN with 2,3-diacyl-GlcN-1-P to form 2′,3′-diacylglucosamine-(β,1′-6)-2,3-diacylglucosamine-1-phosphate (DSMP) and UDP (Scheme 1). Four additional enzymes convert DSMP to Kdo_2-lipid A (*28, 219*).

The characterization of LpxB affords an opportunity to gain new insights into the biochemistry of glycosyl transferases, which comprise 1-2% of the biomass of all life forms (*118*). LpxB is a member of the GT-B super-family, which encompasses a diverse subset of enzymes (*118*). There are currently ~90 CAZy families in the GT-B super-family (http://www.cazy.org/), of which one, family 19, consists exclusively of LpxB orthologs (*118*). However, no LpxB structures have been determined.

Here, we report the over-expression and purification of *E. coli* and *Haemophilus influenzae* LpxB to near-homogeneity on a 10-100 mg scale. We also describe an improved LpxB assay and characterize *E. coli* LpxB's peripheral association with the cytoplasmic membrane. We demonstrate by mass spectrometry and autoradiography that 1.6 to 3.5 phospholipid molecules co-purify with each LpxB monomer, and we identify conserved residues required for LpxB activity. Our findings set the stage for mechanistic studies and x-ray crystallography of LpxB.

5.2 Materials and Methods

5.2.1 Molecular biology protocols

Plasmids described in this study (Table 5.1) were amplified in *E. coli* strain XL1-Blue (Stratagene, La Jolla, CA) and purified using Qiagen Mini-Prep kits (Qiagen, Valencia, CA). DNA fragments were purified using Quiaquick Spin kits (Qiagen, Valencia, CA). Both kits were employed according to the manufacturer's recommendations. Restriction endonucleases, T4 DNA ligase, and calf intestinal alkaline phosphatase were obtained from New England Biolabs

(Ipswich, MA). Pfu Turbo DNA polymerase, the 100 mM dNTP stocks (20 mM each of dATP, dTTP, dGTP and dCTP), and Pfu Turbo polymerase reaction buffer were obtained from Strategene (La Jolla, CA). Polymerase chain reaction (PCR) conditions were those recommended by Strategene, except for inclusion of 1% v/v dimethyl sulfoxide.

5.2.2 Cloning of *E. coli* and H. *influenzae lpxB* genes

DNA oligomers (Erofins MWG Operon Huntsville, AL) were used to amplify *lpxB* genes from *E. coli* and *H. influenzae* genomic DNA (obtained from ATCC, Rockville, MD). The sequences of these primers are shown in Supporting Table 5.1. For the *E. coli* gene, primers were designed to confer 5' *ndeI* or *hindIII* restriction sites, and 3' *xhoI* or *kpnI* restriction sites. For *H. influenzae lpxB*, primers conferred 5' *ndeI* and 3' *xhoI* sites. Amplification from genomic DNA by PCR was accomplished using a Mastercycler Gradient thermocycler (Eppendorf, Hamburg, Germany). Amplified inserts were digested by the appropriate restriction endonuclease and ligated into similarly digested vectors (EMD Chemicals, Inc., Darmstadt, Germany) (Table 5.1) that had been treated with calf intestinal alkaline phosphatase. Ligation was performed using T4 ligase. *E. coli lpxB* was cloned into pET21a(+) and pET23b at 5' *hindIII* and 3' *xhoI* restriction sites, into pET30b at 5' *ndeI* and 3' *kpnI* sites, and into pET19b and pET16b at 5' *ndeI* and 3' *xhoI* sites (Table 1.1), using the designated primers shown in Supporting Table 1. *H. influenzae lpxB* was cloned into pET16b at 5' *ndeI* and 3' *xhoI* sites. For pECLpxB23 and pECLpxB30 (Table 5.1), the *lpxB* stop codons were removed to allow fusion to the C-terminal tag, using the primers EC_*xhoI* and EC_*kpnI*, as summarized in Supporting Table 1. The restriction endonucleases *xbaI* and *xhoI* were employed to sub-clone *E. coli lpxB* from pET21a into the low-copy plasmid pWSK29 (*234*). The use of these restriction endonucleases allowed for the transfer of the 5' ribosome-binding site of pET21a together with *E. coli lpxB*. The vectors pET23b, pET30b, pET19b, pET16b confer a *C*-terminal non-cleavable His_6 tag, a *C*-terminal factor Xa-cleavable His_8 tag, a *N*-terminal enterokinase-cleavable His_{10} tag, or a N-terminal factor Xa-cleavable His_{10} tag, respectively (Table 5.1). Ligation was followed by heat-shock enhanced transformation into

competent *E. coli* XL1-Blue cells (Novagen, EMD Chemicals, Inc., Darmstadt, Germany). The pET16b constructs expressing *E. coli* or *H. influenzae* LpxB were further altered to convert the factor Xa cleavage site into a tobacco etch virus (TEV) protease cleavage site with the sequence ENLYFSQS (*235*), using the Quick-Change mutagenesis kit (Stratagene, La Jolla, CA) with appropriate primers. All constructs were confirmed by DNA sequencing.

5.2.3 Optimization of the *in vitro* assay for LpxB

The radiochemical LpxB assay described previously (*116*) was optimized and adapted to a thin-layer chromatography (TLC) system. The non-radioactive LpxB substrates lipid X and UDP-2,3-diacylglucosamine were prepared as described (*116*). The ^{32}P-lipid X was prepared from *E. coli* mutant strain MN7 (Table 5.1) (*111, 116*). Unless otherwise indicated, the purified ^{32}P-lipid X was re-suspended in a buffer containing 0.05% w/v Triton X-100, 1 mM EDTA, and 1 mM EGTA. The addition of detergent resulted in improved recovery of ^{32}P-lipid X when stored in polypropylene tubes. Before use, 5 mM stocks of the two non-radioactive substrates (re-suspended in 20 mM HEPES pH 8.0) were mixed by vortexing, followed by immersion in a bath sonicator (Avanti Polar Lipids, Alabaster, AL) for 2 min. Typically, 25 μl reactions were prepared in 0.5 ml polypropylene tubes (Eppendorf, Hamburg, Germany), containing 0 – 1 % w/v fatty-acid free bovine serum albumin (BSA) (Sigma-Aldrich, St. Louis, MO), 0 – 2 % w/v Triton X-100 (Pierce), 400 μM lipid X, 600 μM UDP-2,3-diacylglucosamine, 20 mM HEPES pH 8.0, ~1000 cpm/μl ^{32}P lipid X, and enzyme. Prior to enzyme addition, these components were equilibrated in a laboratory heat block for 10 min at 30°C. Reactions were usually initiated by the addition of 5 μl of enzyme to 20 μl of the reaction mixture. At various time-points, 3 μl portions were removed and spotted onto 10 x 20 cm silica gel TLC plates (250 μm) (EMD Chemicals, Inc., Darmstadt, Germany). TLC plates were air-dried at room temperature and developed in a system consisting of $CHCl_3$/MeOH/H_2O/acetic acid (25:15:4:2 v/v/v/v). When the solvent front reached ~0.5 cm from the top edge, the plates were dried with a hot air stream, and exposed to 35 x 43 cm Molecular

Dynamics PhosphorImager Screens (GE Healthcare, Waukesha, WI). After > 5 hr exposure, these screens were scanned and quantified using a Molecular Dynamics Storm 840 PhosphorImager (GE Healthcare, Waukesha, WI) and its associated software.

In the absence of either Triton X-100 or BSA, the LpxB reactions reached ~60% completion and were linear with time for about the first 10% of the progress curve. The inclusion of Triton X-100 stimulated the initial rate ~5-fold and allowed the reactions to proceed to > 90% completion. The inclusion of BSA further improved assay linearity and reproducibility. Triton X-100 and BSA were therefore included in the standard assay and in the enzyme dilution buffer. The optimized LpxB assay contained 400 μM lipid X, 600 μM UDP-diacylglucosamine, 20 mM HEPES, pH 8.0, 0.05 % w/v Triton X-100, and 0.5 mg/ml fatty-acid free BSA.

5.2.4 Large-scale purification of *E. coli* and H. influenzae LpxB constructs

All procedures were carried out a 0-4ºC. For either the pECLpxB-TEV or the pHILpxB-TEV plasmid (Table 1) expressed in C41(DE3) (also see Supporting Methods: optimized expression of *E. coli* and *H. influenzae* LpxB), ~15 g of wet cell pellet were suspended in 225 ml lysis buffer, consisting of 50 mM sodium phosphate buffer, pH 8.0, 250 mM NaCl, 25 mM imidazole, 10 mM β-mercaptoethanol, and 20% v/v glycerol. The mixture was filtered through a Buchner funnel into an ice-chilled Erlenmeyer flask to remove large clumps of cells. The cells were lysed by three passages through an ice-cold Cell-Cracker™ (Microfluidics International Corporation, Newton, MA). Cell debris and membranes were removed by ultracentrifugation at 100,000 *x g* for 1 h. Either 10% w/v Triton X-100 or 10% w/v β-D-dodecylmaltopyranoside (DDM) (Anatrace, Inc., Maumee, OH) were added to the supernatant to yield final concentrations of 0.2 % w/v or 0.1 % w/v, respectively, as indicated below. After mixing with gentle inversion for 30 min at 4 ºC, the sample was loaded overnight onto a 5 ml Ni-NTA Superflow ™ cartridge at a flow rate of 0.25 ml/min, (Qiagen, Valencia, CA). The cartridge was first pre-equilibrated in lysis buffer containing the same detergent concentration as the sample. The flow rate was maintained with a Rabbit-plus peristaltic pump (Rainin Instrument, LLC, Oakland, CA). The column was washed

with 10 bed volumes of lysis buffer containing the appropriate concentration of detergent. Excess detergent and contaminants were removed by washing at 0.25 ml/min with 50 column volumes (250 ml) of lysis buffer without detergent. Twenty column volumes (100 ml) of the same buffer, except containing 50 mM imidazole, were then applied as a wash step at 0.5 ml/min. Elution of LpxB was accomplished with 16 column volumes (80 ml) of the same buffer supplemented with imidazole at 300 mM at 0.5 ml/min. To the entire Ni-NTA eluate, 1 M DTT and 0.5 M EDTA, pH 7.5, were added immediately to yield final concentrations of 5 mM and 10 mM, respectively. Next, 10 ml of 0.5 mg/ml *C*-terminally His_6-tagged TEV protease was added (*235, 236*) and thoroughly mixed with the LpxB by gentle pipetting. After 14 hours at 4 ºC, the sample was dialyzed at 4 ºC against 4 L of 20 mM HEPES pH 8.0, containing 200 mM NaCl, 10% glycerol v/v, and 10 mM β-mercaptoethanol. Following at least 8 h of dialysis, the TEV-digested LpxB was applied at 0.5 ml/min to 7 ml of Ni-NTA Superflow™ resin in a 3.7 cm diameter glass column (Bio-Rad) equilibrated in dialysis buffer. The run-through (~100 ml) was collected and concentrated on a 10,000 molecular weight cut-off YM10 membrane (Millipore, Billercia, MA) under nitrogen pressure in a 50 ml stirred ultra-filtration cell (model 8050, Millipore, Billercia, MA) until the final volume was 5-9 ml.

The sample was next passed through a 0.2 μm filter (Millipore, Billercia, MA) and loaded onto a 320 ml calibrated size exclusion column (Superdex 200 XK26/70, GE Healthcare, Waukesha, WI), equilibrated with a buffer containing 20 mM HEPES, pH 8.0, 150 mM NaCl (for *E. coli* LpxB) or 500 mM NaCl (for *H. influenzae* LpxB), and 5 mM *tris*-(2-carboxyethyl)-phosphine (TCEP). In some preparations, the buffer also contained 0.05% w/v DDM, as indicated. The sample was applied at 0.5 ml/min using an AKTA FPLC system equipped with the UNICORN program (GE Healthcare, Waukesha, WI). Elution with 1.1 column volumes (~350 ml) was at 1 ml/min, and 5 ml fractions were collected after the excluded volume (110 ml) of the column was reached. Fractions containing LpxB, as judged by A_{280} and SDS-PAGE, were pooled and concentrated to 10-20 mg/ml using Amicon Ultra 10,000 molecular weight cut-off centrifugal

concentration devices (Millipore, Billercia, MA). Concentrated LpxB was divided into aliquots, flash-frozen using dry ice in ethanol, and stored at -80 °C. Protein concentration was determined by the bicinchoninic acid assay (*237*). The concentration of NaCl in the *H. influenzae* LpxB size-exclusion chromatography buffer was maintained at 500 mM, because the purified enzyme, when concentrated to > 5 mg/ml, precipitated at lower ionic strength. The protein's apparent molecular mass (M_r) was estimated by fitting the observed elution volume to a set of standards (thyroglobulin, ferritin, aldolase, *E. coli* LpxD, serum albumin, conalbumin, ovalbumin, chymotripsin, and ribonuclease A). Except for lpxD (*185*), standards were obtained from GE Healthcare, Waukesha, WI.

5.2.5 Size exclusion chromatography of *E. coli* LpxB in the presence or absence of detergent

A 500 μl sample of purified *E. coli* LpxB (5 mg/ml) was loaded onto a 24 ml Superdex 200 Preparative grade column (GE Healthcare, Waukesha, WI), attached to an AKTA FPLC system, and eluted at a flow rate of 0.33 ml/min in buffer containing 20 mM Tris, pH 7.4, 200 mM NaCl, and 5% w/v glycerol. Elution was followed by A_{280} and SDS-PAGE analysis of 0.5 ml fractions. To determine whether detergent affects the estimated M_r, another size exclusion experiment was performed as above, except that 0.1% w/v DDM was included in the buffer.

5.2.6 Apparent kinetic parameters and pH dependency of E. coli LpxB

Velocity as a function of lipid X concentration was determined for purified *E. coli* LpxB using the optimized assay conditions, except that UDP-2,3-diacylglucosamine was held constant at 1200 μM, and lipid X was varied from 50 to 1000 μM. The velocities were fit to the Michaelis-Menten equation using KaleidaGraph (*185*). The apparent kinetic parameters with respect to UDP-2,3-diacylglucosamine concentration were determined as above, except that lipid X was held at 1200 μM, while UDP-2,3-diacylglucosamine was varied from 50 to 1000 μM. Typically, 5 nM enzyme was used to start the reaction, and time-points were taken at 3, 15, and 30 min. To determine the pH dependence, LpxB was assayed in a triple-buffer system, consisting of 100 mM

sodium acetate, 50 mM bis(2-hydroxymethyl)-imino-tris(hydroxymethly)-hexane, and 50 mM Tris, ranging in pH from 5.5 to 9.5 (*184*). Standard assay conditions with 5 nM enzyme were used, except that the usual 20 mM HEPES, pH 8.0, was replaced with the triple buffer. Product formation was determined at 15 and 30 min, and experiments were carried out in duplicate. KaleidaGraph was used to fit a two-limb pK_a curve to the data (*184*).

5.2.7 Effect of detergent and surface concentration upon apparent LpxB activity

Purified E. coli LpxB was assayed under standard conditions (400 μM lipid X, 600 μM UDP-2,3-diacylglucosamine), except that the Triton X-100 was varied from 10 μM to 1 mM. To avoid detergent carry-over into the reactions, the purified enzyme was diluted as above, but in the absence of Triton X-100. The final LpxB concentration was 10 nM. For the same reason, 32P-lipid X used in this experiment was re-suspended in a buffer containing EDTA and EGTA, but lacking detergent. To investigate the effects of bulk surface concentration ([lipid X] + [UDP-2,3-diacylglucosamine] + [Triton X-100]) on specific activity, the purified enzyme was assayed under standard assay conditions, except that the mole ratio of lipid X:UDP-2,3-diacylglucosamine:Triton X-100 was held constant at 2:3:4, and the bulk concentration was varied from 0.028 mM to 1.8 mM. The enzyme used in this experiment was diluted in 20 mM HEPES, pH 8.0, and 0.5 mg/ml BSA but without Triton. To determine whether LpxB activity is affected by surface dilution (*238*), the purified enzyme was assayed in the presence of a fixed substrate concentrations (50 μM lipid X and 75 μM UDP-2,3-diacylglucosamine), while Triton X-100 was varied from 0.1 to 13.6 mM to reach a 100-fold excess in relation to the combined substrate concentrations.

Table 5.1. Bacterial strains and plasmids.

Table 1: Relevant strains and plasmids

Strain/plasmid	Description	Source or reference
Strains		
C41(DE3)	F⁻ *ompT hsdS*$_B$ (r_B^- m_B^-) *gal dcm* (DE3) D(srl-recA)306::Tn*10*	Ref. Miroux paper
W3110	wild-type, F⁻, λ⁻	*E. coli* Genetic Stock Center (Yale)
XL1-Blue	*recA1 endA1 gyrA96 thi-1 hsdR17 supE44 relA1 lac [F'proAB lacIqZDM15 Tn10 (Tet^R)]*	Stratagene
MN7	K-12-derived *pgsA444 lpxB1*; accumulates lipid X	Ref. 44 in LpxL paper
Plasmids		
pET21a(+)	expression vector containing a T7 promoter, Amp^R	Novagen
pWSK29	low-copy expression vector containing a T7 promoter, Amp^R	Ref. 33 in LpxL paper
pET23b	expression vector containing a T7 promoter, Amp^R , confers a non-cleavable C-terminal (His)6 tag	Novagen
pET30b	expression vector containing a T7 promoter, Kan^R, confers an enterokinase-cleavable C-terminal (His)^R tag	Novagen
pET19b	expression vector containing a T7 promoter, Amp^R, confers an enterokinase-cleavable N-terminal (His)^{10} tag	Novagen
pET16b	expression vector containing a T7 promoter, Amp^R, confers a factor Xa-cleavable N-terminal (His)^{10} tag	Novagen
pECLpxB21	pET21a(+) containing *E. coli lpxB*	this work
pECLpxBwsk29	pWSK29 containing *E. coli lpxB*	this work
pECLpxB23	pET23b containing *E. coli lpxB*	this work
pECLpxB30	pET30b containing *E. coli lpxB*	this work
pECLpxB19	pET19b containing *E. coli lpxB*	this work
pECLpxB16	pET16b containing *E. coli lpxB*	this work
pHILpxB16	pET16b containing *H. influenzae lpxB*	this work
pECLpxB-TEV	pET16b containing *E. coli lpxB* wherein the factor Xa cleavage site is replaced by a TEV-protease site	this work
pHILpxB-TEV	pET16b containing *H. influenzae lpxB* wherein the factor Xa cleavage site is replaced by a TEV-protease site	this work
pE15A	pET19b containing *E. coli lpxB*-E15A	this work
pS17A	pET19b containing *E. coli lpxB*-S17A	this work
pD98A	pET19b containing *E. coli lpxB*-D98A	this work
pF102A	pET19b containing *E. coli lpxB*-F102A	this work
pW126A	pET19b containing *E. coli lpxB*-W126A	this work
pR210A	pET19b containing *E. coli lpxB*-R210A	this work
pE227A	pET19b containing *E. coli lpxB*-E227A	this work
pL314A	pET19b containing *E. coli lpxB*-L314A	this work
pN316A	pET19b containing *E. coli lpxB*-N316A	this work

5.2.7 Construction, purification, and characterization of *E. coli* LpxB point mutants.

The plasmid pECLpxB19 (Table 1) was mutagenized using a Quick-Change kit (Stratagene, La Jolla, CA) with appropriate primers (Supporting Table 1). Mutagenized plasmids were amplified, purified, and confirmed by DNA sequencing. The plasmids were transformed into the C41(DE3) expression strain. The resultant constructs were inoculated into in LB broth (*239*) supplemented with 100 μg/ml ampicillin, induced at A_{600} of ~0.5 with 1 mM IPTG for 3 hours, and harvested as described in the Supporting Materials. Expression was confirmed by SDS-PAGE of cell lysates. Mutant LpxB enzymes were purified on a small scale in a manner analogous to that

described above (see Supporting Methods), except that the membrane-free lysate was supplemented with DDM to 0.5% w/v, and the Ni-NTA eluant was exchanged into 20 mM HEPES, pH 8.0, 150 mM NaCl, 20% w/v glycerol, and 0.2% w/v DDM using a PD-10 solvent exchange column (GE Healthcare, Waukesha, WI). Purified mutant proteins were analyzed by SDS-PAGE and by the standard *in vitro* LpxB assay. Concentrations of each mutant enzyme were varied from ~1.3 μM to 13 nM as appropriate.

5.2.8 Extraction of phospholipids purifying with *E. coli* LpxB

Cells of C41(DE3)/pECLpxB19 (Table 1) were grown in a 750 ml culture, induced, and harvested as described in the Supporting Methods. Purification was accomplished as described in Supporting Methods, except that the lysate from the 750 ml culture was divided into four portions: one was not incubated with detergent prior to purification, while the other three were incubated at 4 ºC for 30 minutes with either Triton X-100, octyl-β-D-glucopyranoside, or DDM, each of which was added to a final concentration of 1% w/v from 20% w/v stocks. Eluted protein (~0.5 mg/ml) obtained by Ni-NTA chromatography was estimated to be > 95% pure by SDS-PAGE. A 0.8 ml portion (0.4 mg) of each of the four purified protein samples was extracted with a 5.8 ml acidic two-phase Bligh-Dyer mixture (*128*). The lower phase (2 ml), containing phospholipids, was removed and transferred to a fresh glass tube. The lower phase was washed three times with 3.8 ml portions of pre-equilibrated acidic Bligh-Dyer upper phase (*128*). The washed lower phase was dried under N_2, redissolved in 100 μl chloroform/methanol (2:1 v/v), and injected onto a QSTAR XL time-of-flight mass spectrometer (Applied Biosystems, Foster City, CA) operating in the ESI negative ion mode. A spectrum was collected in the *m/z* range of 60 to 2000 amu, with intensity counts accumulated over one minute.

5.2.9 Estimation of the phospholipid to LpxB ratio by quantitative LC/ESI-MS.

A 2.3 μg sample of a synthetic phosphatidylethanolamine (PE) standard, consisting of 17:0, 14:1 PE (Avanti Polar Lipids, Alabaster, AL), was added to 0.4 mg of purified LpxB; this

mixture was extracted by the acidic Bligh-Dyer method (*128, 240*). The lower phase was dried under N_2 and redissolved in 100 μl of chloroform/methanol (2:1 v/v). Next, 20 μl of this material was mixed with 20 μl DMSO and 50 μl of liquid chromatography mobile phase A, consisting of methanol:acetonitrile:aqueous 1 mM ammonium acetate (60:20:20, v/v/v). A 20 μl portion of this mixture was injected onto a Zorbax SB-C8 reverse-phase column (5 μm, 2.1 x 50 mm) obtained from Agilent (Palo Alto, CA), using a Shimadzu LC system composed of a solvent de-gasser, two LC-10A pumps, and a SLC-10A system controller (Shimadzu Scientific Instruments, Kyoto, Japan) coupled to a QSTAR XL quadropole time-of-flight mass spectrometer (Applied Biosystems, Foster City, CA). For chromatography, 100% mobile phase A was run isocratically for 2 minutes, followed by a by a linear gradient from 100% mobile phase A to 100% mobile phase B (100% ethanol containing 1 mM ammonium acetate) over 14 minutes. The flow rate was maintained at 200 μl/min. About 10% of the column eluant was directed to the QSTAR XL for ESI-MS analysis in the negative-ion mode (*241*). The total ion current (TIC) and the derived mass-spectra were analyzed using the Analyst QS software package. Most of the PE species eluted from the C8 column between 8 and 13 minutes. The synthetic 17:0, 14:1 PE standard eluted at 10.59 minutes.

The quantification module of the Analyst software package was used to integrate the area of the extracted ion current (EIC) peak of the synthetic PE and the major endogenous PE species. First, the EIC area corresponding to the PE standard was calculated. Next, the EICs of the three most abundant PE species were integrated. These species were PE(34:1) (at *m/z* 716.51 amu), PE(32:1) (at *m/z* 688.48 amu), and the cyclopropane derivative PE(33:0) (at *m/z* 702.50 amu). To estimate the amount of each endogenous PE species, we calculated the ratio of that species' EIC peak area to the internal standard's EIC peak area. This ratio was then multiplied by the number of moles of internal standard that had been extracted together with the LpxB protein sample, and these values were summed. Given the moles of LpxB extracted, and assuming that the three major PE species accounted for about 50% of the total PE (*242*), and that

PE comprised ~70% of the total phospholipids purifying with the LpxB (see below), we estimated the approximate molar ratio of non-covalently bound phospholipids to purified LpxB.

5.2.10 Estimation of the phospholipid to LpxB ratio by ^{32}P labeling of cells

Cultures (50 ml) of C41(DE3)/pECLpxB19 expressing *E. coli* LpxB or the C41(DE3)/pET19b vector control (Table 1) were grown in LB broth containing 100 μg/ml ampicillin at 37 °C in rotary shaker at 200 rpm. At A_{600} of ~0.5 (mid-log phase), the cultures were induced with 1 mM IPTG. One set of vector-control and LpxB-expressing cultures was labeled with $^{32}P_i$ (Perkin-Elmer, Inc., Waltham, MA) at 10 μCi/ml, while another set was grown without labeling. The cells were harvested after 3 hours, and the pellets were washed with PBS, and divided into two equal portions (each corresponding to 25 ml of culture). One set of pellets from each of the radio-labeled strains (vector-control and LpxB-over-expressing) was extracted in a 5.8 ml acidic two-phase Bligh-Dyer system (*128, 240*). The quantity of total lipid ^{32}P in the washed lower phase of each sample was quantified by liquid scintillation counting (Packard, Inc., Prospect, CT). Approximately 15,000 cpm of each sample were spotted onto a silica TLC plate. The plates were quickly placed (prior to complete drying of the spots) into a tank equilibrated with chloroform/methanol/acetic acid (65/25/10, v/v/v). The developed plates were dried, exposed to PhosphorImager screens, and quantified. Phospholipids were identified by their R_f values.

Cells from the second set of radio-labeled pellets and a corresponding set of unlabeled pellets were lysed by sonic disruption (*243*) in 25 ml 50 mM sodium phosphate, pH 8.0, and 300 mM NaCl. Cell debris and membranes were removed by ultracentrifugation for 1 h at 100,000 x *g*. LpxB from these membrane-free lysates was purified by Ni-NTA chromatography, as described in the Supporting Methods, except that sonic irradiation was used to accomplish cell lysis. Phospholipids that co-purified with LpxB were extracted with an acidic Bligh-Dyer system (*128, 240*), separated and quantified as described above. The LpxB purified from the non-radiolabeled cell pellets was assayed under standard conditions and analyzed by SDS-PAGE to confirm over-expression and purity. The purified enzyme was fully active and greater than > 95% pure. The

molar ratios of the ^{32}P phospholipids to the purified LpxB samples from which they were extracted were estimated as follows: the assumption that ~10 μg of phospholipids can be extracted per A_{600} unit/ml of *E. coli* culture (*108*); the measured amount of LpxB protein purified from the 25 ml of culture; and the assumption that the average molecular weight of *E. coli* phospholipids is ~720 g/mol.

5.2.11. Transmission electron microscopy of *E. coli* cells over-expressing LpxB

The vector-control C41(DE3)pET19b and the LpxB-over-expressing C41(DE3)/pECLpxB19 were grown in LB broth at 37 °C to mid-log phase (A_{600} of ~0.5) and induced with 1 mM IPTG for three h. The cells were harvested by centrifugation at ~2500 x *g* and fixed with 2.5 % w/v glutaraldehyde and 1% w/v tannic acid. Cells were stained with osmium tetroxide, uranyl acetate, and lead acetate (*244*). Sectioning and transmission electron microscopy were conducted at the University of North Carolina: Chapel Hill, Department of Cell Biology and Physiology Electron Microscopy Facility.

5.3 Results

5.3.1 Cloning and expression of *E. coli* and *H. influenzae* LpxB

The *lpxB* genes of *E. coli* and *H. influenzae* were cloned into several vectors, including some that introduced *N*-terminal or *C*-terminal His tags (Table 1). Expression in *E. coli* C41(DE3) (*182*) was monitored by SDS-PAGE and LpxB assay. Maximal over-expression was obtained with high-copy pET plasmids encoding LpxB fused to a *C*-terminal His_6 tag via a short, non-cleavable linker, or with a *N*-terminal His_{10} tag connected by an 8-12 residue protease-cleavable segment. Lysates of the best constructs over-expressed LpxB activity 20-40,000-fold relative to vector controls (Tables 2 and 3 and Supporting Table 2). Similar constructs were used to over-express *H. influenzae* LpxB. Membrane-free lysates of the best *H. influenzae* constructs had specific activities that were 10-fold lower than those of the corresponding *E. coli* lysates (Tables 2 and 3) because of lower protein expression (Figure 1). Extracts of the various *E. coli* constructs (Table 1) with cleavable *N*-terminal His_{10} tags generally had specific activities that were within a factor of two each other, as did the corresponding Ni-NTA purified proteins.

5.3.2 An optimized autoradiographic assay for LpxB

We previously observed that ~2/3 of *E. coli* LpxB activity sediments with *E. coli* membranes prepared from wild-type strains that had been lysed in low-salt buffers (*116*). To explore this issue in more detail, *E. coli* cells expressing LpxB were lysed in PBS, and membranes were separated from the soluble fraction by ultracentrifugation. The membranes contained ~75% of the LpxB activity. Next, they were divided into three portions, which were washed with either PBS, PBS supplemented with 250 mM NaCl, or PBS supplemented with 250 mM KSCN. The membranes were again collected by ultracentrifugation. Whereas over 80% of the LpxB units remained associated with membranes washed in PBS, inclusion of 250-300 mM NaCl reduced the membrane association to 32 %, and 250 mM KSCN released most of the LpxB into the soluble fraction (data not shown). When cells over-expressing LpxB were lysed in the presence of Ni-NTA loading buffer (50 mM sodium phosphate, pH 8.0, 250 mM NaCl, 25 mM

imidazole and 20% glycerol, ~2/3 of the LpxB activity was recovered in the supernatant following ultracentrifugation. The latter procedure was the simplest for recovering LpxB on a large scale.

5.3.3 Peripheral association of *E. coli* LpxB with membranes

We previously observed that ~2/3 of *E. coli* LpxB activity sediments with *E. coli* membranes prepared from wild-type strains that had been lysed in low-salt buffers (*116*). To explore this issue in more detail, *E. coli* cells expressing LpxB were lysed in PBS, and membranes were separated from the soluble fraction by ultracentrifugation. The membranes contained ~75% of the LpxB activity. Next, they were divided into three portions, which were washed with either PBS, PBS supplemented with 250 mM NaCl, or PBS supplemented with 250 mM KSCN. The membranes were again collected by ultracentrifugation. Whereas over 80% of the LpxB units remained associated with membranes washed in PBS, inclusion of 250-300 mM NaCl reduced the membrane association to 32 %, and 250 mM KSCN released most of the LpxB into the soluble fraction (data not shown). When cells over-expressing LpxB were lysed in the presence of Ni-NTA loading buffer (50 mM sodium phosphate, pH 8.0, 250 mM NaCl, 25 mM imidazole and 20% glycerol, ~2/3 of the LpxB activity was recovered in the supernatant following ultracentrifugation. The latter procedure was the simplest for recovering LpxB on a large scale.

5.3.4 Purification of *E. coli* and *H. influenzae* LpxB

The previous purification of *E. coli* LpxB (*116*) used dye-affinity resins that are no longer manufactured and that preceded the advent of pET vectors. Because *N*-terminally His_{10}-tagged LpxBs showed stronger affinity for Ni-NTA columns than those with *C*-terminal His_6 tags, the former were used for large-scale purification. As noted above, membrane-free lysates, prepared in the high-salt Ni-NTA resin-loading buffer, contained about two-thirds of the LpxB activity. The addition of detergents (0.1% w/v DDM in the optimized large-scale purification scheme) to the supernatant at this stage improved LpxB recovery, even when DDM was omitted in the later steps.

Table 5.2. Purification of *E. coli* LpxB from C41(DE3)/pECLpxB-TEV

Step	Total Protein (mg)	Total volume (ml)	Total Units (mmol/min)	Specific activity (μmol/min/mg)	Yield (%)	Fold-purification
Membrane-free lysate	1200	225	7.5	6.1	100	1.0
Ni-NTA column fractions	34	90	4.4	129	58	20
TEV-digested Ni-NTA flow-through	20	100	2.5	125	32	19
Size exclusion chromatography	15	20	1.6	107	21	16

Table 5.3. Purification of *H. influenzae* LpxB from C41(DE3)/pHILpxB-TEV

Step	Total Protein (mg)	Total Volume (ml)	Total Units (mmol/min)	Specific activity (μmol/min/mg)	Yield (%)	Fold-purification
Membrane-free lysate	930	225	42	45	100	1.0
Ni-NTA column fractions	110	90	19	173	44	3.9
TEV-digested Ni-NTA flow-through	100	100	17	170	39	3.6
Size exclusion chromatography	52	25	9.5	183	23	4.0

Table 5.4. Relative specific activities of purified *E. coli* LpxB point mutants.

Substitution	Conservation of mutated residue among LpxB orthologs	Wild-type specific activity %
E15A	highly conserved	0.99
S17A	highly conserved	2.70
D98A	absolutely conserved	< 0.01 (none detected)
F102A	highly conserved	3.20
W126A	absolutely conserved	3.72
R201A	absolutely conserved	< 0.01 (none detected)
L314A	highly conserved	9.47
N316A	absolutely conserved	0.10

Table 5.5 ESI/MS quantification of the three most abundant phosphatidylethanolamine species associated with *E. coli* LpxB

PE species	Exact mass	Peak area (counts)	Estimated PE (pmols)
PE: 31:1 (internal standard)	675.48	4.83 x 104	3.00*
PE: 34:1	717.53	8.82 x 104	6.21
PE 32:1	689.50	4.48 x 104	3.15
PE 33:0 cyclopropane form	703.52	1.90 x 104	1.34

Table 5.6 ^{32}P-phospholipid counts in whole cell pellets and purified *E. coli* LpxB fractions.

Sample	32P (cpm ± range* x 10-6)
C41(DE3)/pET19b whole cell pellet	12.2 ± 1.1
C41(DE3)/pET19b Ni-NTA fractions	0.003 ± 0.001
C41(DE3)/pECLpxB19 whole cell pellet	23.0 ± 2.2
C41(DE3)/pECLpxB19 Ni-NTA fractions	0.29 ± 0.06

Table 5.7 Composition of ^{32}P-labeled phospholipids purifying with *E. coli* LpxB.

Source of phospholipid	PE*	PG*	CL*
C41(DE3)/pET19b whole cell pellet	74 ± 1	22 ± 2	3 ± 2
C41(DE3)/pECLpxB19 whole cell pellet	65 ± 1	17 ± 3	15 ± 2
LpxB purified from C41(DE3)/pECLpxB19	72 ± 2	21 ± 1	7 ± 3

N-terminally His_{10}-tagged *E. coli* or *H. influenzae* LpxB, present in the DDM-treated supernatants of *E. coli* C41(DE3)/pECLpxB-TEV or *E. coli* C41(DE3)/pHILpxB-TEV (Table 1), was purified to about 95% homogeneity, as described in the methods section, by chromatography on Ni-NTA columns (Tables 2 and 3, and Fig. 2). This step also removed the bulk DDM and the phospholipids that are otherwise non-covalently associated with LpxB (see below). TEV-protease (*235, 236*) was then used to cleave the His_{10} tag, after which both *E. coli* and *H. influenzae* LpxB were passed through the same Ni-NTA column to remove the cleaved tag, the remaining His_{10}-tagged LpxB, the *C*-terminally His_6-tagged TEV-protease, and minor contaminating *E. coli* proteins. The cleavage of the His_{10} tag was detected by gel electrophoresis of the initial Ni-NTA column eluate (Fig. 1, lane 2) versus the TEV-treated LpxB after the second Ni-NTA column (Fig. 1, lane 3). The shift in LpxB migration corresponded to the loss of ~2.5 kDa upon cleavage of the tag and its linker.

Size-exclusion chromatography was employed as the final purification step. *E. coli* and *H. influenzae* LpxBs were purified 3.9 and 16-fold, from their respective membrane-free lysates (Tables 2 and 3, and Figure 1). From a 12 L induced culture grown to A_{600} = 3.5, about 50 mg of *E. coli* LpxB was obtained with an overall activity yield of 23% (Table 2), and 15 mg of *H. influenzae* LpxB was obtained with a yield of 21% (Table 3). The sequences of these purified constructs were confirmed by ESI/MS of the intact proteins. For the *E. coli* LpxB construct, a de-convoluted molecular weight of 42741.00 was measured (expected: 42737.80). For the *H.*

influenzae LpxB construct, a de-convoluted molecular weight of 43995.00 was measured (expected: 43992.50). Each cleaved, purified protein contains three additional amino acid residues (SHM) at its *N*-terminus compared to wild-type. These residues are artifacts of the TEV protease cleavage sequence and the *ndeI* restriction site.

5.3.5 Size of *E. coli* and *H. influenzae* LpxB as judged by gel filtration.

When analyzed in a detergent-free buffer on a calibrated Superdex 200 column, *E. coli* LpxB elutes at a volume consistent with a M_r of ~360 kDA (Figure 3A), whereas *H. influenzae* LpxB elutes with a M_r of ~42 kDA (Figure 3B). The estimated M_rs of *E. coli* and *H. influenzae* LpxB are consistent with an octamer and a monomer, respectively. When *E. coli* LpxB is passed through a similar gel filtration column in the presence of 0.1% w/v DDM, the peak shifts from one consistent with an octamer to a smaller species (Figure 3C).

5.3.6 Apparent kinetic parameters and pH rate profile for *E. coli* LpxB.

The apparent K_M for lipid X was 381 ± 23 μM, and the apparent V_{max} was 271 ± 6 nmol/min/mg with UDP-2,3-diacyglucosamine held at 1200 μM (Figure 4A). The apparent K_M and V_{max} when varying UDP-2-3-diacylglucosamine were 287 ± 34 μM and 147 ± 7 nmol/min/mg (Figure 4B). These values are "apparent" because of the surface dilution effects inherent in mixed-micelle systems (*238*). To determine its pH dependency, purified *E. coli* LpxB was assayed in a three-buffer system over the range of pH values shown in Figure 4C (*184*). An apparent pK_a of 5.9 ± 0.2 and a pK_b of 9.0 ± 0.4 were estimated from the data.

5.3.7 Effect of detergent on *E. coli* LpxB activity

Purified enzyme was assayed under standard assay conditions at varying concentrations of Triton X-100. Between 0 and 500 μM Triton X-100 increased the apparent specific activity five-fold (Figure 5A) with lipid X and UDP-2-3-diacylglucosamine concentrations held at 400 μM and 600 μM, respectively. The Triton X-100 concentration in this experiment never exceeded 1 mM.

To determine whether LpxB activity is dependent upon the bulk concentration of the micelle surface (*238*), the molar ratios of lipid X, UDP-2-3-diacylglucosamine, and Triton X-100 were fixed with respect to each other. The bulk concentration ([lipid X] + [UDP-2-3-diacylglucosamine] + [Triton X-100]) was then varied from 28 μM to 1.8 mM (Figure 5B). A sigmoidal relationship, highlighted in the inset, is seen when the bulk surface concentration is varied between ~60 and 230 μM. This behavior is suggestive of interfacial activation, because the apparent specific activity drops sharply as the mixed micelle surface approaches the critical micelle concentration of Triton X-100 (50-100 μM) (*238*).

To probe the effect of surface dilution on the apparent specific activity of *E. coli* LpxB, the Triton X-100 concentration was varied over a larger concentration range (50 μM to 14 mM) than used in Figure 5A. Moreover, the substrate concentrations were fixed at ~10-fold lower values (50 μM and 75 μM for lipid X and UDP-2-3-diacylglucosamine, respectively) than those used in the standard assay condition. The resulting curve was fit to a single exponential decay (Figure 5C), consistent with the dilution of the LpxB substrates at the micelle surface by Triton X-100 (*238*).

5.3.8 Site directed mutagenesis of conserved *E. coli* LpxB residues.

Highly (~90%) or absolutely conserved residues present in the available LpxB orthologs were mutated to alanine. These mutant proteins were expressed, purified, and assayed for activity as described in the Supporting Information. As judged by SDS-PAGE analysis, the expression levels and purification behaviors of the mutant proteins were similar to the wild-type (data not shown). Among the subset of absolutely conserved residues, two LpxB variants (D98A an R201A) had no detectable activity, suggesting that they may play important roles in catalysis or substrate binding. Substitution of the other residues with alanine resulted in mutant proteins that retained between 1 and 10% of the wild-type LpxB activity (Table 4). The absolutely conserved residues T277 and E281 and the highly conserved residue E326 were not investigated.

5.3.9 Identification of bound phospholipids purifying with *E. coli* LpxB

LpxB that was not exposed to DDM or Triton X-100 after the initial ultracentrifugation step could be purified by the standard metal affinity chromatography and TEV protease cleavage protocols. The phospholipids associated with the protein were extracted using a two-phase Bligh-Dyer system and analyzed in the negative ion mode by ESI-MS (Figure 6A). The major phospholipids associated with LpxB are similar in composition to the total *E. coli* phospholipids (*245*), suggesting that LpxB does not bind a particular molecular species. Upon repetition of this experiment with purified LpxB that had been treated with or 1% w/v DDM prior to Ni-NTA chromatography, a ~100-fold reduction in LpxB-associated phospholipids was observed (Figure 6B). Treatment with 1% w/v Triton X-100 or 1% w/v octyl-β-D-glucopyranoside yielded similar results (data not shown).

In order to quantify the ratio of bound phospholipids per LpxB monomer, purified *E. coli* LpxB that had not been treated with detergent was extracted together with a known amount of a synthetic phosphatidylethanolamine standard (17:0, 14:1) with an exact mass of 675.48. The extracted phospholipids were then fractionated by reverse-phase chromatography, and the effluent was continuously monitored by ESI-MS (*241*). The area of the extracted ion current (EIC) of the standard was compared to the corresponding areas of the three most abundant endogenous phosphatidylethanolamine species (Table 5), allowing us to estimate the approximate molar quantity of each (Table 5). With the additional assumptions described in the Materials and Methods section, the molar ratio of phospholipids to LpxB monomer was about 1:1.6.

5.3.10 Quantification of phospholipids bound to E. coli LpxB by 32P-labeling.

The molar ratio of phospholipids bound to LpxB (purified without exposure to detergent) was confirmed by labeling cultures of *E. coli* C41(DE3)/pECLpxB19 and the vector control C41(DE3)/pET19b with $^{32}P_i$. The cell pellets were divided into two portions: one was directly

extracted by the Bligh-Dyer method to determine the total phospholipid content. The cells in the other portion were lysed and subjected to Ni-NTA affinity chromatography. The LpxB-containing fractions in the 300 mM imidazole eluate were then extracted with the Bligh-Dyer method. The total number of counts in each fraction was quantified. There were 100 times fewer counts in the Ni-NTA fractions from the vector control than from the $(His)_{10}$-tagged LpxB fractions (Table 6), confirming that some phospholipid molecules are indeed associated with LpxB. Assuming that ~10 μg of phospholipids are present per ml of culture at A_{600} = 1.0 (*108*) and knowing the amount of LpxB protein recovered, we calculated that 9.3 nmol or 12.6 nmol of phospholipids were purified together with 2.9 nmol of LpxB in two separate experiments, corresponding to an average protein to phospholipid to molar ratio of 1:3.5 (Table 6). Although this value is slightly higher than the amount determined by mass spectrometry (Table 5), both results exclude the possibility of a phospholipid vesicle being associated with the purified LpxB protein (*246*).

Nearly two times more total ^{32}P-labeled phospholipids were extracted from the cell pellets of the LpxB over-expressing strain relative to the vector control (Table 5). To determine whether or not the over-expression of LpxB altered the phospholipid composition of the host cells, we separated the labeled phospholipids by TLC and quantified their relative amounts. The LpxB over-expressing strain contained somewhat more phosphatidylglycerol and cardiolipin than the vector control (Table 7). However, the composition of the phospholipids associated with LpxB was indistinguishable from that of the total wild-type cell pellet.

5.3.11 Transmission electron microscopy of E. coli cells over-expressing LpxB.

E. coli cells in which LpxB is massively over-expressed contain nearly twice the quantity of phospholipids as paired vector-controls (Table 6), suggesting that LpxB over-expression perturbs the membrane phospholipid biosynthesis. LpxB-expressing and vector-control strains were therefore examined by thin-section transmission electron microscopy. The vector-control strain showed a typical *E. coli* cell envelope (Figure 8A and B). In contrast, at least 50% of the

LpxB-expressing cells accumulated aberrant tubular membranes (Figure 8C and D) of a uniform diameter, situated mainly along the inner surface of the inner membrane.

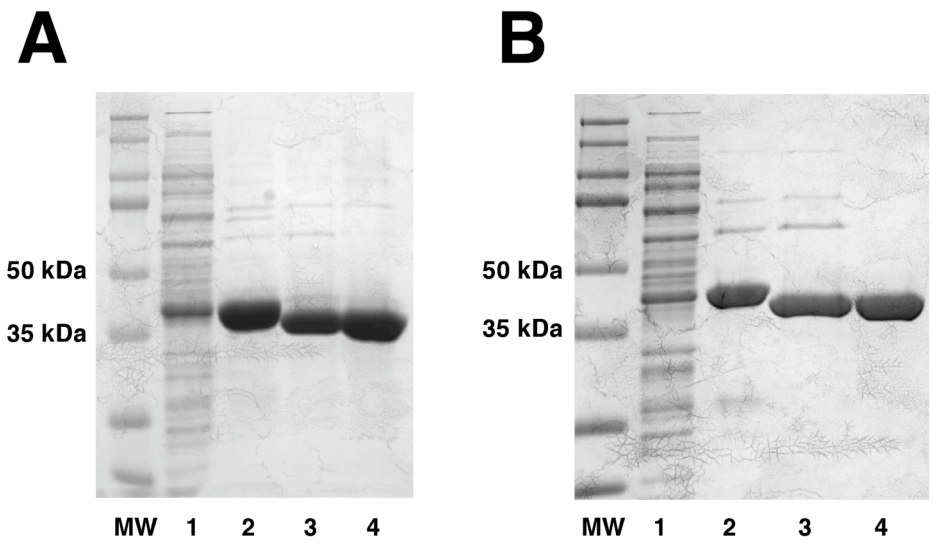

Figure 5.1. Purification of *E. coli* and *H. influenzae* LpxB to near-homogeneity. These 12% SDS-Tris-polyacrylamide gels show 30 μg protein samples from each step of the optimized purifications of *N*-terminally His_{10}-tagged and TEV-protease cleavable *E. coli* (**Panel A**) and *H. influenzae* (**Panel B**) LpxB. The far left lanes are the molecular weight standards. **Lane 1**, membrane-free lysates; **lane 2**, the Ni-NTA column 300 mM imidazole fraction; **lane 3**, the TEV-protease digested protein after passage through a second Ni-NTA column; **lane 4**, the final material after purification by size-exclusion chromatography. MW denotes the molecular weights of the proteins standards. The molecular weights of the tagged and cleaved *E. coli* LpxB constructs are 45.9 kDa and 42.7 kDa, respectively, while those of the tagged and cleaved *H. influenzae* LpxB constructs are 46.1 kDa and 43.9 kDa. The activity yields for these *E. coli* and *H. influenzae* LpxB preparations are shown in Tables 2 and 3 respectively.

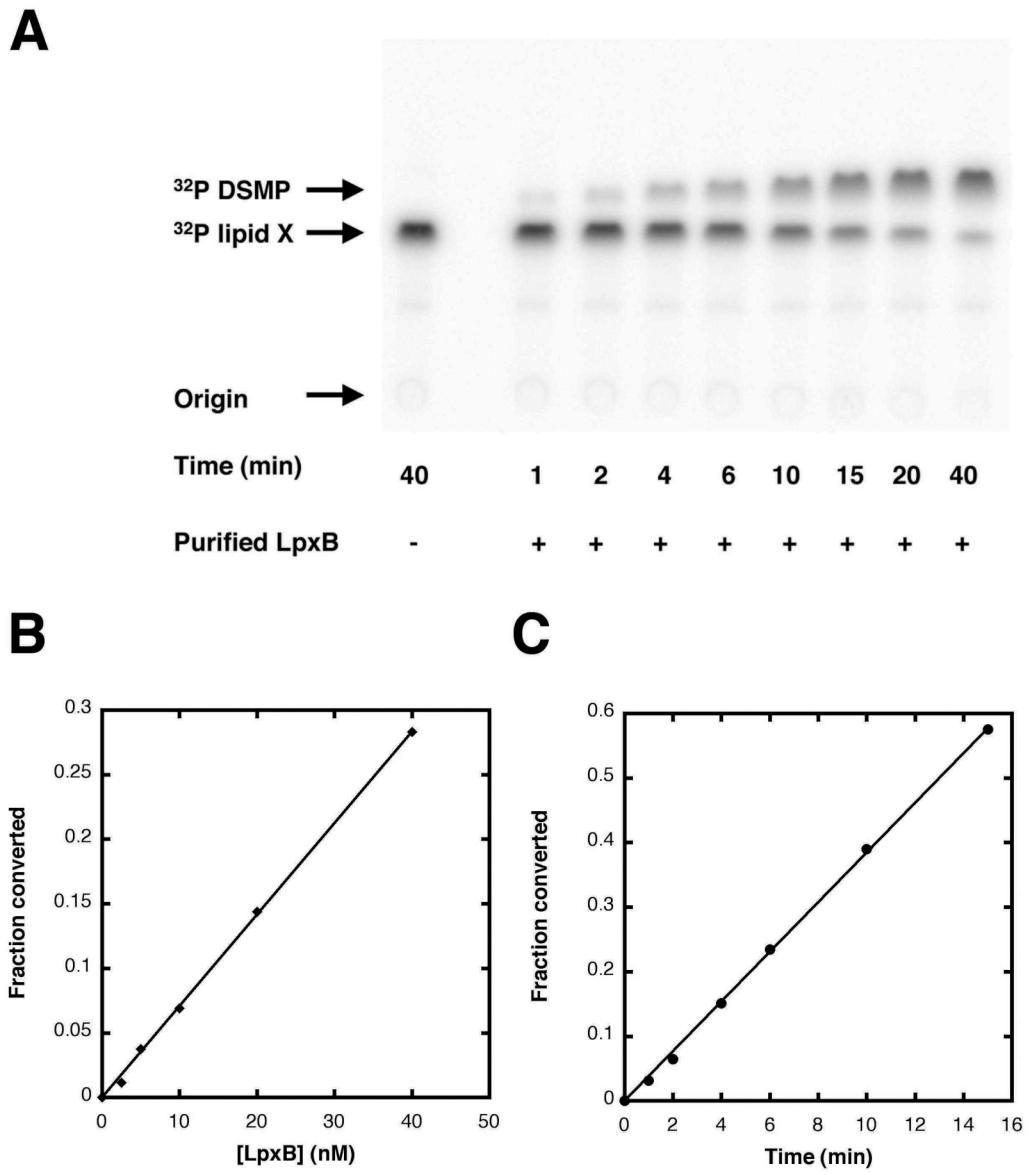

Figure 5.2. An optimized quantitative *in vitro* assay for LpxB activity. Reaction mixtures at 30 °C contained 400 μM lipid X, 1000 cpm/μl ^{32}P-lipid X, 600 μM UDP-2,3-diacylglucosamine, 20 mM HEPES, pH 8.0, 0.5 mg/ml BSA, 0.05% w/v Triton X-100 and enzyme, as indicated in a final volume of 25 μL. At various times 3 μl portions were spotted onto a Silica Gel 60 plate and developed in chloroform/methanol/water/acetic acid (25/15/4/2, v/v/v/v). The plates were subsequently dried, and radioactivity was quantified using a PhosphorImager. **Panel A**. Image of a typical time course with LpxB purified from C41(DE3)/pECLpxB19 at 20 nM. **Panel B**. LpxB activity is linear with protein concentration, which was varied from 2.5 to 40 nM. Reactions were stopped after 3 min. **Panel C**. LpxB product formation is linear with time.

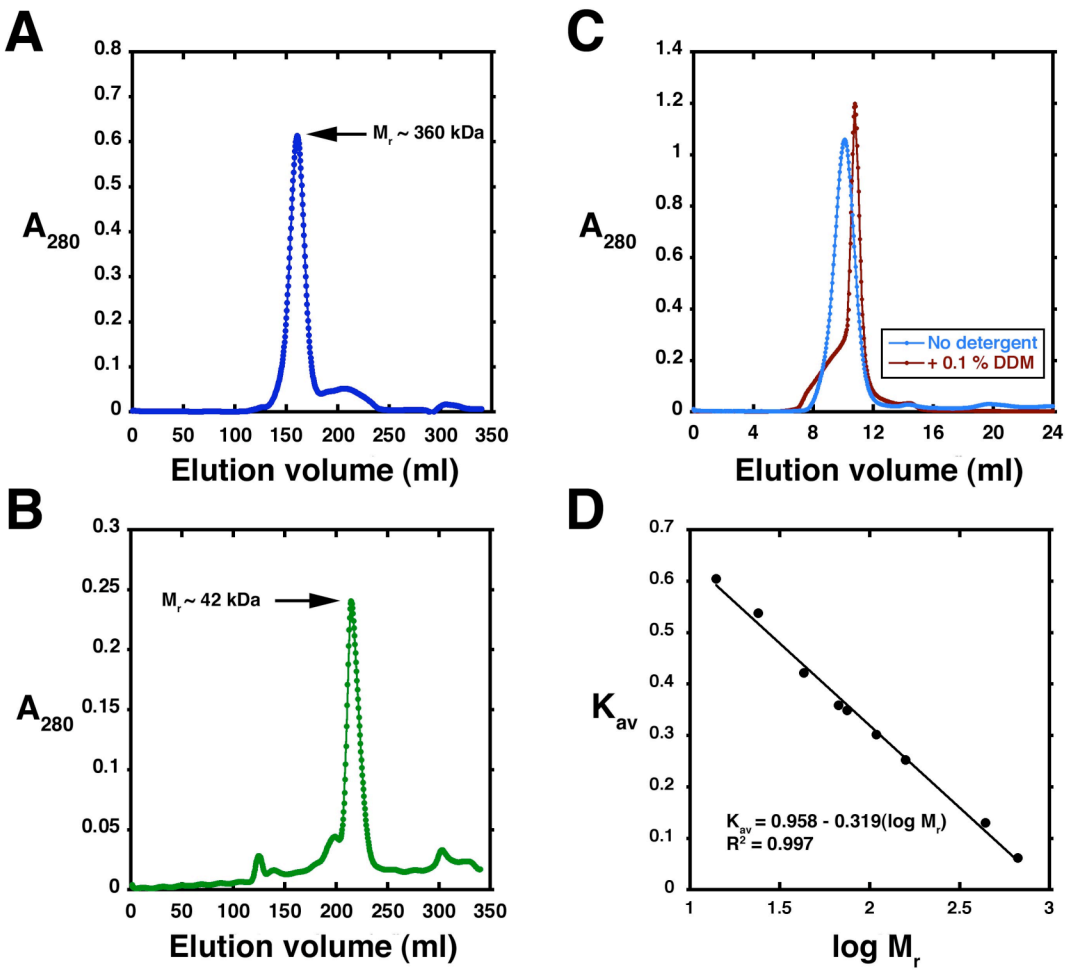

Figure 5.3. Size exclusion chromatography of *E. coli* and *H. influenzae* LpxB. Panel A. As shown by the A_{280} profile, pure *E. coli* LpxB (21 mg as prepared in Table 2) emerges as an apparent octamer on a 350 ml Superdex 200 column, run at 1.0 ml/min in 20 mM HEPES, pH 8.0, 150 mM NaCl, and 5 mM TCEP. **Panel B**. *H. influenzae* LpxB (15 mg as prepared in Table 3) emerges as an apparent monomer under chromatographic conditions identical to those used for the *E. coli* enzyme, except for the inclusion of 500 mM NaCl to prevent precipitation above 5 mg/ml. **Panel C.** *E. coli* LpxB is shifted from an apparent octamer (blue trace) to an apparent dimer (red trace) when 0.1% w/v DDM is included in the buffer. In this experiment, a 24 ml Superdex 200 column was run at a flow rate of 0.33 ml/min in 20 mM Tris, pH 7.4, 200 mM NaCl, 5 mM TCEP, and 5% w/v glycerol. **Panel D.** The 350 ml Superdex 200 sizing column used in Panels A and B was calibrated with indicated protein standards to estimate the molecular weights of the LpxB peaks.

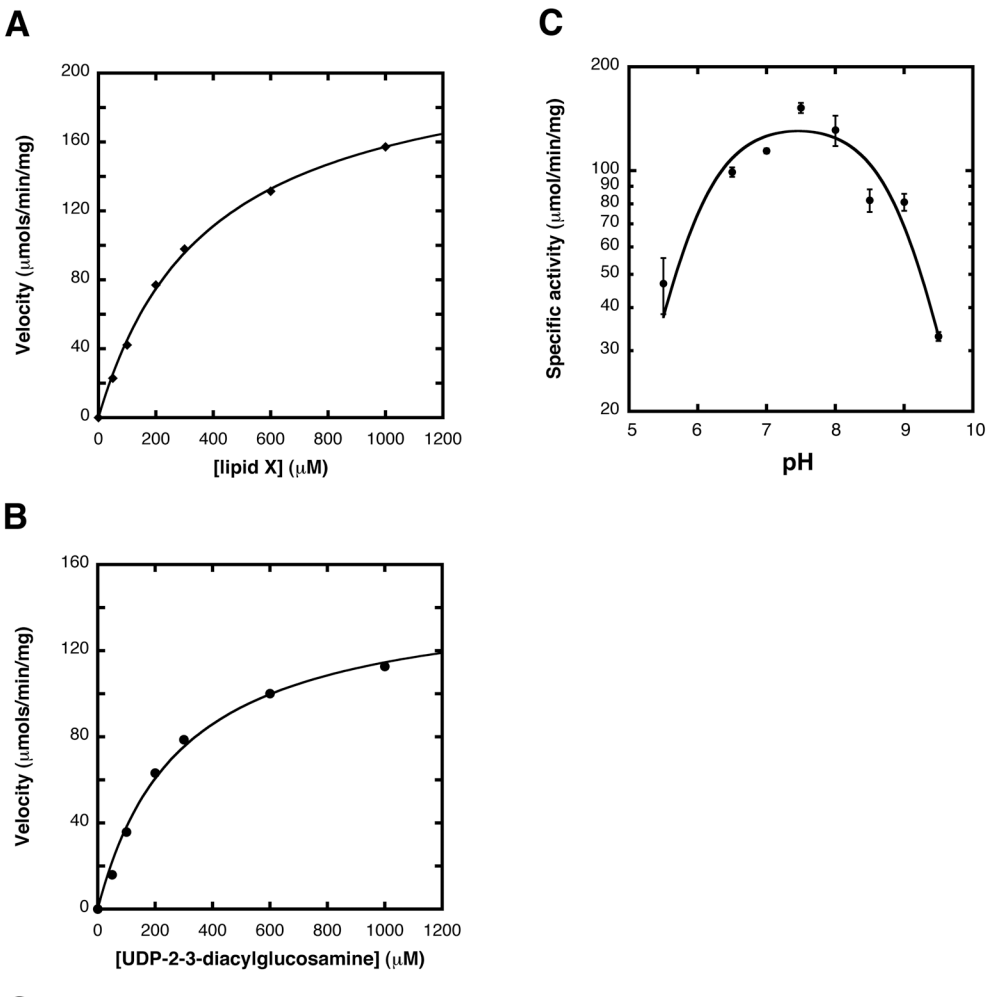

Figure 5.4. Apparent kinetic parameters and pH rate profile of *E. coli* LpxB. Panel A. Purified *E. coli* LpxB from strain C41(DE3)/pECLpxB19 was assayed under standard conditions except that UDP-2,3-diacyl-GlcN was constant at 1200 μM, and lipid X was varied from 50 to 1000 μM. The velocities were fit to a standard Michaelis-Menten function using the program KaleidaGraph. With respect to lipid X, the apparent K_M was 381 ± 23 μM, and the apparent V_{max} was 271 ± 6 nmol/min/mg. **Panel B**. In this experiment lipid X was held at 1200 μM, while UDP-2,3-diacyl-GlcN was varied from 50 to 1000 μM. With respect to UDP-2,3-diacyl-GlcN, the apparent K_M was 287 ± 34 μM, and the apparent V_{max} was 147 ± 7 nmol/min/mg. **Panel C**. *E. coli* LpxB was assayed over the indicated pH range under optimized assay conditions with a triple-buffer system consisting of 100 mM sodium acetate, 50 mM bis(2-hydroxymethyl)-imino-tris(hydroxymethly)-hexane, and 50 mM Tris (*184*).

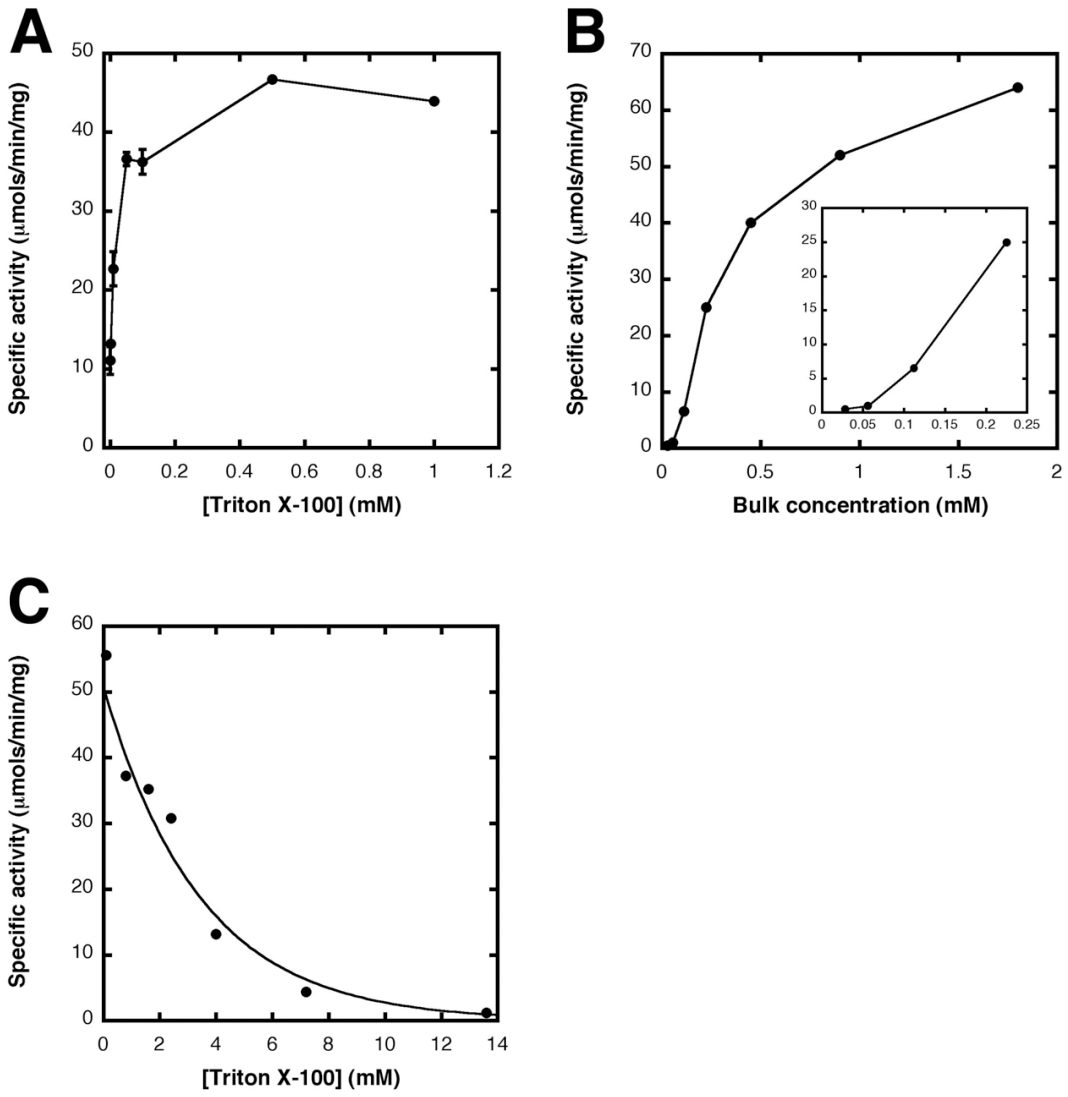

Figure 5.5. Effect of detergent concentration on *E. coli* LpxB activity. Panel A. Pure LpxB from C41(DE3)/pECLpxB23 (Table 1) was assayed under standard conditions (400 μM lipid X and 600 μM UDP-2,3-diacyl-GlcN), except that the concentration of Triton X-100 (estimated average molecular of 647) was varied from 10 μM to 1 mM. Each point represents the average of two identical experiments. **Panel B**. Pure LpxB from C41(DE3)/pECLpxB-TEV was assayed under conditions similar to those in Panel A, except that the molar ratio of lipid X:UDP-2,3-diacyl-GlcN:Triton X-100 was held constant at 2:3:4, and then varied from 0.028 mM to 1.8 mM. The inset shows the sigmoidal behavior of the reaction velocity at low bulk concentrations. **Panel C**. To evaluate the effects of surface dilution, pure LpxB from C41(DE3)/pECLpxB-TEV was assayed with 50 μM lipid X and 75 μM UDP-2,3-diacylglucosamine, and the concentration of Triton X-100 was varied from 0.1 to 13.6 mM. The resulting curve was fit to a single exponential decay function.

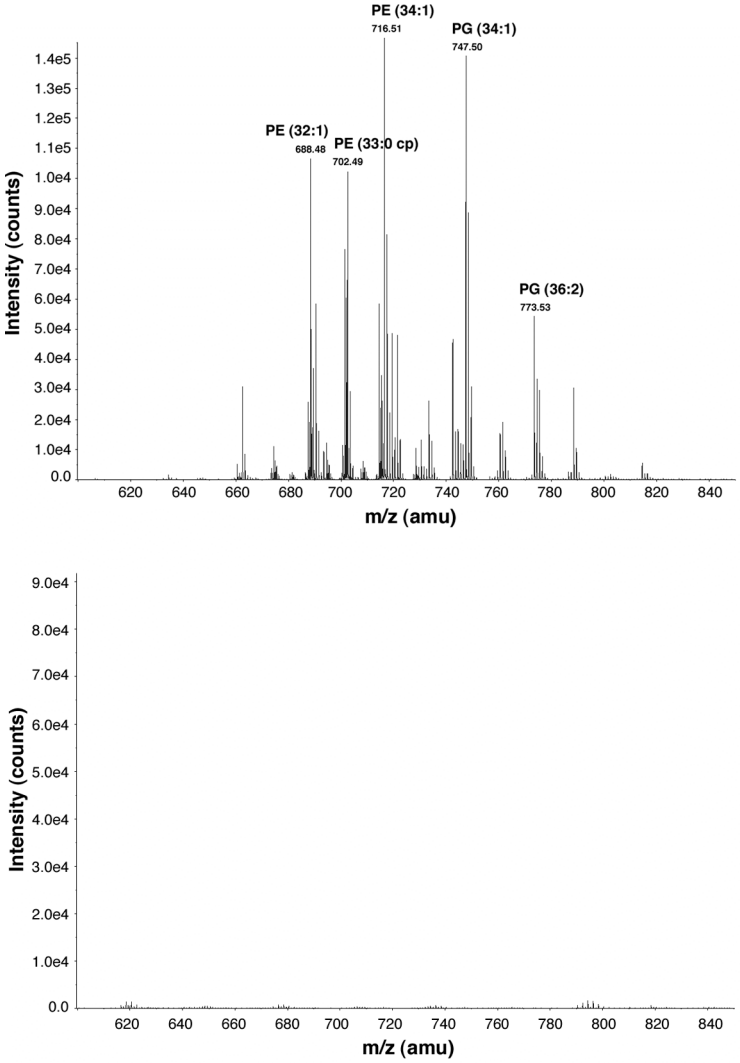

Figure 5.6. Phospholipids are bound to *E. coli* LpxB purified in the absence of detergents. Panel A. Pure LpxB, prepared without exposure to detergent from C41(DE3)/pECLpxB19 (Table 1), was extracted with a two-phase Bligh-Dyer system. The lower phase was dried under N_2, re-dissolved in chloroform/methanol (2:1, v/v), and analyzed by ESI/MS in the negative ion mode following direct injection into an ABI QSTAR-XL time-of-flight mass spectrometer. The phospholipids species are: PE, phosphoethanolamine; and PG, phosphatidylglycerol. **Panel B**. *E. coli* LpxB was purified as above, except that the Ni-NTA-immobilized enzyme was washed with buffer containing 1% w/v DDM, as in the preparation shown in Table 2. There is a 100-fold decrease in the amount of phospholipids recovered in comparison to Panel A.

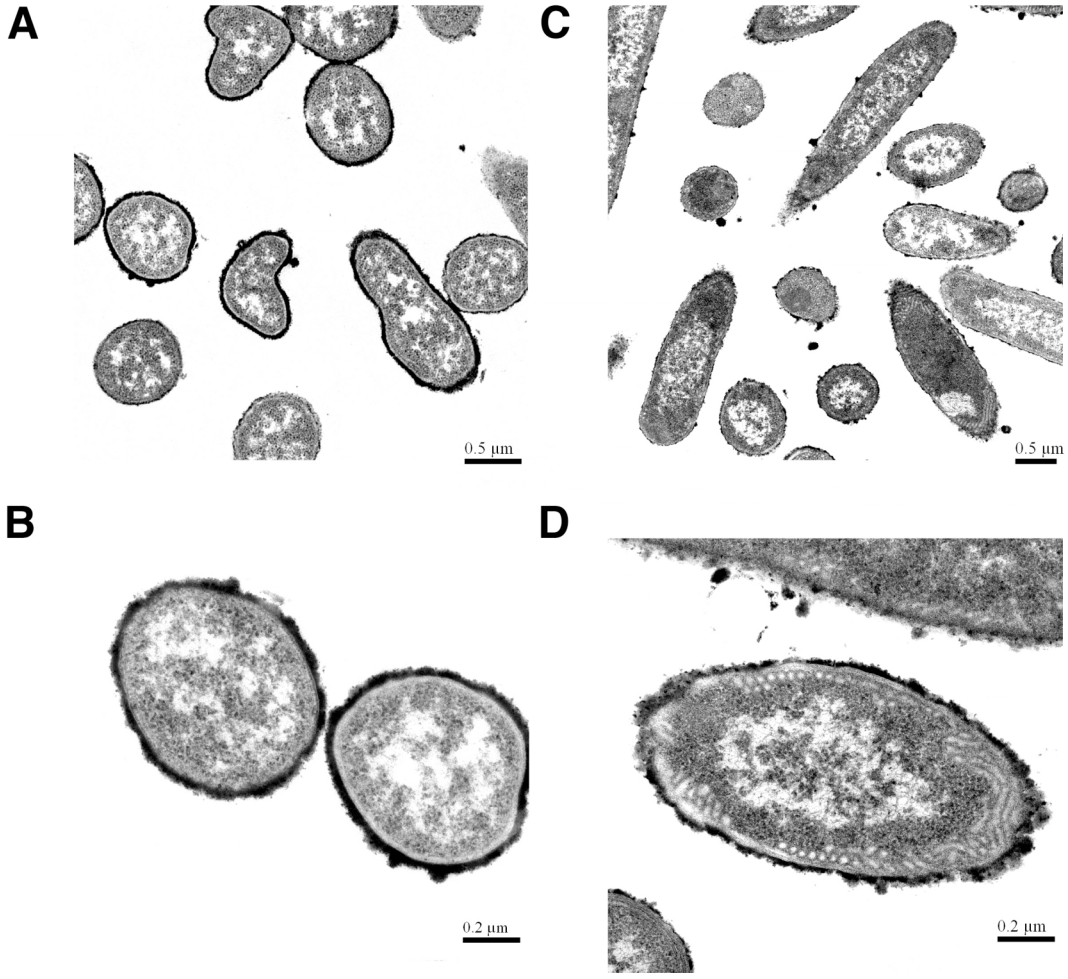

Figure 5.7. Transmission electron microscopy of *E. coli* cells over-expressing LpxB. Thin-section transmission electron micrographs of induced C41(DE3)/pET19b vector control cells (**Panels A** and **B**) compared to induced C41(DE3)/pECLpxB19 cells (**Panels C** and **D**). Cells were fixed with 2.5 % w/v glutaraldehyde and 1% w/v tannic acid, and then were stained with osmium tetroxide, uranyl acetate, and lead acetate (*244*). Aberrant tubular membranes were observed in over 50% of the induced C41(DE3)/pECLpxB19 cells.

5.4 Discussion

LpxB, the lipid A disaccharide synthase, is an essential enzyme in nearly all Gram-negative bacteria (*219*). As members of the GT-B superfamily of glycosyltransferases, *E. coli* and *H. influenzae* LpxB are inverting glycosyltransferases in CAZy sub-family 19 (http://www.cazy.org/), a grouping of hundreds of putative LpxB orthologs. While abundant in nature, relatively few GT-B type glycosyl transferases have been structurally and enzymatically characterized (*118*). Equipped with an improved autoradiographic LpxB assay (Figure 2), we have now developed robust expression and purification procedures for *E. coli* and *H. influenzae* LpxB (Figure 1). *E. coli* LpxB activity is surface-concentration dependent (Figure 5), but its surface association is largely mediated by ionic interactions. Phospholipids co-purify with *E. coli* LpxB, as demonstrated by radioactive labeling and mass-spectrometry (Figure 6 and Tables 5, 6 and 7). Alanine-scanning mutagenesis of a subset of conserved LpxB residues, and purification of the mutant gene products, allowed us to identify two conserved residues without which there is no measurable LpxB activity (Table 4).

High-copy pET plasmids, induced in the *E. coli* BLR(DE3)-derived strain, C41(DE3) (*182*), yielded nearly 100-fold greater LpxB over-expression than our previously reported strains (*116*). Moreover, the addition of a *C*- or *N*-terminal polyhistidine tag to LpxB was crucial for over-expression. This observation has precedent, although it is unclear whether the polyhisitidine tag is disrupting regulatory mRNA structure, preventing protein degradation, or enhancing protein folding. The use of these tags also facilitated the development of a rapid purification by Ni-NTA affinity chromatography. Moreover, the use of TEV-protease-cleavable polyhistidine tags (*235, 236*) facilitated the efficient removal of co-purifying contaminant proteins, and permitted us to purify both *E. coli* and *H. influenzae* LpxB to near-homogeneity (Figure 1).

The oligomerization states of *E. coli* and *H. influenzae* LpxB were probed by size exclusion chromatography (Figure 3). *E. coli* LpxB, in the absence of detergent, elutes as an apparent octamer (Figure 3A), while the *H. influenzae* enzyme is an apparent monomer under

similar conditions (Figure 3B). When sizing chromatography is performed on *E. coli* LpxB in the presence of DDM, the octamer shifts to a smaller species consistent with either a monomer or a dimer (Figure 3C). This observation further suggests that the self-association of purified *E. coli* LpxB may be mediated, at least in part, by hydrophobic contacts.

To characterize the activity of our purified enzyme preparations, we developed an improved LpxB assay, using TLC in conjunction with quantitative PhosphorImager analysis (Figure 3). The inclusion of 0.05% w/v Triton X-100 significantly increased the reaction's initial rate and linearity. It may be that detergents disaggregate *E. coli* LpxB, or that Triton X-100 promotes rapid mixing of the LpxB substrates, thereby allowing the entire substrate pool to be presented to the enzyme. The inclusion of BSA further enhanced the reproducibility of the assay.

We determined the apparent kinetic parameters for purified *E. coli* LpxB (Figure 4). With respect to lipid X, the apparent K_M was 381 ± 23 μM and the apparent V_{max} was 271 ± 6 nmol/min/mg. With respect to UDP-2-3-diacylglucosamine, the apparent K_M and V_{max} were 287 ± 34 μM and 147 ± 7 nmol/min/mg, respectively. The K_M values were within two-fold of those that we previously reported in the absence of Triton X-100 (*116*), while the apparent V_{max} values were about 10-fold higher, probably because of the optimized assay. Given that surface dilution effects are observed in this system (Figure 5), the physiological relevance of these apparent kinetic parameters is difficult to evaluate. When the substrate concentrations were fixed at low values and the concentration of Triton was varied from 1 to 112-fold that of the substrates (Figure 5C), the apparent LpxB activity decreased dramatically. This dilution effect is characteristic of surface-active enzymes (*238*).

If LpxB is not exposed to detergent during purification, it contains several bound *E. coli* phospholipid molecules per monomer, as judged by negative-mode ESI-MS analysis (Figure 6 and Table 5) and ^{32}P labeling studies (Tables 6 and 7). The bound lipids were not enriched for any particular species. LpxB activity is not stimulated by *E. coli* phospholipids, nor is the phospholipid free preparation less active than the phospholipid-containing enzyme (data not

shown). Since LpxB catalyzes the condensation of two diacylated lipid molecules (Scheme 1), it is possible that glycerophospholipids can bind non-specifically at low affinity to the unoccupied LpxB substrate-binding sites. Alternatively, the phospholipids may be bound to other sites that enhance the interaction of the LpxB protein with the inner membrane.

When comparing the total ^{32}P-labelled phospholipid content of an *E. coli* LpxB over-expressing strain to that of a matched vector control, we noted a two-fold accumulation of phospholipids in cells over-producing LpxB (Table 6). Moreover, we observed a statistically significant relative increase in the amount of anionic phospholipids (Table 7). We therefore examined the morphology of these LpxB over-expressing strains by transmission electron microscopy and noted the accumulation of tubules of uniform diameter along the inner membrane (Figure 7). Similar, aberrant membrane phenotypes have been observed in *E. coli* strains that over-express *sn*-glycerol-3-phosphate acyltransferase (*247*) and the peptidoglycan biosynthetic glycosyl transferase MurG (*246, 248*). How the overproduction of a specific membrane protein stimulates *de novo* phospholipid synthesis requires further exploration.

Alanine-scanning mutagenesis of a subset of conserved LpxB residues was carried out, and the mutant proteins were expressed, purified to homogeneity, and assayed. Two mutants, D98A and R201A, had no detectable catalytic activity (Table 4). Given that these constructs did not form inclusion bodies and purified in a manner similar to the wild-type enzyme, it is unlikely that either mutation caused gross protein misfolding. The micellar nature of the LpxB substrates (*116, 117*) (Figure 5) precludes the facile analysis of these mutants by standard enzyme kinetics.

Our analysis of LpxB's behavior at the membrane surface (Figure 5) and its purification with a small number of lipid molecules (Figure 6) may facilitate its crystallization. The identification of key functional residues (Table 4) should further aid in mechanistic and structural studies. Precedent exists for using inactive point mutants to capture membrane proteins in conformations that promote crystal formation (*249*). Although LpxB has a predicted secondary structure that is similar to those of other glycosyl transferases, including MurG for which a

structure is available (*248*), the diversity of glycosyl transferase substrate binding sites and catalytic strategies probably arises from the variable loops between the regions of conserved secondary structure (*118*). Knowledge of the structure of LpxB should reveal its unique lipid-binding properties (Scheme 1) and may facilitate the development of novel inhibitors with utility as antibiotics.

5. Dissertation Summary

Discovery and characterization of LpxI: a novel UDP-2-,3-diacylglucosamine hydrolase

Gram-negative bacteria possess an asymmetric outer membrane in which the inner leaflet is composed primarily of phospholipids while the outer leaflet contains both phospholipids and lipopolysaccharide (LPS). LPS forms a structural barrier that protects Gram-negative bacteria from antibiotics and other environmental stressors. The lipid A anchor of LPS is a glucosamine-based saccharolipid that is further modified with core and O-antigen sugars. In addition to serving a structural role as the hydrophobic anchor of LPS, lipid A is recognized by the innate immune system in animal cells and macrophages. In macrophages, lipid A has been found to stimulate TLR4 (toll like receptor 4), which in turn activates the inflammatory cascade.

The enzymes of Lipid A biosynthesis are conserved in Gram-negative bacteria; in most species, a single copy of each bio-synthetic gene is present. The exception is *lpxH*, which is an essential gene encoding a membrane-associated UDP-2,3-diacylglucosamine hydrolase, which catalyzed the attack of water upon the alpha-phosphate of its substrate and the leaving of UMP, resulting in the formation of lipid X. About 30% of Gram-negatives lack an *lpxH* orthologue, yet these species must possess an activity analogous to that of LpxH. We used bioinformatics approaches to identify this transformational analogue in the model organism *Caulobacter crescentus*, which we designated *lpxI.* We were then able to demonstrate that *lpxI* covers for a strain of *Escherichia coli* with deficient LpxH. Moreover, we have shown that LpxI possesses robust and specific UDP-2,3-diacylglucosamine hydrolase activity *in vitro*. This *in vitro* activity assay allowed us to develop high-yield purification schema for *Caulobacter crescentus* LpxI (CcLpxI) that had been expressed in *E. coli*. Protein crystallization screening was performed on the purified enzyme, and crystallization conditions identified. We were ultimately able to determine the x-ray crystal structure of this enzyme to 2.6 angstroms, utilizing single-wavelength anomalous dispersion (SAD) data for phasing.

Like any new finding, the structural characterization of LpxI yielded surprises. CcLpxI, which has homology to no other known enzymes, consists of two novel domains connected by a linker. CcLpxI co-purifies and co-crystallizes in a 0.95:1 stoichiometric ratio with its saccharolipid product, lipid X. The lipid X binding domain, in particular, displays an unexpected fold, with a deep hydrophobic tunnel completely enveloping lipid X's acyl chains. Based upon this observation, we constructed mutants of CcLpxI and determined whether their over-expression in *E. coli* strains causes lipid X or UDP-2,3-diacylglucosamine to accumulate in those cells' total lipids. By this method, we identified an alanine mutant of an absolutely-conserved aspartate (D225), which sequesters and co-purifies with its UDP-2,3-diacylglucosamine substrate. This construct was purifed, crystallized, and its structure solved to 3.0 angstroms. Large conformational differences between the CcLpxI and CcLpxI-D225A models are observed. Analytical ultracentrifugation experiments suggest that these conformational differences may be representatitive of behavior in solution. Refinement and analysis of the LpxI structured is ongoing.

This work sets the stage for further biochemical and structural characterization of this unusual peripheral-membrane enzyme binding to its unique sccharolipid substrate. From a macroscopic perspective, this work contributes to our knowledge of the small but growing set of structurally-characterized lipid-protein complexes, and the interesting binding modalities that these display. Moreover, such work is applicable to antibacterial drug design.

Purification and Characterization of LpxB, the Lipid A Disaccharide Synthase

E. coli LpxB, an inverting glycosyl transferase, catalyzes the condensation of 2,3-diacyl-GlcN-1-P (lipid X) and UDP-2-3-diacyl-GlcN (UDP-diacyl-glucosamine) to form 2',3'-diacyl-GlcN (β,1'→ 6)2,3-diacyl-GlcN-1-P (disaccharide monophosphate) and UDP. The LpxB product, disaccharide monophosphate (DSMP), constitutes the basic molecular scaffold of lipid A. The *lpxB* gene is essential in nearly all Gram-negative bacteria, making its product an excellent drug target.

LpxB orthologues exist in hundreds of bacterial species. Members of the functionally diverse, metal-independent Type B superfamily of glycosyltransferases, these comprise a distinct family (CAZy database family 19). At present, all members of this family remain enzymatically and structurally uncharacterized. Acting upon unusual saccharolipid substrates in an essential biological pathway, LpxB is an interesting target for biochemical analysis in the context of both enzymological structure-function relationships and antibacterial drug development.

My work addresses three questions: How does LpxB behave at membrane and protein interfaces? In what manner does LpxB accomplish catalysis? What does the disaccharide synthase's molecular structure reveal about its enzymatic properties, and how do these structure-function relationships contribute to the biochemical understanding of lipid substrate recognition?

We have developed a method by which to purify *E. coli* and *H. influenzae* LpxB to near-homogeneity in 10-mg quantities. The purified enzymes are active and can be concentrated to > 20 mg/ml in a minimal buffer. Our work prepares for future structure-function analysis of this unique glycosyltransferase. The preceding findings represent a significant contribution to the fields of lipid biochemistry, membrane assembly, bacterial pathogenesis, and membrane-protein structural biology.

Works Cited

(1) Khan, S. A., Everest, P., Servos, S., Foxwell, N., Zahringer, U., Brade, H., Rietschel, E. T., Dougan, G., Charles, I. G., and Maskell, D. J. (1998) A lethal role for lipid A in *Salmonella* infections. *Mol. Microbiol. 29*, 571-579.

(2) Ohl, M. E., and Miller, S. I. (2001) Salmonella: a model for bacterial pathogenesis. *Annu. Rev. Med. 52*, 259-274.

(3) Croxen, M. A., and Finlay, B. B. (2010) Molecular mechanisms of Escherichia coli pathogenicity. *Nature Reviews Microbiology 8*, 26-38.

(4) Masson-Boivin, C., Giraud, E., Perret, X., and Batut, J. (2009) Establishing nitrogen-fixing symbiosis with legumes: how many rhizobium recipes? *Trends in Microbiology 17*, 458-466.

(5) de Lorenzo, V. (2008) Systems biology approaches to bioremediation. *Current Opinion in Biotechnology 19*, 579-589.

(6) Raetz, C. R. H., and Whitfield, C. (2002) Lipopolysaccharide endotoxins. *Annual Review of Biochemistry 71*, 635-700.

(7) Raetz, C. R. H., Reynolds, C. M., Trent, M. S., and Bishop, R. E. (2007) Lipid a modification systems in gram-negative bacteria. *Annual Review of Biochemistry 76*, 295-329.

(8) Reynolds, C. M., and Raetz, C. R. H. (2009) Replacement of Lipopolysaccharide with Free Lipid A Molecules in Escherichia coli Mutants Lacking All Core Sugars. *Biochemistry 48*, 9627-9640.

(9) Boyle, E. C., and Finlay, B. B. (2003) Bacterial pathogenesis: exploiting cellular adherence. *Curr. Opin. Cell. Biol. 15*, 633-639.

(10) Miller, S. I., Ernst, R. K., and Bader, M. W. (2005) LPS, TLR4 and infectious disease diversity. *Nat. Rev. Microbiol. 3*, 36-46.

(11) Levy, S. B. (2005) Antibiotic resistance-the problem intensifies. *Adv. Drug Deliv. Rev. 57*, 1446-1450.

(12) Godfroid, F., Cloeckaert, A., Taminiau, B., Danese, I., Tibor, A., de Bolle, X., Mertens, P., and Letesson, J. J. (2000) Genetic organisation of the lipopolysaccharide O-antigen biosynthesis region of *Brucella melitensis* 16M (wbk). *Res. Microbiol. 151*, 655-668.

(13) Mantur, B. G., and Amarnath, S. K. (2008) Brucellosis in India - a review. *Journal of Biosciences 33*, 539-547.

(14) Mauldin, P. D., Salgado, C. D., Hansen, I. S., Durup, D. T., and Bosso, J. A. (2010) Attributable Hospital Cost and Length of Stay Associated with Health Care-Associated Infections Caused by Antibiotic-Resistant Gram-Negative Bacteria. *Antimicrobial Agents and Chemotherapy 54*, 109-115.

(15) Evrard, B., Balestrino, D., Dosgilbert, A., Bouya-Gachancard, J. L. J., Charbonnel, N., Forestier, C., and Tridon, A. (2010) Roles of Capsule and Lipopolysaccharide O Antigen in Interactions of Human Monocyte-Derived Dendritic Cells and Klebsiella pneumoniae. *Infection and Immunity 78*, 210-219.

(16) Armitage, J. P. (1999) Bacterial tactic responses. *Adv. Microb. Physiol. 41*, 229-289.

(17) Chevalier, J., Mulfinger, C., Garnotel, E., Nicolas, P., Davin-Regli, A., and Pages, J. M. (2008) Identification and Evolution of Drug Efflux Pump in Clinical Enterobacter aerogenes Strains Isolated in 1995 and 2003. *Plos One 3*, -.

(18) Ashida, H., Ogawa, M., Mimuro, H., and Sasakawa, C. (2009) Shigella Infection of Intestinal Epithelium and Circumvention of the Host Innate Defense System. *Molecular Mechanisms of Bacterial Infection Via the Gut 337*, 231-255.

(19) Chase, J. C., and Bosio, C. M. (2010) The Presence of CD14 Overcomes Evasion of Innate Immune Responses by Virulent Francisella tularensis in Human Dendritic Cells In Vitro and Pulmonary Cells In Vivo. *Infection and Immunity 78*, 154-167.

(20) Drawz, S. M., and Bonomo, R. A. (2010) Three Decades of beta-Lactamase Inhibitors. *Clinical Microbiology Reviews 23*, 160-+.

(21) Mamelli, L., Petit, S., Chevalier, J., Giglione, C., Lieutaud, A., Meinnel, T., Artaud, I., and Pages, J. M. (2009) New Antibiotic Molecules: Bypassing the Membrane Barrier of Gram Negative Bacteria Increases the Activity of Peptide Deformylase Inhibitors. *Plos One 4*, -.

(22) Tran, A. X., Lester, M. E., Stead, C. M., Raetz, C. R. H., Maske
ll, D. J., McGrath, S. C., Cotter, R. J., and Trent, M. S. (2005) Resistance to the antimicrobial peptide polymyxin requires myristoylation of Escherichia coli and Salmonella typhimurium lipid A. *Journal of Biological Chemistry 280*, 28186-28194.

(23) Yan, A. X., Guan, Z. Q., and Raetz, C. R. H. (2007) An undecaprenyl phosphate-aminoarabinose flippase required for polymyxin resistance in Escherichia coli. *Journal of Biological Chemistry 282*, 36077-36089.

(24) Goossens, H. (2009) Antibiotic consumption and link to resistance. *Clinical Microbiology and Infection 15*, 12-15.

(25) Fallon, E. O., Pop-Vicas, A., and Agata, E. D. (2009) The Emerging Threat of Multidrug-Resistant Gram-Negative Organisms in Long-Term Care Facilities. *Journals of Gerontology Series a-Biological Sciences and Medical Sciences 64*, 138-141.

(26) Gould, I. M. (2008) The epidemiology of antibiotic resistance. *International Journal of Antimicrobial Agents 32*, S2-S9.

(27) Metzger, L. E., and Raetz, C. R. H. (2009) Purification and Characterization of the Lipid A Disaccharide Synthase (LpxB) from Escherichia coli, a Peripheral Membrane Protein. *Biochemistry 48*, 11559-11571.

(28) Raetz, C. R. H., and Whitfield, C. (2002) Lipopolysaccharide endotoxins. *Annu. Rev. Biochem. 71*, 635-700.

(29) Coleman, J., and Raetz, C. R. H. (1988) First committed step of lipid A biosynthesis in *Escherichia coli*: sequence of the *lpxA* gene. *J. Bacteriol. 170*, 1268-1274.

(30) Young, K., Silver, L. L., Bramhill, D., Caceres, C. A., Stachula, S. A., Shelly, S. E., Raetz, C. R. H., and Anderson, M. S. (1993) The second step of lipid A biosynthesis, UDP-3-*O*-acyl-GlcNAc deacetylase is encoded by the pleiotropic permeability/cell division gene *envA* of *Escherichia coli*. *FASEB J. 7*, A1268.

(31) Kelly, T. M., Stachula, S. A., Raetz, C. R. H., and Anderson, M. S. (1993) The *firA* gene of *Escherichia coli* encodes UDP-3-*O*-(*R*-3-hydroxymyristoyl)-α-D-glucosamine *N*-acyltransferase: the third step of endotoxin biosynthesis. *J. Biol. Chem. 268*, 19866-19874.

(32) Stukey, J., and Carman, G. M. (1997) Identification of a novel phosphatase sequence motif. *Protein Sci. 6*, 469-472.

(33) Babinski, K. J., and Raetz, C. R. H. (1998) Identification of a gene encoding a novel *Escherichia coli* UDP-2,3-diacylglucosamine hydrolase. *FASEB J. 12*, A1288.

(34) Babinski, K. J., Kanjilal, S. J., and Raetz, C. R. H. (2002) Accumulation of the lipid A precursor UDP-2,3-diacylglucosamine in an *Escherichia coli* mutant lacking the *lpxH* gene. *J. Biol. Chem. 277*, 25947-25956.

(35) Crowell, D. N., Anderson, M. S., and Raetz, C. R. H. (1986) Molecular cloning of the genes for lipid A disaccharide synthase and UDP-*N*-acetylglucosamine acyltransferase in *Escherichia coli*. *J. Bacteriol. 168*, 152-159.

(36) Garrett, T. A., Kadrmas, J. L., and Raetz, C. R. H. (1997) Identification of the gene encoding the *Escherichia coli* lipid A 4'-kinase: facile phosphorylation of endotoxin analogs with recombinant LpxK. *Journal of Biological Chemistry 272*, 21855-21864.

(37) Belunis, C. J., Clementz, T., Carty, S. M., and Raetz, C. R. H. (1995) Inhibition of lipopolysaccharide biosynthesis and cell growth following inactivation of the *kdtA* gene in *Escherichia coli*. *J. Biol. Chem. 270*, 27646-27652.

(38) Clementz, T., Zhou, Z. M., and Raetz, C. R. H. (1997) Function of the *Escherichia coli msbB* gene, a multicopy suppressor of *htrB* knockouts, in the acylation of lipid A: acylation by MsbB follows laurate incorporation by HtrB. *Journal of Biological Chemistry 272*, 10353-10360.

(39) Karow, M., Fayet, O., Cegielska, A., Ziegelhoffer, T., and Georgopoulos, C. (1991) Isolation and characterization of the *Escherichia coli htrB* gene, whose product is essential for bacterial viability above 33 degrees C in rich media. *Journal of Bacteriology 173*, 741-750.

(40) Babinski, K. J., Ribeiro, A. A., and Raetz, C. R. H. (2002) The *Escherichia coli* gene encoding the UDP-2,3-diacylglucosamine pyrophosphatase of lipid A biosynthesis. *J. Biol. Chem. 277*, 25937-25946.

(41) Albers, U., Reus, K., Shuman, H. A., and Hilbi, H. (2005) The amoebae plate test implicates a paralogue of *lpxB* in the interaction of *Legionella pneumophila* with *Acanthamoeba castellanii*. *Microbiology 151*, 167-182.

(42) Zavaleta-Pastor, M., Sohlenkamp, C., Gao, J. L., Guan, Z. Q., Zaheer, R., Finan, T. M., Raetz, C. R. H., Lopez-Lara, I. M., and Geiger, O. (2010) Sinorhizobium meliloti phospholipase C required for lipid remodeling during phosphorus limitation. *Proceedings of the National Academy of Sciences of the United States of America 107*, 302-307.

(43) Whitfield, C., Kaniuk, N., and Frirdich, E. (2003) Molecular insights into the assembly and diversity of the outer core oligosaccharide in lipopolysaccharides from Escherichia coli and Salmonella. *Journal of Endotoxin Research 9*, 244-249.

(44) Doerrler, W. T., and Raetz, C. R. H. (2002) ATPase activity of the MsbA lipid flippase of *Escherichia coli*. *J. Biol. Chem. 277*, 36697-36705.

(45) Karow, M., and Georgopoulos, C. (1993) The essential *Escherichia coli msbA* gene, a multicopy suppressor of null mutations in the *htrB* gene, is related to the universally conserved family of ATP-dependent translocators. *Molecular Microbiology 7*, 69-79.

(46) Liu, D., Cole, R. A., and Reeves, P. R. (1996) An O-antigen processing function for Wzx (RfbX): A promising candidate for O-unit flippase. *Journal of Bacteriology 178*, 2102-2107.

(47) Paramonov, N. A., Aduse-Opoku, J., Hashim, A., Rangarajan, M., and Curtis, M. A. (2009) Structural Analysis of the Core Region of O-Lipopolysaccharide of Porphyromonas gingivalis from Mutants Defective in O-Antigen Ligase and O-Antigen Polymerase. *Journal of Bacteriology 191*, 5272-5282.

(48) Ma, C., and Chang, G. (2007) Structure of the multidrug resistance efflux transporter EmrE from *Escherichia coli*. *Proc. Natl. Acad. Sci. U S A 104*, 3668.

(49) Sperandeo, P., Cescutti, R., Villa, R., Di Benedetto, C., Candia, D., Deho, G., and Polissi, A. (2007) Characterization of lptA and lptB, two essential genes implicated in lipopolysaccharide transport to the outer membrane of *Escherichia coli. J. Bacteriol. 189*, 244-253.

(50) Ruiz, N., Gronenberg, L. S., Kahne, D., and Silhavy, T. J. (2008) Identification of two inner-membrane proteins required for the transport of lipopolysaccharide to the outer membrane of *Escherichia coli*. *Proc. Natl. Acad. Sci. U S A 105*, 5537-5542.

(51) Sperandeo, P., Lau, F. K., Carpentieri, A., De Castro, C., Molinaro, A., Deho, G., Silhavy, T. J., and Polissi, A. (2008) Functional analysis of the protein machinery required for the transport of lipopolysaccharide to the outer membrane of *Escherichia coli*. *J. Bacteriol.*, in press.

(52) Tate, C. G. (2006) Comparison of three structures of the multidrug transporter EmrE. *Curr. Opin. Struct. Biol. 16*, 457-464.

(53) Wu, T., McCandlish, A. C., Gronenberg, L. S., Chng, S. S., Silhavy, T. J., and Kahne, D. (2006) Identification of a protein complex that assembles lipopolysaccharide in the outer membrane of Escherichia coli. *Proceedings of the National Academy of Sciences of the United States of America 103*, 11754-11759.

(54) Bryant, C. E., Spring, D. R., Gangloff, M., and Gay, N. J. (2010) The molecular basis of the host response to lipopolysaccharide. *Nature Reviews Microbiology 8*, 8-14.

(55) Takeda, K. (2009) The Lipid A Receptor. *Lipid a in Cancer Therapy 667*, 53-58.

(56) Andra, J., Gutsmann, T., Muller, M., and Schromm, A. B. (2009) Interactions between Lipid A and Serum Proteins. *Lipid a in Cancer Therapy 667*, 39-51.

(57) Mitchell, J. A., Paul-Clark, M. J., Clarke, G. W., McMaster, S. K., and Cartwright, N. (2007) Critical role of toll-like receptors and nucleotide oligomerisation domain in the regulation of health and disease. *Journal of Endocrinology 193*, 323-330.

(58) O'Neill, L. A. J., and Bowie, A. G. (2007) The family of five: TIR-domain-containing adaptors in Toll-like receptor signalling. *Nature Reviews Immunology 7*, 353-364.

(59) Carpenter, S., and O'Neill, L. A. J. (2009) Recent insights into the structure of Toll-like receptors and post-translational modifications of their associated signalling proteins. *Biochemical Journal 422*, 1-10.

(60) Park, B. S., Song, D. H., Kim, H. M., Choi, B. S., Lee, H., and Lee, J. O. (2009) The structural basis of lipopolysaccharide recognition by the TLR4-MD-2 complex. *Nature 458*, 1191-U130.

(61) Nagai, Y., Akashi, S., Nagafuku, M., Ogata, M., Iwakura, Y., Akira, S., Kitamura, T., Kosugi, A., Kimoto, M., and Miyake, K. (2002) Essential role of MD-2 in LPS responsiveness and TLR4 distribution. *Nature Immunology 3*, 667-672.

(62) Verstak, B., Nagpal, K., Bottomley, S. P., Golenbock, D. T., Hertzog, P. J., and Mansell, A. (2009) MyD88 Adapter-like (Mal)/TIRAP Interaction with TRAF6 Is Critical for TLR2-and TLR4-mediated NF-kappa B Proinflammatory Responses. *Journal of Biological Chemistry 284*, 24192-24203.

(63) Walsh, C., Gangloff, M., Monie, T., Smyth, T., Wei, B., McKinley, T. J., Maskell, D., Gay, N., and Bryant, C. (2008) Elucidation of the MD-2/TLR4 interface required for signaling by lipid IVa. *Journal of Immunology 181*, 1245-1254.

(64) Knirel, Y. A., Lindner, B., Vinogradov, E. V., Kocharova, N. A., Senchenkova, S. N., Shaikhutdinova, R. Z., Dentovskaya, S. V., Fursova, N. K., Bakhteeva, I. V., Titareva, G. M., Balakhonov, S. V., Holst, O., Gremyakova, T. A., Pier, G. B., and Anisimov, A. P. (2005) Temperature-dependent variations and intraspecies diversity of the structure of the lipopolysaccharide of *Yersinia pestis*. *Biochemistry 44*, 1731-1743.

(65) Kanistanon, D., Hajjar, A. M., Pelletier, M. R., Gallagher, L. A., Kalhorn, T., Shaffer, S. A., Goodlett, D. R., Rohmer, L., Brittnacher, M. J., Skerrett, S. J., and Ernst, R. K. (2008) A *Francisella* mutant in lipid A carbohydrate modification elicits protective immunity. *PLoS Pathog. 4*, e24.

(66) Tanabe, H., Ayabe, T., Bainbridge, B., Guina, T., Ernst, R. K., Darveau, R. P., Miller, S. I., and Ouellette, A. J. (2005) Mouse Paneth cell secretory responses to cell surface glycolipids of virulent and attenuated pathogenic bacteria. *Infection and Immunity 73*, 2312-2320.

(67) Kim, S. K., Kim, Y. M., Yeum, C. E., Jin, S. H., Chae, G. T., and Lee, S. B. (2009) Rifampicin Inhibits the LPS-induced Expression of Toll-like Receptor 2 via the Suppression of NF-kappa B DNA-binding Activity in RAW 264.7 Cells. *Korean Journal of Physiology & Pharmacology 13*, 475-482.

(68) Liu, T., Konig, R., Sha, J., Agar, S. L., Tseng, C. T. K., Klimpel, G. R., and Chopra, A. K. (2008) Immunological responses against Salmonella enterica serovar Typhimurium Braun lipoprotein and lipid A mutant strains in Swiss-Webster mice: Potential use as live-attenuated vaccines. *Microbial Pathogenesis 44*, 224-237.

(69) Telepnev, M. V., Klimpel, G. R., Haithcoat, J., Knirel, Y. A., Anisimov, A. P., and Motin, V. L. (2009) Tetraacylated Lipopolysaccharide of Yersinia pestis Can Inhibit Multiple Toll-Like Receptor-Mediated Signaling Pathways in Human Dendritic Cells. *Journal of Infectious Diseases 200*, 1694-1702.

(70) Soderberg, M. A., and Cianciotto, N. P. (2010) Mediators of Lipid A Modification, RNA Degradation, and Central Intermediary Metabolism Facilitate the Growth of Legionella pneumophila at Low Temperatures. *Current Microbiology 60*, 59-65.

(71) Albers, U., Tiaden, A., Spirig, T., Al Alam, D., Goyert, S. M., Gangloff, S. C., and Hilbi, H. (2007) Expression of Legionella pneumophila paralogous lipid A biosynthesis genes under different growth conditions. *Microbiology-Sgm 153*, 3817-3829.

(72) Raetz, C. R. H., Guan, Z. Q., Ingram, B. O., Six, D. A., Song, F., Wang, X. Y., and Zhao, J. S. (2009) Discovery of new biosynthetic pathways: the lipid A story. *Journal of Lipid Research 50*, S103-S108.

(73) Delano, W. L., and Lam, J. W. (2005) PyMOL: A communications tool for computational models. *Abstracts of Papers of the American Chemical Society 230*, U1371-U1372.

(74) Kim, H. M., Park, B. S., Kim, J. I., Kim, S. E., Lee, J., Oh, S. C., Enkhbayar, P., Matsushima, N., Lee, H., Yoo, O. J., and Lee, J. O. (2007) Crystal structure of the TLR4-MD-2 complex with bound endotoxin antagonist Eritoran. *Cell 130*, 906-917.

(75) Sweet, C. R., and Raetz, C. R. H. (2001) Identification of two enzymes from *Thiobacillus ferrooxidans* that catalyze the oxidation and transamination of UDP-GlcNac. *FASEB J. 15*, A194.

(76) Sweet, C. R., Williams, A. H., Karbarz, M. J., Werts, C., Kalb, S. R., Cotter, R. J., and Raetz, C. R. H. (2004) Enzymatic synthesis of lipid A molecules with four amide-linked acyl chains. LpxA

acyltransferases selective for a new analogue of UDP-*N*-acetylglucosamine in which an amine replaces the 3"-hydroxyl group. *J. Biol. Chem. 279*, 25411-25419.

(77) Trent, M. S., Pabich, W., Raetz, C. R. H., and Miller, S. I. (2001) A PhoP/PhoQ-induced lipase (PagL) that catalyzes 3-*O*-deacylation of lipid A precursors in membranes of *Salmonella typhimurium*. *J. Biol. Chem. 276*, 9083-9092.

(78) Reynolds, C. M., Ribeiro, A. A., McGrath, S. C., Cotter, R. J., Raetz, C. R. H., and Trent, M. S. (2006) An outer membrane enzyme encoded by *Salmonella typhimurium lpxR* that removes the 3'-acyloxyacyl moiety of lipid A. . *J. Biol. Chem. 281*, 21974-21987.

(79) Bishop, R. E. (2005) The lipid A palmitoyltransferase PagP: molecular mechanisms and role in bacterial pathogenesis. *Mol. Microbiol. 57*, 900-912.

(80) Karbarz, M. J., Six, D. A., and Raetz, C. R. H. (2009) Purification and Characterization of the Lipid A 1-Phosphatase LpxE of Rhizobium leguminosarum. *Journal of Biological Chemistry 284*, 414-425.

(81) Wang, X., McGrath, S. C., Cotter, R. J., and Raetz, C. R. H. (2006) Expression cloning and periplasmic orientation of the *Francisella novicida* lipid A 4'-phosphatase LpxF. *J. Biol. Chem. 281*, 9321-9330.

(82) Que-Gewirth, N. L. S., Karbarz, M. J., Kalb, S. R., Cotter, R. J., and Raetz, C. R. H. (2003) Origin of the 2-amino-2-deoxy-gluconate unit in *Rhizobium leguminosarum* lipid A. Expression cloning of the outer membrane oxidase LpxQ. *J. Biol. Chem. 278*, 12120-12129.

(83) Reynolds, C. M., Kalb, S. R., Cotter, R. J., and Raetz, C. R. H. (2005) A phosphoethanolamine transferase specific for the outer 3-deoxy-D-*manno*-octulosonic acid residue of *Escherichia coli* lipopolysaccharide. Identification of the *eptB* gene and Ca^{2+} hypersensitivity of an *eptB* deletion mutant. *J. Biol. Chem. 280*, 21202-21211.

(84) Breazeale, S. D., Ribeiro, A. A., and Raetz, C. R. H. (2003) Origin of lipid A species modified with 4-amino-4-deoxy-L-arabinose in polymyxin-resistant mutants of *Escherichia coli. J. Biol. Chem. 279*, 24731–24739.

(85) Trent, M. S., Ribeiro, A. A., Doerrler, W. T., Lin, S. H., Cotter, R. J., and Raetz, C. R. H. (2001) Accumulation of a polyisoprene-linked amino sugar in polymyxin-resistant *Salmonella typhimurium* and *Escherichia coli*: structural characterization and transfer to lipid A in the periplasm. *Journal of Biological Chemistry 276*, 43132-43144.

(86) Curtiss, R., Wanda, S. Y., Gunn, B. M., Zhang, X., Tinge, S. A., Ananthnarayan, V., Mo, H., Wang, S. F., and Kong, W. (2009) Salmonella enterica Serovar Typhimurium Strains with Regulated Delayed Attenuation In Vivo. *Infection and Immunity 77*, 1071-1082.

(87) Li, Y., Wang, S., Scarpellini, G., Gunn, B., Xin, W., Wanda, S. Y., Roland, K. L., and Curtiss, R. (2009) Evaluation of new generation Salmonella enterica serovar Typhimurium vaccines with regulated delayed attenuation to induce immune responses against PspA. *Proceedings of the National Academy of Sciences of the United States of America 106*, 593-598.

(88) Branger, C. G., Torres-Escobar, A., Sun, W., Perry, R., Fetherston, J., Roland, K. L., and Curtiss, R. (2009) Oral vaccination with LcrV from Yersinia pestis KIM delivered by live attenuated Salmonella enterica serovar Typhimurium elicits a protective immune response against challenge with Yersinia pseudotuberculosis and Yersinia enterocolitica. *Vaccine 27*, 5363-5370.

(89) Peschel, A., and Sahl, H. G. (2006) The co-evolution of host cationic antimicrobial peptides and microbial resistance. *Nature Reviews Microbiology 4*, 529-536.

(90) Williams, A. H., Immormino, R. M., Gewirth, D. T., and Raetz, C. R. H. (2006) Structure of UDP-N-acetylglucosamine acyltransferase with a bound antibacterial pentadecapeptide. *Proc. Natl. Acad. Sci. U S A 103*, 10877-10882.

(91) Ulaganathan, V., Buetow, L., and Hunter, W. N. (2007) Nucleotide Substrate Recognition by UDP-N-acetylglucosamine Acyltransferase (LpxA) in the First Step of Lipid A Biosynthesis. *J. Mol. Biol. 369*, 305-312.

(92) Barb, A. W., Leavy, T. M., Robins, L. I., Guan, Z. Q., Six, D. A., Zhou, P., Hangauer, M. J., Bertozzi, C. R., and Raetz, C. (2009) Uridine-Based Inhibitors as New Leads for Antibiotics Targeting Escherichia coli LpxC (vol 48, pg 3068, 2009). *Biochemistry 48*, 7776-7776.

(93) Barb, A. W., Jiang, L., Raetz, C. R. H., and Zhou, P. (2007) Structure of the deacetylase LpxC bound to the antibiotic CHIR-090: Time-dependent inhibition and specificity in ligand binding. *Proceedings of the National Academy of Sciences of the United States of America 104*, 18433-18438.

(94) Coggins, B. E., Li, X., McClerren, A. L., Hindsgaul, O., Raetz, C. R. H., and Zhou, P. (2003) Structure of the LpxC deacetylase with a bound substrate-analog inhibitor. *Nat. Struct. Biol. 10*, 645-651.

(95) Coggins, B. E., McClerren, A. L., Jiang, L., Li, X., Rudolph, J., Hindsgaul, O., Raetz, C. R. H., and Zhou, P. (2005) Refined solution structure of the LpxC-TU-514 complex and pKa analysis of an active site histidine: insights into the mechanism and inhibitor design. *Biochemistry 44*, 1114-11126.

(96) Kennedy, E., Gennity, J., and Jackson, B. (1986) Regulation of the Balanced Synthesis of Membrane-Lipids in Escherichia-Coli. *Federation Proceedings 45*, 1592-1592.

(97) Hirschbe.Cb, and Kennedy, E. P. (1972) Mechanism of Enzymatic-Synthesis of Cardiolipin in Escherichia-Coli. *Proceedings of the National Academy of Sciences of the United States of America 69*, 648-&.

(98) Raetz, C. R. H., Wickner, W. T., Hirschbe.Cb, Kennedy, E. P., and Dowhan, W. (1972) Specific Membrane Bound Enzyme in Escherichia-Coli Catalyzing Hydrolyzing Hydrolysis of Nucleoside Diphosphate Diglycerides. *Federation Proceedings 31*, A896-&.

(99) Schulman, H., and Kennedy, E. P. (1977) Identification of Udp-Glucose as an Intermediate in Biosynthesis of Membrane-Derived Oligosaccharides of Escherichia-Coli. *Journal of Biological Chemistry 252*, 6299-6303.

(100) Schulman, H., and Kennedy, E. P. (1977) Relation of Turnover of Membrane Phospholipids to Synthesis of Membrane-Derived Oligosaccharides of Escherichia-Coli. *Journal of Biological Chemistry 252*, 4250-4255.

(101) Schneider, J. E., Schulman, H., and Kennedy, E. P. (1977) Membrane-Derived Oligosaccharides of Cell-Envelope of Escherichia-Coli. *Federation Proceedings 36*, 897-897.

(102) Raetz, C. R. H., and Kennedy, E. P. (1974) Partial-Purification and Properties of Phosphatidylserine Synthetase from Escherichia-Coli. *Journal of Biological Chemistry 249*, 5038-5045.

(103) Raetz, C. R. H., Dowhan, W., and Kennedy, E. P. (1976) Partial-Purification and Characterization of Cytidine 5'-Diphosphate-Diglyceride Hydrolase from Membranes of Escherichia-Coli. *Journal of Bacteriology 125*, 855-863.

(104) Raetz, C. R. H., and Kennedy, E. P. (1973) Function of Cytidine Diphosphate-Diglyceride and Deoxycytidine Diphosphate-Diglyceride in Biogenesis of Membrane Lipids in Escherichia-Coli. *Journal of Biological Chemistry 248*, 1098-1105.

(105) Raetz, C. R. H., Wickner, W. T., Kennedy, E. P., Hirschbe.Cb, and Dowhan, W. (1972) Membrane-Bound Pyrophosphatase in Escherichia-Coli Catalyzing Hydrolysis of Cytidine Diphosphate-Diglyceride. *Journal of Biological Chemistry 247*, 2245-&.

(106) Raetz, C. R. H., and Kennedy, E. P. (1972) Association of Phosphatidylserine Synthetase with Ribosomes in Extracts of Escherichia-Coli. *Journal of Biological Chemistry 247*, 2008-&.

(107) Raetz, C. R. H. (1975) Isolation of *Escherichia coli* mutants defective in enzymes of membrane lipid synthesis. *Proc. Natl. Acad. Sci. USA 72*, 2274-2278.

(108) Raetz, C. R. H., Kantor, G. D., Nishijima, M., and Newman, K. F. (1979) Cardiolipin accumulation in the inner and outer membranes of *Escherichia coli* mutants defective in phosphatidylserine synthetase. *J. Bacteriol. 139*, 544-551.

(109) Nishijima, M., and Raetz, C. R. H. (1979) Membrane lipid biogenesis in *Escherichia coli*: identification of genetic-loci for phosphatidylglycerophosphate synthetase and construction of mutants lacking phosphatidylglycerol. *Journal of Biological Chemistry 254*, 7837-7844.

(110) Bligh, E. G., and Dyer, W. J. (1959) A rapid method of total lipid extraction and purification. *Canaidan Journal of Biochemical Physiology 37*, 911-917.

(111) Nishijima, M., Bulawa, C. E., and Raetz, C. R. H. (1981) Two interacting mutations causing temperature-sensitive phosphatidylglycerol synthesis in *Escherichia coli* membranes. *J. Bacteriol. 145*, 113-121.

(112) Nishijima, M., and Raetz, C. R. H. (1981) Characterization of two membrane-associated glycolipids from an *Escherichia coli* mutant deficient in phosphatidylglycerol. *J. Biol. Chem. 256*, 10690-10696.

(113) Raetz, C. R. H., Purcell, S., Meyer, M. V., Qureshi, N., and Takayama, K. (1985) Isolation and characterization of eight lipid A precursors from a 3-deoxy-D-*manno*-octulosonic acid-deficient mutant of *Salmonella typhimurium*. *J. Biol. Chem. 260*, 16080-16088.

(114) Strain, S. M., Armitage, I. M., Anderson, L., Takayama, K., Qureshi, N., and Raetz, C. R. H. (1985) Location of polar substituents and fatty acyl chains on lipid A precursors from a 3-deoxy-D-*manno*-octulosonic acid-deficient mutant of *Salmonella typhimurium*: Studies by ^{1}H, ^{13}C and ^{31}P nuclear magnetic resonance. *J. Biol. Chem. 260*, 16089-16098.

(115) Crowell, D. N., Reznikoff, W. S., and Raetz, C. R. H. (1987) Nucleotide sequence of the *Escherichia coli* gene for lipid A disaccharide synthase. *J. Bacteriol. 169*, 5727-5734.

(116) Radika, K., and Raetz, C. R. H. (1988) Purification and properties of lipid A disaccharide synthase of *Escherichia coli*. *J. Biol. Chem. 263*, 14859-14867.

(117) Lipka, G., Demel, R. A., and Hauser, H. (1988) Phase behaviour of lipid X. *Chem. Phys. Lipids 48*, 267-280.

(118) Lairson, L. L., Henrissat, B., Davies, G. J., and Withers, S. G. (2008) Glycosyltransferases: structures, functions, and mechanisms. *Annu. Rev. Biochem. 77*, 521-555.

(119) Gross, B. J., Kraybill, B. C., and Walker, S. (2005) Discovery of O-GlcNAc transferase inhibitors. *Journal of the American Chemical Society 127*, 14588-14589.

(120) Cantarel, B. L., Coutinho, P. M., Rancurel, C., Bernard, T., Lombard, V., and Henrissat, B. (2009) The Carbohydrate-Active EnZymes database (CAZy): an expert resource for Glycogenomics. *Nucleic Acids Research 37*, D233-D238.

(121) Chen, L., Men, H., Ha, S., Ye, X. Y., Brunner, L., Hu, Y., and Walker, S. (2002) Intrinsic lipid preferences and kinetic mechanism of Escherichia coli MurG. *Biochemistry 41*, 6824-6833.

(122) Ha, S., Walker, D., Shi, Y. G., and Walker, S. (2000) The 1.9 angstrom crystal structure of Escherichia coli MurG, a membrane-associated glycosyltransferase involved in peptidoglycan biosynthesis. *Protein Science 9*, 1045-1052.

(123) Helm, J. S., Hu, Y. N., Chen, L., Gross, B., and Walker, S. (2003) Identification of active-site inhibitors of MurG using a generalizable, high-throughput glycosyltransferase screen. *Journal of the American Chemical Society 125*, 11168-11169.

(124) Takayama, K., Qureshi, N., Mascagni, P., Anderson, L., and Raetz, C. R. H. (1983) Glucosamine-derived phospholipids in *Escherichia coli*: Structure and chemical modification of a triacyl GlcN-1-P found in a phosphatidylglycerol-deficient mutant. *J. Biol. Chem. 258*, 14245-14252.

(125) Takayama, K., Qureshi, N., Mascagni, P., Nashed, M. A., Anderson, L., and Raetz, C. R. H. (1983) Fatty acyl derivatives of glucosamine 1-phosphate in *Escherichia coli* and their relation to lipid A: complete structure of a diacyl GlcN-1-P found in a phosphatidylglycerol-deficient mutant. *J. Biol. Chem. 258*, 7379-7385.

(126) Rietschel, E. T., Sidorczyk, A., Zahringer, U., Wollenweber, H. W., and Luderitz, O. (1983) in *Bacterial Lipopolysaccharides, ACS Symposium Series* (Anderson, L., and Unger, F. M., Ed.) pp 214, American Chemical Society, Washington, D. C.

(127) Bulawa, C. E., and Raetz, C. R. H. (1984) The Biosynthesis of gram-negative endotoxin: identification and function of UDP-2,3-diacylglucosamine in Escherichia coli. *Journal of Biological Chemistry 259*, 4846-4851.

(128) Bligh, E. G., and Dyer, J. J. (1959) A rapid method of total lipid extraction and purification. *Can. J. Biochem. Physiol. 37*, 911-917.

(129) Ray, B. L., Painter, G., and Raetz, C. R. H. (1984) The biosynthesis of gram-negative endotoxin: formation of lipid A disaccharides from monosaccharide precursors in extracts of *Escherichia coli*. *J. Biol. Chem. 259*, 4852-4859.

(130) Anderson, M. S., Bulawa, C. E., and Raetz, C. R. H. (1985) The biosynthesis of Gram-negative endotoxin: formation of lipid A precursors from UDP-GlcNAc in Extracts of Escherichia coli. *Journal of Biological Chemistry 260*, 5536-5541.

(131) Bulawa, C. E., and Raetz, C. R. H. (1984) Isolation and characterization of *Escherichia coli* strains defective in CDP-diglyceride hydrolase. *Journal of Biological Chemistry 259*, 1257-1264.

(132) Raetz, C. R. H., Hirschberg, C. B., Dowhan, W., Wickner, W. T., and Kennedy, E. P. (1972) A membrane-bound pyrophosphatase in *Escherichia coli* catalyzing the hydrolysis of cytidine diphosphate-diglyceride. *J. Biol. Chem. 247*, 2245-2247.

(133) Raetz, C. R. H., Dowhan, W., and Kennedy, E. P. (1976) Partial purification and characterization of cytidine 5'-diphosphate-diglyceride hydrolase from membranes of Escherichia coli. *Journal of Bacteriology 125*, 855-863.

(134) Bulawa, C. E., Hermes, J. D., and Raetz, C. R. H. (1983) Chloroform-soluble nucleotides in *Escherichia coli*. Role of CDP-diglyceride in the enzymatic cytidylylation of phosphomonoester acceptors. *J. Biol. Chem. 258*, 14974-14980.

(135) Icho, T., Bulawa, C. E., and Raetz, C. R. H. (1985) Molecular cloning and sequencing of the gene for CDP-diglyceride hydrolase of Escherichia coli. *Journal of Biological Chemistry 260*, 2092-2098.

(136) Anderson, M. S., Bulawa, C. E., and Raetz, C. R. H. (1985) The biosynthesis of gram-negative endotoxin: formation of lipid A precursors from UDP-GlcNAc in extracts of *Escherichia coli*. *J. Biol. Chem. 260*, 15536-15541.

(137) Kohara, Y., Akiyama, K., and Isono, K. (1987) The physical map of the whole *Escherichia coli* chromosome: application of a new strategy for rapid analysis and sorting of a large genomic library. *Cell 50*, 495-508.

(138) Gahan, L. R., Smith, S. J., Neves, A., and Schenk, G. (2009) Phosphate Ester Hydrolysis: Metal Complexes As Purple Acid Phosphatase and Phosphotriesterase Analogues. *European Journal of Inorganic Chemistry*, 2745-2758.

(139) Barker, C. J., Illies, C., Gaboardi, G. C., and Berggren, P. O. (2009) Inositol pyrophosphates: structure, enzymology and function. *Cellular and Molecular Life Sciences 66*, 3851-3871.

(140) Maceyka, M., Milstien, S., and Spiegel, S. (2009) Sphingosine-1-phosphate: the Swiss army knife of sphingolipid signaling. *Journal of Lipid Research 50*, S272-S276.

(141) McLennan, A. G. (2006) The Nudix hydrolase superfamily. *Cellular and Molecular Life Sciences 63*, 123-143.

(142) Sigal, Y. J., McDermott, M. I., and Morris, A. J. (2005) Integral membrane lipid phosphatases/phosphotransferases: common structure and diverse functions. *Biochemical Journal 387*, 281-293.

(143) McIntosh, E. M., and Haynes, R. H. (1997) dUTP pyrophosphatase as a potential target for chemotherapeutic drug development. *Acta Biochimica Polonica 44*, 159-171.

(144) Persson, R., Cedergren-Zeppezauer, E. S., and Wilson, K. S. (2001) Homotrimeric dUTPases; Structural solutions for specific recognition and hydrolysis of dUTP. *Current Protein & Peptide Science 2*, 287-300.

(145) McLennan, A. G. (1999) The MutT motif family of nucleotide phosphohydrolases in man and human pathogens (Review). *International Journal of Molecular Medicine 4*, 79-89.

(146) Liu, H., and Kiledjian, M. (2006) Decapping the message: a beginning or an end. *Biochemical Society Transactions 34*, 35-38.

(147) Tadokoro, T., and Kanaya, S. (2009) Ribonuclease H: molecular diversities, substrate binding domains, and catalytic mechanism of the prokaryotic enzymes. *Febs Journal 276*, 1482-1493.

(148) English, D. (1996) Phosphatidic acid: A lipid messenger involved in intracellular and extracellular signalling. *Cellular Signalling 8*, 341-347.

(149) Das, R., and Pandey, G. K. (2010) Expressional Analysis and Role of Calcium Regulated Kinases in Abiotic Stress Signaling. *Current Genomics 11*, 2-13.

(150) Schenk, G., Elliott, T. W., Leung, E., Carrington, L. E., Mitic, N., Gahan, L. R., and Guddat, L. W. (2008) Crystal structures of a purple acid phosphatase, representing different steps of this enzyme's catalytic cycle. *Bmc Structural Biology 8*, -.

(151) Voegtli, W. C., White, D. J., Reiter, N. J., Rusnak, F., and Rosenzweig, A. C. (2000) Structure of the bacteriophage λ Ser/Thr protein phosphatase with sulfate ion bound in two coordination modes. *Biochemistry 39*, 15365-15374.

(152) Mildvan, A. S., Xia, Z., Azurmendi, H. F., Saraswat, V., Legler, P. M., Massiah, M. A., Gabelli, S. B., Bianchet, M. A., Kang, L. W., and Amzel, L. M. (2005) Structures and mechanisms of Nudix hydrolases. *Archives of Biochemistry and Biophysics 433*, 129-143.

(153) Conyers, G. B., Wu, G., Bessman, M. J., and Mildvan, A. S. (2000) Metal requirements of a diadenosine pyrophosphatase from Bartonella bacilliformis: Magnetic resonance and kinetic studies of the role of Mn2+. *Biochemistry 39*, 2347-2354.

(154) Gabelli, S. B., Bianchet, M. A., Azurmendi, H. F., Xia, Z. Y., Sarawat, V., Mildvan, A. S., and Amzel, L. M. (2004) Structure and mechanism of GDP-mannose glycosyl hydrolase, a nudix enzyme that cleaves at carbon instead of phosphorus. *Structure 12*, 927-935.

(155) Weber, D. J., Bhatnagar, S. K., Bullions, L. C., Bessman, M. J., and Mildvan, A. S. (1992) Nmr and Isotopic Exchange Studies of the Site of Bond-Cleavage in the Mutt Reaction. *Journal of Biological Chemistry 267*, 16939-16942.

(156) Legler, P. M., Massiah, M. A., Bessman, M. J., and Mildvan, A. S. (2000) GDP-Mannose mannosyl hydrolase catalyzes nucleophilic substitution at carbon, unlike all other nudix hydrolases. *Biochemistry 39*, 8603-8608.

(157) Vertessy, B. G., and Toth, J. (2009) Keeping Uracil Out of DNA: Physiological Role, Structure and Catalytic Mechanism of dUTPases. *Accounts of Chemical Research 42*, 97-106.

(158) Kovari, J., Barabas, O., Varga, B., Bekesi, A., Tolgyesi, F., Fidy, J., Nagy, J., and Vertessy, B. G. (2008) Methylene substitution at the alpha-beta bridging position within the phosphate chain of dUDP profoundly perturbs ligand accommodation into the dUTPase active site. *Proteins-Structure Function and Bioinformatics 71*, 308-319.

(159) Varga, B., Barabas, O., Kovari, J., Toth, J., Hunyadi-Gulyas, E., Klement, E., Medzihradszky, K. F., Tolgyesi, F., Fidy, J., and Vertessy, B. G. (2007) Active site closure facilitates juxtaposition of reactant atoms for initiation of catalysis by human dUTPase. *Febs Letters 581*, 4783-4788.

(160) Tarbouriech, N., Buisson, M., Seigneurin, J. M., Cusack, S., and Burmeister, W. P. (2005) The monomeric dUTPase from Epstein-Barr virus mimics trimeric dUTPases. *Structure 13*, 1299-1310.

(161) Moorhead, G. B. G., De Wever, V., Templeton, G., and Kerk, D. (2009) Evolution of protein phosphatases in plants and animals. *Biochemical Journal 417*, 401-409.

(162) Gerlt, J. A., and Babbitt, P. C. (2001) Divergent evolution of enzymatic function: Mechanistically diverse superfamilies and functionally distinct suprafamilies. *Annual Review of Biochemistry 70*, 209-246.

(163) Sakai, A., Fedorov, A. A., Fedorov, E. V., Schnoes, A. M., Glasner, M. E., Brown, S., Rutter, M. E., Bain, K., Chang, S., Gheyi, T., Sauder, J. M., Burley, S. K., Babbitt, P. C., Almo, S. C., and Gerlt, J. A. (2009) Evolution of Enzymatic Activities in the Enolase Superfamily: Stereochemically Distinct Mechanisms in Two Families of cis,cis-Muconate Lactonizing Enzymes. *Biochemistry 48*, 1445-1453.

(164) Rakus, J. F., Kalyanaraman, C., Fedorov, A. A., Fedorov, E. V., Mills-Groninger, F. P., Toro, R., Bonanno, J., Bain, K., Sauder, J. M., Burley, S. K., Almo, S. C., Jacobson, M. P., and Gerlt, J. A. (2009) Computation-Facilitated Assignment of the Function in the Enolase Superfamily: A Regiochemically Distinct Galactarate Dehydratase from Oceanobacillus iheyensis. *Biochemistry 48*, 11546-11558.

(165) Gerlt, J. A., and Babbitt, P. C. (2009) Enzyme (re)design: lessons from natural evolution and computation. *Current Opinion in Chemical Biology 13*, 10-18.

(166) Kanjilal, S. J., Basu, S. S., Kanipes, M. I., and Raetz, C. R. H. (2005) Origin of the galacturonic acid modifications to the inner core of *Rhizobium leguminosarum* lipopolysaccharides. *Glycobiology 15*, 1194.

(167) Kanjilal-Kolar, S., Basu, S. S., Kanipes, M. I., Guan, Z., Garrett, T. A., and Raetz, C. R. H. (2006) Expression cloning of three *Rhizobium leguminosarum* lipopolysaccharide core galacturonosyltransferases. *J. Biol. Chem. 281*, 12865-12878.

(168) Yethon, J. A., Heinrichs, D. E., Monteiro, M. A., Perry, M. B., and Whitfield, C. (1998) Involvement of *waaY*, *waaQ*, and *waaP* in the modification of *Escherichia coli* lipopolysaccharide and their role in the formation of a stable outer membrane. *J. Biol. Chem. 273*, 26310-26316.

(169) Schaaf, G., Betts, L., Garrett, T. A., Raetz, C. R. H., and Bankaitis, V. A. (2006) Crystallization and preliminary X-ray diffraction analysis of phospholipid-bound Sfh1p, a member of the Saccharomyces cerevisiae Sec14p-like phosphatidylinositol transfer protein family. *Acta Crystallogr. Sect. F Struct. Biol. Cryst. Commun. 62*, 1156-1160.

(170) Schaaf, G., Ortlund, E. A., Tyeryar, K. R., Mousley, C. J., Ile, K. E., Garrett, T. A., Ren, J., Woolls, M. J., Raetz, C. R. H., Redinbo, M. R., and Bankaitis, V. A. (2008) Functional anatomy of phospholipid binding and regulation of phosphoinositide homeostasis by proteins of the Sec14 superfamily. *Molecular Cell 29*, 191-206.

(171) Silk, J. D., Salio, M., Brown, J., Jones, E. Y., and Cerundolo, V. (2008) Structural and Functional Aspects of Lipid Binding by CD1 Molecules. *Annual Review of Cell and Developmental Biology 24*, 369-395.

(172) Wang, J., Li, Y. L., Kinjo, Y., Mac, T. T., Gibson, D., Painter, G. F., Kronenberg, M., and Zajonc, D. M. (2010) Lipid binding orientation within CD1d affects recognition of Borrelia burgorferi antigens by NKT cells. *Proceedings of the National Academy of Sciences of the United States of America 107*, 1535-1540.

(173) Wyckoff, T. J., and Raetz, C. R. H. (1999) The active site of *Escherichia coli* UDP-*N*-acetylglucosamine acyltransferase. Chemical modification and site-directed mutagenesis. *J. Biol. Chem. 274*, 27047-27055.

(174) Williams, A. H., and Raetz, C. R. H. (2007) Structural basis for the acyl chain selectivity and mechanism of UDP-N-acetylglucosamine acyltransferase. *Proc. Natl. Acad. Sci. U S A 104*, 13543-13550.

(175) Robins, L. I., Williams, A. H., and Raetz, C. R. H. (2009) Structural Basis for the Sugar Nucleotide and Acyl-Chain Selectivity of Leptospira interrogans LpxA. *Biochemistry 48*, 6191-6201.

(176) Sweet, C. R., Preston, A., Toland, E., Ramirez, S. M., Cotter, R. J., Maskell, D. J., and Raetz, C. R. H. (2002) Relaxed acyl chain specificity of *Bordetella* UDP-N-acetylglucosamine acyltransferases. *J. Biol. Chem. 277*, 18281-18290.

(177) Petrek, M., Otyepka, M., Banas, P., Kosinova, P., Koca, J., and Damborsky, J. (2006) CAVER: a new tool to explore routes from protein clefts, pockets and cavities. *Bmc Bioinformatics 7*, -.

(178) Guzman, L. M., Belin, D., Carson, M. J., and Beckwith, J. (1995) Tight regulation, modulation, and high-level expression by vectors containing the arabinose PBAD promoter. *J. Bacteriol. 177*, 4121-4130.

(179) Yu, D., Smith, G. A., Enquist, L. W., and Shenk, T. (2002) Construction of a self-excisable bacterial artificial chromosome containing the human cytomegalovirus genome and mutagenesis of the diploid TRL/IRL13 gene. *Journal of Virology 76*, 2316-2328.

(180) Ma, B., Reynolds, C. M., and Raetz, C. R. H. (2008) Periplasmic orientation of nascent lipid A in the inner membrane of an Escherichia coli LptA mutant. *Proceedings of the National Academy of Sciences of the United States of America 105*, 13823-13828.

(181) Miller, J. R. (1972) *Experiments in Molecular Genetics*, Cold Spring Harbor Laboratory, Cold Spring Harbor, NY.

(182) Miroux, B., and Walker, J. E. (1996) Over-production of proteins in Escherichia coli: mutant hosts that allow synthesis of some membrane proteins and globular proteins at high levels. *J. Mol. Biol. 260*, 289-298.

(183) Doerrler, W. T., Gibbons, H. S., and Raetz, C. R. H. (2004) MsbA-dependent translocation of lipids across the inner membrane of *Escherichia coli*. *J. Biol. Chem. 279*, 45102-45109.

(184) McClerren, A. L., Zhou, P., Guan, Z., Raetz, C. R. H., and Rudolph, J. (2005) Kinetic analysis of the zinc-dependent deacetylase in the lipid A biosynthetic pathway. *Biochemistry 44*, 1106-1113.

(185) Bartling, C. M., and Raetz, C. R. H. (2008) Steady-state kinetics and mechanism of LpxD, the *N*-acyltransferase of lipid A biosynthesis. *Biochemistry 47*, 5290-5302.

(186) Wheeler, D. L., Church, D. M., Federhen, S., Lash, A. E., Madden, T. L., Pontius, J. U., Schuler, G. D., Schriml, L. M., Sequeira, E., Tatusova, T. A., and Wagner, L. (2003) Database resources of the National Center for Biotechnology. *Nucleic Acids Research 31*, 28-33.

(187) Nierman, W. C., Feldblyum, T. V., Laub, M. T., Paulsen, I. T., Nelson, K. E., Eisen, J., Heidelberg, J. F., Alley, M. R., Ohta, N., Maddock, J. R., Potocka, I., Nelson, W. C., Newton, A., Stephens, C., Phadke, N. D., Ely, B., DeBoy, R. T., Dodson, R. J., Durkin, A. S., Gwinn, M. L., Haft, D. H., Kolonay, J. F., Smit, J., Craven, M. B., Khouri, H., Shetty, J., Berry, K., Utterback, T., Tran, K., Wolf, A., Vamathevan, J., Ermolaeva, M., White, O., Salzberg, S. L., Venter, J. C., Shapiro, L., and Fraser, C. M. (2001) Complete genome sequence of *Caulobacter crescentus*. *Proc. Natl. Acad. Sci. U S A 98*, 4136-4141.

(188) Smit, J., Kaltoshov, I. A., Cotter, R. J., Vinogradov, E., Perry, M. B., Haider, H., and Qureshi, N. (2008) Structure of a novel lipid A obtained from the lipopolysaccharide of Caulobacter crescentus. *Innate Immunity 14*, 25-37.

(189) Snyder, D. S., Brahamsha, B., Azadi, P., and Palenik, B. (2009) Structure of Compositionally Simple Lipopolysaccharide from Marine Synechococcus. *Journal of Bacteriology 191*, 5499-5509.

(190) Kapust, R. B., and Waugh, D. S. (2000) Controlled intracellular processing of fusion proteins by TEV protease. *Protein Expression and Purification 19*, 312-318.

(191) Melcher, K. (2000) A modular set of prokaryotic and eukaryotic expression vectors. *Analytical Biochemistry 277*, 109-120.

(192) Guan, Z., Breazeale, S. D., and Raetz, C. R. H. (2005) Extraction and identification by mass spectrometry of undecaprenyl diphosphate-MurNAc-pentapeptide-GlcNAc from *Escherichia coli*. *Anal. Biochem. 345*, 336-339.

(193) Pudney, C. R., Hay, S., and Scrutton, N. S. (2009) Bipartite recognition and conformational sampling mechanisms for hydride transfer from nicotinamide coenzyme to FMN in pentaerythritol tetranitrate reductase. *Febs Journal 276*, 4780-4789.

(194) Berman, H. M., Westbrook, J., Feng, Z., Gilliland, G., Bhat, T. N., Weissig, H., Shindyalov, I. N., and Bourne, P. E. (2000) The Protein Data Bank. *Nucleic Acids Research 28*, 235-242.

(195) Epand, R. M., and Epand, R. F. (2009) Lipid domains in bacterial membranes and the action of antimicrobial agents. *Biochimica Et Biophysica Acta-Biomembranes 1788*, 289-294.

(196) Stahelin, R. V. (2009) Lipid binding domains: more than simple lipid effectors. *Journal of Lipid Research 50*, S299-S304.

(197) Studier, F. W. (2005) Protein production by auto-induction in high-density shaking cultures. *Protein Expression and Purification 41*, 207-234.

(198) Six, D. A., Carty, S. M., Guan, Z. Q., and Raetz, C. R. H. (2008) Purification and mutagenesis of LpxL, the lauroyltransferase of Escherichia coli lipid a biosynthesis. *Biochemistry 47*, 8623-8637.

(199) Holton, J., and Alber, T. (2004) Automated protein crystal structure determination using ELVES. *Proceedings of the National Academy of Sciences of the United States of America 101*, 1537-1542.

(200) Adams, P. D., Afonine, P. V., Bunkoczi, G., Chen, V. B., Davis, I. W., Echols, N., Headd, J. J., Hung, L. W., Kapral, G. J., Grosse-Kunstleve, R. W., McCoy, A. J., Moriarty, N. W., Oeffner, R., Read, R. J., Richardson, D. C., Richardson, J. S., Terwilliger, T. C., and Zwart, P. H. (2010) PHENIX: a comprehensive Python-based system for macromolecular structure solution. *Acta Crystallographica Section D-Biological Crystallography 66*, 213-221.

(201) Emsley, P., and Cowtan, K. (2004) Coot: model-building tools for molecular graphics. *Acta Crystallographica Section D-Biological Crystallography 60*, 2126-2132.

(202) Potterton, L., McNicholas, S., Krissinel, E., Gruber, J., Cowtan, K., Emsley, P., Murshudov, G. N., Cohen, S., Perrakis, A., and Noble, M. (2004) Developments in the CCP4 molecular-graphics project. *Acta Crystallographica Section D-Biological Crystallography 60*, 2288-2294.

(203) Davis, I. W., Murray, L. W., Richardson, J. S., and Richardson, D. C. (2004) MOLPROBITY: structure validation and all-atom contact analysis for nucleic acids and their complexes. *Nucleic Acids Res. 32*, W615-619.

(204) Pettersen, E. F., Goddard, T. D., Huang, C. C., Couch, G. S., Greenblatt, D. M., Meng, E. C., and Ferrin, T. E. (2004) UCSF chimera - A visualization system for exploratory research and analysis. *Journal of Computational Chemistry 25*, 1605-1612.

(205) Ebel, C. (2004) Analytical ultracentrifugation for the study of biological macromolecules. *Analytical Ultracentrifugation Vii 127*, 73-82162.

(206) Lebowitz, J., Lewis, M. S., and Schuck, P. (2002) Modern analytical ultracentrifugation in protein science: A tutorial review. *Protein Science 11*, 2067-2079.

(207) Laue, T. M., and Stafford, W. F. (1999) Modern applications of analytical ultracentrifugation. *Annual Review of Biophysics and Biomolecular Structure 28*, 75-100.

(208) Schuck, P. (2003) On the analysis of protein self-association by sedimentation velocity analytical ultracentrifugation. *Analytical Biochemistry 320*, 104-124.

(209) Schwede, T., Kopp, J., Guex, N., and Peitsch, M. C. (2003) SWISS-MODEL: an automated protein homology-modeling server. *Nucleic Acids Research 31*, 3381-3385.

(210) Rajagopalan, P. T. R., and Benkovic, S. J. (2002) Preorganization and protein dynamics in enzyme catalysis. *Chemical Record 2*, 24-36.

(211) Zimmer, J., Li, W. K., and Rapoport, T. A. (2006) A novel dimer interface and conformational changes revealed by an X-ray structure of B-subtilis SecA. *Journal of Molecular Biology 364*, 259-265.

(212) Chen, C. K. M., Lee, G. C., Ko, T. P., Guo, R. T., Huang, L. M., Liu, H. J., Ho, Y. F., Shaw, J. F., and Wang, A. H. J. (2009) Structure of the Alkalohyperthermophilic Archaeoglobus fulgidus Lipase

Contains a Unique C-Terminal Domain Essential for Long-Chain Substrate Binding. *Journal of Molecular Biology 390*, 672-685.

(213) Lundgren, S., Andersen, B., Piskur, J., and Dobritzsch, D. (2007) Crystallization and preliminary X-ray data analysis of beta-alanine synthase from Drosophila melanogaster. *Acta Crystallographica Section F-Structural Biology and Crystallization Communications 63*, 874-877.

(214) Wolthers KR, L. C., Scrutton NS, Leys D. (2010) Large-scale domain dynamics and adenosylcobalamin reorientation orchestrate radical catalysis in ornithine 4,5 aminomutase. *Journal of Biological Chemistry*.

(215) Epand, R. M., and Epand, R. F. (2009) Domains in bacterial membranes and the action of antimicrobial agents. *Molecular Biosystems 5*, 580-587.

(216) Lemmon, M. A. (2008) Membrane recognition by phospholipid-binding domains. *Nature Reviews Molecular Cell Biology 9*, 99-111.

(217) Kutateladze, T. G. (2007) Mechanistic similarities in docking of the FYVE and PX domains to phosphatidylinositol 3-phosphate containing membranes. *Progress in Lipid Research 46*, 315-327.

(218) Nikaido, H. (2003) Molecular basis of bacterial outer membrane permeability revisited. *Microbiol. Mol. Biol. Rev. 67*, 593-656.

(219) Raetz, C. R. H., Reynolds, C. M., Trent, M. S., and Bishop, R. E. (2007) Lipid A modification systems in gram-negative bacteria. *Annu. Rev. Biochem. 76*, 295-329.

(220) Brade, H., Opal, S. M., Vogel, S. N., and Morrison, D. C. (1999) pp 950, Marcel Dekker, Inc., New York.

(221) Meredith, T. C., Aggarwal, P., Mamat, U., Lindner, B., and Woodard, R. W. (2006) Redefining the requisite lipopolysaccharide structure in *Escherichia coli*. *ACS Chem. Biol. 1*, 33-42.

(222) Medzhitov, R., and Janeway, C., Jr. (2000) Innate immunity. *N. Engl. J. Med. 343*, 338-344.

(223) Akira, S., Uematsu, S., and Takeuchi, O. (2006) Pathogen recognition and innate immunity. *Cell 124*, 783-801.

(224) Gay, N. J., and Gangloff, M. (2007) Structure and function of toll receptors and their ligands. *Annu. Rev. Biochem. 76*, 141-165.

(225) Poltorak, A., He, X., Smirnova, I., Liu, M. Y., Huffel, C. V., Du, X., Birdwell, D., Alejos, E., Silva, M., Galanos, C., Freudenberg, M., Ricciardi-Castagnoli, P., Layton, B., and Beutler, B. (1998) Defective LPS signaling in C3H/HeJ and C57BL/10ScCr mice: mutations in Tlr4 gene. *Science 282*, 2085-2088.

(226) Hoshino, K., Takeuchi, O., Kawai, T., Sanjo, H., Ogawa, T., Takeda, Y., Takeda, K., and Akira, S. (1999) Cutting edge: Toll-like receptor 4 (TLR4)-deficient mice are hyporesponsive to lipopolysaccharide: evidence for TLR4 as the Lps gene product. *J. Immunol. 162*, 3749-3752.

(227) Park, B. S., Song, D. H., Kim, H. M., Choi, B. S., Lee, H., and Lee, J. O. (2009) The structural basis of lipopolysaccharide recognition by the TLR4-MD-2 complex. *Nature 458*, 1191-1195.

(228) Li, A., Chang, A. C., Peer, G. T., Hinshaw, L. B., and Taylor, F. B., Jr. (1996) Comparison of the capacity of rhTNF-alpha and Escherichia coli to induce procoagulant activity by baboon mononuclear cells in vivo and in vitro. *Shock 5*, 274-279.

(229) Drake, T. A., Cheng, J., Chang, A., and Taylor, F. B., Jr. (1993) Expression of tissue factor, thrombomodulin, and E-selectin in baboons with lethal *Escherichia coli* sepsis. *Am. J. Pathol. 142*, 1458-1470.

(230) Russell, J. A. (2006) Management of sepsis. *N. Engl. J. Med. 355*, 1699-1713.

(231) Rietschel, E. T., Kirikae, T., Schade, F. U., Mamat, U., Schmidt, G., Loppnow, H., Ulmer, A. J., Zähringer, U., Seydel, U., Di Padova, F., Schreier, M., and Brade, H. (1994) Bacterial endotoxin: molecular relationships of structure to activity and function. *FASEB Journal 8*, 217-225.

(232) Onishi, H. R., Pelak, B. A., Gerckens, L. S., Silver, L. L., Kahan, F. M., Chen, M. H., Patchett, A. A., Galloway, S. M., Hyland, S. A., Anderson, M. S., and Raetz, C. R. H. (1996) Antibacterial agents that inhibit lipid A biosynthesis. *Science 274*, 980-982.

(233) McClerren, A. L., Endsley, S., Bowman, J. L., Andersen, N. H., Guan, Z., Rudolph, J., and Raetz, C. R. H. (2005) A slow, tight-binding inhibitor of the zinc-dependent deacetylase LpxC of lipid A biosynthesis with antibiotic activity comparable to ciprofloxacin. *Biochemistry 44*, 16574-16583.

(234) Wang, R. F., and Kushner, S. R. (1991) Construction of versatile low-copy-number vectors for cloning, sequencing and gene expression in *Escherichia coli. Gene 100*, 195-199.

(235) Lucast, L. J., Batey, R. T., and Doudna, J. A. (2001) Large-scale purification of a stable form of recombinant tobacco etch virus protease. *Biotechniques 30*, 544-550.

(236) Phan, J., Zdanov, A., Evdokimov, A. G., Tropea, J. E., Peters, H. K., 3rd, Kapust, R. B., Li, M., Wlodawer, A., and Waugh, D. S. (2002) Structural basis for the substrate specificity of tobacco etch virus protease. *J. Biol. Chem. 277*, 50564-50572.

(237) Smith, P. K., Krohn, R. I., Hermanson, G. T., Mallia, A. K., Gartner, F. H., Provenzano, M. D., Fujimoto, E. K., Goeke, N. M., Olson, B. J., and Klenk, D. C. (1985) Measurement of protein using bicinchoninic acid. *Anal. Biochem. 150*, 76-85.

(238) Carman, G. M., Deems, R. A., and Dennis, E. A. (1995) Lipid signaling enzymes and surface dilution kinetics. *J. Biol. Chem. 270*, 18711-18714.

(239) Miller, J. R. (1972) *Experiments in Molecular Genetics*., Cold Spring Harbor Laboratory, Cold Spring Harbor, NY.

(240) Nishijima, M., and Raetz, C. R. H. (1979) Membrane lipid biogenesis in *Escherichia coli*: identification of genetic loci for phosphatidylglycerophosphate synthetase and construction of mutants lacking phosphatidylglycerol. *J. Biol. Chem. 254*, 7837-7844.

(241) Guan, Z., Li, S., Smith, D. C., Jr., Shaw, W. A., and Raetz, C. R. H. (2007) Identification of *N*-acyl phosphatidylserine molecules in eukaryotic cells. *Biochemistry*, Submitted.

(242) Cronan, J. E. (2003) Bacterial membrane lipids: where do we stand? *Annu. Rev. Microbiol. 57*, 203-224.

(243) Doerrler, W. T., Reedy, M. C., and Raetz, C. R. H. (2001) An *Escherichia coli* mutant defective in lipid export. *J. Biol. Chem. 276*, 11461-11464.

(244) Robertson, J. D., Schreil, W., and Reedy, M. (1982) *Halobacterium halobium*. I. A thin-sectioning electron-microscopic study. *J. Ultrastruct. Res. 80*, 148-162.

(245) Raetz, C. R. H. (1986) Molecular genetics of membrane phospholipid synthesis. *Annu. Rev. Genet. 20*, 253-295.

(246) van den Brink-van der Laan, E., Boots, J. W., Spelbrink, R. E., Kool, G. M., Breukink, E., Killian, J. A., and de Kruijff, B. (2003) Membrane interaction of the glycosyltransferase MurG: a special role for cardiolipin. *J. Bacteriol. 185*, 3773-3779.

(247) Wilkison, W. O., Bell, R. M., Taylor, K. A., and Costello, M. J. (1992) Structural characterization of ordered arrays of sn-glycerol-3-phosphate acyltransferase from Escherichia coli. J. Bacteriol. 174, 6608-6616.

(248) Hu, Y., Chen, L., Ha, S., Gross, B., Falcone, B., Walker, D., Mokhtarzadeh, M., and Walker, S. (2003) Crystal structure of the MurG:UDP-GlcNAc complex reveals common structural principles of a superfamily of glycosyltransferases. Proc. Natl. Acad. Sci. U S A 100, 845-849.

(249) Guan, L., Mirza, O., Verner, G., Iwata, S., and Kaback, H. R. (2007) Structural determination of wild-type lactose permease. Proc. Natl. Acad. Sci. U S A 104, 15294-15298.

Biography

Louis Eugene Metzger IV was born in Winfield, Illinois on May 25th, 1982 to Louis Eugene Metzger III and Janet Marie Metzger *née* Foehringer. He passed most of his youth in Arizona and New Mexico. He attended Cibola High School (Albuquerque, New Meixco) where, in 2000, he graduated first in his class. He then matriculated into the University of New Mexico as a Regents' Scholar (that university's most prestigious undergraduate scholarship), where he pursued research in structure-based drug design under the guidance of Professor David L. Van der Jagt and Dr. William Michael Brown. In 2003, he was named a Goldwater Scholar in Mathematics, Science, and Engineering. In 2004, he earned a B.Sc. in biochemistry, *summa cum laude*.

Metzger matriculated into Duke University's Doctoral Program in Biochemistry in 2004 as a James B. Duke Fellow. There, he joined the laboratory of Professor Christian R. H. Raetz. In 2005, he was named a National Science Foundation Graduate Research Fellow.

Scientific Publications to Date:

Metzger, L. E., and Raetz, C. R. H. (2009) Purification and Characterization of the Lipid A Disaccharide Synthase (LpxB) from Escherichia coli, a Peripheral Membrane Protein. *Biochemistry 48*, 11559-11571.

Immormino R.M., Metzger L.E. 4th, Reardon P.N., Dollins D.E., Blagg B.S., Gewirth D.T. (2009) Different poses for ligand and chaperone in inhibitor-bound Hsp90 and GRP94: implications for paralog-specific drug design. *J Mol Biol. 388(5)*, 1033-42.

Brown W.M., Metzger L.E., Barlow J.P., Hunsaker L.A., Deck L.M., Royer R.E., Vander Jagt D.L. (2003) 17-beta-Hydroxysteroid dehydrogenase type 1: computational design of active site inhibitors targeted to the Rossmann fold. *Chem Biol Interact.143-144*, 481-91.